THE GEOCHEMISTRY AND PETROGENESIS OF LAVAS FROM THE COMORES ARCHIPELAGO, WESTERN INDIAN OCEAN

Andreas Späth

VOLUME 1: TEXT

Department of Geological Sciences
University of Cape Town
September 1994

Thesis submitted to the University of Cape Town in fulfilment of the requirements for the degree of Master of Science

DECLARATION

I hereby declare that all of the work presented in this thesis is my own, except where otherwise stated in the text.

Signed by candidate

A. Späth

TABLE OF CONTENTS

ABSTRACT I

1. INTRODUCTION 1

2. REGIONAL GEOLOGY 5
The Tectonic History of the Western Indian Ocean 5
Cenozoic Volcanism in the Western Indian Ocean 8

3. LOCAL GEOLOGY: PREVIOUS STUDIES 10
The Geology of the Comores Archipelago 10
Grande Comore 12
Moheli 14
Anjouan 16
Mayotte 18

4. THE PETROLOGY OF LAVAS FROM GRANDE COMORE 21
4.1 Classification of the Rocks 21
4.2 Petrography and Mineralogy 22
Karthala Lavas 22
La Grille Lavas 23
4.3 Mineral Chemistry 23
Clinopyroxene 24
Olivine 26
4.4 Bulk Rock Chemistry 27
Major and Minor Elements 27
Trace Elements 31
Isotopes 36

5. THE PETROLOGY OF LAVAS FROM MOHELI 38
5.1 Classification of the Rocks 38
5.2 Petrography and Mineralogy 39
Alkali Basalts 40
Basanites 40
Nephelinites 41
Clinopyroxene Phenocrysts in Moheli Lavas 42
5.3 Mineral Chemistry 43
Clinopyroxene 43
Olivine 45
5.4 Bulk Rock Chemistry 47
Major and Minor Elements 47
Trace Elements 50
Isotopes 57

6. THE PETROLOGY OF LAVAS FROM MAYOTTE 58
6.1 Classification of the Rocks 58
6.2 Petrography and Mineralogy 59
Shield-building Phase Lavas 59
Post-erosional Phase Lavas 60
Rejuvenescent Phase Lavas 62
Clinopyroxene Phenocrysts in Mayotte Lavas 66
6.3 Mineral Chemistry 66
Clinopyroxene 67
Olivine 72
Feldspar 74
Fe-Ti Oxide 76
6.4 Bulk Rock Chemistry 79
Major and Minor Elements 79
Trace Elements 84
Isotopes 91

7. PRIMARY MELTS 93
Grande Comore 94
Moheli 94
Mayotte 96

8. FRACTIONAL CRYSTALLISATION 97
Grande Comore 97
Moheli 101
Mayotte 108
Green-core Clinopyroxenes 115
Amphibole Fractionation 118
Depth of Crystallisation 120

9. PARTIAL MELTING 122

10. THE ORIGIN OF LA GRILLE-TYPE INCOMPATIBLE ELEMENT PATTERNS 131
Fractional Crystallisation of Amphibole 133
Fractional Crystallisation of Phlogopite 134
Partial Melting of a Phlogopite-bearing Source 136
Partial Melting of an Amphibole-bearing Source 138

11. SOURCE REGION CHARACTERISTICS 141
Incompatible Elements 141
Radiogenic Isotopes 143
Mantle Depletion and Enrichment Events 148

12. THE EVOLUTION OF COMORES VOLCANISM IN SPACE AND TIME - A SYNTHESIS 151

13. CONCLUSIONS 158

ACKNOWLEDGMENTS 161

REFERENCES 162

ABSTRACT

The islands of the Comores Archipelago define a short, NNW-trending, volcanic lineament across the northern entrance to the Mozambique Channel in the western Indian Ocean and are considered to represent the surface expression of the Comores mantle plume. New mineral and bulk-rock analyses, as well as selected rare earth element (REE), $^{87}Sr/^{86}Sr$ and $^{143}Nd/^{144}Nd$ compositions for lavas from three of the four main islands of the archipelago are presented.

The alkaline lavas of the Comores range in texture from sparsely to strongly porphyritic, containing phenocrysts of olivine, clinopyroxene, amphibole, feldspar, Fe-Ti oxide and in one sample nepheline and garnet, which are typically set in a fine-grained groundmass of clinopyroxene, feldspar or nepheline, Fe-Ti oxide, lesser olivine and accessory apatite and titanite (sphene). With the exception of a few hypersthene- and even quartz-normative samples, all of the rocks analysed are moderately to strongly silica-undersaturated, nepheline-normative lavas. On *Grande Comore*, the youngest island in the archipelago, a clear distinction exists between the generally alkali basaltic lavas erupted by Karthala volcano and the basanites of La Grille volcano. The samples from the island of *Moheli* are classified as alkali basalts, basanites and nephelinites. The lavas of *Mayotte*, the oldest Comorean island, were erupted during three phases of volcanic activity and display greater chemical variation than both Grande Comore and Moheli lavas. Mayotte lavas range in composition from alkali basalt through trachybasalt, basaltic trachyandesite and trachyandesite to trachyte, and from basanite and nephelinite through phonotephrite to phonolite. Comorean lavas have high incompatible element abundances and display strongly light rare earth element-enriched chondrite-normalised REE patterns. On the basis of their primitive mantle-normalised incompatible element patterns (spidergrams), all of the lavas analysed may be assigned to one of two very distinct Comorean lava types: La Grille-type (LGT) lavas display strong relative depletions in K (and sometimes Rb), whereas Karthala-type (KT) lavas do not show such depletions. Both LGT and KT lavas were erupted on Grande Comore, Moheli and Mayotte.

With the exception of the lavas erupted by La Grille volcano, which exhibit the petrographic and geochemical characteristics expected of primary mantle magmas, all

Comorean lavas analysed have experienced compositional modifications after they segregated from their source regions. Quantitative major and trace element modelling suggests that much of the compositional variation observed amongst Comorean lavas is explicable in terms of fractional crystallisation processes dominated by the early fractionation of olivine and clinopyroxene. Plagioclase appears to have been an additional fractionating phase during the evolution of Moheli basanites. The more advanced stages of the differentiation history of Mayotte lavas were dominated by the fractionation of increasing quantities of feldspar and amphibole, as well as smaller amounts of clinopyroxene, Fe-Ti oxide and accessory apatite and titanite. The presence of high-pressure clinopyroxene, amphibole and possibly garnet crystals in Comorean lavas suggests that the crystal fractionation processes involved in their differentiation may have been initiated at relatively elevated pressures.

Partial melting in the presence of residual amphibole is proposed to be the most likely mode of origin for the K-depletions which characterise LGT Comorean lavas. It is suggested that primary LGT magmas were generated by small degrees of partial melting of an amphibole-bearing garnet-lherzolite mantle source at depths corresponding to pressures greater than 25 kb. Primary KT magmas, on the other hand, are considered to be the product of somewhat larger degrees of partial melting of an amphibole-free spinel-lherzolite source at shallower depths.

The Nd and Sr isotopic compositions of Comorean lavas bear evidence for a time-averaged depletion in incompatible elements, whereas the high incompatible element abundances of these lavas are proposed to reflect the effects of a recent mantle enrichment event. It is suggested that the garnet-lherzolite source of LGT Comorean lavas experienced recent modal metasomatism, resulting in the precipitation of amphibole, whereas the shallower spinel-lherzolite source of KT lavas underwent cryptic metasomatism only, without the introduction of new minerals. The ambient sub-Comorean upper mantle is proposed to consist of a mixture between the HIMU mantle component and a depleted component (DMM, PREMA or a component on the mantle array). The Nd and Sr isotope signature of the majority of Comorean lavas (both LGT and KT) may be explained as a mixture dominated by the components comprising the sub-Comorean mantle with limited contributions from the EM I-type Comorean mantle plume itself. The lavas erupted by Karthala volcano (the youngest Comorean lavas),

however, have significantly different isotopic compositions than all other Comorean lavas (lower $^{143}Nd/^{144}Nd$ and higher $^{87}Sr/^{86}Sr$), suggesting significantly increased contributions from the Comores mantle plume. An alternative model, equally consistent with the present data, involves an ambient sub-Comorean mantle consisting of a depleted component that is mixed with a Comores mantle plume which contains both HIMU and EM I components. In this scenario, the character of the plume would have to change from one dominated by the HIMU component during most of the volcanic history of the Comores, to one dominated by the EM I component during the generation of the lavas erupted by Karthala.

An internally consistent, broadly chronological petrogenetic model for the evolution of Comorean volcanism is presented.

1. INTRODUCTION

The Comores Archipelago is located between approximately 11°30'S 43°30'E and 13°S 45°15'E, at the northern end of the Mozambique Channel in the western Indian Ocean, and is comprised of the four main islands Grande Comore, Moheli, Anjouan and Mayotte.

The geological setting of this group of young volcanic islands is very similar to that of numerous islands in ocean basins worldwide. The lavas erupted on such intraplate oceanic islands far removed from active mid-ocean spreading centres and destructive plate margins are generally referred to as ocean island basalts (OIB), although they are by no means all strictly basaltic in composition. The volcanic activity that gives rise to these islands is widely regarded to be the result of partial mantle melting at so-called hotspots, which represent the surface expressions of localised areas of anomalously high mantle heat flow associated with relatively narrow plumes of upwelling mantle material rising towards the Earth's surface from significant depths. Such mantle plumes are thought to remain more or less stationary within the Earth's mantle, creating linear chains of ocean islands and seamounts on overriding oceanic plates, the Hawaiian islands and the adjoining Emperor seamount chain being the classic example. Mantle plumes may also have played an important role during various episodes of continental breakup (e.g. southern Atlantic) and in the generation of continental flood basalts (e.g. Deccan Traps). Numerous hotspots have been identified worldwide, including several in the Indian Ocean, one of which may in fact have produced the islands of the Comores Archipelago.

Although OIB comprise only a very small percentage of igneous rocks worldwide, they have been studied in great detail since they contrast with continental igneous rocks (e.g. continental flood basalts) in that they were erupted through comparatively thin, basaltic, oceanic crust, and with mid-ocean ridge basalts in that they are considered to originate from significantly deeper, less depleted mantle domains. OIB therefore represent essentially uncontaminated melts produced by partial melting of the Earth's upper mantle. Over the last few decades, the study of OIB has led to significant advances in our

understanding of the petrogenesis of basaltic magmas, particularly in terms of the nature of partial melting, melt segregation and melt propagation processes in the upper mantle, as well as the evolution of basaltic mantle melts by processes such as shallow-level and polybaric fractional crystallisation. Since they represent a virtually unobstructed "window" into the oceanic mantle, OIB have provided a wealth of information concerning the geochemical characteristics, mineralogy and evolution of the source regions of basaltic magmas and have furthermore helped to identify geochemical heterogeneities and various geochemically distinct domains in the Earth's mantle. Another objective of studying OIB is the accurate determination of any age progressions amongst the eruptive products of plume-generated volcanic lineaments. Such age progressions can provide powerful, independent constraints on the absolute motions of lithospheric plates with respect to a global framework of stationary mantle plumes. Age determinations of OIB furthermore allow investigations of possible temporal variations in the geochemistry of the lavas produced by a mantle plume. Besides providing invaluable information about the geochemical nature and evolution of the Earth's mantle in general and of mantle plumes in particular, the study of OIB has also led to sophisticated theoretical and experimental investigations into the structure of such mantle plumes, illuminating the geophysical and fluid-dynamical principles involved in their formation and their propagation through the mantle.

The aims of the present study are to investigate the petrology and geochemistry of lavas from three of the four main Comores islands (Grande Comore, Moheli, Mayotte) with a view towards explaining their petrogenesis and furthermore to constrain the geochemical characteristics of their mantle source region(s). All of the samples that were analysed during this study were kindly donated by R. A. Duncan of Oregon State University, USA. The sample collection includes many of the specimen investigated by Emerick (1980, 1985) and Emerick and Duncan (1982, 1983). No samples from Anjouan were available. Where possible, individual sampling sites on Grande Comore, Moheli and Mayotte are indicated in Figures 3.1, 3.2a and 3.3 (Chapter 3) respectively.

For the purposes of a brief outline, the main body of this dissertation may be divided into three parts:

- Part I. Geological Background

  Chapters 2 and 3 summarize aspects of both the geological history and setting of the western Indian Ocean and the geology of the Comores Archipelago as described in the literature.

- Part II. Descriptions

  Descriptive accounts of the petrography as well as the mineral and bulk rock chemistry of all the Grande Comore, Moheli and Mayotte samples investigated in this study are contained in Chapters 4, 5 and 6 respectively.

- Part III. Interpretations

  Using the data presented in Part II, the petrogenesis and evolution of Comorean lavas, as well as the geochemistry of their mantle source region(s) are discussed in Chapters 7 to 13. In Chapter 7, the present data are evaluated to establish whether any of the lavas exhibit the characteristics expected of primary mantle melts. In Chapters 8 and 9, evidence for the role played by fractional crystallisation and partial melting processes in the petrogenesis of Comorean lavas is presented. Possible modes of origin for two distinct lava types encountered on the Comores are evaluated in Chapter 10, whilst Chapter 11 investigates the geochemical characteristics of the mantle source region of Comorean lavas. In Chapter 12, the results and interpretations from previous chapters are combined into an internally consistent model for the evolution of Comorean volcanism in space and time. The most important conclusions drawn in this study are summarized briefly in Chapter 13.

The appendices, which are contained in a separate volume, include brief summaries of

the analytical techniques employed, tables listing additional mineral chemistry data, a table listing the mineral-melt distribution coefficients used for quantitative modelling of partial melting and fractional crystallisation processes, petrographic descriptions of all samples for which thin sections were made, and photomicrographs of selected samples.

2. REGIONAL GEOLOGY

The Tectonic History of the Western Indian Ocean

The location of the Comores Archipelago warrants a brief review of the tectonic framework and history of the western Indian Ocean as described in the literature. The term "western Indian Ocean" is used here, to describe broadly the area between the African east coast and the Carlsberg, Central Indian and eastern Southwest Indian Ridges (Fig. 2.1).

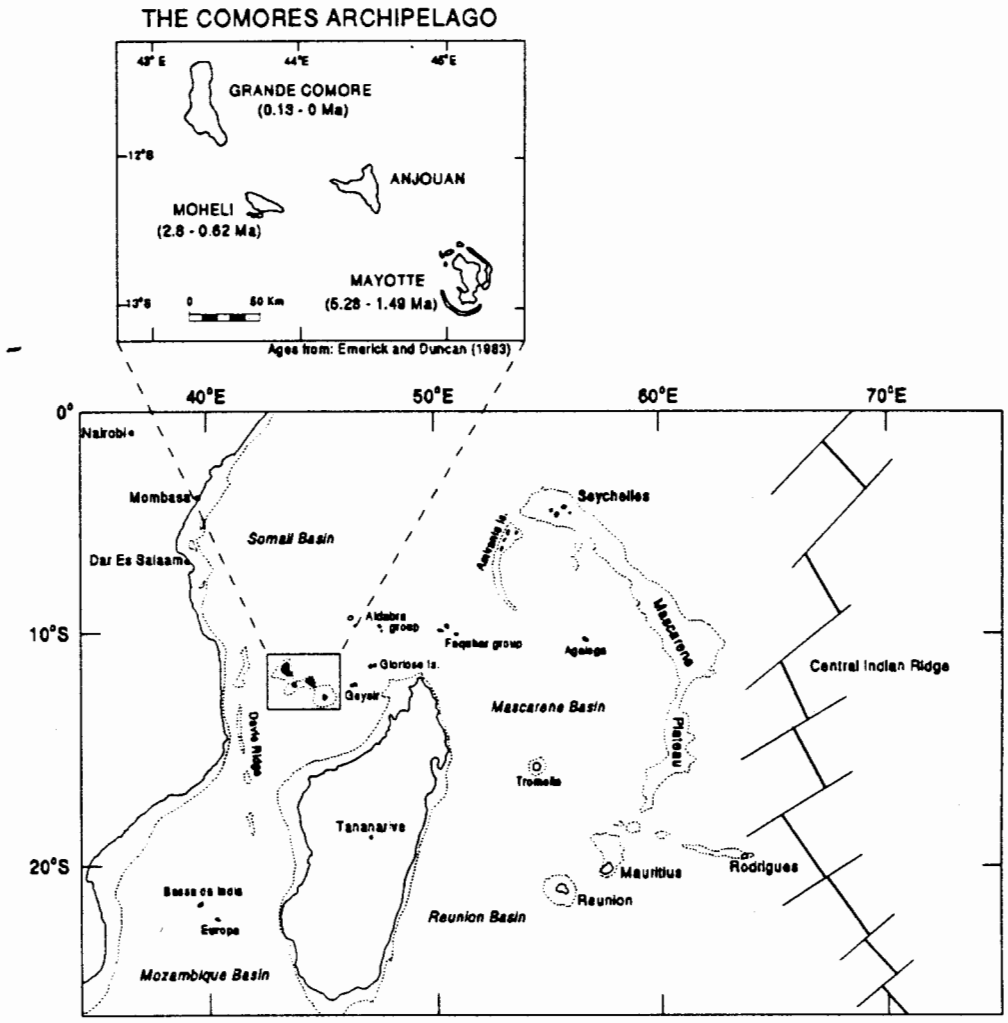

Fig. 2.1. Map of the western Indian Ocean, Madagascar and the southeast coast of Africa. The inset shows a close-up of the Comores Archipelago (the range of K-Ar ages of lavas from three of the islands is indicated).

The palaeoposition of *Madagascar* prior to the breakup of Gondwanaland and by implication the opening of the Mozambique Channel and the Somali Basin, has long been a point of debate (e.g. Wegener, 1924; Du Toit, 1937). One suggestion has been that Madagascar has remained in its present position with respect to Africa since at least mid-Mesozoic times and that the Mozambique Channel is underlain by subsided continental crust (e.g. Flower and Strong, 1969). According to this model the Comores islands should be underlain, at least partially, by continental crustal material. In contrast, a number of workers have argued for a pre-rifting fit of Madagascar against the coastlines of present-day Mozambique and Natal (Flores, 1970; Wright and McCurry, 1970; Green, 1972; Kent, 1972). In this scenario, Madagascar moved east- and northwards during the Mesozoic to reach its present location.

The bulk of the recent literature on this debate, has, however, vindicated the suggestion by Du Toit (1937), that Madagascar was situated adjacent to present-day Kenya, Tanzania and southern Somalia prior to the breakup of Gondwanaland and was subsequently displaced towards the south and slightly to the east (Bunce and Molnar, 1977; Norton and Sclater, 1979; Rabinowitz *et al.*, 1983). Bunce and Molnar (1977) identified three north-south trending, en echelon basement ridges on seismic reflection profiles of the Somali Basin and interpreted them as fracture zones which are approximately parallel to the Davie Ridge further to the south. The Davie Ridge itself is proposed to be a curvilinear fracture zone (Davie Fracture Zone), extending from 5°S (off Kenya) to 26°S (south of Madagascar) (Scrutton, 1978; Bassias, 1992). Several workers have argued that the southward drift of Madagascar proceeded along these fracture zones (Heirtzler and Burroughs, 1971; Bunce and Molnar, 1977; Scrutton, 1978; Norton and Sclater, 1979). This model is supported by a sequence of east-west trending magnetic anomalies of Mesozoic age in the western Somali Basin, which have been interpreted to indicate that the separation between Africa and Madagascar started during the time of the Jurassic Quiet Zone (~165 Ma) and ended at the time of the formation of anomaly M9 (~121 Ma) (Rabinowitz *et al.*, 1983). According to this model, the Comores Archipelago should be underlain by oceanic, rather than continental crust.

During the initial stages of the breakup of Gondwanaland, Madagascar was probably a

part of the Indian plate, but in the late Cretaceous (~80-90 Ma), the spreading axis between Madagascar and Africa jumped to a new position between India and Madagascar, commencing the separation between these two landmasses, with the Indian plate moving northward (Norton and Sclater, 1979; Dickin *et al.*, 1986/1987; Dostal *et al.*, 1992). Evidence for the initiation of rifting exists in the form of extensive lower Campanian (~73 Ma) volcanism along the east coast of Madagascar (Norton and Sclater, 1979; Dostal *et al.*, 1992).

The *Seychelles Archipelago*, north of Madagascar, is comprised of a large number of islands, rising from the submarine Seychelles Bank. Most of the islands are composed of anorogenic granite, the Precambrian ages of which are consistent with a continental origin (Miller and Mudie, 1961; Wasserburg *et al.*, 1963; Baker and Miller, 1963). From the interpretation of seismic refraction profiles and gravity anomaly measurements, Matthew and Davies (1966), concluded that the granitic rocks extend to a depth of about 15 km beneath the central part of the Seychelles Bank and that the crust in this area has both continental character and thickness. In 1937, Du Toit suggested that the Seychelles may rēpresent "fragments left behind in the rear of India" during its northward movement. Several workers have since argued that at about 64 Ma, the active spreading ridge situated between Madagascar and India jumped northward to a location between India and the Seychelles, forming the present-day Carlsberg Ridge (Fisher *et al.*, 1967; Norton and Sclater, 1979; Dickin *et al.*, 1986/1987; Dostal *et al.*, 1992) and separating the Seychelles from the Indian plate.

The Seychelles Bank is topographically linked to the northern extremity of the flat-topped *Mascarene Plateau*. This plateau is a major structural element of the western Indian Ocean and extends for more than 2300 km from the Seychelles across the Saya de Malha, Nazareth and Cargados Carajos Banks towards the volcanic islands of Mauritius and Réunion. No consensus exists in the literature as to the origin of the Mascarene Plateau. Several workers have suggested that parts of the plateau consist of continental crustal material that is structurally linked to the Seychelles Bank (Baker and Miller, 1963; Matthews and Davies, 1966; Fisher *et al.*, 1967). According to some other authors, however, the principle volume of the Mascarene Plateau consists of volcanic

material or at least is underlain by volcanic basement (Shor and Pollard, 1963; Meyerhoff and Kame-Kaye, 1981). Recent biostratigraphical, geochronological and geochemical studies have provided evidence consistent with the suggestion that the three Mascarene islands of Rodrigues, Mauritius and Réunion, together with much of the Mascarene Plateau, the Chagos-Laccadive Ridge and the Deccan flood basalt province, are all products of the Réunion mantle plume (Fisk *et al.*, 1989; Duncan *et al.*, 1989; Duncan, 1990; Duncan and Hargraves, 1990; Baxter, 1990; White *et al.*, 1990). Earlier, Duncan (1981) showed that, geometrically and chronologically, these features match the linear pattern of topographic anomalies expected from calculated motions of the Indian and African plates over this hotspot.

The *Amirante Ridge and Islands* and the associated Amirante Trench southwest of the Seychelles remain somewhat enigmatic features of the western Indian Ocean. The Amirante Islands are coral atolls and sand cays and although no volcanic rocks are exposed at the surface, magnetic anomaly profiles suggest the presence of a basaltic foundation at a depth of less than 1 km below sea-level (Matthews and Davies, 1966). The Amirante Ridge and islands have been interpreted as an extinct subduction zone and its associated island arc (Matthews and Davies, 1966; Green, 1972), as a structural part of the Seychelles Bank (Baker and Miller, 1963) and more exotically, as the astrobleme formed by the impact of a hypothetical K-T boundary extinction bolide (Hartnady, 1986).

Cenozoic Volcanism in the Western Indian Ocean

Besides the volcanism on the Comores, Tertiary and Quaternary intraplate volcanic activity has been fairly wide-spread throughout the western Indian Ocean.

Upton (1982) suggested that some of the very small islands to the east and south of the Comores (e.g. the *Glorioso Islands*, *Geysir Reef*, *Juan de Nova Island*) may represent limestone growths capping earlier Tertiary volcanoes.

Emerick and Duncan (1982) determined the K-Ar ages of several lavas from *northern Madagascar* and proposed that the alkaline magmatic activity in this region commenced at least 10 Ma ago and continued for about 9 Ma.

The slightly elevated coral reefs of the islands of the *Aldabra group*, northeast of the Comores, are situated on the summits of mountains that rise about 4000 metres from the relatively flat seafloor of the Somali Basin and may consist of late Cretaceous or early Tertiary volcanic cones (Stoddart *et al.*, 1971). On the basis of a single magnetic anomaly profile, Green (1972) suggested that the Aldabra islands may be connected by a "submarine intrusion or extrusion" to the volcanic northeastern region of Madagascar or even the Comores.

The islands of the *Faquhar group*, located just north of Madagascar, are capped by sea-level coral reefs (Stoddart *et al.*, 1971), but the nature of their (possibly volcanic ?) basement is unknown.

During Tertiary times, the Precambrian granites of the *Seychelles Bank* were intruded by alkaline complexes and north-westerly trending basaltic dike swarms (Baker and Miller, 1963; Fisher *et al.*, 1967). Emerick and Duncan (1982) proposed that this volcanic activity represents the earliest manifestation of the Comores hotspot. Dickin *et al.* (1986/1987), however, suggested that the good agreement between the ages of alkaline complexes on the islands of Silhouette and Ile du Nord (about 63 Ma) and the postulated age of the initiation of spreading on the Carlsberg Ridge (about 64 Ma), provides evidence that the younger igneous activity on the Seychelles is intimately associated with continental rifting.

3. LOCAL GEOLOGY: PREVIOUS STUDIES

The Geology of the Comores Archipelago

The islands of the Comores Archipelago represent the emergent peaks of a north-northwest trending submarine ridge that rises from the abyssal depths (>3500m) of the Comores Basin and straddles the northern entrance of the Mozambique Channel (Fig. 2.1). From Grande Comore in the northwest via Moheli and Anjouan to Mayotte in the southeast, the four main Comores islands define a roughly linear chain, approximately 275 km in length. The islands are entirely volcanic in nature and consist predominantly of silica-undersaturated, alkaline lavas, including alkali basalts, basanites, nephelinites, trachybasalts, mugearites, benmoreites, phonolites and trachytes. Lacroix (1922) and Krenkel (1925) provided some of the earliest geological accounts of the Archipelago, while more recent summaries were published by Esson *et al.* (1970) and Upton (1982).

A lack of consensus about the geological history of the western Indian Ocean and the surprisingly widespread evidence for Cenozoic volcanic activity in the region are two factors which have contributed to diverging ideas concerning the tectonic setting, nature and evolution of the Comores. As noted in the previous chapter, the preferred model for the southeastward migration of Madagascar from a pre-rift setting adjacent to present-day Kenya, Tanzania and Somalia, predicts that the Comores Archipelago is underlain by oceanic crust. Some workers have argued, however, that the presence of sedimentary xenoliths in Comorean lavas provides evidence for the existence of continental crustal material beneath the Archipelago (Flower and Strong, 1969; Esson *et al.*, 1970). As pointed out by Wright and McCurry (1970), however, the occurrence of these xenoliths is evidence merely for the presence of sediments beneath the islands and does by no means constitute conclusive proof that this part of the Indian Ocean is underlain by non-oceanic crust. Nougier *et al.* (1986) suggested that the Comores are located near the continental margin in a transitional zone between oceanic and continental crust.

Just as the nature of the basement underlying the Comores Archipelago is a contentious issue, there are diverging opinions about the nature and evolution of Comorean

volcanism itself. The near-linear northwesterly trend of the island chain and the apparent westward decrease in age from the oldest, most severely eroded island of Mayotte to the younger, volcanically active Grande Comore, have been noted by several workers (e.g. Krenkel, 1925; Flower and Strong, 1969; Esson *et al.*, 1970; Strong, 1972b). More recently, the age progression has been confirmed by radiometric K-Ar dating (Hajash and Armstrong, 1972; Emerick and Duncan, 1982, 1983) which showed Comorean lavas to be late Tertiary to Quaternary in age, ranging from 5.28 ± 0.26 Ma for the oldest rocks analysed from Mayotte to 0.13 ± 0.02 Ma for the oldest Grande Comore samples analysed (see Fig. 2.1). Based on these ages, the apparent rate of migration of the magma source beneath the islands has been estimated at 45 to 70 $mm.a^{-1}$ (Hajash and Armstrong, 1972; Emerick and Duncan, 1982; Emerick, 1985).

Emerick (1980) and Emerick and Duncan (1982), in agreement with Morgan (1971, 1972) and others (e.g. Burke and Wilson, 1976; Crough, 1983; Vink *et al.*, 1985) concluded that the geometry and age progression of the Comores Archipelago are consistent with a hotspot origin and proposed that the trace of the Comores hotspot can be followed in a curvilinear trend along the length of the Comores Archipelago itself, through the northern tip of Madagascar and several atolls north of Madagascar (Faquhar and Amirante Islands) to the late Tertiary basaltic dikes dissecting the Seychelles Plateau.

This "classical" Grande Comore-Seychelles hotspot hypothesis was questioned by Nougier *et al.* (1986), who argued that, based on published and new K-Ar age data (including new ages of approximately 7.7 Ma old nephelinites from Mayotte and an 11.1 Ma old syenite from Anjouan), no obvious migration of volcanic activity can be demonstrated on the Archipelago. As an alternative hypothesis, these authors suggested that the Comores were produced by more or less synchronous volcanic activity along deep lithospheric fractures related to west-northwest trending fault zones in northern Madagascar and in the Mozambique Channel.

Yet another model for Comorean volcanism has been put forward by Upton (1982), who proposed that the Comores Ridge represents a very slow and consequently partly

emergent spreading ridge. Emerick and Duncan (1982), however, have cited the absence of any significant seismic activity or young magnetic anomalies, the alkaline composition of Comorean lavas and the regular age progression of volcanism on the islands as evidence against such a hypothesis.

The published evidence for a hotspot model is found to be compelling and data from the present study are entirely consistent with such a model.

Grande Comore

Grande Comore, the youngest, largest and most westerly island of the Comores Archipelago is situated about 280 km east of Africa (Fig. 2.1) and consists of two large shield volcanoes: La Grille in the north and Karthala in the south (Fig. 3.1). The island has a smooth and undissected coastline along which an incipient reef is relatively poorly developed. The dormant La Grille volcano has gentle slopes (~6-7°), is covered by numerous cinder cones and lacks any caldera or well-defined summit crater (Esson *et al.*, 1970; Upton, 1982). The significantly steeper (10-15°) Karthala volcano reaches a maximum elevation of 2560 metres above sealevel and above 2000 metres is capped by a steep dome which is itself truncated by a complex caldera (Strong and Jacquot, 1970). The structure and development of this caldera, which appears to be located at the intersection of two regional fissure systems trending north-south and NNW-SSE respectively (Esson *et al.*, 1970), has been described in detail by Strong and Jacquot (1970). Karthala has erupted frequently in the past 120 years and although historic eruptions were distributed along a broad (6-8 km wide) NNW-SSE trending rift zone which extends across the island for some 45 km, all eruptions since 1918 have been much more localised and confined to the summit area, within or very close to the caldera (Upton *et al.*, 1974). K-Ar age dating (Hajash and Armstrong, 1972; Emerick and Duncan, 1982,1983) has confirmed the very youthful nature of Grande Comore, with lava ages ranging from 0.01 ± 0.01 Ma to 0.13 ± 0.02 Ma.

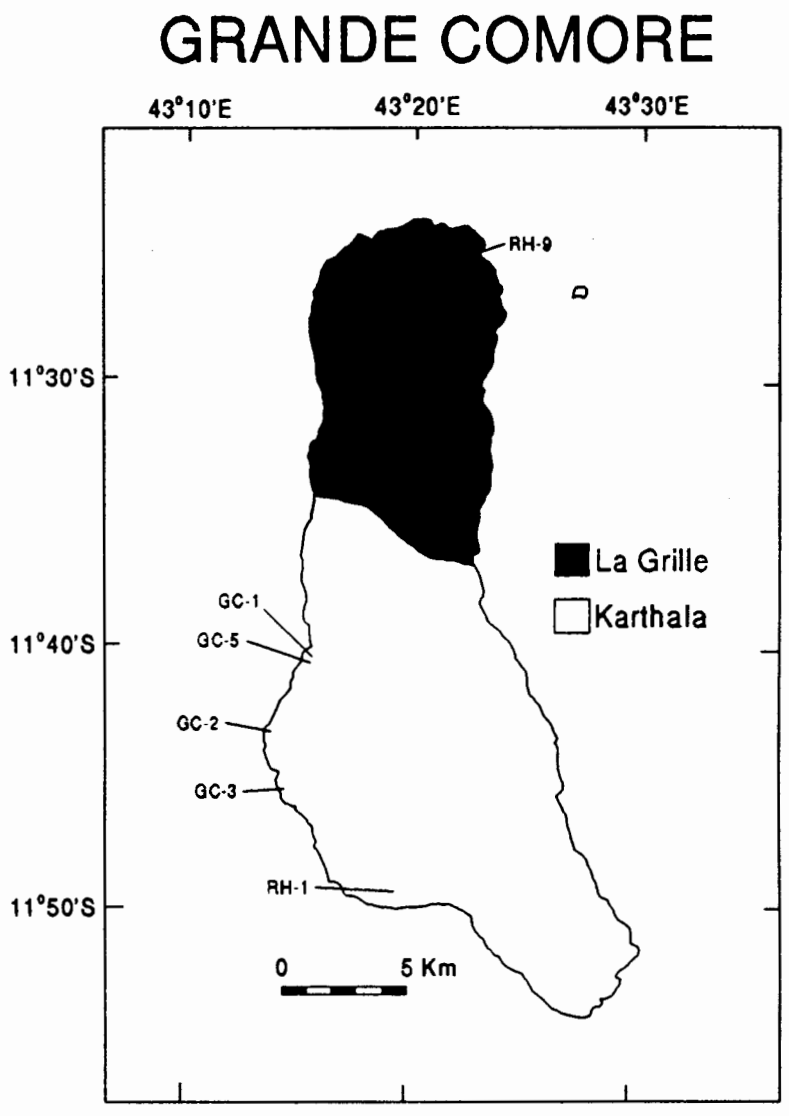

Fig. 3.1. Geological map of Grande Comore (after Strong, 1972b). Where known, sampling sites are indicated (after Emerick, 1985).

The only detailed petrological investigation of Grande Comore lavas was presented by Strong (1972b), who studied their petrography, mineralogy and geochemistry and noted that although Karthala and La Grille have been simultaneously active in the same geological setting, each volcano has its own distinct lava chemistry. He proposed that the parental magmas of La Grille and Karthala lavas were produced by less than 10% and more than 10% partial melting of a garnet-lherzolite mantle source at pressures of around 25 to 30 kb respectively. Strong (1972b) furthermore suggested that after

segregation from their source, these magmas experienced high-pressure fractionation of olivine, orthopyroxene, garnet and clinopyroxene, followed by polybaric olivine, clinopyroxene, orthopyroxene and spinel fractionation during ascent towards the surface and in the case of Karthala lavas, by significant amounts of predominantly olivine and clinopyroxene fractionation at shallow depths (probably < 10 km).

Moheli

Moheli, the smallest island of the Comores Archipelago, is situated 40 km southeast of Grande Comore and 45 km southwest of Anjouan (Fig. 2.1). The island is roughly elliptical in shape (about 30 km by 20 km), with its long axis approximately parallel to the Archipelago's principal axis (NNW) (Fig. 3.2).

The relatively low-lying eastern plateau (<400 m above sealevel) with its deep soil cover contrasts strongly with the more mountainous western parts of the island, which are dominated by a jagged median ridge that rises to a maximum elevation of 790 metres. Moheli has a rugged and embayed coastline and is entirely surrounded by a relatively mature fringing reef. The elongate shape of Moheli has been interpreted to be the result of repeated eruptions along north-northwest trending fissures, although the nearly circular submarine contours of the island and the radiating flows preserved as peninsulas and small, elongate islets on the southern coast suggest the former existence of a large central shield volcano (Esson *et al.*, 1970; Strong, 1972a).

Strong (1972a) suggested that evidence for three phases of volcanic activity exists on Moheli (Fig. 3.2a). The *Older Phase* predominates in the low-lying eastern parts of the island, including the southern islets, whereas the *Middle Phase* forms most of the rugged central and western regions. Localised areas of fresh lava flows along the northern and western coastal regions represent the *Younger Phase*. Numerous well-preserved cinder cones are found throughout Moheli, generally aligned with the island's long axis, and appear to be of similar age as the Younger Phase lavas. Radiometric K-Ar dating (Emerick and Duncan, 1982, 1983) has confirmed Strong's stratigraphy of the island and

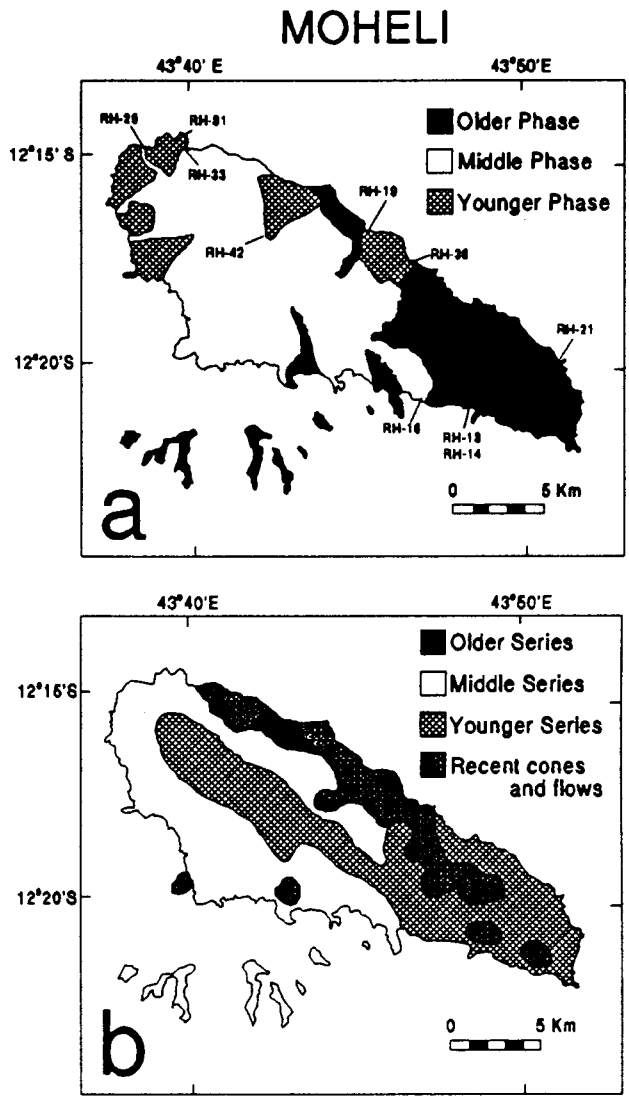

Fig. 3.2. a. Geological map of Moheli after Strong (1972a). Where known, sampling sites are indicated (after Emerick, 1985). **b.** Geological map of Moheli after Nougier *et al.* (1986).

suggests average ages of 1.71 ± 0.07 Ma, 1.14 ± 0.08 Ma and 0.68 ± 0.09 Ma for the Older, Middle and Younger Phases respectively. In addition, however, Emerick and Duncan (1982, 1983) provided evidence for an earlier *Shield-building Phase* at 2.75 ± 0.13 Ma, underlying the Younger Phase in western Moheli. An alternative geochronology for Moheli was proposed by Nougier *et al.* (1986) (Fig. 3.2b). According to these authors, a basal *Older Series* (dated at 5 Ma and older) is observed locally on the north coast, while outcrops of the *Middle Series* (from 4 to 2.5 Ma) cover large parts of the central and western regions of the island. In contrast to Strong's (1972a) stratigraphic model, Nougier

et al. (1986) suggested that most of the eastern areas, as well as the median ridge are comprised of *Younger Series* lavas (from 2.5 to 1.5 Ma) and that recent cones and valley-filling flows (from 0.8 to 0.5 Ma) occur along the northern coast and at several localities in the south of the island. A comparison of Figures 3.2a and 3.2b reveals considerable differences between the stratigraphic models of Strong (1972a) and Emerick and Duncan (1982, 1983) on the one hand and Nougier *et al.* (1986) on the other. It appears that the debate about the precise stratigraphic subdivision of Moheli lavas and the age and areal extent of the different chronostratigraphic units remains unresolved and awaits more detailed field and geochronological investigations.

The only detailed petrological study of this island was carried out by Strong (1972a), who investigated the petrography and geochemistry of Moheli lavas and classified them as alkali basalts, basanites, melanephelinites, nepheline hawaiites, trachytes and phonolites. He suggested that Moheli lavas define two separate petrochemical variation trends: a "high-pressure trend" from alkali basalt through basanite to nephelinite, interpreted to be the result of variable degrees of partial melting in the upper mantle (nephelinite representing very small degrees of melting and basanite and alkali basalt representing progressively larger degrees of melting); and a "low-pressure trend" from nephelinite to trachyte and phonolite, generated by shallow-level fractional crystallisation of initially olivine plus clinopyroxene, later joined by apatite, Fe-Ti oxides and eventually feldspar.

Anjouan

Anjouan, situated 40 km east-northeast of Moheli (Fig. 2.1), has a rugged topography that rises to a maximum elevation of 1595 metres in the central peak of N'Tingui, which represents the deeply dissected remains of a large shield volcano. The island's strongly embayed coastline is completely surrounded by a mature fringing reef. A barrier reef is in its early stages of development off the western coast of Anjouan.

K-Ar dating has shown Anjouan lavas to range from 3.9 Ma to about 0.36 Ma in age (Hajash and Armstrong, 1972; Emerick and Duncan, 1982, 1983; Nougier *et al.*, 1986)

and a syenite from the island has been dated at 11.1±0.5 Ma by Nougier *et al.* (1986). A three-stage evolutionary history has been suggested for Anjouan by Flower (1972, 1973a). The early *Shield-building Stage* involved the relatively uninterrupted outpouring of fairly homogeneous ankaramitic and basaltic lavas with very minor eruptions of hawaiites, benmoreites and trachytes. During the subsequent *Fissure-eruptive Stage*, the island's three peninsulas (M'Jimilimé to the north, Nioumakélé to the south and Sima to the west) were constructed by erupting lavas and pyroclastics. This phase of volcanism produced mainly alkali basalts, basanites and hawaiites. Following a period of erosion, the *Rejuvenescent Stage* involved the eruption of basanites, nepheline-hawaiites, nepheline-mugearites, nepheline-benmoreites and phonolites which filled erosional valleys and flooded coastal plains.

Flower (1972) proposed the existence of three geochemically distinct differentiation trends amongst the lavas of the island: the *hypersthene-normative trend* is almost exclusively restricted to the Shield-building Stage, whereas the lavas of the Fissure-eruptive and Rejuvenescent Stages erupted lavas which belong to the *alkalic* and *basanitic trends*. Clinopyroxene and olivine are the dominant phenocryst phases in the basic and intermediate lavas of Anjouan, whereas kaersutitic amphibole and plagioclase become important in the mugearites and benmoreites (Flower, 1972, 1973a). One-atmosphere melting experiments (Thompson and Flower, 1971; Thompson, 1972) have shown that clinopyroxene, together with olivine is a liquidus or near-liquidus phase in Anjouan lavas and that plagioclase crystallises at significantly lower temperatures than these minerals.

The geochemical variations observed *within* the hypersthene-normative, alkalic and basanitic differentiation trends have been attributed to low-pressure fractional crystallisation of the principal phenocryst minerals in the lavas, starting with olivine and clinopyroxene, followed at more evolved stages by plagioclase, apatite, Fe-Ti oxides and amphibole (Flower, 1971a, 1972, 1973a, 1973b). The variation from hypersthene-normative to alkali basaltic and basanitic lavas, on the other hand, has been proposed to be the result of high-pressure processes reflecting mantle source characteristics and the effects of variable degrees and depths of partial melting (Flower, 1973a, 1973b).

Mafic and ultramafic xenoliths commonly occur in the alkali basalts and basanites of the Fissure-eruptive and Rejuvenescent Stages, but are only rarely found in Shield-building lavas (Flower, 1971a, 1972, 1973a). Ludden (1977) divided xenoliths occurring in Anjouan lavas into three groups: a *syenite-gabbro suite* (nepheline- and sodalite-syenites and gabbros), a *dunite-wehrlite suite* and a *lherzolite suite* (spinel-lherzolites). Ludden (1977) interpreted the gabbroic xenoliths to represent high-level intrusions generated by cotectic fractionation of either alkali basaltic liquids of the Fissure-eruptive Stage, or evolved liquids associated with the hypersthene-normative Shield-building lavas. The sodalite- and nepheline-syenite xenoliths, on the other hand, appear to represent high-level intrusions with the normative characteristics of trachytes and phonolites respectively. The dunite-wehrlite xenoliths were proposed by Ludden (1977) to have been derived from layered cumulate sequences which precipitated from hypersthene-normative basaltic Shield-building liquids in floored magma chambers at pressures of less than 9 kb. Ludden (1977) suggested that 5 to 7% partial melting of a spinel-peridotite source at pressures below 20-25 kb was required to produce the hypersthene-normative Anjouan lavas. The REE-depleted (Flower, 1971a) spinel-lherzolite residuum produced by this melting process was subsequently sampled accidentally by the basanites and alkali basalts, which were themselves generated from a garnet-peridotite source by relatively smaller degrees of melting at greater mantle depths (pressures greater than 20-25 kb).

Mayotte

The island of Mayotte consists of a partially submerged, severely eroded volcanic pile with a relatively subdued topography. The deeply embayed and irregular coastline is bounded by highly developed fringing reefs and a continuous barrier reef that encloses a 3 to 12 km wide lagoon (Esson *et al.*, 1970; Guilcher, 1965) (Fig. 3.3).

Relatively little is known about the geology of Mayotte. Esson *et al.* (1970) suggested that the geological and topographical development of the island was controlled by fissuring and faulting along west-northwest and north-northeast trending lineations, whereas Nougier *et al.* (1986) proposed that the island's structure is explicable either as that of

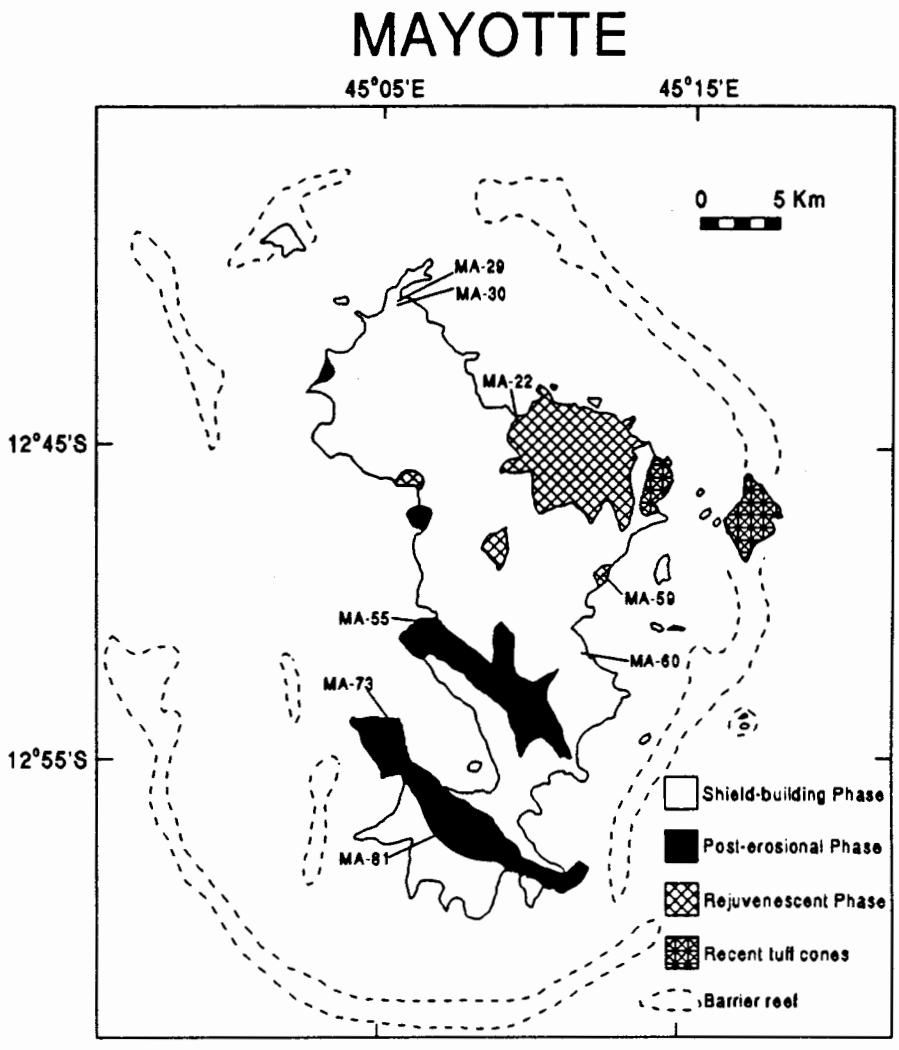

Fig. 3.3. Geological map of Mayotte (after Emerick and Duncan, 1982, 1983 and Nougier *et al.*, 1986). Where known, sampling sites are indicated (after Emerick, 1985).

a collapsed large shield volcano, or that of a coalescent chain of several smaller volcanoes. The K-Ar ages determined for Mayotte lavas range from 7.7±1 Ma to 1.49±0.1 Ma (Hajash and Armstrong, 1972; Emerick and Duncan, 1982, 1983; Nougier *et al.*, 1986). Nougier *et al.* (1986) estimated the age of initial volcanism at roughly 10-15 Ma. The production of a primitive shield by basaltic, basanitic and nephelinitic flows appears to have lasted until around 3.75 Ma (Emerick and Duncan, 1982, 1983; Nougier *et al.*, 1986). According to Emerick and Duncan (1982, 1983) and Nougier *et al.* (1986),

this initial *Shield-building Phase* was followed by a fissure-erupted *Post-erosional Phase* from 3.75±0.12 Ma to 2.5±0.09 Ma and a *Rejuvenescent Phase* between 2.5±0.09 Ma and 1.49±0.10 Ma. Emerick and Duncan's (1982, 1983) model for the geochronology and evolution of Mayotte appears to be reasonably consistent with that proposed by Nougier *et al.* (1986) (Fig. 3.3).

4. THE PETROLOGY OF LAVAS FROM GRANDE COMORE

Detailed accounts of the petrography, mineralogy and geochemistry of Grande Comore lavas were published by Strong (1972b), who presented olivine and clinopyroxene analyses as well as bulk-rock compositions (major, minor and trace elements) for several samples from Karthala and La Grille. Flower (1971a) published the rare earth element (REE) concentrations of two Grande Comore lavas. The observations made during the present investigation of Grande Comore lavas are entirely consistent with Strong's (1972b) description of the rocks from this island and expand the existing dataset.

4.1 Classification of the Rocks

Lavas from Grande Comore are conveniently classified according to whether they were erupted by La Grille volcano or by Karthala volcano. Although thin-sections of 12 lavas from Grande Comore were made (seven from Karthala; five from La Grille), only seven of these samples (four from Karthala; three from La Grille) could be analysed for their major, minor and trace element composition, due to a shortage of sample in some cases. According to the classification scheme of le Bas *et al.* (1986), based on the total alkali-silica diagram (Fig. 4.1), three of the analysed Karthala samples are alkali basalts (GC-1, GC-3, RH-1b) and one is a hawaiite (GC-5). All La Grille samples analysed (RH-7, RH-9, RH-11) are basanitic in composition.

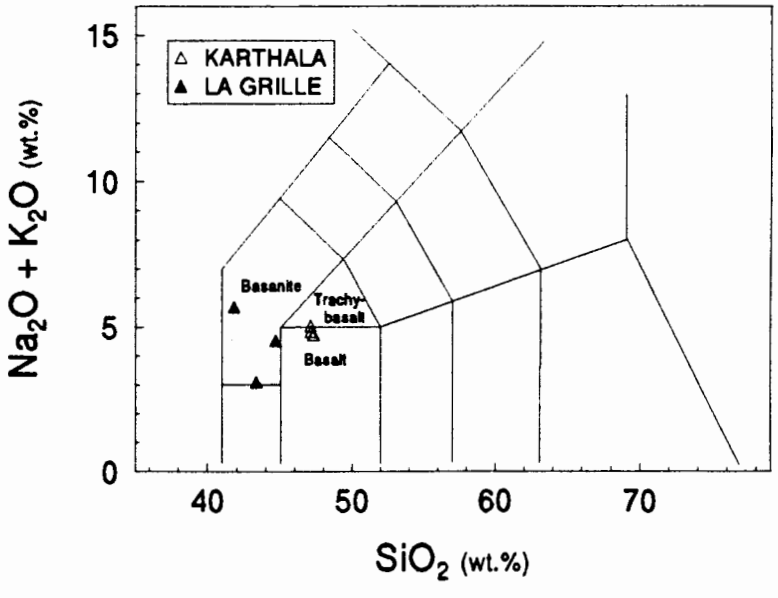

Fig. 4.1. Total alkali-silica diagram for Grande Comore lavas. Classification grid after le Bas *et al.* (1986).

4.2 Petrography and Mineralogy

In general, Grande Comore rocks are vesicular, sparsely to coarsely olivine and clinopyroxene phyric lavas with a very fine-grained, partly glassy groundmass that contains mainly clinopyroxene, Fe-Ti oxide, small amounts of olivine and variable quantities of plagioclase. Detailed petrographic descriptions of individual Grande Comore samples are contained in Appendix A4.1. The petrographic characteristics of lavas from the two volcanoes are summarised below. All plates (photomicrographs) referred to in the text are contained in Appendix A5.

Karthala Lavas

The lavas from Karthala volcano have textures that range from slightly to highly vesicular and from sparsely to coarsely olivine and clinopyroxene phyric. Olivine is generally the dominant phenocryst phase and of the alkali basalts, only one may be classified as an ankaramite (clinopyroxene predominates over olivine as phenocryst phase), whereas all the remaining samples are alkali olivine basalts (olivine predominates over clinopyroxene as phenocryst phase). The euhedral to anhedral macrophenocrysts (up to around 5 mm in diameter) and phenocrysts of olivine are relatively fresh (Plate 1), or only slightly altered around the edges and often contain fine-grained inclusions of Fe-Ti oxides. Clinopyroxene typically occurs as fresh, grey to pale tan phenocrysts and microphenocrysts (Plate 1) and as abundant tan to tan-violet, fine-grained groundmass phase. Clinopyroxene phenocrysts frequently have pale grey-tan cores, but darker tan to tan-violet rims (Plate 2). Oscillatory zonation and simple twinning occur amongst the clinopyroxene phenocrysts, and clinopyroxene microphenocrysts frequently occur as glomerophyric aggregates (Plate 3). Very rarely, clinopyroxene phenocrysts with greenish-grey, sieve-textured cores, containing Fe-Ti oxide inclusions, and clear tan-coloured rims are observed. Some Karthala lavas contain rare plagioclase microphenocrysts, but in general, this phase is present as abundant, fine-grained laths in the groundmass (Plate 2). Karthala lavas typically exhibit a dark-grey, fine-grained to cryptocrystalline, often partly glassy groundmass that contains predominantly plagioclase laths, tan-coloured clinopyroxene and finely disseminated Fe-Ti oxide, with smaller amounts of olivine and

on occasion, accessory biotite and apatite (Plates 1 to 3).

La Grille Lavas

The basanitic lavas erupted from La Grille volcano are vesicular and porphyritic rocks. In most of the La Grille samples investigated, olivine is by far the dominant phenocryst phase, with the exception of one sample (RH-11), in which clinopyroxene phenocrysts predominate over olivine phenocrysts. On the whole, the ratio of olivine to clinopyroxene phenocrysts is significantly greater in La Grille lavas than in Karthala lavas. In terms of modal compositions, too, olivine is commonly the dominant phase in La Grille lavas, whereas in Karthala lavas, it is usually subordinate to clinopyroxene. In contrast to Karthala lavas, where plagioclase phenocrysts are present on occasion, plagioclase is confined to the groundmass in the case of La Grille lavas and may even be entirely absent. The relatively fresh to slightly altered olivine phenocrysts of La Grille lavas range in size from macrophenocrysts (up to about 5 mm in diameter) to microphenocrysts (0.5 mm and less in diameter) and frequently display signs of partial resorption. The subhedral, zoned and sometimes twinned, phenocrysts and microphenocrysts of clinopyroxene range in size from around 1 mm to less than 0.5 mm and often have pale grey cores, but darker tan to violet titanaugite rims. The clinopyroxene microphenocrysts frequently occur as glomerophyric clusters. Some clinopyroxene phenocrysts have sieve-textured cores, but clear rims. The very fine-grained to cryptocrystalline and sometimes partly glassy groundmass of La Grille lavas typically contains tan-coloured clinopyroxene and Fe-Ti oxide, with smaller amounts of olivine. Plagioclase may be a significant groundmass phase, but may also be entirely absent from these rocks. Xenolithic fragments, apparently of harzburgitic (possibly lherzolitic) composition, were identified in two of the lavas (RH-2b, RH-7).

4.3 Mineral Chemistry

Clinopyroxene and olivine phenocrysts in the lavas of Grande Comore were analysed using a CAMECA Camebax electron microprobe at operating conditions described in

Appendix A1.1.

Clinopyroxene

Electron microprobe analyses of Grande Comore clinopyroxene phenocrysts are reported in Table 4.1 and the range in composition is depicted in Fig. 4.2. The clinopyroxenes of Grande Comore are diopsides and salites that have a relatively limited compositional range from $Wo_{47}En_{47}Fs_6$ to $Wo_{51}En_{36}Fs_{13}$. Fig. 4.2 shows the compositions of clinopyroxenes in Karthala lavas to overlap with those in La Grille lavas. The FeO content of these clinopyroxenes varies from 3.93 to 8.00 wt.%. The TiO_2 (0.27-3.13 wt.%), Na_2O (0.26-1.10 wt.%) and Al_2O_3 (0.27-9.60 wt.%) abundances are variable and range to fairly high values, possibly reflecting the effects of magmatic fractionation.

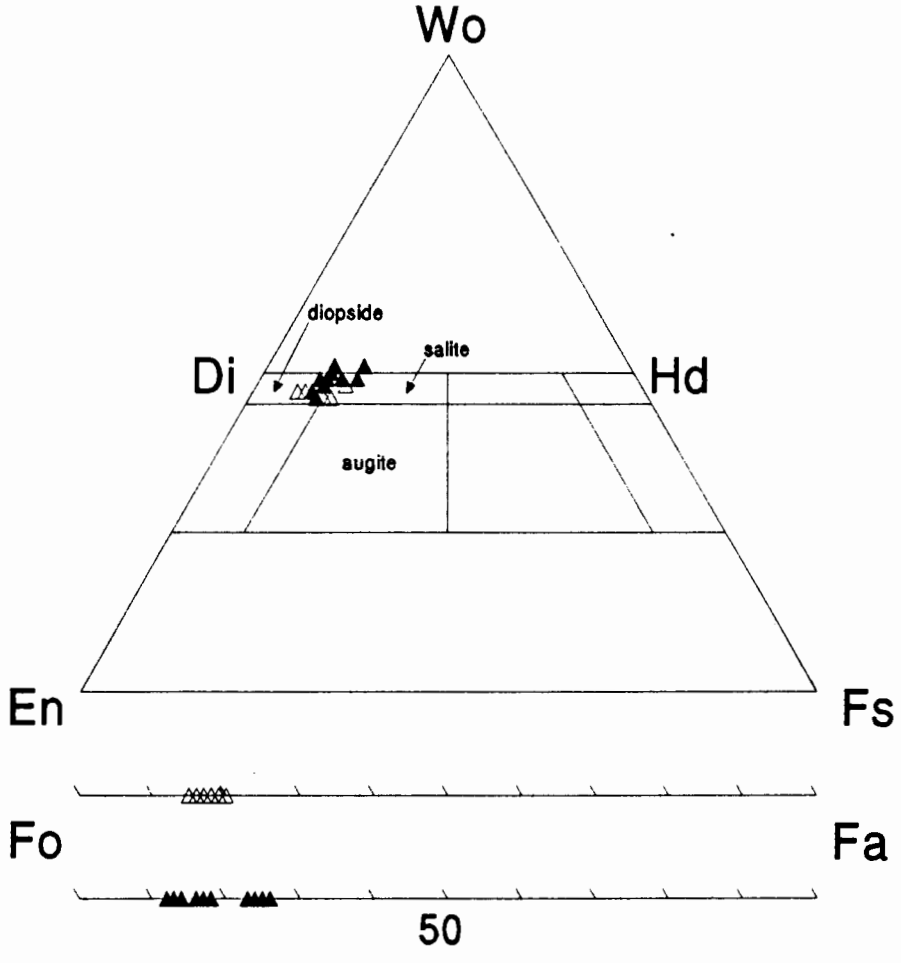

Fig. 4.2. Mineral chemistry of clinopyroxenes and olivines in Grande Comore lavas. Open symbols: Karthala; filled symbols: La Grille.

TABLE 4.1
Clinopyroxene analyses from Grande Comore lavas

	Karthala				*La Grille*								
Sample	*GC-1*	*GC-1*	*GC-1*	*GC-3*	*RH-7*	*RH-7*	*RH-7*	*RH-9*	*RH-9*	*RH-9*	*RH-11*	*RH-11*	*RH-11*
SiO_2	49.60	50.84	52.14	47.97	47.91	52.82	54.68	46.95	48.92	50.24	44.64	49.01	49.71
TiO_2	1.58	1.11	0.59	2.22	2.07	0.27	*n.d.*	2.39	1.66	1.09	3.13	1.20	1.22
Al_2O_3	4.90	3.43	2.29	5.19	6.20	3.14	0.27	6.05	5.18	4.60	9.60	6.60	5.64
Cr_2O_3	*n.d.*	*n.d.*	1.01	*n.d.*	0.43	0.11	0.48	*n.d.*	0.36	0.18	*n.d.*	1.10	0.80
FeO	6.40	6.43	3.93	7.40	6.57	5.23	4.71	8.00	5.58	5.31	7.38	4.63	4.73
MnO	0.15	0.13	*n.d.*	*n.d.*	*n.d.*	0.13	*n.d.*	*n.d.*	*n.d.*	*n.d.*	*n.d.*	*n.d.*	*n.d.*
MgO	14.97	15.22	16.40	13.62	13.53	15.18	15.78	12.59	14.09	14.89	11.60	14.11	14.64
CaO	22.10	22.24	22.72	22.52	23.17	21.98	23.08	23.13	23.95	23.11	23.29	22.61	22.71
Na_2O	0.29	0.28	0.26	0.41	0.37	0.90	1.10	0.40	0.32	0.44	0.35	0.55	0.46
Total	99.99	99.69	99.36	99.32	100.26	99.76	100.10	99.51	100.05	99.85	99.99	99.80	99.90
Wo	0.46	0.46	0.47	0.48	0.49	0.46	0.47	0.49	0.50	0.48	0.51	0.49	0.49
En	0.43	0.44	0.47	0.40	0.40	0.45	0.45	0.38	0.41	0.43	0.36	0.43	0.43
Fs	0.11	0.10	0.06	0.12	0.11	0.09	0.08	0.13	0.09	0.09	0.13	0.08	0.08

n.d. = not detected

TABLE 4.2
Olivine analyses from Grande Comore lavas

	Karthala					*La Grille*													
Sample	*GC-1*	*GC-1*	*GC-1*	*GC-1*	*GC-3*	*RH-7*	*RH-7*	*RH-7*	*RH-7*	*RH-9*	*RH-9*	*RH-9*	*RH-9*	*RH-9*	*RH-9*	*RH-11*	*RH-11*	*RH-11*	*RH-11*	*RH-11*
SiO_2	39.15	39.76	40.08	40.22	39.74	40.11	40.12	40.24	40.38	37.97	38.47	38.48	39.75	39.83	40.10	37.99	38.85	39.17	39.22	39.41
Al_2O_3	*n.d.*	*n.d.*	0.07	*n.d.*	*n.d.*	0.08	0.08	0.09	0.09	*n.d.*	*n.d.*	*n.d.*	0.09	0.06	*n.d.*	*n.d.*	*n.d.*	*n.d.*	0.09	*n.d.*
Cr_2O_3	*n.d.*	*n.d.*	*n.d.*	*n.d.*	*n.d.*	*n.d.*	0.09	*n.d.*	0.09	*n.d.*	*n.d.*	*n.d.*	*n.d.*	*n.d.*	*n.d.*	*n.d.*	*n.d.*	*n.d.*	*n.d.*	*n.d.*
FeO	17.84	14.70	14.80	13.81	15.14	11.05	11.31	10.76	10.70	23.49	20.45	22.35	12.53	12.43	11.71	21.51	20.26	16.66	16.17	14.78
MnO	0.23	0.23	0.26	0.25	0.28	0.14	0.13	0.16	0.17	0.33	0.24	0.32	0.23	0.20	0.20	0.28	0.21	0.21	0.22	0.19
MgO	42.07	44.27	44.17	44.82	43.60	47.58	47.39	47.58	47.59	38.19	40.30	38.83	46.37	46.94	47.26	39.51	40.09	43.59	44.24	44.65
CaO	0.44	0.42	0.38	0.38	0.43	0.24	0.21	0.23	0.18	0.15	0.12	0.19	0.31	0.26	0.23	0.19	0.10	0.21	0.23	0.25
NiO	0.26	0.21	0.24	0.22	0.23	0.33	0.35	0.38	0.30	n.d.	0.14	0.15	0.27	0.27	0.37	0.17	0.22	0.10	0.10	0.22
Total	99.99	99.59	99.98	99.70	99.42	99.53	99.67	99.44	99.52	100.12	99.72	100.32	99.55	100.00	99.86	99.66	99.72	99.94	100.27	99.50
Fo	0.80	0.84	0.84	0.85	0.83	0.88	0.88	0.88	0.88	0.74	0.78	0.75	0.86	0.87	0.87	0.76	0.78	0.82	0.83	0.84

n.d. = not detected

Olivine

Analyses of olivine phenocrysts in Grande Comore lavas are presented in Table 4.2 and the compositional range is shown in Fig. 4.2. The Fo-content of olivines in Karthala lavas ranges from 80 to 85, whereas La Grille olivines display somewhat greater compositional variability, ranging to both higher and lower Fo contents (from Fo_{74} to Fo_{88}). Roeder and Emslie (1970) quantified the temperature-independent partitioning of iron and magnesium between olivine and melt in terms of the distribution coefficient $K_D^{Fe\text{-}Mg}$ *. The value of $K_D^{Fe\text{-}Mg}$ for individual olivine crystals gives an indication of the state of equilibrium or disequilibrium of these olivines with respect to their host rocks. Fig. 4.3 shows a graphical representation of this relationship for olivines from Grande Comore lavas.

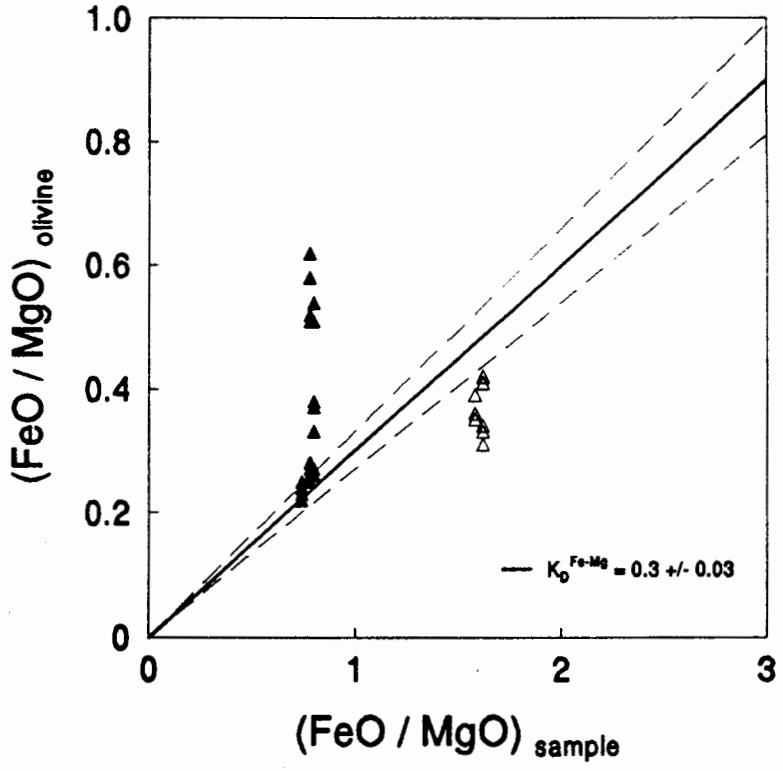

Fig. 4.3. Plot of $(FeO/MgO)_{olivine}$ vs $(FeO/MgO)_{sample}$ for olivine phenocrysts from Grande Comore. Open symbols: Karthala; filled symbols: La Grille. Solid line: $K_D^{Fe\text{-}Mg}=0.3$. Stippled lines: $K_D^{Fe\text{-}Mg}=0.33$ and $K_D^{Fe\text{-}Mg}=0.27$.

$$* K_D^{Fe\text{-}Mg} = \frac{\left(\frac{FeO}{MgO}\right)^{olivine}}{\left(\frac{FeO}{MgO}\right)^{melt}}$$

Some of the La Grille olivine phenocrysts fall into the range of $K_D^{Fe-Mg} = 0.3 \pm 0.03$, indicating equilibrium conditions. Several other La Grille olivines, however, have K_D^{Fe-Mg} values significantly greater than 0.3, suggesting disequilibrium conditions. These olivines are too rich in FeO, relative to MgO, to be in equilibrium with their host rocks. All of the Karthala olivine phenocrysts, on the other hand, have K_D^{Fe-Mg} values below the equilibrium value of 0.3. These olivines are too magnesian to be in equilibrium with their host rocks. K_D^{Fe-Mg} values are observed to vary significantly amongst the olivine phenocrysts of individual Grande Comore samples, ranging from near-equilibrium values to values significantly greater or smaller than 0.3. The disequilibrium observed between several olivine phenocrysts and their Grande Comore host lavas suggests that they may be xenocrystic in nature.

4.4 Bulk Rock Chemistry

As mentioned in Chapter 3, Strong (1972b) noted that Karthala and La Grille, the two volcanic centres on Grande Comore, have erupted lavas of distinctly different geochemical character - an observation which is confirmed by the bulk rock chemistry of the Grande Comore lavas analysed in the present study.

Major and Minor Elements

The major and minor element compositions of seven lavas from Grande Comore (three from La Grille and four from Karthala) were determined by XRF spectrometry as described in Appendix A1.2 and are presented in Table 4.3. The compositional range of the Grande Comore lavas is depicted in Figures 4.1, 4.4 and 4.5. Before plotting on diagrams, the major and minor element data were normalised to 100 per cent on a volatile free basis.

It was noted previously, that the lavas from La Grille are basanites, whereas the Karthala lavas are alkali basalts and one hawaiite (Fig. 4.1). All Grande Comore lavas analysed are nepheline-normative (Fig. 4.4) and one (RH-11) also contains normative leucite. La Grille lavas have markedly higher concentrations of normative nepheline (average: 13.6 wt.%) and olivine (average: 24.6 wt.%), but have lower contents of normative plagioclase

TABLE 4.3

Bulk-rock analysis and selected trace element ratios of Grande Comore lavas

	Karthala				*La Grille*		
Sample	*GC-1*	*GC-3*	*GC-5*	*RH-1b*	*RH-7*	*RH-9*	*RH-11*
	AB	*AB*	*Ha*	*AB*	*Bas*	*Bas*	*Bas*
SiO_2	46.47	46.60	46.80	46.91	42.81	42.38	41.48
TiO_2	2.67	2.69	2.65	2.49	1.92	2.34	2.17
Al_2O_3	14.38	14.96	14.63	14.29	12.96	12.45	12.08
Fe_2O_3	1.58	1.59	1.59	1.58	1.38	1.56	1.54
FeO	10.51	10.58	10.59	10.55	9.21	10.40	10.25
MnO	0.19	0.18	0.18	0.19	0.18	0.19	0.20
MgO	6.48	6.72	6.81	6.88	12.44	13.39	12.78
CaO	10.81	10.25	10.64	11.09	10.12	11.43	12.20
Na_2O	3.39	3.47	3.78	3.47	3.49	2.43	4.34
K_2O	1.34	1.38	1.28	1.25	0.84	0.60	1.29
P_2O_5	0.48	0.50	0.47	0.42	0.44	0.55	0.78
LOI	1.64	0.84	0.12	0.82	3.42	1.40	0.89
H_2O-	0.54	0.18	0.68	0.28	0.97	0.20	0.13
Total	100.47	99.95	100.22	100.21	100.16	99.33	100.12
Zr	223	226	224	208	223	202	226
Nb	52	56	52	47	87	71	92
Y	29	30	29	27	24	24	29
Rb	31	32	31	29	30	8.10	46
Ba	363	405	374	324	709	534	623
Sr	542	603	557	495	659	628	764
Th	6.2	5.2	5.6	4.9	9.2	8.6	9.9
Co	52	50	53	53	64	72	68
Cr	143	142	145	166	535	613	603
Ni	117	122	115	121	327	373	338
V	260	249	253	248	208	246	238
Zn	237	110	107	111	89	92	93
Cu	270	65	94	87	66	66	78
Sc	26	21	24	28	22	27	28
La	41	46	-	39	-	-	-
Ce	81	90	-	79	-	-	-
Nd	41	42	-	39	-	-	-
Zr/Nb	4.3	4.0	4.3	4.4	2.6	2.9	2.5
Zr/Y	7.7	7.5	7.7	7.7	9.3	8.4	7.8
Y/Nb	0.56	0.54	0.56	0.57	0.28	0.34	0.32
Ba/Nb	7.0	7.2	7.2	6.9	8.2	7.5	6.8
Mg#	0.52	0.53	0.53	0.54	0.71	0.70	0.69

Fe_2O_3 calculated assuming $Fe_2O_3/FeO = 0.15$; La,Ce and Nd determined by XRF; *Mg#* = atomic $Mg/(Mg+Fe^{2+})$ with $Fe_2O_3/FeO = 0.15$; *AB*=alkali basalt, *Ha*=hawaiite, *Bas*=basanite.

(average: 21.1 wt.%) than Karthala lavas (averages: nepheline: 6.5 wt.%; olivine: 13.8 wt.%; plagioclase: 38.3 wt.%).

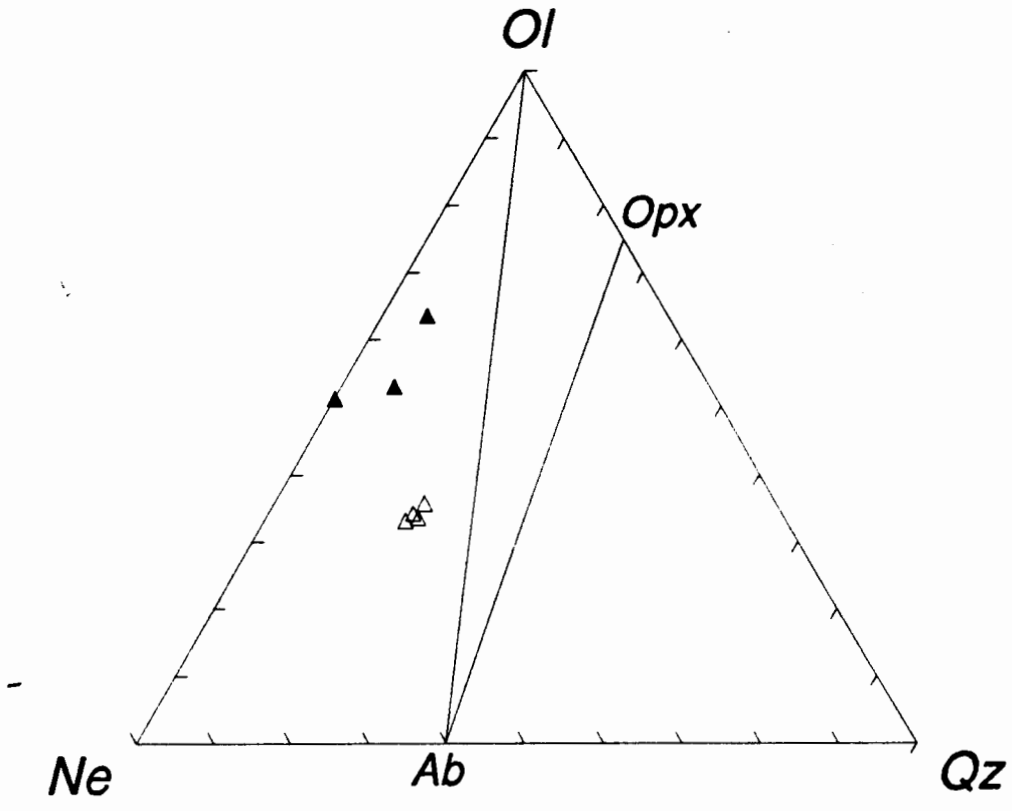

Fig. 4.4. Grande Comore lavas plotted on the basal projection of the normative Cpx-Ol-Ne-Qz tetrahedron, projected from cpx according to Irvine and Baragar (1971). Open symbols: Karthala; filled symbols: La Grille.

In Fig. 4.5, several major and minor elements from Grande Comore lavas are plotted against *Mg-number* (atomic $Mg/Mg+Fe^{2+}$, with $Fe_2O_3/FeO=0.15$), which is considered to be a measure of differentiation in these rocks. Grande Comore lavas exhibit relatively limited variation in terms of their major and minor element compositions. La Grille lavas have slightly lower concentrations of SiO_2, TiO_2, Al_2O_3, FeO and K_2O than Karthala lavas. The most notable difference between the lavas from the two volcanoes, however, lies in their MgO contents and *Mg-numbers*: La Grille lavas have significantly higher MgO concentrations and *Mg-numbers* (0.69-0.71) than Karthala lavas (*Mg-numbers*: 0.52-0.54). The major and minor element abundances of Karthala lavas fall within the overall compositional ranges of lavas from Moheli and Mayotte, but La Grille lavas have the

highest Mg-numbers of all Comores lavas analysed in this study.

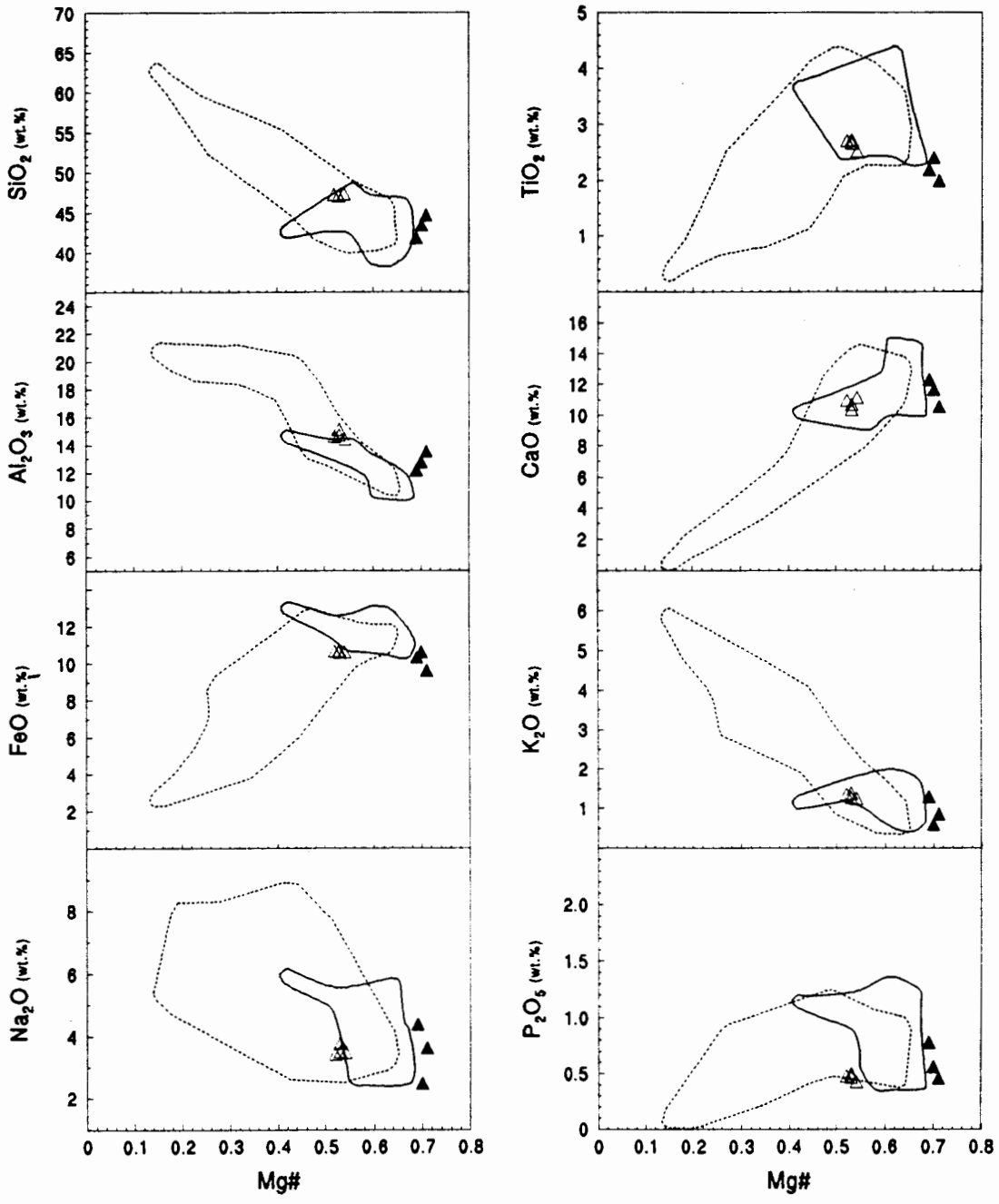

Fig. 4.5. Plots of major and minor elements (wt.%) vs *Mg-number* (atomic $Mg/Mg+Fe^{2+}$ with Fe_2O_3/FeO = 0.15) for Grande Comore lavas. Open symbols: Karthala; filled symbols: La Grille. For comparison, the fields for Moheli and Mayotte data, delineated by solid and stippled lines respectively, are shown.

Trace Elements

The trace element compositions of Grande Comore lavas were determined by XRF spectrometry as described in Appendix A1.2 and are presented in Table 4.3. In addition, the REE compositions of five Grande Comore lavas were determined by high-performance ion chromatography (HPIC), as described in Appendix A1.3. These REE concentrations are reported in Table 4.4.

TABLE 4.4
REE contents (ppm) of some Grande Comore lavas

	Karthala		*La Grille*		
Sample	*GC-2*	*GC-5*	*RH-7*	*RH-9*	*RH-11*
La	19.3	42.0	55.9	47.6	73.8
Ce	38.3	74.7	96.8	89.3	131
Pr	4.71	9.44	10.4	10.5	13.9
Nd	18.7	35.7	38.5	39.4	53.0
Sm	4.23	8.64	6.82	8.44	9.60
Eu	1.27	2.61	2.08	2.59	2.71
Gd	3.98	7.91	5.76	6.97	7.52
Tb	0.58	1.13	0.81	1.01	1.15
Dy	3.29	6.07	4.46	5.18	5.30
Er	1.52	3.19	2.14	2.55	2.56
Yb	1.31	2.75	1.55	2.14	2.05
$(La/Sm)_n$	2.9	3.1	5.3	3.6	5.0
$(La/Yb)_n$	10.6	11.0	25.9	16.0	25.8
La/Nb	-	0.81	0.64	0.67	0.80

$(La/Sm)_n$ and $(La/Yb)_n$ are chondrite-normalised ratios (normalising values from Sun and McDonough, 1989).

The compatible ferromagnesian trace elements Ni and Cr, as well as the compatible element Sc, are plotted against *Mg-number* in Fig. 4.6. La Grille lavas are significantly richer in Ni and Cr and also in Co than Karthala lavas. There is no difference in the Sc

content of the lavas from the two volcanoes, however. Karthala lavas contain more V, Zn and Cu than La Grille lavas.

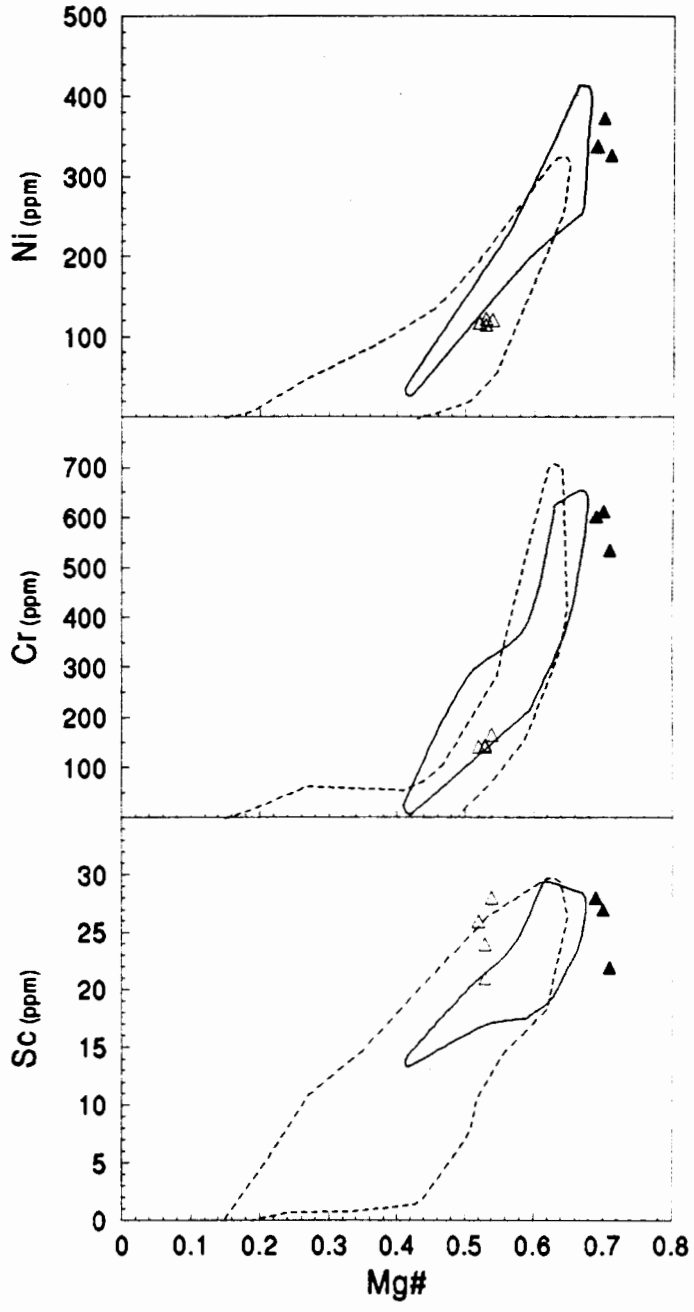

Fig. 4.6. Plots of Ni, Cr and Sc (ppm) vs *Mg-number* for Grande Comore lavas. Open symbols: Karthala; filled symbols: La Grille. For comparison, the fields for Moheli and Mayotte data, delineated by solid and stippled lines respectively, are shown.

Several incompatible trace elements from Grande Comore lavas are plotted against Zr in Fig. 4.7. The Zr, Y and Rb contents of La Grille and Karthala lavas overlap, but La Grille lavas are enriched in Nb, Th, Sr and Ba relative to Karthala lavas. The incompatible trace element ratios Ba/Nb and La/Nb ratios of Grande Comore lavas have limited ranges from 6.8 to 8.2 and from 0.67 to 0.85 respectively. Karthala lavas have higher Zr/Nb (4.0-4.4) and Y/Nb (0.54-0.57) ratios than La Grille lavas (Zr/Nb: 2.5-2.9; Y/Nb: 0.28-0.34).

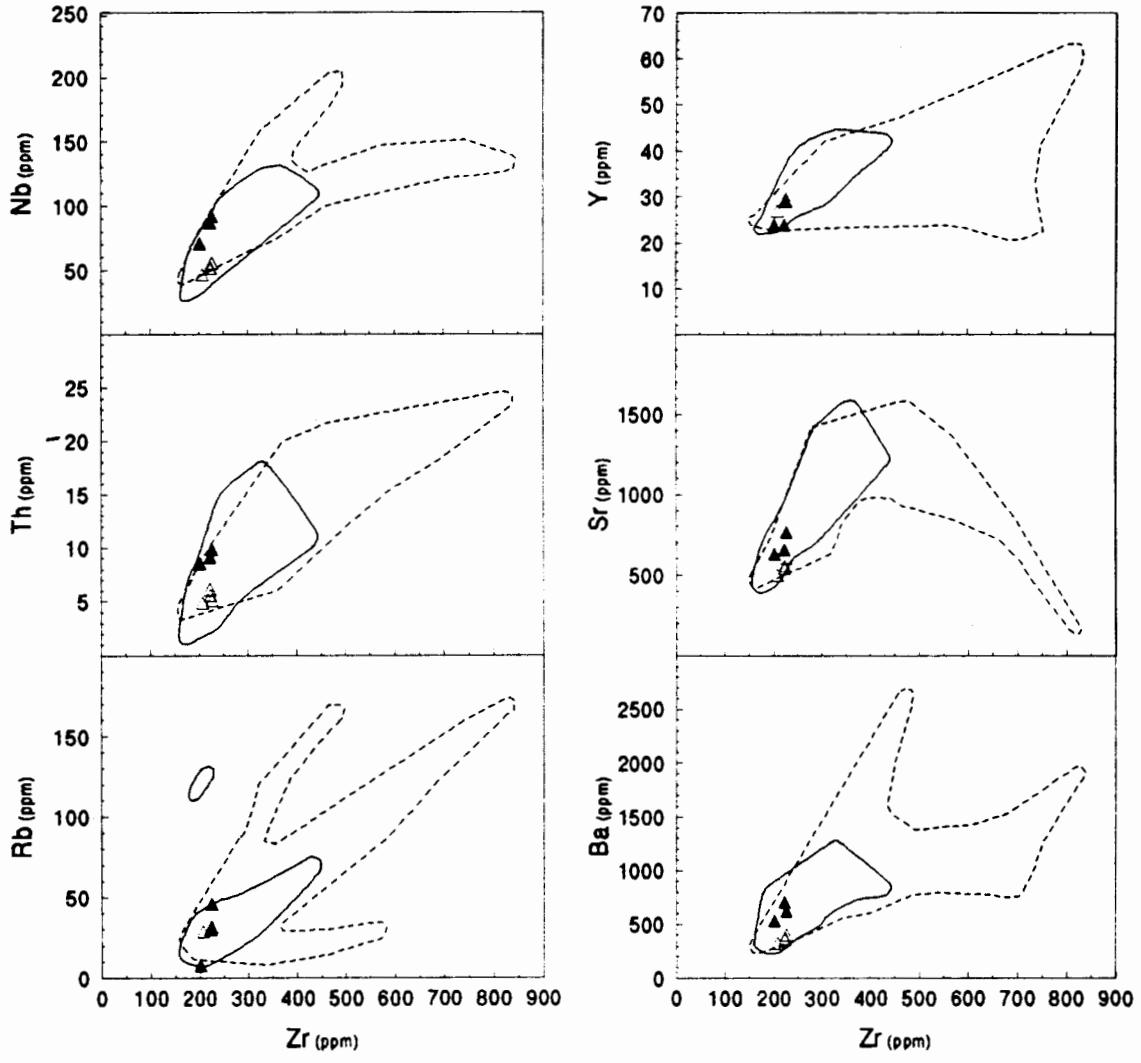

Fig. 4.7. Plots of incompatible trace elements vs Zr (all in ppm) for Grande Comore lavas. Open symbols: Karthala; filled symbols: La Grille. For comparison, the fields for Moheli and Mayotte data, delineated by solid and stippled lines respectively, are shown.

In Fig. 4.8, a number of incompatible elements, normalised to a hypothetical primitive mantle composition, are plotted in order of decreasing incompatibility (spidergrams).

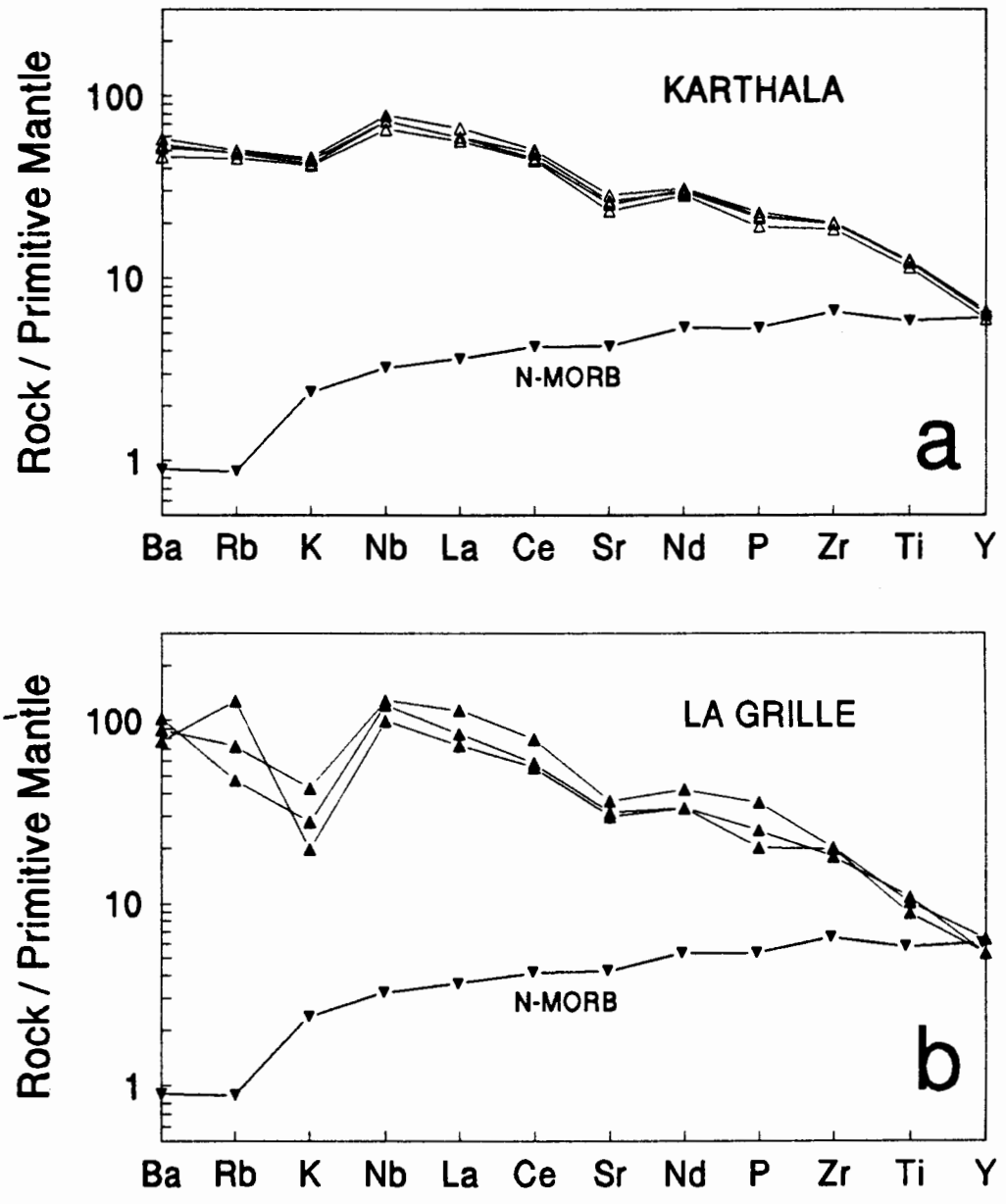

Fig. 4.8. Plots of primitive mantle-normalised incompatible trace elements, arranged (from left to right) in order of decreasing incompatibility for Grande Comore lavas. (**a**) Karthala lavas; (**b**) La Grille lavas. A pattern of N-type MORB (Sun and McDonough, 1989) is shown for comparison. Normalising values after Sun and McDonough (1989).

Although both La Grille and Karthala lavas are highly enriched relative to primitive mantle and N-type mid-ocean ridge basalt (N-MORB) in all of the elements considered,

Karthala and La Grille lavas are shown to have fundamentally different incompatible element patterns. Karthala lavas display very limited variability in normalised incompatible element patterns, whereas La Grille lavas display notably greater variability and, compared to Karthala lavas, are more enriched in Ba, Nb, La and Ce. The most noticeable difference between La Grille and Karthala spidergrams, however, is the behaviour of K and to a lesser extent Rb. K shows considerable variability and is significantly depleted relative to Ba and Nb in all of the La Grille lavas analysed. Rb also shows great variability in La Grille lavas, but in two of the three samples is depleted relative to Ba. It will be shown in subsequent chapters, that this distinction between the primitive mantle-normalised incompatible element patterns of La Grille and Karthala lavas can be extended to lavas on the two other Comorean islands investigated in this study. On both Moheli and Mayotte, lavas with distinctive relative depletions in K (and in some cases Rb) and lavas without such relative depletions were encountered. These two distinct groups of Comorean lavas will be referred to as "La Grille-type" (LGT) and "Karthala-type" (KT) lavas respectively.

The chondrite-normalised REE patterns of two Karthala and three La Grille lavas are shown in Fig. 4.9. The La Grille lavas have significantly steeper REE patterns and greater normalised La/Yb ratios (15.9-25.9) than the Karthala lavas (La/Yb: 10.6-10.9). All of the La Grille REE patterns cut across one of the Karthala patterns.

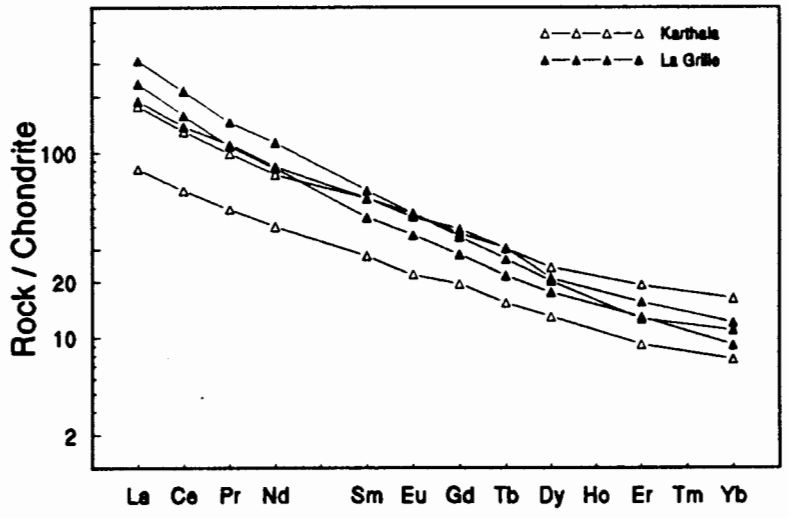

Fig. 4.9. Chondrite-normalised REE patterns of selected Grande Comore lavas. Normalising values after Sun and McDonough (1989).

Isotopes

A total of five samples from Grande Comore, four from Karthala and one from La Grille, were analysed for their Sr and Nd isotopic compositions according to the analytical method outlined in Appendix A1.4 and all of these isotopic data are listed in Table 4.5.

TABLE 4.5
Sr and Nd isotope data for selected Grande Comore lavas

	Sample	$^{87}Sr/^{86}Sr$	$^{143}Nd/^{144}Nd$
Karthala	*GC-1*	0.70390±1	0.51265±1
Karthala	*GC-3*	0.70378±1	0.51268±1
Karthala	*GC-5*	0.70393±1	0.51266±1
Karthala	*RH-1b*	0.70391±1	0.51263±1
La Grille	*RH-9*	0.70325±1	0.51284±1

errors are $2\sigma_{mean}$ on in-run statistics and correspond to least significant digits.

Lavas erupted from Karthala volcano display very limited isotopic variability and have isotopic signatures which are distinctly different from those of all other Comores lavas analysed, with $^{87}Sr/^{86}Sr$ values ranging from 0.70378±1 to 0.70393±1 and $^{143}Nd/^{144}Nd$ values between 0.51263±1 and 0.51268±1. The $^{87}Sr/^{86}Sr$ (0.703888) and $^{143}Nd/^{144}Nd$ (0.512635) values reported for a single Comores sample by Hart et al. (1986) are identical to those determined for Karthala lavas in the present study. Emerick (1985) reported the Sr isotopic compositions of several Karthala lavas and although two of these analyses (GC-2: $^{87}Sr/^{86}Sr=0.703861$; GC-5: $^{87}Sr/^{86}Sr=0.703972$) are similar to those determined in the present study, she reported significantly lower $^{87}Sr/^{86}Sr$ values for samples GC-1 (0.703255) and RH-1b (0.703294) than were measured for the same samples in the present study. In the light of the excellent internal consistency of the present data, it is suggested that Emerick's (1985) Sr isotope data for GC-1 and RH-1b are in error. The single La Grille lava analysed, with its significantly lower $^{87}Sr/^{86}Sr$ (0.70325±1) and higher $^{143}Nd/^{144}Nd$ (0.51284±1) has a very different isotopic signature

than all of the Karthala lavas, but falls into the isotopic compositional range defined by all Moheli and Mayotte lavas analysed (see Chapters 5 and 6). Emerick (1985) reported a significantly higher $^{87}Sr/^{86}Sr$ value for the same La Grille sample (0.703941), but once again, considering the excellent and internally consistent data presented in the present study, the validity of this particular analysis is highly questionable. Dupré and Allègre (1983) reported $^{87}Sr/^{86}Sr$ values of two Comores samples which are somewhat intermediate between the present data for Karthala and La Grille lavas (0.70367, 0.70369). It is, however, unclear from which of the islands these samples originate.

5. THE PETROLOGY OF LAVAS FROM MOHELI

Strong (1972a) described the petrography of lavas from Moheli and published the major, minor and trace element compositions of rocks from this island, whereas Emerick (1985) presented $^{87}Sr/^{86}Sr$ ratios for several Moheli lavas. New bulk-rock and mineral chemistry data for Moheli lavas, as well as REE concentrations and Sr and Nd isotope compositions of selected samples from this island are presented here.

5.1 Classification of the Rocks

According to the classification scheme of le Bas *et al.* (1986), the samples from Moheli may be classified into three groups (Fig. 5.1): five of the analysed samples are alkali basalts (RH-15, RH-16, RH-17, RH-28, RH-42), ten are basanites (RH-12a, RH-13, RH-21, RH-26, RH-27, RH-29, RH-30, RH-33, RH-36, RH-39) and five are nephelinites (RH-14, RH-18, RH-19, RH-31, RH-41).

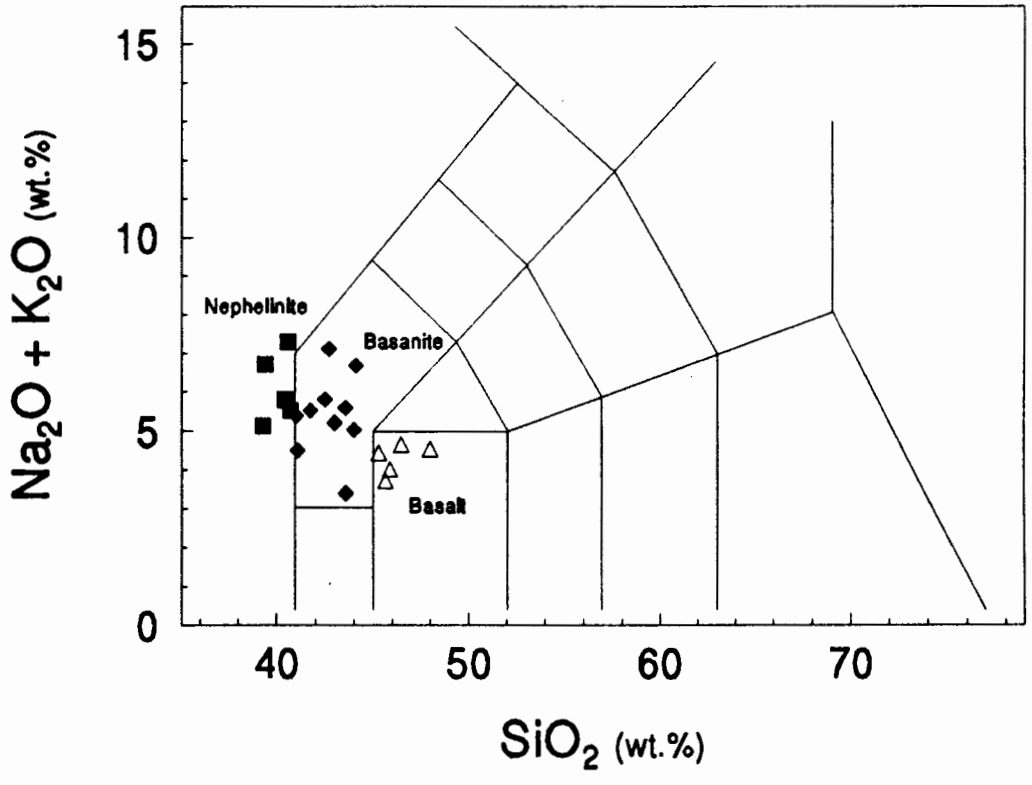

Fig. 5.1. Total alkali-silica diagram for Moheli lavas. Symbols: open triangles: alkali basalts; filled diamonds: basanites; filled squares: nephelinites. Classification grid after le Bas *et al.* (1986).

The alkali basalts may further be subdivided into alkali olivine basalts (olivine phenocrysts predominate over clinopyroxene phenocrysts) and ankaramites (clinopyroxene phenocrysts predominate over olivine phenocrysts). Nephelinites in which olivine is the predominant phenocryst phase are termed olivine nephelinites. Although K-Ar ages are available for several of the Moheli lavas (Emerick and Duncan, 1983), the samples were not classified according to geochronological considerations (i.e. into Older, Middle or Younger Phase/Series lavas), because of the unresolved nature of the stratigraphy and geochronology of the island (see Chapter 3).

It should be noted at this point, that the sample collection considered in this study does not represent the entire compositional range of lavas encountered on Moheli. Although the majority of the rocks analysed by Strong (1972a) are alkali basalts, basanites and nephelinites, he also reported a number of more differentiated lavas of trachytic and phonolitic composition which he considered to be the products of low-pressure fractional crystallisation of the more primitive rocks. Strong (1972a) furthermore identified several types of intrusive rocks on Moheli, namely alkali gabbro, theralite and ijolite (being the approximate intrusive equivalents of alkali basalt, basanite and nephelinite respectively). The present investigation is confined to a study of the alkali basalts, basanites and nephelinites only.

5.2 Petrography and Mineralogy

Since Strong (1972a) has described the petrography of Moheli lavas in some detail, only those aspects important to this study are presented here. In general, Moheli rocks are slightly vesicular, moderately to sparsely olivine and clinopyroxene phyric lavas with a fine-grained to cryptocrystalline groundmass. The ratio of olivine to clinopyroxene phenocrysts is typically greater in the nephelinites than it is in the alkali basalts and basanites. Plagioclase is an abundant groundmass phase in the alkali basalts, but is not present in the basanites and nephelinites. Instead of plagioclase, nepheline is a groundmass phase in the basanites and nephelinites and the nepheline content generally increases from the basanites to the nephelinites. Detailed petrographic descriptions of

all Moheli samples for which thin-sections were available are contained in Appendix A4.2. No thin-sections could be made for samples RH-13 and RH-19. The overall petrographic characteristics of each of the three groups of rocks from Moheli are summarised below.

Alkali Basalts

Moheli alkali basalts vary in texture from slightly to highly vesicular and from coarsely through moderately porphyritic to sparsely microporphyritic, containing phenocrysts and microphenocrysts of olivine and clinopyroxene. Three of the samples are alkali olivine basalts (RH-15, RH-16, RH-28) and one is an ankaramite (RH-17). Two of the lavas (RH-15, RH-17) are notable for their coarsely porphyritic textures, containing macrophenocrysts of olivine and clinopyroxene that measure up to 5 mm in diameter, suggesting a possible cumulate origin (Plates 4 and 5). The olivine phenocrysts display variable degrees of iddingsitisation and in some cases show signs of resorption. Phenocrysts of clinopyroxene commonly exhibit oscillatory zonation patterns (Plates 4 and 5) and some have sieve-textured cores (Plate 6). Clinopyroxene microphenocrysts often occur in small glomerophyric aggregates of radiating crystals. The fine-grained groundmass of the alkali basalts consists predominantly of flow-aligned laths of plagioclase with intergranular clinopyroxene and Fe-Ti oxide and much smaller amounts of olivine. One sample of alkali basalt composition (RH-42) differs texturally from the others, although having the same mineralogical characteristics. RH-42 is a medium-grained rock with a seriate texture of interlocking crystals of plagioclase, clinopyroxene, olivine and lesser Fe-Ti oxide (Plate 6). This rock may be of shallow intrusive origin or alternatively may represent the slow-cooling centre of a thick lava flow.

Basanites

Moheli basanites are generally slightly vesicular and range in texture from moderately porphyritic to microporphyritic, containing phenocrysts (up to about 2 mm in diameter) and microphenocrysts (usually around 0.5 mm or less in diameter) of olivine and clinopyroxene. Although some basanites contain predominantly olivine phenocrysts, on

average, the proportions of olivine and clinopyroxene phenocrysts are probably close to equal, and no constant increase in the ratio of olivine to clinopyroxene phenocrysts from the alkali basalts to the basanites (as suggested by Strong, 1972a) is recognised in the present collection of samples. The anhedral to subhedral olivine phenocrysts and microphenocrysts usually have clear and almost inclusion-free cores, but often display brown iddingsitised rims (Plate 7) and are even totally iddingsitised in some cases. Olivine phenocrysts frequently show signs of embayment and resorption (Plate 7). Clinopyroxene occurs mainly as microphenocrysts with grey cores and tan- to violet-coloured titanaugite rims. Many of the phenocryst-sized clinopyroxene crystals have irregular, sieve-textured, grey to pale-green cores that are surrounded by clear, zoned rims of grey to tan-violet titanaugite (Plates 8 and 9). Oscillatory and hourglass zonation are common amongst clinopyroxene phenocrysts. The fine-grained and sometimes cryptocrystalline and partly glassy groundmass of the basanites consists predominantly of clinopyroxene, Fe-Ti oxide, small amounts of nepheline and even less olivine. Some accessory apatite microlites may occur. In contrast to the basanites of La Grille (see Chapter 4), no plagioclase is present in Moheli basanites.

Nephelinites

The nephelinites from Moheli are slightly vesicular and moderately olivine and clinopyroxene phyric lavas. Three of the samples are olivine nephelinites (RH-14, RH-18, RH-31), olivine being by far the predominant (and in the case of RH-18 the only) phenocryst phase (Plate 10). The anhedral to subhedral phenocrysts (up to 2.5 mm in diameter) and microphenocrysts of olivine have clear, inclusion-free cores, but often exhibit iddingsitised rims and show signs of resorption. Clinopyroxene occurs mainly as microphenocrysts, often with lighter-coloured grey or greenish, sieve-textured cores and tan- to violet-coloured titanaugite rims. Oscillatory and hourglass zonation are common amongst clinopyroxene phenocrysts. The very fine-grained to cryptocrystalline groundmass consists predominantly of clinopyroxene, nepheline and Fe-Ti oxide and in some cases contains very small amounts of olivine and accessory biotite.

Clinopyroxene Phenocrysts in Moheli Lavas

As described above, clinopyroxene phenocrysts and microphenocrysts in Moheli lavas typically consist of light grey to pale grey-tan cores that are surrounded by darker tan to tan-violet rims. The transition from core to rim is commonly gradational, rather than sharp and the colour of the rim zone generally appears to be the same as that of clinopyroxene crystals in the groundmass. In many of the rocks, however, clinopyroxene phenocrysts with slightly more complex structures are observed. These phenocrysts have irregular to rounded, sieve-textured cores, some containing Fe-Ti oxide inclusions, that are surrounded by pale grey to pale tan and sometimes almost colourless mantles grading into darker tan to tan-violet rims (Plates 6,8 and 9).

The sieve-textured cores range in colour from pale grey to pale green and on occasion to darker green and pleochroic green. Amongst Moheli lavas, distinctly darker green clinopyroxene cores occur in the basanites and less commonly the nephelinites, but were not observed in the alkali basalts. The dark green cores of these phenocrysts are often irregular and rounded and exhibit optically sharp contacts with the surrounding mantles. Clinopyroxene phenocrysts with sieve-textured cores occur in the lavas of all three islands considered in this study, but the distinctly darker green-core clinopyroxenes appear to be more common amongst the basanites and nephelinites of Moheli and some of the mafic to intermediate Mayotte lavas (see Chapter 6).

Sieve-textured and green core clinopyroxene phenocrysts, similar to the ones found in Comores lavas, have been described in many mafic and intermediate alkaline lavas from intraoceanic and intracontinental settings (e.g. Scott, 1976; Brooks and Printzlau, 1978; Wass, 1979; Barton and van Bergen, 1981; Barton *et al.*, 1982; Duda and Schmincke, 1985; Haase and Devey, 1994).

5.3 Mineral Chemistry

Clinopyroxene and olivine phenocrysts in the lavas of Moheli were analysed using the electron microprobe.

Clinopyroxene

Clinopyroxene analyses from Moheli lavas are presented in Table 5.1 and the compositional range is depicted in Fig. 5.2. The clinopyroxenes in Moheli lavas are diopsides, salites and augites. Clinopyroxenes in the alkali basalts range in composition from $Wo_{48}En_{43}Fs_9$ to $Wo_{45}En_{35}Fs_{20}$. Amongst these rocks, the coarsely porphyritic RH-15, contains clinopyroxene phenocrysts with significantly lower FeO/MgO ratios than the sparsely porphyritic RH-16. Clinopyroxenes in the basanites range from $Wo_{42}En_{48}Fs_{10}$ to $Wo_{49}En_{36}Fs_{14}$, whereas those in the nephelinites range from $Wo_{50}En_{40}Fs_{10}$ to $Wo_{51}En_{36}Fs_{13}$.

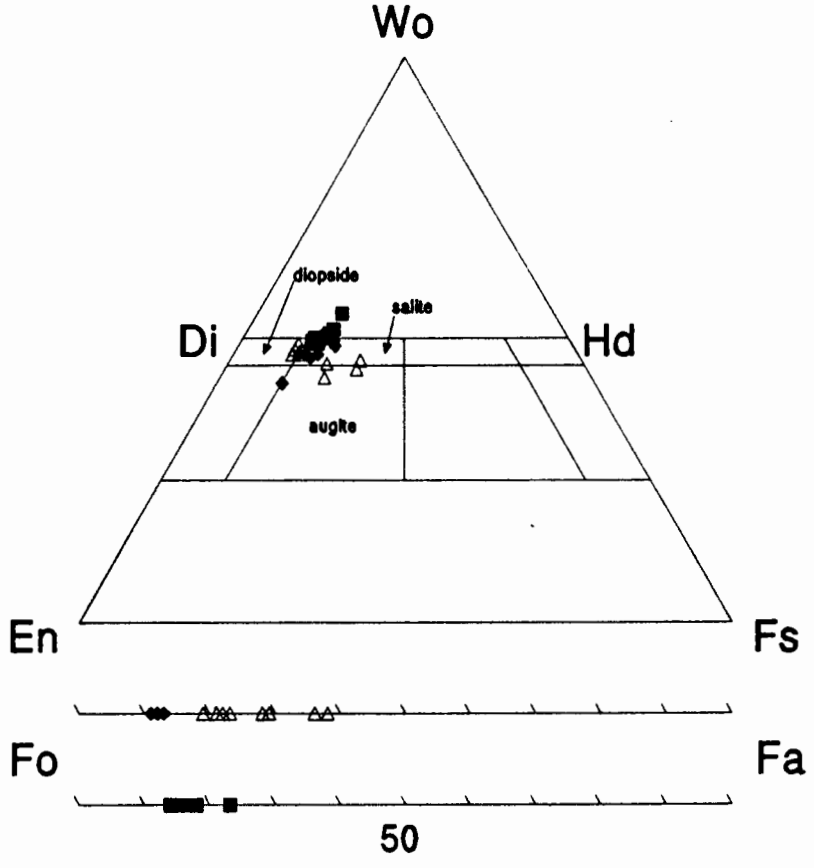

Fig. 5.2. Mineral chemistry of clinopyroxenes and olivines from Moheli lavas. Symbols: open triangles: alkali basalts; filled diamonds: basanites; filled squares: nephelinites.

TABLE 5.1
Clinopyroxene analyses from Moheli lavas

	Alkali Basalts										*Nephelinite*
Sample	*RH-15*	*RH-15*	*RH-15*	*RH-15*	*RH-15*	*RH-15*	*RH-16*	*RH-16*	*RH-16*	*RH-16*	*RH-18*
SiO_2	49.72	49.77	49.77	50.03	50.13	50.31	46.14	48.09	49.82	49.88	47.98
TiO_2	1.70	1.61	1.77	1.43	1.52	1.20	2.42	1.58	0.79	0.82	2.42
Al_2O_3	4.15	4.46	4.48	4.04	4.05	3.57	7.01	6.12	4.21	3.89	5.02
Cr_2O_3	0.24	0.42	0.28	0.46	0.44	0.61	0.42	0.15	*n.d.*	0.09	*n.d.*
FeO	6.57	5.71	6.36	6.14	5.72	5.70	8.88	9.28	11.31	11.69	7.14
MnO	0.13	*n.d.*	*n.d.*	*n.d.*	*n.d.*	*n.d.*	0.14	0.11	0.27	0.31	*n.d.*
MgO	14.35	14.46	14.15	14.48	14.70	15.13	13.12	13.86	11.11	11.73	13.29
CaO	22.54	22.72	22.56	22.37	23.13	22.55	21.09	20.14	20.55	20.52	24.07
Na_2O	0.45	0.42	0.42	0.46	0.41	0.41	0.58	0.69	1.58	1.27	0.57
Total	99.87	99.57	99.80	99.42	100.11	99.48	99.79	100.09	99.64	100.19	100.48
Wo	0.47	0.48	0.48	0.47	0.48	0.47	0.45	0.43	0.46	0.45	0.50
En	0.42	0.43	0.42	0.43	0.43	0.44	0.40	0.41	0.34	0.35	0.38
Fs	0.11	0.09	0.10	0.10	0.09	0.09	0.15	0.16	0.20	0.20	0.12

TABLE 5.1 continued

	Nephelinites						*Basanites*			
Sample	*RH-18*	*RH-31*	*RH-31*	*RH-31*	*RH-31*	*RH-31*	*RH-33*	*RH-36*	*RH-36*	*RH-36*
SiO_2	48.33	44.39	47.28	47.30	47.63	48.60	47.03	46.14	47.68	50.52
TiO_2	2.34	5.58	2.70	2.65	2.58	2.20	2.28	2.73	2.29	0.70
Al_2O_3	4.53	7.80	5.49	5.56	5.18	4.89	6.26	7.89	6.23	4.91
Cr_2O_3	*n.d.*	*n.d.*	*n.d.*	*n.d.*	*n.d.*	*n.d.*	*n.d.*	0.13	0.12	0.80
FeO	6.78	7.90	7.14	7.30	6.92	6.60	8.37	7.15	7.03	6.12
MnO	*n.d.*	*n.d.*	*n.d.*	*n.d.*	*n.d.*	*n.d.*	0.20	0.15	*n.d.*	0.19
MgO	13.60	11.89	13.26	13.50	13.46	13.77	12.28	12.24	13.26	15.94
CaO	23.93	23.96	24.11	23.91	24.00	24.19	23.10	23.78	23.47	19.54
Na_2O	0.46	0.55	0.39	0.38	0.39	0.39	0.67	0.45	0.35	0.72
Total	99.96	100.07	100.36	100.59	100.17	100.63	100.18	100.66	100.42	99.44
Wo	0.50	0.51	0.50	0.49	0.50	0.50	0.50	0.51	0.50	0.42
En	0.39	0.36	0.38	0.39	0.39	0.40	0.36	0.37	0.39	0.48
Fs	0.11	0.13	0.12	0.12	0.11	0.10	0.14	0.12	0.11	0.10

n.d. = not detected

In Fig. 5.2, clinopyroxenes in the basanites and nephelinites define a short trend, directed away from the En-apex, from augitic to more calcic, Wo-rich compositions and the relatively high Na_2O content of clinopyroxenes in Moheli lavas (0.35-1.58 wt.%), typical for alkaline lavas, suggests an appreciable aegirine content and a trend towards aegirine-augite compositions. On average, the clinopyroxenes in the basanites and nephelinites tend to have greater abundances of TiO_2, Al_2O_3, and CaO than the clinopyroxenes in the alkali basalts.

Olivine

Analyses of olivines from Moheli lavas are reported in Table 5.2 and the range in composition is shown in Fig. 5.2. The olivines in the alkali basalts span a compositional range from Fo_{62} to Fo_{81}, whereas olivines in the basanites and nephelinites are more Mg-rich and range from Fo_{87} to Fo_{89} and from Fo_{77} to Fo_{86} respectively. The FeO/MgO ratio of the olivine phenocrysts tends to increase from the cores to the rims.

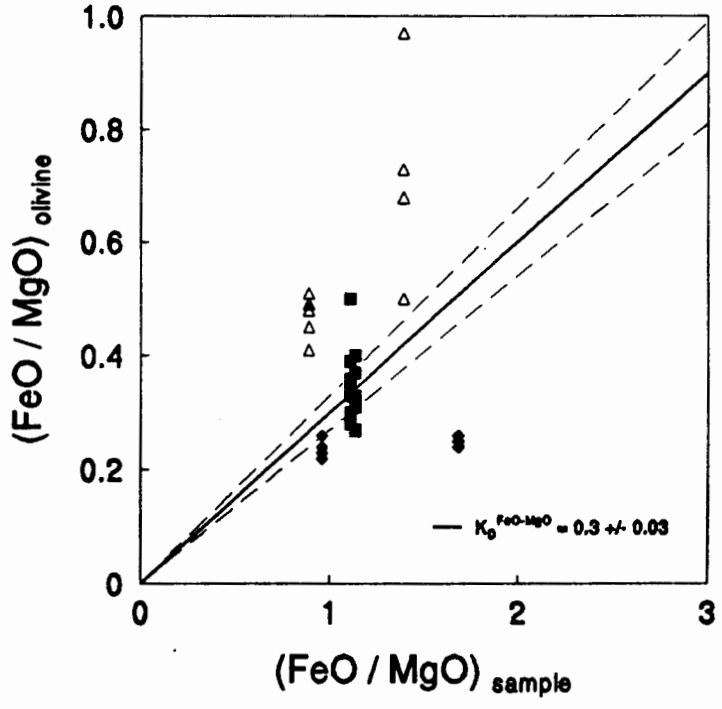

Fig. 5.3. Plot of $(FeO/MgO)_{olivine}$ vs $(FeO/MgO)_{sample}$ for olivine phenocrysts from Moheli. Symbols: open triangles: alkali basalts; filled diamonds: basanites; filled squares: nephelinites. Solid line: $K_D^{Fe-Mg}=0.3$. Stippled lines: $K_D^{Fe-Mg}=0.33$ and $K_D^{Fe-Mg}=0.27$.

Most of the olivines in the nephelinites have K_D^{Fe-Mg} values close to 0.3 (Fig. 5.3), indicating equilibrium or near-equilibrium conditions with their host rocks. The alkali

TABLE 5.2
Olivine analyses from Moheli lavas

	Alkali Basalts									*Nephelinites*				
Sample	*RH-15*	*RH-15*	*RH-15*	*RH-15*	*RH-16*	*RH-16*	*RH-16*	*RH-16*	*RH-16*	*RH-18*	*RH-18*	*RH-31*	*RH-31*	*RH-31*
SiO_2	36.76	38.90	39.05	39.65	35.82	36.05	37.47	38.25	36.69	39.33	39.37	38.44	39.10	39.36
Al_2O_3	*n.d.*	*n.d.*	*n.d.*	*n.d.*	*n.d.*	*n.d.*	*n.d.*	*n.d.*	*n.d.*	0.06	0.08	*n.d.*	*n.d.*	*n.d.*
Cr_2O_3	*n.d.*	*n.d.*	*n.d.*	*n.d.*	*n.d.*	*n.d.*	*n.d.*	*n.d.*	*n.d.*	*n.d.*	*n.d.*	*n.d.*	*n.d.*	*n.d.*
FeO	20.42	18.76	18.61	17.37	31.31	33.06	25.14	20.19	26.08	17.24	14.06	20.22	15.35	15.00
MnO	0.26	0.25	0.25	0.23	0.50	0.61	0.35	0.24	0.35	0.27	0.18	0.49	0.17	0.14
MgO	41.30	41.26	41.09	42.77	32.19	30.43	37.02	40.61	35.82	43.47	45.91	40.17	44.43	45.27
CaO	0.43	0.43	0.46	0.41	0.30	0.34	0.25	0.26	0.22	0.29	0.20	0.23	0.21	0.20
NiO	0.16	0.22	0.17	0.20	0.12	*n.d.*	0.27	0.33	0.15	*n.d.*	0.23	0.10	0.25	0.21
Total	99.33	99.82	99.64	100.64	100.23	100.49	100.49	99.88	99.31	100.66	100.02	100.43	99.51	100.19
Fo	0.78	0.79	0.79	0.81	0.64	0.62	0.72	0.78	0.71	0.82	0.85	0.77	0.83	0.84

n.d. = not detected

TABLE 5.2 continued

	Nephelinite				*Basanites*								
Sample	*RH-31*	*RH-31*	*RH-31*	*RH-31*	*RH-33*	*RH-33*	*RH-33*	*RH-33*	*RH-36*	*RH-36*	*RH-36*	*RH-36*	*RH-36*
SiO_2	39.47	39.52	39.57	40.03	39.76	39.76	39.77	39.81	39.71	39.72	40.09	40.14	40.32
Al_2O_3	*n.d.*	*n.d.*	*n.d.*	0.08	0.06	0.09	0.06	0.09	0.07	0.06	0.12	*n.d.*	0.15
Cr_2O_3	*n.d.*	*n.d.*	*n.d.*	*n.d.*	*n.d.*	*n.d.*	*n.d.*	*n.d.*	*n.d.*	*n.d.*	0.10	*n.d.*	0.16
FeO	16.13	15.41	15.51	12.95	11.92	11.54	12.08	12.01	10.78	10.73	11.18	12.27	11.32
MnO	0.16	0.18	0.19	0.15	0.15	0.16	0.16	0.15	0.17	0.13	0.13	0.18	0.16
MgO	44.24	44.91	44.79	46.72	47.14	47.30	47.24	46.83	48.32	48.30	48.36	47.26	47.87
CaO	0.22	0.23	0.21	0.25	0.23	0.22	0.24	0.24	0.23	0.21	0.23	0.23	0.23
NiO	0.25	0.27	0.26	0.31	0.28	0.34	0.32	0.32	0.32	0.31	0.29	0.21	0.30
Total	100.46	100.53	100.54	100.50	99.55	99.41	99.87	99.45	99.60	99.47	100.50	100.28	100.50
Fo	0.83	0.83	0.83	0.86	0.87	0.88	0.87	0.87	0.88	0.89	0.88	0.87	0.88

n.d. = not detected

basalts, on the other hand, contain olivine phenocrysts which have K_D^{Fe-Mg} values significantly greater than 0.3 (Fig. 5.3). These olivines contain too much FeO, relative to MgO, to be in equilibrium with their host rocks. The olivine phenocrysts in the basanites are too magnesian to be in equilibrium with their host rocks, having K_D^{Fe-Mg} values below 0.3 (Fig. 5.3). Some individual Moheli samples show a considerable range in K_D^{Fe-Mg} values amongst their olivine phenocrysts. The presence in Moheli lavas of olivine phenocrysts which are in disequilibrium with their host rocks implies that a significant proportion of these phenocrysts may in fact be xenocrysts, with a possible origin by, for instance, accumulation or wall-rock assimilation processes.

5.4 Bulk Rock Chemistry

Major and Minor Elements

The major and minor element compositions of Moheli lavas are presented in Table 5.3. The compositional range of Moheli lavas is depicted in Figures 5.1, 5.4 and 5.5. Major and minor element data were normalised to 100 per cent on a volatile free basis before plotting.

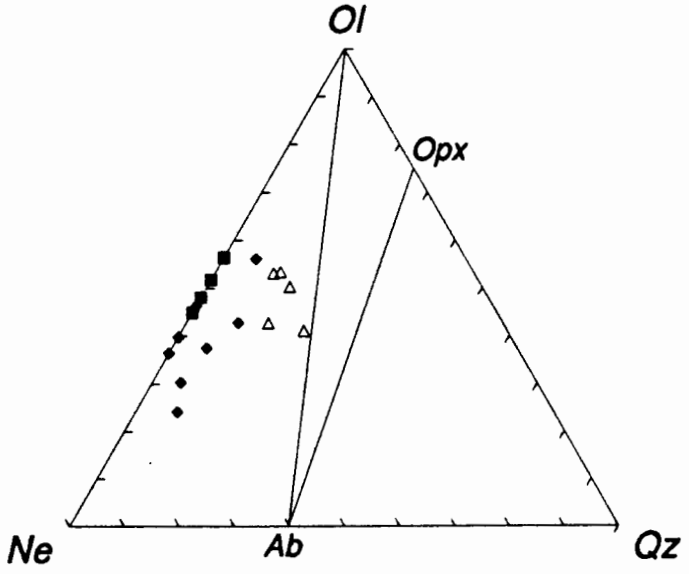

Fig. 5.4. Moheli lavas plotted on the basal projection of the normative Cpx-Ol-Ne-Qz tetrahedron, projected from Cpx according to Irvine and Baragar (1971). Symbols: open triangles: alkali basalts; filled diamonds: basanites; filled squares: nephelinites.

TABLE 5.3
Bulk-rock analyses and selected trace element ratios of Moheli lavas

	Alkali Basalts					*Basanites*										*Nephelinites*				
Sample	*RH-15*	*RH-16*	*RH-17*	*RH-28*	*RH-42*	*RH-12a*	*RH-13*	*RH-21*	*RH-26*	*RH-27*	*RH-29*	*RH-30*	*RH-33*	*RH-36*	*RH-39*	*RH-14*	*RH-18*	*RH-19*	*RH-31*	*RH-41*
SiO_2	44.97	47.25	45.06	43.46	46.30	39.05	42.79	42.29	40.81	39.35	41.22	41.72	42.72	42.17	47.38	39.50	38.76	39.96	37.83	39.96
TiO_2	2.38	2.50	2.60	2.88	2.67	2.64	2.79	2.47	4.20	3.38	3.53	2.47	2.41	2.32	3.33	3.25	2.91	2.70	2.90	2.59
Al_2O_3	10.34	13.70	10.92	13.00	12.91	11.55	12.68	11.22	11.33	10.45	14.16	11.74	12.99	11.67	12.10	11.15	10.64	10.67	10.29	11.00
Fe_2O_3	1.69	1.64	1.63	1.74	1.68	1.81	1.74	1.61	1.69	1.69	1.88	1.64	1.72	1.62	1.64	1.70	1.84	1.70	1.82	1.60
FeO	11.24	10.94	10.88	11.63	11.18	12.09	11.59	10.71	11.24	11.29	12.54	11.35	11.47	10.82	10.92	11.30	12.28	11.36	12.15	10.64
MnO	0.18	0.19	0.18	0.20	0.20	0.27	0.20	0.20	0.19	0.21	0.24	0.21	0.27	0.21	0.19	0.22	0.23	0.26	0.22	0.22
MgO	12.59	7.80	11.63	8.41	9.10	9.72	9.16	11.69	10.08	11.10	5.07	10.27	6.78	11.31	9.84	11.32	10.75	11.16	10.92	11.60
CaO	10.21	9.40	11.70	9.55	10.56	11.80	10.46	12.63	12.07	13.02	9.88	12.13	10.92	12.04	10.78	12.66	13.01	12.41	14.00	13.90
Na_2O	3.06	3.08	2.68	2.59	3.39	4.07	3.97	2.69	4.74	3.71	5.74	4.86	4.98	4.35	4.76	4.41	4.83	5.50	3.49	3.93
K_2O	0.88	1.38	1.00	1.66	1.24	1.07	0.93	0.61	0.66	0.60	1.14	0.84	1.49	0.76	0.68	1.25	1.80	1.69	1.46	1.48
P_2O_5	0.43	0.59	0.43	0.75	0.42	1.09	0.83	0.89	0.72	0.98	1.11	0.89	1.03	0.72	0.63	0.88	1.27	1.01	1.24	1.17
LOI	1.07	0.97	1.54	2.36	0.69	3.61	2.52	2.56	2.41	3.36	2.88	2.12	2.71	2.08	2.21	2.23	1.56	1.49	2.48	1.83
H_2O-	0.71	0.41	0.45	0.88	0.17	0.95	0.98	0.56	0.97	0.82	0.96	0.67	0.77	0.39	1.07	0.65	0.22	0.37	0.30	0.52
Total	99.75	99.85	100.70	99.11	100.51	99.72	100.64	100.13	101.14	99.96	100.35	100.91	100.26	100.46	100.53	100.55	100.10	100.28	99.10	100.44
Zr	174	228	200	278	189	359	311	229	192	207	430	248	328	211	214	237	359	262	299	2.48
Nb	34	50	38	66	59	124	96	68	65	76	112	74	124	79	64	88	127	105	103	82
Y	24	27	24	29	25	42	30	29	26	30	42	36	43	30	27	32	36	39	32	34
Rb	17	32	23	40	36	45	31	15.5	117	13.1	72	27	51	20	128	20	48	34	50	44
Ba	369	416	306	550	477	1003	726	639	800	747	844	596	1236	693	679	806	802	599	657	703
Sr	446	634	487	731	566	1404	813	909	710	658	1225	837	1283	754	751	792	1527	1060	1367	912
Th	2.3	3.5	5.3	6.3	3.2	15.0	12.0	9.4	7.1	8.3	11.0	10.4	17.8	9.4	9.1	9.8	14.7	15.3	11.8	14.0
Co	76	55	69	61	58	59	63	63	68	63	46	69	47	67	67	71	65	67	66	61
Cr	644	263	612	268	369	221	350	601	454	557	20	485	277	606	387	392	356	615	403	519
Ni	403	184	375	219	214	201	245	343	254	288	34	317	141	338	269	301	260	318	267	257
V	240	181	240	207	220	208	242	242	290	262	219	237	196	252	249	257	224	235	216	246
Zn	107	146	108	127	109	158	159	107	96	100	150	103	116	102	104	109	156	125	141	101
Cu	90	98	80	67	76	56	105	77	77	68	58	59	63	89	71	81	67	67	71	84
Sc	28	20	28	18.8	22	17.9	23	24	22	25	13.8	29	19.8	28	21	23	22	22	19.7	26
La	-	-	31	-	33	-	66	-	-	61	-	69	105	61	53	-	-	98	-	92
Ce	-	-	64	-	70	-	131	-	-	120	-	136	194	110	99	-	-	188	-	173
Nd	-	-	32	-	34	-	61	-	-	58	-	59	79	49	45	-	-	78	-	76
Zr/Nb	5.1	4.6	5.3	4.2	3.2	2.9	3.2	3.4	3.0	2.7	3.8	3.4	2.7	2.7	3.3	2.7	2.8	2.5	2.9	3.0
Zr/Y	7.3	8.4	8.3	9.6	7.6	8.6	10.4	7.9	7.4	6.9	10.2	6.9	7.6	7.0	7.9	7.4	10.0	6.7	9.3	7.3
Y/Nb	0.71	0.54	0.63	0.44	0.42	0.34	0.31	0.43	0.40	0.39	0.38	0.49	0.35	0.38	0.42	0.36	0.28	0.37	0.31	0.41
Ba/Nb	10.9	8.3	8.1	8.3	8.1	8.1	7.6	9.4	12.3	9.8	7.5	8.1	10.0	8.8	10.6	9.2	6.3	5.7	6.4	8.6
Mg#	0.67	0.56	0.66	0.56	0.59	0.59	0.58	0.66	0.62	0.64	0.42	0.62	0.51	0.65	0.62	0.64	0.61	0.64	0.62	0.66

Fe_2O_3 calculated assuming $Fe_2O_3/FeO = 0.15$; La, Ce and Nd determined by XRF; *Mg#* = atomic $Mg/(Mg+Fe^{2+})$ with $Fe_2O_3/FeO = 0.15$.

As noted previously, the Moheli lavas analysed in this study have been classified into alkali basalts, basanites and nephelinites, according to the total alkali-silica diagram of le Bas *et al.* (1986) (Fig. 5.1). All of the Moheli lavas analysed are nepheline-normative (Fig. 5.4) and some of the basanites as well as all of the nephelinites also contain normative leucite. There is a consistent increase in the average contents of normative nepheline from the alkali basalts (5.4 wt.%) to the basanites (18.8 wt.%) and nephelinites (20.6 wt.%). On average, the alkali basalts are richer in normative plagioclase (32.1 wt.%) than both the basanites (14.4 wt.%) and nephelinites (5.1 wt.%), whereas the basanites contain less normative olivine (16.9 wt.%) than the alkali basalts (20.4 wt.%) and nephelinites (22.8 wt.%).

A number of major and minor elements are plotted against *Mg-number* in Fig. 5.5. The data from Moheli alkali basalts, basanites and nephelinites overlap on most of these variation diagrams, although the average CaO, Na_2O and P_2O_5 contents of the basanites and nephelinites are higher than those of the alkali basalts. The nephelinites are distinctly more potassic than most of the basanites. Amongst the three rock types investigated, the basanites show the greatest range in *Mg-number* (0.42-0.66). Well-defined linear trends are uncommon in the Moheli major and minor element variation diagrams, but with decreasing *Mg-number*, a general increase in Al_2O_3 and FeO is observed. Amongst the basanites, there is a reasonably well-defined increase in Na_2O and decrease in CaO with decreasing *Mg-number*.

Moheli lavas have similar ranges of major and minor element abundances as the more primitive lavas from Mayotte. The major and minor element compositions of Moheli lavas also tend to overlap with those of the lavas from Grande Comore, although for a given *Mg-number*, most Moheli lavas are somewhat richer in FeO and P_2O_5, but poorer in Al_2O_3 than Grande Comore lavas.

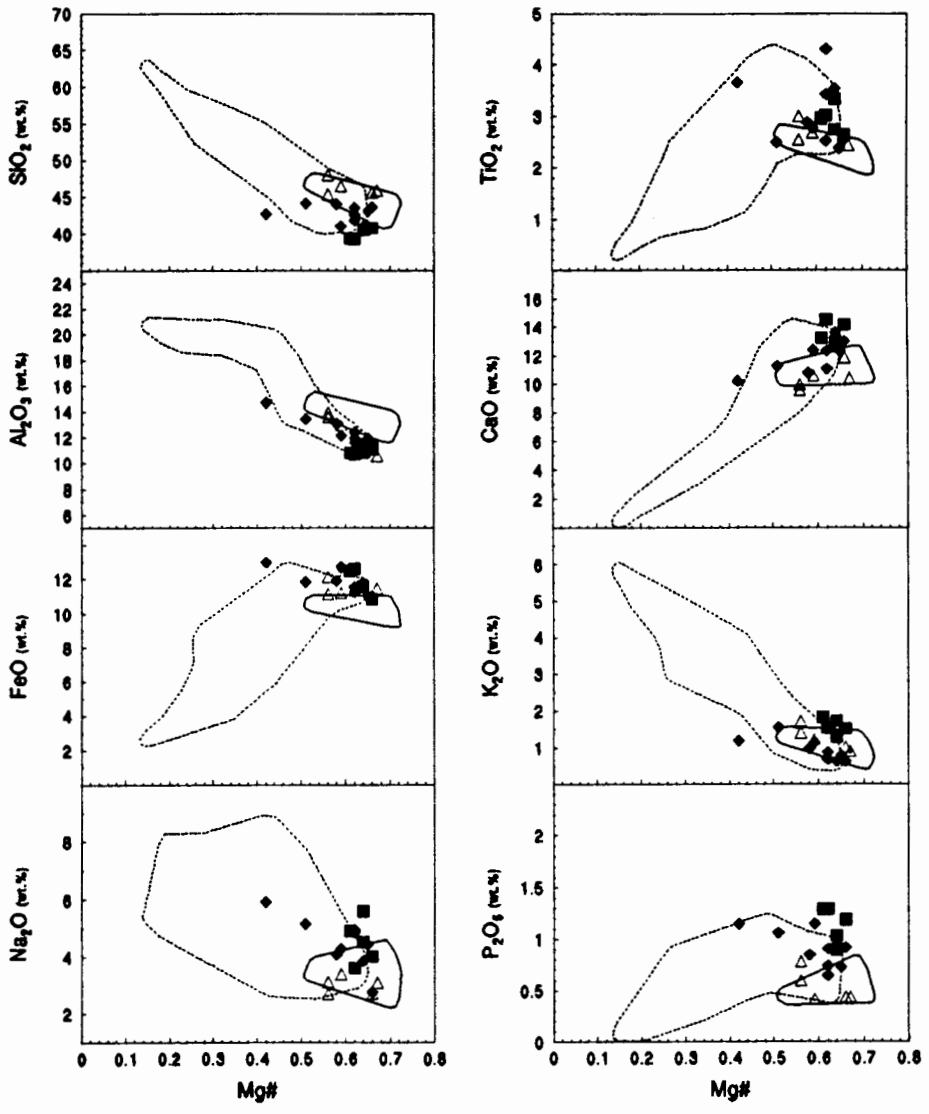

Fig. 5.5. Plots of major and minor elements (wt.%) vs *Mg-number* for Moheli lavas. Symbols: open triangles: alkali basalts; filled diamonds: basanites; filled squares: nephelinites. For comparison, the fields for Grande Comore and Mayotte data, delineated by solid and stippled lines respectively, are shown.

Trace Elements

Trace element compositions of Moheli lavas are presented in Table 5.3 and the REE compositions of ten Moheli lavas are reported in Table 5.4.

Considerable ranges in the concentrations of the ferromagnesian elements Ni and Cr are observed amongst Moheli lavas and well-defined trends of decreasing Ni, Cr and Sc with

decreasing *Mg-number* are shown in Fig. 5.6.

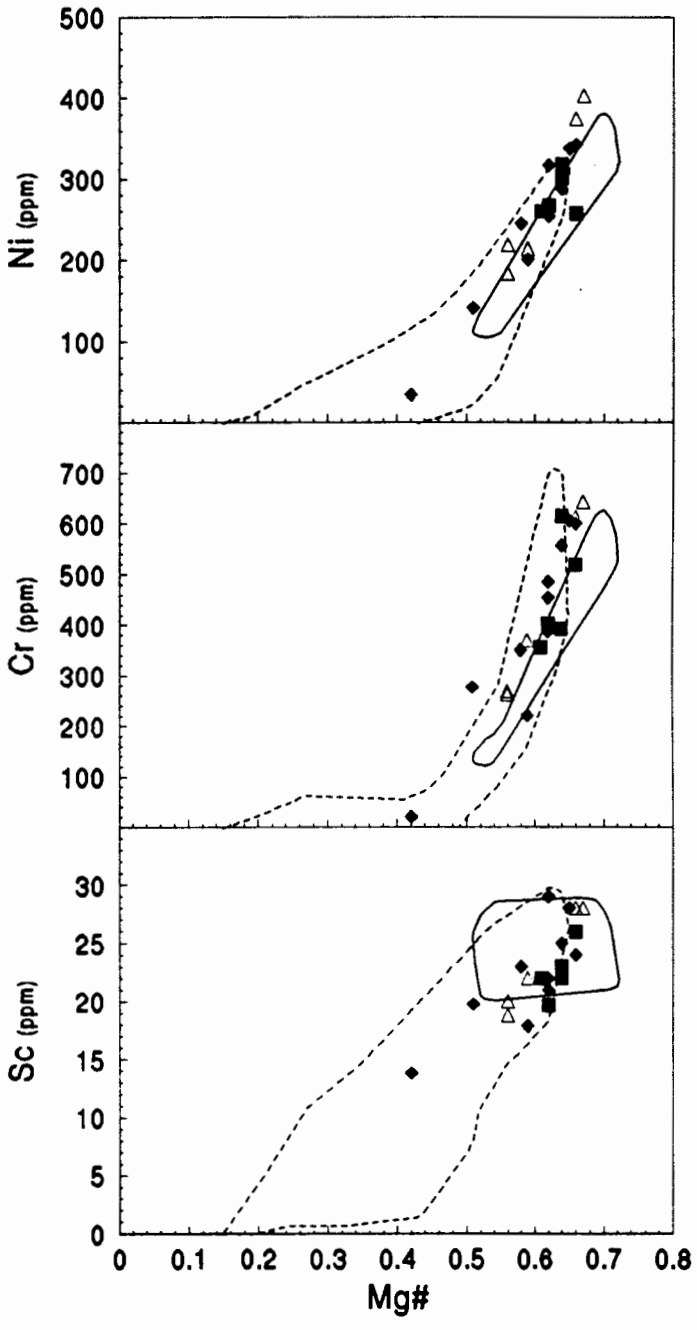

Fig. 5.6. Plots of Ni, Cr and Sc (ppm) vs *Mg-number* for Moheli lavas. Symbols: open triangles: alkali basalts; filled diamonds: basanites; filled squares:nephelinites. For comparison, the field for Grande Comore and Mayotte data, delineated by solid and stippled lines respectively, are shown.

Several incompatible trace elements are plotted against Zr in Fig. 5.7. All of these diagrams show broad positive correlations of increasing trace element concentrations

with increasing Zr content and in some of these diagrams (e.g. Nb vs Zr, Th vs Zr, Sr vs Zr) more than one linear trend may possibly be inferred. The alkali basalts, which appear to define an independent, short linear trend on some of the diagrams (e.g. Nb vs Zr, Sr vs Zr, Th vs Zr), tend to have lower abundances of Nb, Th, Sr and Ba for a given Zr content than the basanites and nephelinites.

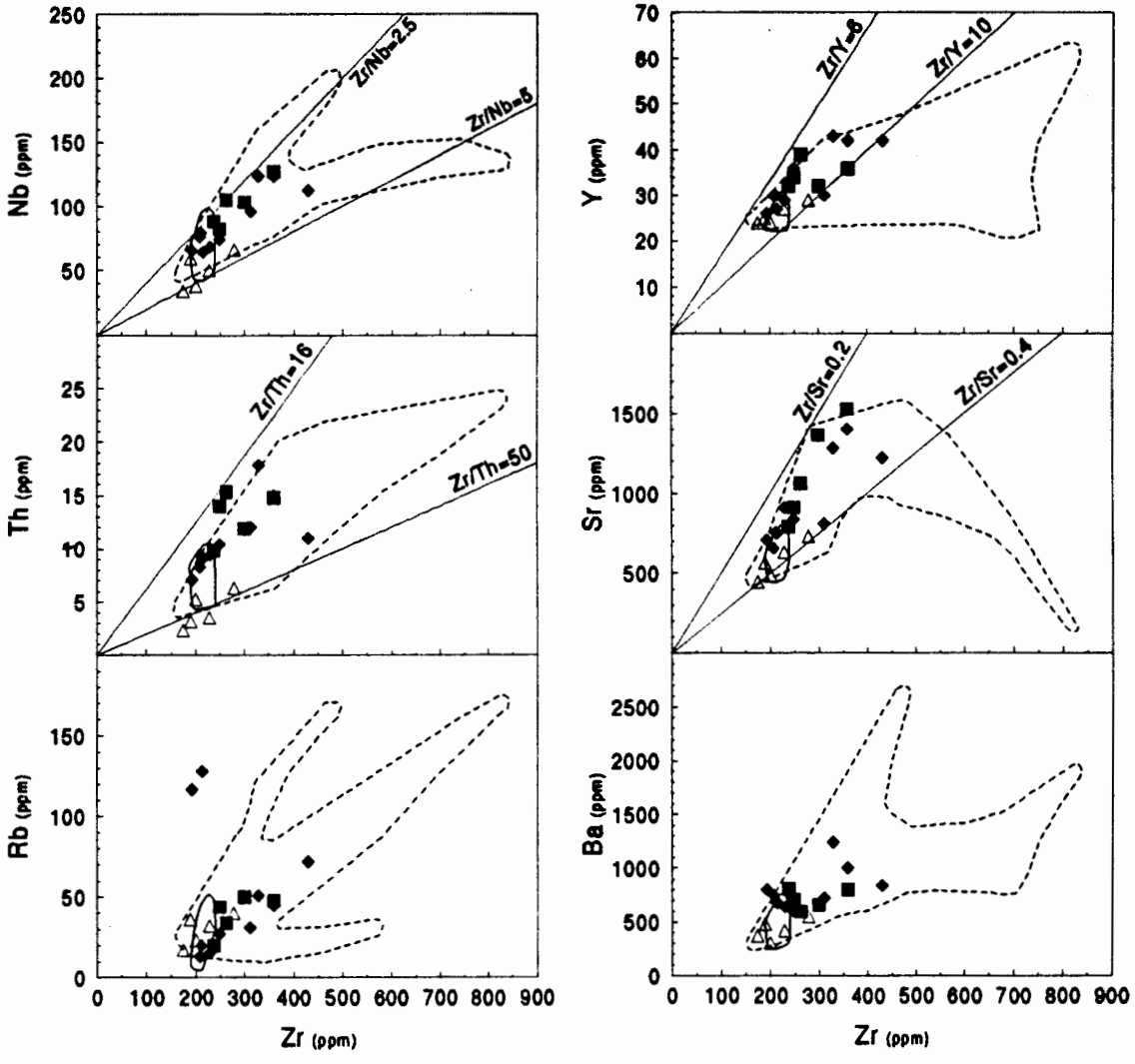

Fig. 5.7. Plots of incompatible trace elements vs Zr (all in ppm) for Moheli lavas. Symbols: open triangles: alkali basalts; filled diamonds: basanites; filled squares: nephelinites. For comparison, the fields for Grande Comore and Mayotte data, delineated by solid and stippled lines respectively, are shown.

Incompatible trace element ratios are plotted against Zr in Fig. 5.8. On the Zr/Nb vs Zr and Y/Nb vs Zr diagrams, the alkali basalts (with the exception of RH-42) once again

define a linear trend that is independent of and significantly different from the basanite and nephelinite data. Since fractional crystallisation processes are incapable of causing significant changes in these ratios, the relatively marked variation in Zr/Nb and Y/Nb amongst Moheli alkali basalts may point towards either the effects of variable degrees of partial melting or to an origin from distinctly different source regions. The fact that sample RH-42 falls off the linear trend defined by the alkali basalts on diagrams involving Nb in the Y-axis ratio might at first suggest that the analytical result for the Nb abundance in this particular sample are in error, being anomalously high. However, a re-analysis of RH-42, several months after the initial analysis, yielded a Nb abundance identical (within analytical error) to the first and the apparently anomalous Nb concentration of this sample and its location on plots such as those in Fig. 5.8 remains enigmatic. All Moheli lavas show a similar range in terms of Ba/Nb (5.7-12.3) and La/Nb (0.56-1.12) ratios, but the alkali basalts (with the exception of RH-42) tend to have higher Zr/Nb (4.2-5.3) and Y/Nb (0.44-0.71) ratios than the basanites and nephelinites (joined ranges: Zr/Nb: 2.5-3.8; Y/Nb: 0.28-0.49).

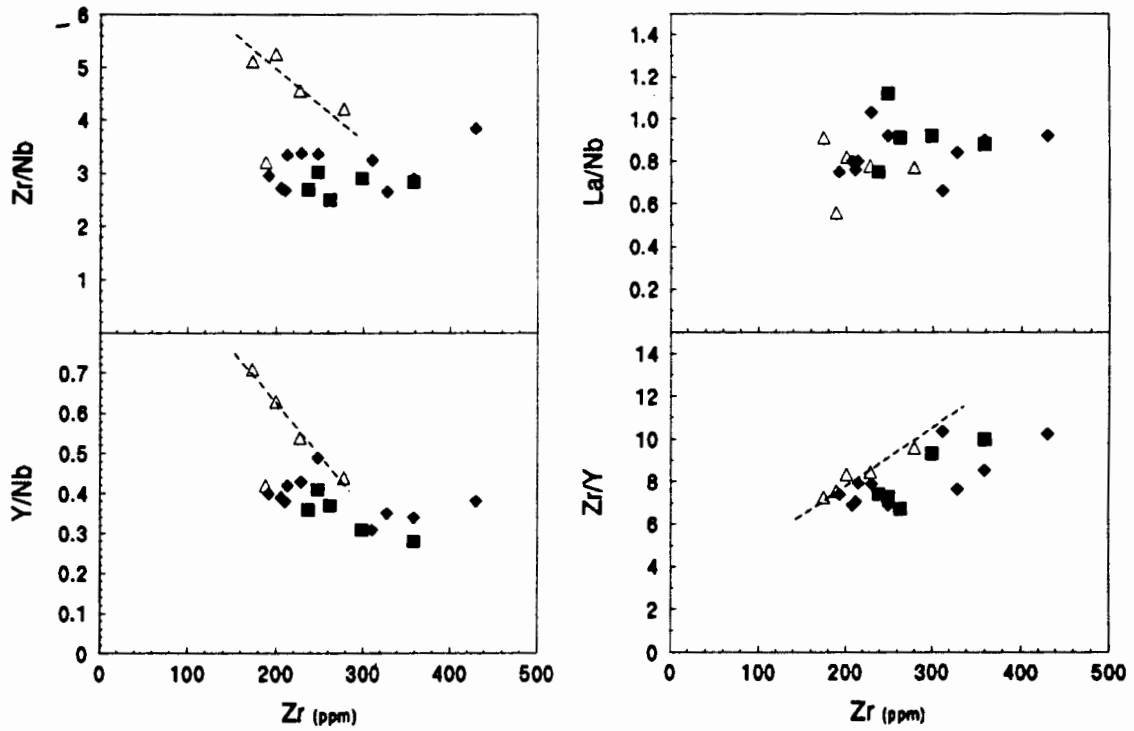

Fig. 5.8. Plots of incompatible trace element ratios vs Zr (ppm) for Moheli lavas. Symbols: open triangles: alkali basalts; filled diamonds: basanites; filled squares: nephelinites.

Primitive mantle-normalised incompatible element diagrams (spidergrams) of Moheli lavas are shown in Fig. 5.9. The highly incompatible element enriched nature of Moheli lavas relative to primitive mantle and N-type MORB is evident from these diagrams. Although slightly more variable in their degree of relative enrichment, the Moheli alkali basalts have incompatible element patterns that are strikingly similar to those of Karthala lavas from Grande Comore (compare Fig. 5.9a with Fig. 4.8a) and for this reason, Moheli alkali basalts are considered to be Karthala-type lavas. The basanites and nephelinites show greater overall enrichment in the highly incompatible elements than the alkali basalts, but like the lavas from La Grille (Fig. 4.8b), they are significantly depleted in K and are thus considered to belong to the La Grille-type of lavas. Rb shows considerable variation in the basanites and nephelinites, but in the majority of cases also shows significant depletion relative to Nb and Ba.

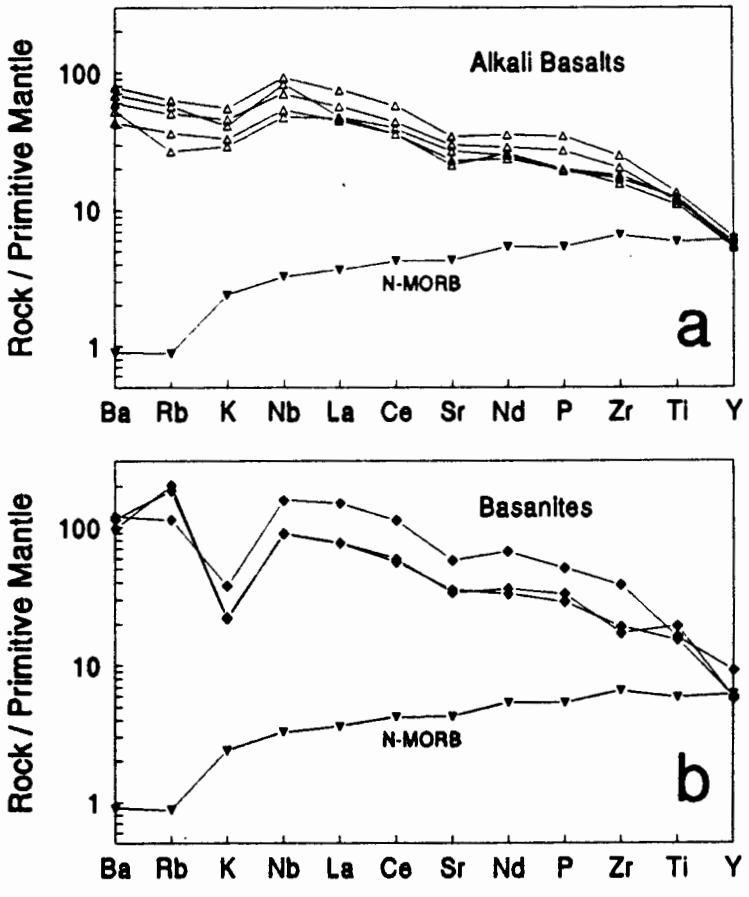

Fig. 5.9. Plots of primitive mantle-normalised incompatible elements, arranged (from left to right) in order of decreasing incompatibility for Moheli lavas. (**a**) Alkali basalts; (**b**) basanites; (**c**) and (**d**) basanites and nephelinites. A pattern of N-type MORB (Sun and McDonough, 1989) is shown for comparison. Normalising values after Sun and McDonough (1989).

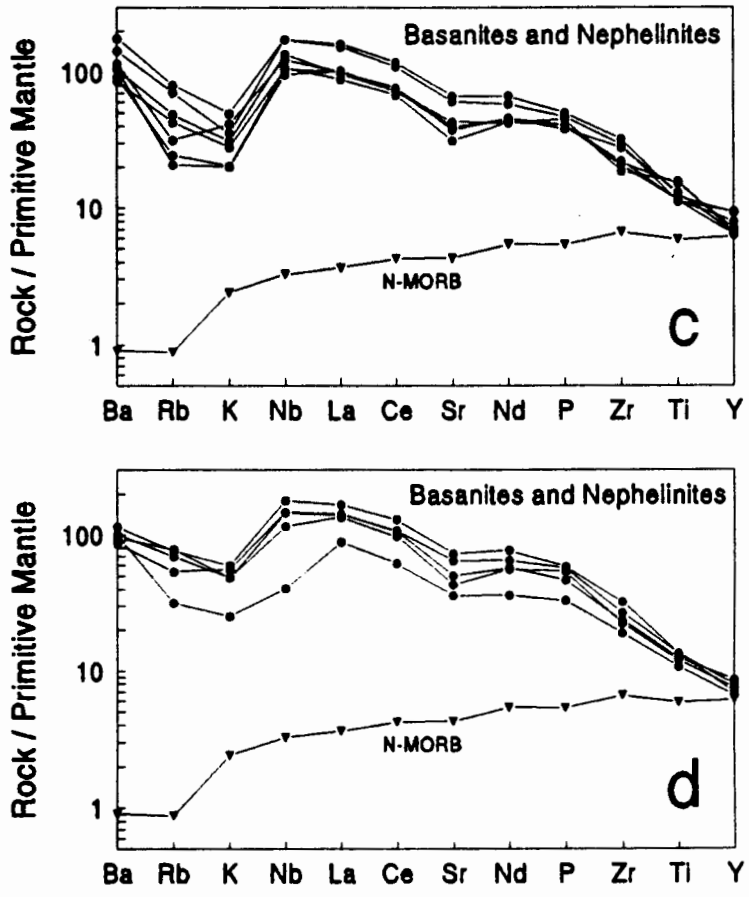

Fig. 5.9 ***continued.***

The chondrite-normalised REE patterns of ten Moheli lavas are shown in Fig. 5.10. Typically, the nephelinites are more strongly enriched in the light and middle REE, but have lower chondrite-normalised heavy rare earth element (HREE) abundances than the basanites. The basanites themselves, show greater overall REE enrichment than the alkali basalts. The nephelinites analysed have steeper REE patterns and greater normalised La/Yb ratios (28-52) than the basanites (16.8-39) and alkali basalts (12.4-22), and cross-cut the REE patterns of the basanites and alkali basalts in the middle to heavy REE range.

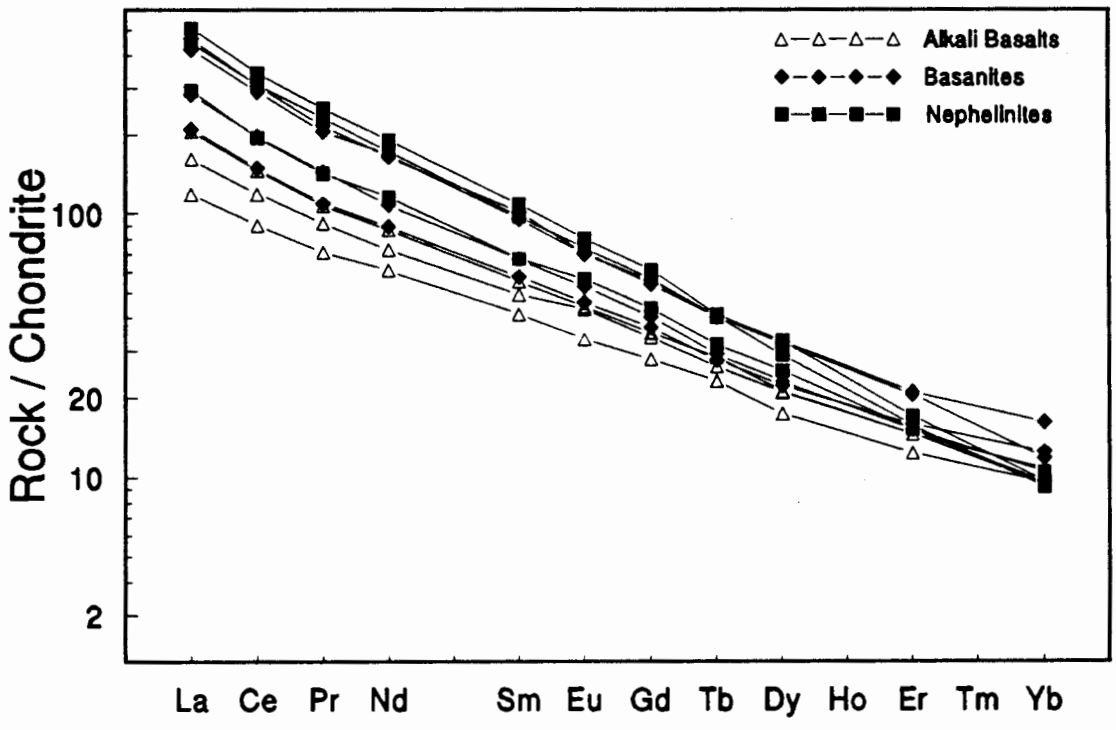

Fig. 5.10. Chondrite-normalised REE patterns of selected Moheli lavas. Normalising values after Sun and McDonough (1989).

TABLE 5.4
REE contents (ppm) of selected Moheli lavas

	Alkali Basalts			*Basanites*				*Nephelinites*		
Sample	*RH-15*	*RH-16*	*RH-28*	*RH-12a*	*RH-21*	*RH-26*	*RH-29*	*RH-14*	*RH-18*	*RH-31*
La	28.2	38.4	48.9	110	67.6	49.9	100	70.0	120	106
Ce	55.3	72.8	89.9	188	121	91.5	179	120	211	190
Pr	6.77	8.76	10.2	20.7	13.8	10.4	19.6	13.6	24.1	22.1
Nd	28.4	34.1	40.6	77.2	50.6	41.9	78.4	54.3	89.4	81.1
Sm	6.34	7.50	8.44	15.6	10.3	8.80	14.6	10.3	16.6	15.0
Eu	1.92	2.50	2.56	4.11	3.04	2.67	4.05	3.27	4.66	4.29
Gd	5.74	6.92	7.24	11.1	8.30	7.55	11.4	8.94	12.5	11.6
Tb	0.86	0.98	1.06	1.52	1.09	1.03	1.51	1.18	1.54	1.51
Dy	4.41	5.31	5.35	8.15	5.84	5.65	8.30	6.40	8.33	7.37
Er	2.05	2.42	2.40	3.40	2.50	2.62	3.48	2.52	2.82	2.60
Yb	1.63	1.61	1.83	2.01	1.64	2.13	2.75	1.78	1.65	1.56
$(La/Sm)_n$	2.9	3.3	3.7	4.6	4.2	3.7	4.4	4.4	4.7	4.6
$(La/Yb)_n$	12.4	17.1	19.2	39.3	29.6	16.8	26.1	28.2	52.2	48.7
La/Nb	0.83	0.77	0.74	0.89	0.99	0.77	0.89	0.80	0.94	1.0

$(La/Sm)_n$ and $(La/Yb)_n$ are chondrite-normalised ratios (normalising values from Sun and McDonough, 1989).

Isotopes

A total of six samples from Moheli, including four alkali basalts, one basanite and one nephelinite, were analysed for their $^{87}Sr/^{86}Sr$ and $^{143}Nd/^{144}Nd$ ratios which are listed in Table 5.5. The isotopic compositions of all three rock types overlap, showing relatively limited variability, with $^{87}Sr/^{86}Sr$ values ranging from 0.70323±1 to 0.70349±2 and $^{143}Nd/^{144}Nd$ values ranging from 0.51279±1 to 0.51285±1. The range of $^{87}Sr/^{86}Sr$ ratios for several Moheli lavas (0.703185-0.703443) presented by Emerick (1985) is consistent with this data. The Nd and Sr isotopic compositions of Moheli lavas overlap with those of lavas from La Grille and Mayotte (see Chapters 4 and 6).

TABLE 5.5
Sr and Nd isotope data for selected Moheli lavas

	Sample	$^{87}Sr/^{86}Sr$	$^{143}Nd/^{144}Nd$
Alkali Basalt	*RH-15*	0.70342±1	0.51279±1
Alkali Basalt	*RH-16*	0.70324±1	0.51285±1
Alkali Basalt	*RH-17*	0.70349±2	-
Alkali Basalt	*RH-28*	0.70335±2	0.51282±1
Basanite	*RH-26*	0.70323±1	0.51283±1
Nephelinite	*RH-14*	0.70326±1	0.51285±1

errors are $2\sigma_{mean}$ on in-run statistics and correspond to least significant digits.

6.1 Classification of the Rocks

Mayotte lavas may be classified into different rock types according to the total alkali-silica diagram of le Bas *et al.* (1986; Fig. 6.1).

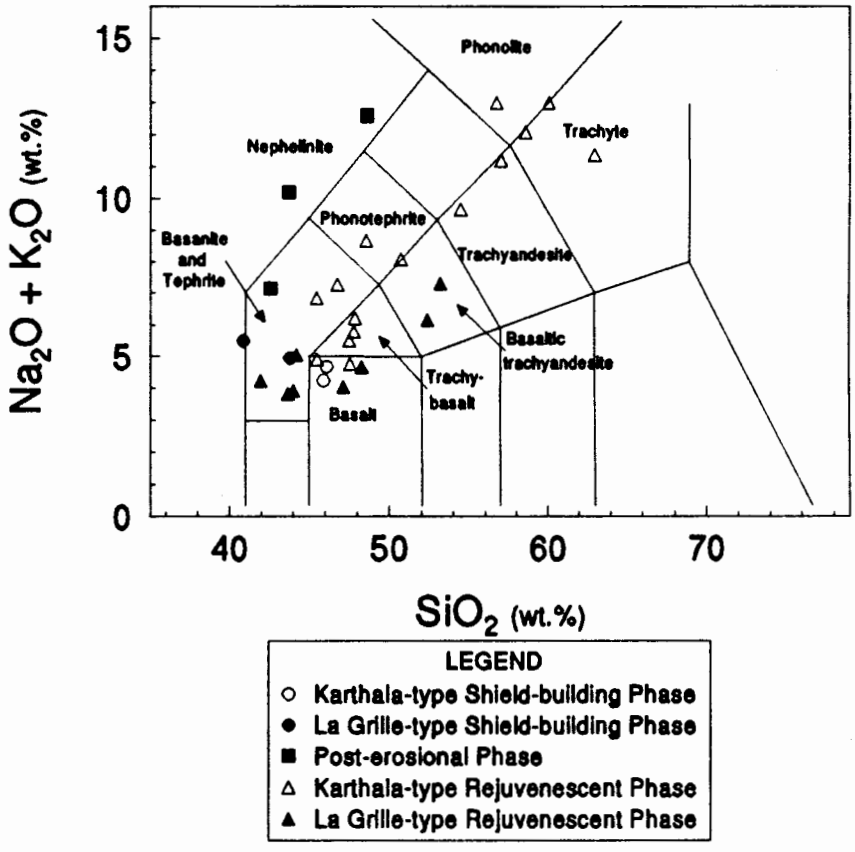

Fig. 6.1. Total alkali-silica diagram for Mayotte lavas. Classification grid after le Bas *et al.* (1986).

Mayotte samples were further divided into several groups according to two criteria. *Firstly*, based on the K-Ar data and geological maps of Emerick and Duncan (1982, 1983) and Nougier *et al.* (1986), the lavas were classified according to the phase of volcanic activity during which they were erupted. *Secondly*, using mantle-normalised incompatible element patterns described in detail below (Fig. 6.13), lavas were further classified according to whether they belong to the La Grille-type or the Karthala-type of lavas. The

classification of Mayotte lavas according to these two criteria is summarised in Table 6.1.

TABLE 6.1
Classification of Mayotte lavas according to phase of volcanism and lava type

	Shield-building Phase	Post-erosional Phase	Rejuvenescent Phase
Karthala-type	MA-29, MA-30	-	MA-1, MA-3, MA-5, MA-6, MA-8, MA-9, MA-11, MA-14, MA-18, MA-20, MA-35, MA-59, MA-65, MA-66, MA-67
La Grille-type	MA-60, MA-61	MA-55, MA-73, MA-81	MA-2, MA-4, MA-7, MA-12, MA-17, MA-22, MA-33, MA-34

6.2 Petrography and Mineralogy

Detailed petrographic descriptions of all Mayotte samples for which thin-sections were available are contained in Appendix A4.3. The petrographic characteristics of the various groups of samples from the island are summarised below.

Shield-building Phase Lavas

Only four samples from this phase of volcanism were analysed and as described above, these have been divided into two groups.

La Grille-type lavas :
Of the two La Grille-type Shield-building lavas, one is a basanite (MA-60) and the other is a nephelinite (MA-61) (Fig. 6.1). These lavas are slightly altered, porphyritic rocks, containing phenocrysts and microphenocrysts of clinopyroxene. Olivine is also a phenocryst phase in MA-60, but it is entirely absent from MA-61, in which microphenocrysts of Fe-Ti oxide are present. The clinopyroxene phenocrysts and microphenocrysts contain inclusions of Fe-Ti oxide and are typically pale tan to tan-violet in colour and in the case of MA-60 frequently have pale grey-green or pleochroic green cores (Plate 11). The partly to strongly altered olivine phenocrysts of MA-60 commonly

show signs of partial resorption. The fine- to very fine-grained and partly glassy groundmass of these lavas contains clinopyroxene, Fe-Ti oxide, nepheline, olivine (MA-60 only) and accessory amounts of biotite and apatite. No plagioclase is present in the rocks.

Karthala-type lavas :

Both Karthala-type Shield-building lavas are alkali basaltic (Fig. 6.1), vesicular and porphyritic lavas. Slightly iddingsitised and partially resorbed olivine is an abundant phenocryst phase in both lavas, whereas clinopyroxene phenocrysts and microphenocrysts occur commonly in MA-30, but are rare in MA-29. The clinopyroxene phenocrysts are typically pale tan in colour and often occur in small glomerophyric aggregates. The fine- to very fine-grained groundmass contains clinopyroxene, plagioclase, olivine and Fe-Ti oxide.

Post-erosional Phase Lavas

One of the Post-erosional Phase lavas is a tephrite (MA-55) and two are nephelinites (MA-73, MA-81; no thin-section for MA-81) (Fig. 6.1). Both MA-55 and MA-73 are porphyritic rocks, but their phenocryst assemblages differ considerably. MA-55 contains phenocrysts and microphenocrysts of mainly clinopyroxene and fewer titanomagnetite microphenocrysts. The zoned clinopyroxene phenocrysts in this rock are typically pale tan in colour, but often have pleochroic green or violet cores and pale tan to tan-violet rims (Plate 12). MA-73, on the other hand, has the most extreme mineralogy of all samples investigated, containing abundant phenocrysts and microphenocrysts of nepheline, clinopyroxene (pleochroic green aegirine-augite) and dark brown garnet (Plates 13 and 14). Several electron microprobe analyses of nepheline phenocrysts from MA-73 are presented in Table 6.2. and two analyses of garnet phenocrysts from this sample are shown in Table 6.3. The garnets are schorlomites, containing between 14.0 and 15.4 wt.% TiO_2. Schorlomite is a very dark brown to black, titanium-rich variety of andradite garnet, which has been reported to occur in nepheline-syenite and ijolite and in their volcanic equivalents, phonolite, nephelinite, etc. (Deer *et al.*, 1962a, Table 15, analyses 10 and 11). It is not known whether this mineral has been recognised in other ocean island basalts and the implications of its occurrence in terms of the physico-chemical

TABLE 6.2
Nepehline analyses from Mayotte lavas

	Post-erosional Phase					
Sample	*MA-73*	*MA-73*	*MA-73*	*MA-73*	*MA-73*	*MA-73*
SiO_2	44.53	44.32	44.89	43.52	45.33	44.79
Al_2O_3	34.76	34.01	35.06	33.96	34.05	34.63
FeO	0.66	0.58	0.75	0.68	0.63	0.73
MgO	*n.d.*	*n.d.*	*n.d.*	*n.d.*	*n.d.*	*n.d.*
CaO	1.01	0.26	0.68	0.27	0.45	0.44
Na_2O	13.34	14.40	12.51	15.10	13.68	11.85
K_2O	5.47	6.23	6.77	7.08	5.88	6.78
Total	99.78	99.80	100.66	100.62	100.01	99.22

n.d. = not detected.

TABLE 6.3
Garnet analyses from MA-73

	Post-erosional Phase	
Sample	*MA-73*	*MA-73*
SiO_2	29.64	29.46
TiO_2	13.95	15.40
Al_2O_3	2.43	2.10
Cr_2O_3	*n.d.*	*n.d.*
FeO	20.15	19.41
MnO	0.44	0.46
MgO	0.76	0.86
CaO	32.71	32.33
Na_2O	0.17	*n.d.*
K_2O	*n.d.*	*n.d.*
Total	100.25	100.02

n.d. = not detected.

conditions of crystallisation is unclear. The fine- to very fine-grained groundmass of the Post-erosional Phase lavas contains nepheline, clinopyroxene (tan-violet titanaugite in MA-55; pleochroic green aegirine-augite in MA-73), Fe-Ti oxide and accessory apatite.

Rejuvenescent Phase Lavas

As described above, the lavas erupted during the Rejuvenescent Phase of volcanism have been divided into two distinct groups.

***La Grille-type lavas*:**

Four samples in this group are basanites (MA-2, MA-4, MA-22, MA-33), two are basalts (one alkali basalt: MA-12; one subalkali basalt: MA-7) and two are shoshonites (MA-17, MA-34) (Fig. 6.1).

The *basanites* are slightly vesicular, typically seriate-textured lavas, ranging from slightly to moderately porphyritic. They contain between 5 and 35 vol.% phenocrysts and microphenocrysts of primarily clinopyroxene and olivine. Titanomagnetite microphenocrysts also commonly occur in small quantities. Most of the phenocrysts and microphenocrysts in one of the samples (MA-2) are pseudomorphs after olivine and amphibole. There are too few samples in this group to ascertain whether clinopyroxene or olivine is the predominant phenocryst phase. Clinopyroxene phenocrysts and microphenocrysts typically have pale grey-tan to pale green, occasionally sieve-textured, cores and darker tan to tan-violet rims. They frequently include fine Fe-Ti oxide grains and some display oscillatory or more irregular zonation patterns. The phenocrysts and microphenocrysts of olivine are moderately to very strongly iddingsitised and commonly show signs of partial resorption (Plate 15). The fine- to medium-grained groundmass of these La Grille-type Rejuvenescent Phase lavas typically contains tan-violet titaniferous clinopyroxene, plagioclase, Fe-Ti oxide, smaller amounts of olivine and accessory apatite. In one sample (MA-22), nepheline occurs as a groundmass phase instead of plagioclase.

The *basalts* of this group are vesicular, porphyritic and seriate-textured lavas, containing phenocrysts and microphenocrysts of clinopyroxene and olivine in nearly equal proportions (Plate 16). The moderately to strongly and sometimes entirely iddingsitised olivine phenocrysts and microphenocrysts show signs of partial resorption. The zoned clinopyroxene phenocrysts and microphenocrysts are generally pale tan in colour, but often have pale green, sometimes sieve-textured and Fe-Ti oxide-rich cores and tan to

tan-violet rims. The fine-grained groundmass of these rocks contains abundant plagioclase with subordinate amounts of clinopyroxene, Fe-Ti oxide, olivine and accessory alkali feldspar and apatite.

The *shoshonites* are porphyritic rocks with subtrachytic texture, containing phenocrysts of amphibole, clinopyroxene and feldspars. The abundant amphibole phenocrysts and microphenocrysts typically have thick, opaque reaction rims, rich in Fe-Ti oxide. Electron microprobe analyses of amphibole phenocrysts in Rejuvenescent Phase Mayotte lavas are reported in Table 6.4. These amphiboles are kaersutitic in composition (Ti atomic proportions > 0.5; Leake, 1978), containing 4.7 to 6.3 wt.% TiO_2. Clinopyroxene occurs as pale tan to pale green phenocrysts and microphenocrysts. The fine-grained, light-grey groundmass is dominated by flow-aligned laths of plagioclase, with subordinate interstitial Fe-Ti oxide, alkali feldspar, clinopyroxene, amphibole and apatite.

Karthala-type lavas:

Of all the subgroups defined within the present Mayotte sample collection, the Karthala-type Rejuvenescent Phase lavas display the greatest compositional range. Using the total alkali-silica diagram (Fig. 6.1), they may be classified as alkali basalts (MA-8, MA-35), basanites (MA-1, MA-66), trachybasalts (two hawaiites: MA-9, MA-67; one potassic trachybasalt: MA-11), one phonotephrite (MA-3), one mugearite (MA-6), benmoreites (MA-14a, MA-59), one phonolite (MA-18) and trachytes (MA-5, MA-65, MA-20).

The *alkali basalts, basanites and trachybasalts* range in texture from slightly to highly vesicular and from microporphyritic to seriate-textured and porphyritic. As in the case of other relatively mafic Comores lavas, clinopyroxene and olivine tend to be the dominant phenocryst phases, but other minerals, such as amphibole, alkali feldspar, titanomagnetite and rarely plagioclase also occur as phenocrysts and microphenocrysts in these rocks. Amphibole is in fact the dominant phenocryst phase in one alkali basalt (MA-35) and comprises about a third of all phenocrysts in one of the basanites (MA-66), whereas the potassic trachybasalt (MA-11) contains alkali feldspar as a major phenocryst phase. The typically subhedral phenocrysts and microphenocrysts of olivine often display signs of partial resorption and their degree of alteration ranges from slight to complete

TABLE 6.4
Amphibole analyses from Mayotte lavas

	Karthala-type Rejuvenescent Phase															
Sample	*MA-3*	*MA-3*	*MA-3*	*MA-6*	*MA-6*	*MA-6*	*MA-6*	*MA-6*	*MA-11*	*MA-14a*	*MA-14a*	*MA-18*	*MA-18*	*MA-18*	*MA-35*	*MA-35*
SiO_2	39.84	40.00	39.83	40.57	40.07	40.20	40.65	40.35	38.81	40.08	39.61	38.93	38.54	40.08	39.76	40.25
TiO_2	6.05	5.76	5.75	4.86	4.66	5.27	5.71	5.81	5.88	5.53	4.92	5.34	5.13	5.20	5.20	5.46
Al_2O_3	13.71	13.44	13.42	13.62	13.07	13.44	13.65	13.54	13.35	13.30	13.34	13.49	13.10	13.13	13.50	13.47
FeO	11.66	12.10	11.92	14.52	16.39	12.47	12.90	11.18	13.12	11.71	14.56	15.86	17.45	13.72	13.65	12.82
MnO	0.14	*n.d.*	0.19	0.26	0.28	*n.d.*	0.19	*n.d.*	0.23	0.13	0.22	0.27	0.33	0.22	0.21	0.15
MgO	12.49	12.24	12.33	11.01	10.08	12.09	11.70	12.87	11.78	12.51	10.77	9.70	8.94	11.22	11.30	11.83
CaO	12.47	12.22	12.31	11.86	11.68	11.85	11.91	12.09	11.99	11.97	11.87	11.88	11.81	11.77	12.46	12.35
Na_2O	2.63	2.80	2.72	2.59	2.64	2.62	2.78	2.55	2.56	2.67	2.67	2.77	2.79	3.00	2.65	2.66
K_2O	0.81	0.81	0.81	1.11	1.13	1.09	0.90	1.03	0.98	1.03	1.09	1.21	1.33	1.04	1.30	1.25
Total	99.79	99.36	99.29	100.40	100.00	99.03	100.38	99.42	99.68	99.93	99.06	99.43	99.41	99.36	100.03	100.23

n.d. = *not detected*

TABLE 6.4 *continued*

	Karthala-type Rejuvenescent Phase								*La Grille-type Rejuvenescent Phase*						
Sample	*MA-35*	*MA-35*	*MA-35*	*MA-59*	*MA-59*	*MA-59*	*MA-59*	*MA-66*	*MA-17*	*MA-17*	*MA-17*	*MA-17*	*MA-17*	*MA-34*	*MA-34*
SiO_2	39.25	39.69	39.21	38.63	39.14	39.01	39.20	40.13	39.57	40.07	39.76	40.02	40.00	39.40	39.44
TiO_2	6.26	5.97	6.03	5.10	5.10	5.19	5.12	5.71	5.88	5.81	5.08	5.57	5.59	5.40	6.56
Al_2O_3	13.72	13.71	13.67	13.61	13.39	13.67	13.40	12.98	13.60	13.29	13.21	13.37	13.26	13.52	13.84
FeO	11.38	11.63	11.92	16.14	15.10	15.79	14.72	11.18	11.75	11.35	14.35	12.50	12.08	12.60	12.83
MnO	*n.d.*	0.16	*n.d.*	0.36	0.23	0.25	0.26	*n.d.*	*n.d.*	0.14	0.28	0.15	0.15	0.14	0.14
MgO	12.65	12.40	13.38	9.47	10.45	9.72	10.41	12.94	12.68	13.01	11.12	12.07	12.54	12.31	12.02
CaO	12.64	12.68	12.58	12.25	12.03	12.18	12.17	12.34	12.01	12.25	11.75	11.91	11.94	12.08	11.91
Na_2O	2.40	2.44	2.50	2.59	2.61	2.63	2.69	2.48	2.58	2.50	2.72	2.66	2.74	2.48	2.50
K_2O	1.21	1.28	1.13	1.37	1.33	1.32	1.36	1.15	1.03	1.03	1.10	0.96	1.06	1.20	1.23
Total	99.50	99.95	99.42	99.51	99.37	99.77	99.32	98.92	99.10	99.44	99.37	99.20	99.36	99.14	99.47

n.d. = *not detected*

iddingsitisation. Clinopyroxene phenocrysts and microphenocrysts are typically pale tan in colour, but frequently have lighter grey-tan to pale green and sometimes sieve-textured cores, and clear, darker tan to tan-violet rims (Plates 17 and 18). Concentric oscillatory and more irregular zonation patterns and inclusions of Fe-Ti oxide are common features in clinopyroxene phenocrysts and microphenocrysts which often occur as glomerophyric aggregates. Where amphibole phenocrysts occur, they have thick, opaque rims (Plate 19) and sometimes they are completely replaced by Fe-Ti oxide. Inclusions of clinopyroxene and Fe-Ti oxide are frequent in amphibole phenocrysts. The fine- to very fine-grained and occasionally partly glassy groundmass of these Karthala-type basalts, basanites and trachybasalts contains predominantly plagioclase, clinopyroxene and Fe-Ti oxide, with generally smaller amounts of alkali feldspar and olivine and at times accessory apatite and amphibole.

In the Karthala-type Rejuvenescent Phase rocks of *phonotephritic and mugearitic* compositions, which are seriate-textured, porphyritic lavas, olivine is not an important phenocryst phase. Amphibole is the dominant phenocryst mineral together with smaller quantities of clinopyroxene, plagioclase and titanomagnetite (Plate 20). MA-6 also contains a small number of alkali feldspar and olivine phenocrysts. The abundant amphibole phenocrysts have Fe-Ti oxide-rich reaction rims and frequently contain inclusions of clinopyroxene, plagioclase, Fe-Ti oxide and apatite. Clinopyroxene is present as zoned, pale tan to pale green and pale tan-violet phenocrysts and microphenocrysts, often containing Fe-Ti oxide inclusions (Plates 20 and 21). The subtrachytic groundmass of these lavas contains predominantly plagioclase laths with intergranular Fe-Ti oxide, pale tan to pale green clinopyroxene, alkali feldspar and accessory apatite.

In the *benmoreites* of this group of samples, which are slightly to moderately porphyritic lavas with subtrachytic to trachytic textures, amphibole is the dominant phenocryst phase together with feldspar (plagioclase and alkali feldspar). Titanomagnetite microphenocrysts occur in small numbers. Amphibole phenocrysts and microphenocrysts display Fe-Ti oxide-rich reaction rims (Plate 22). The amphibole phenocrysts, some of which show simple twinning, commonly contain inclusions of Fe-Ti oxide, apatite, feldspar and clinopyroxene. The groundmass is dominated by flow-aligned plagioclase

laths with intergranular Fe-Ti oxide, alkali feldspar and apatite.

The most evolved rocks amongst the Karthala-type Rejuvenescent Phase lavas are *trachytic and phonolitic* in composition. Their textures range from sparsely to moderately porphyritic and from subtrachytic to trachytic. Feldspar (plagioclase and alkali feldspar) tends to predominate over amphibole as phenocryst phase in these rocks (Plate 23), while clinopyroxene and titanomagnetite phenocrysts are rare. Where amphibole phenocrysts and microphenocrysts occur, they have thick, opaque reaction rims and in some cases they are totally replaced by Fe-Ti oxide. The light-grey, fine-grained groundmass is dominated by flow-aligned plagioclase laths (Plate 23) and alkali feldspar, with interstitial pale green aegirine-augite, Fe-Ti oxide, accessory apatite and in MA-18, titanite (sphene) (Plate 24).

Clinopyroxene Phenocrysts in Mayotte Lavas

Various kinds of clinopyroxene phenocrysts have already been described in Moheli lavas (see Chapter 5). Similar observations can be made for clinopyroxene phenocrysts in mafic to intermediate Mayotte lavas. Typically, these phenocrysts display pale grey-tan to pale green cores and darker tan to tan-violet rims. In many of the lavas, however, clinopyroxene phenocrysts show irregular sieve-textured cores, surrounded by pale grey-tan mantles and darker tan to tan-violet rims. In several Mayotte lavas, distinctly darker green and sometimes pleochroic green cores, which may or may not be sieve-textured, are observed (e.g. Plates 11, 17, 18 and 25).

6.3 Mineral Chemistry

Clinopyroxene, olivine, feldspar, Fe-Ti oxide, amphibole, nepheline and garnet phenocrysts from Mayotte lavas were analysed using the electron microprobe. The nepheline, garnet and amphibole analyses were reported in the previous section.

Clinopyroxene

A selection of analyses of clinopyroxene phenocrysts from Mayotte lavas are presented in Table 6.5 and the range in composition is depicted in Fig. 6.2. The complete dataset of Mayotte clinopyroxene analyses acquired during this study is contained in Table A2.1, Appendix A2.

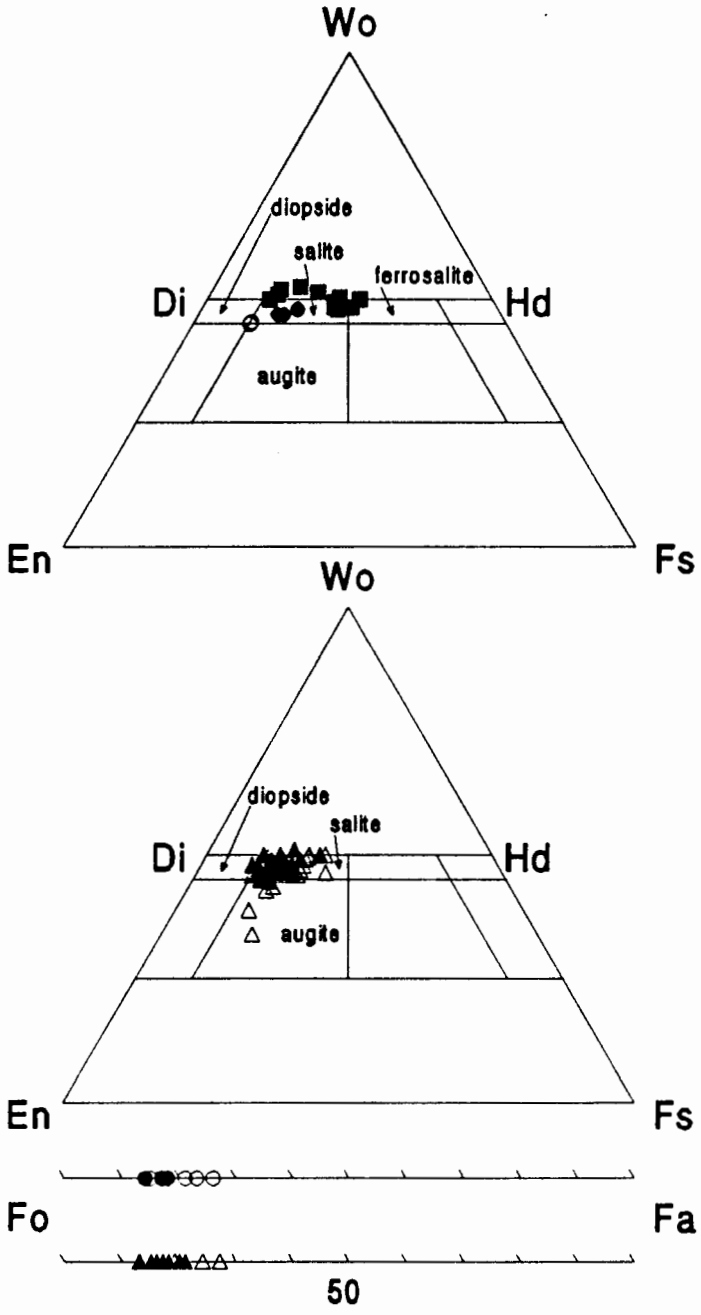

Fig. 6.2. Mineral chemistry of clinopyroxenes and olivines in Mayotte lavas. Symbols as in Fig. 6.1.

TABLE 6.5
Selected clinopyroxene analyses from Mayotte lavas

	KT Shield-building Phase		*LGT Shield-building Phase*		*Post-erosional Phase*			*Karthala-type Rejuvenescent Phase*		
Sample	*MA-30*	*MA-30*	*MA-60*	*MA-60*	*MA-55*	*MA-55*	*MA-73*	*MA-1*	*MA-3*	*MA-6*
SiO_2	50.94	50.96	49.23	49.56	43.70	45.36	48.60	50.19	47.76	45.43
TiO_2	1.05	1.13	1.43	0.99	4.37	3.20	1.21	1.37	2.28	2.83
Al_2O_3	2.76	2.79	4.20	4.08	9.29	7.30	3.52	3.01	6.16	7.54
Cr_2O_3	0.52	0.40	*n.d.*	*n.d.*	*n.d.*	*n.d.*	*n.d.*	*n.d.*	0.13	*n.d.*
FeO	6.05	6.23	8.17	8.77	8.45	12.71	13.30	7.89	7.06	10.03
MnO	0.15	0.15	0.24	0.21	*n.d.*	0.32	0.49	0.15	0.15	0.20
MgO	15.61	15.54	13.35	12.82	10.14	8.27	9.06	14.40	13.47	10.98
CaO	21.87	22.01	22.36	22.12	22.86	22.01	21.71	22.04	22.93	21.89
Na_2O	0.29	0.25	0.66	0.87	0.73	1.11	1.33	0.45	0.46	0.78
Total	99.23	99.45	99.64	99.41	99.53	100.28	99.22	99.50	100.40	99.68
Wo	0.45	0.46	0.47	0.47	0.52	0.50	0.48	0.46	0.48	0.48
En	0.45	0.44	0.39	0.38	0.32	0.26	0.28	0.41	0.40	0.34
Fs	0.10	0.10	0.14	0.15	0.15	0.23	0.24	0.13	0.12	0.18

TABLE 6.5 *continued*

	Karthala-type Rejuvenescent Phase						*La Grille-type Rejuvenescent Phase*			
Sample	*MA-8*	*MA-9*	*MA-14a*	*MA-35*	*MA-59*	*MA-67*	*MA-7*	*MA-12*	*MA-17*	*MA-33*
SiO_2	48.88	49.02	49.79	45.99	47.34	49.50	48.07	47.73	49.82	47.71
TiO_2	1.68	1.73	1.38	2.26	1.89	1.64	1.90	2.14	1.42	2.20
Al_2O_3	5.71	4.76	4.88	6.91	6.14	3.74	5.78	6.16	3.95	5.45
Cr_2O_3	*n.d.*	*n.d.*	0.30	*n.d.*	*n.d.*	*n.d.*	*n.d.*	0.17	*n.d.*	0.14
FeO	8.55	7.55	7.09	10.45	10.31	9.16	8.45	7.35	7.41	6.36
MnO	0.13	0.13	0.13	0.29	0.30	*n.d.*	0.16	*n.d.*	0.14	*n.d.*
MgO	12.86	14.07	14.46	10.39	10.63	14.30	12.60	13.38	14.49	13.61
CaO	21.51	21.82	21.49	22.49	22.59	20.83	21.85	22.15	21.63	23.63
Na_2O	0.77	0.44	0.54	0.99	0.95	0.42	0.77	0.51	0.51	0.47
Total	100.10	99.51	100.07	99.76	100.15	99.58	99.58	99.60	99.37	99.56
Wo	0.47	0.46	0.45	0.50	0.50	0.44	0.47	0.48	0.45	0.50
En	0.39	0.41	0.43	0.32	0.32	0.42	0.38	0.40	0.42	0.40
Fs	0.14	0.13	0.12	0.18	0.18	0.15	0.15	0.12	0.13	0.10

n.d. = not detected. KT=Karthala-type; LGT=La Grille-type.

Most of the clinopyroxenes are salites, although a few diopsides, augites and ferrosalites also occur. Clinopyroxenes in lavas of the Shield-building Phase ($Wo_{45}En_{45}Fs_{10}$ to $Wo_{47}En_{38}Fs_{15}$) and the Rejuvenescent Phase ($Wo_{46}En_{44}Fs_{10}$ to $Wo_{50}En_{30}Fs_{20}$) overlap in the compositional fields of salite, augite and diopside. Clinopyroxene phenocrysts from the Post-erosional Phase lavas define a trend of iron-enrichment from salite to ferrosalite ($Wo_{50}En_{39}Fs_{11}$ to $Wo_{48}En_{26}Fs_{26}$). Like their counterparts in Grande Comore and Moheli lavas, clinopyroxene phenocrysts in Mayotte lavas are relatively rich and variable in TiO_2, Al_2O_3 and Na_2O. The relatively sodic nature of these clinopyroxenes is consistent with the alkaline character of their host lavas, suggesting an appreciable aegirine content and a trend towards aegirine-augite compositions.

Green-core clinopyroxene phenocrysts:

It was noted in the previous section, that some of the mafic to intermediated Mayotte lavas contain clinopyroxene phenocrysts with distinctly darker green, sometimes pleochroic cores, pale grey-tan to almost colourless mantles and darker tan to tan-violet rims. The cores of these phenocrysts, some of which are sieve-textured, are often rounded or irregular in shape and exhibit optically sharp contacts with their surrounding mantles. The transition from mantle to rim, on the other hand, is gradational, rather than sharp. Several of these green-core clinopyroxene phenocrysts in Mayotte lavas were analysed with the electron microprobe. Analyses of cores, mantles and rims of these phenocrysts are presented in Table 6.6.

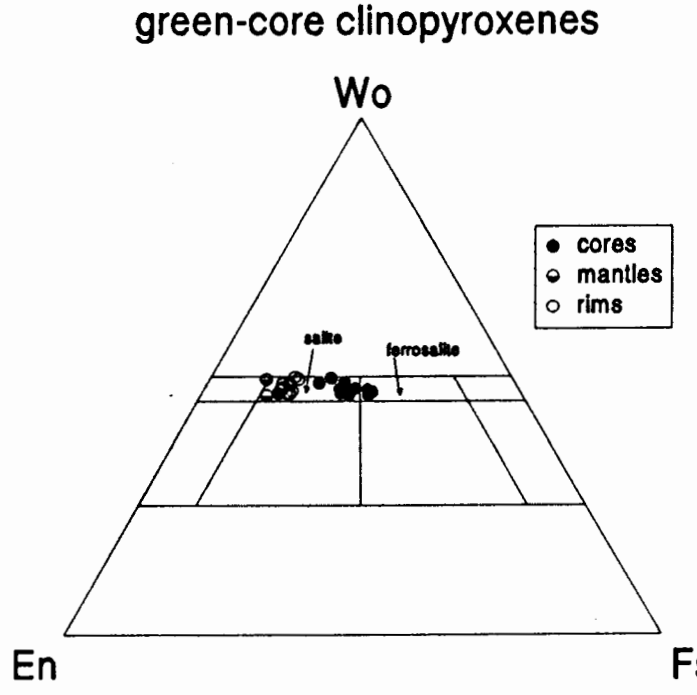

Fig. 6.3. En-Wo-Fs triangular diagram showing core, mantle and rim composition of green-core clinopyroxene phenocrysts in Mayotte lavas.

TABLE 6.6
Green-core clinopyroxene analyses from Mayotte lavas

	LGT Shield-building Phase		*Karthala-type Rejuvenescent Phase*				*La Grille-type Rejuvenescent Phase*					
Sample	*MA-60*		*MA-11*				*MA-7*					
	core	*core*	*core*	*core*	*rim*	*rim*	*core*	*core*	*mantle*	*mantle*	*rim*	*rim*
SiO_2	47.79	48.35	48.81	49.44	47.37	46.73	48.52	49.40	47.81	46.84	48.12	47.14
TiO_2	1.17	1.16	0.99	0.88	2.29	2.53	1.01	0.80	2.00	2.45	2.70	2.70
Al_2O_3	5.33	4.57	3.52	3.37	5.95	6.82	3.14	2.76	5.66	6.40	4.90	5.49
Cr_2O_3	*n.d.*	*n.d.*	*n.d.*	*n.d.*	*n.d.*	*n.d.*	*n.d.*	*n.d.*	*n.d.*	*n.d.*	*n.d.*	*n.d.*
FeO	13.55	12.45	13.96	13.15	8.24	8.51	15.38	15.44	7.59	7.70	8.80	8.70
MnO	0.50	0.48	0.65	0.62	0.24	0.15	0.78	0.79	0.14	*n.d.*	0.18	0.16
MgO	8.52	9.56	9.56	9.98	13.18	12.89	8.29	8.19	13.81	13.45	12.83	13.09
CaO	20.82	21.26	21.42	21.70	21.90	21.65	20.95	21.21	22.18	22.24	22.27	22.03
Na_2O	2.00	1.84	1.13	1.13	0.58	0.60	1.55	1.59	0.51	0.54	0.52	0.54
Total	99.67	99.66	100.04	100.26	99.74	99.89	99.62	100.18	99.70	99.62	100.29	99.86
Wo	0.48	0.47	0.46	0.47	0.47	0.47	0.46	0.47	0.47	0.47	0.47	0.47
En	0.27	0.30	0.29	0.30	0.39	0.39	0.26	0.25	0.40	0.40	0.38	0.38
Fs	0.25	0.23	0.25	0.23	0.14	0.14	0.28	0.28	0.13	0.13	0.15	0.15

TABLE 6.6 *continued*

	La Grille-type Rejuvenescent Phase											
Sample	*MA-33*				*MA-33*			*MA-33*				
	core	*core*	*mantle*	*rim*	*core*	*mantle*	*rim*	*core*	*core*	*mantle*	*rim*	
SiO_2	45.85	46.55	49.15	48.18	47.22	45.54	45.37	46.85	45.17	47.55	43.47	
TiO_2	2.46	1.90	1.79	2.37	1.44	2.92	3.47	1.99	2.75	2.09	3.76	
Al_2O_3	7.06	5.75	4.22	5.17	5.75	8.27	7.62	6.46	7.88	5.92	9.06	
Cr_2O_3	*n.d.*	*n.d.*	0.22	*n.d.*	*n.d.*	0.09	*n.d.*	*n.d.*	*n.d.*	*n.d.*	*n.d.*	
FeO	12.19	15.00	6.82	7.34	14.56	8.04	8.03	10.49	11.09	7.67	8.44	
MnO	0.41	0.56	*n.d.*	0.20	0.60	0.13	0.14	0.33	0.34	0.15	0.14	
MgO	8.81	7.64	14.78	13.06	7.84	12.47	11.78	10.65	9.62	13.18	11.60	
CaO	21.13	20.21	22.31	22.76	20.55	22.48	22.72	22.13	22.12	22.45	22.40	
Na_2O	1.68	2.01	0.41	0.53	2.01	0.60	0.58	1.02	1.18	0.64	0.63	
Total	99.59	99.62	99.70	99.62	99.97	100.54	99.71	99.92	100.15	99.65	99.51	
Wo	0.49	0.47	0.46	0.49	0.48	0.49	0.50	0.49	0.50	0.48	0.49	
En	0.28	0.25	0.43	0.39	0.25	0.37	0.36	0.33	0.30	0.39	0.36	
Fs	0.23	0.28	0.11	0.12	0.27	0.14	0.14	0.18	0.20	0.13	0.15	

n.d. = not detected; LGT = La Grille-type.

The green cores differ significantly in composition from the mantles and rims (Figures 6.3 and 6.4). In the majority of cases, the cores have significantly higher FeO and Na_2O contents and lower MgO contents and *Mg-numbers* than the mantles and rims (Fig. 6.4). CaO is usually slightly lower in the cores than in the mantles and rims. SiO_2, Al_2O_3 and TiO_2 contents are somewhat more variable, but in general, SiO_2 concentrations tend to be higher in the cores than in the mantles and rims, whereas Al_2O_3 and TiO_2 contents tend to be lower in the cores than in the mantles and rims.

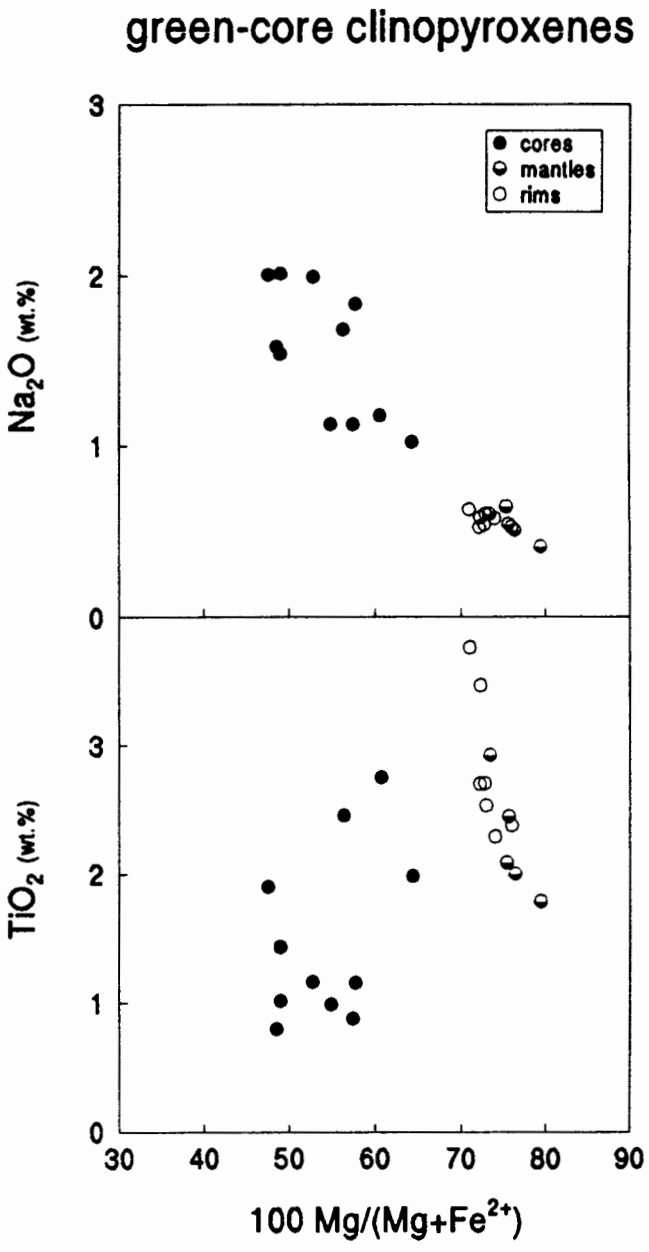

Fig. 6.4. Plots of Na_2O and Ti_2O (wt.%) vs Mg-number (atomic $100Mg/(Mg+Fe^{2+})$) for cores, mantles and rims of green-core clinopyroxene phenocrysts in Mayotte lavas.

Once again, the relatively high Na_2O contents (1.0-2.0 wt.%) of these green clinopyroxene cores are particularly noteworthy, since they imply appreciable aegirine contents and compositions approaching aegirine-augite. The chemical variations in the solid solution series augite→aegirine-augite(→aegirine) are dominated by the replacement reaction $NaFe^{3+} \rightleftharpoons \square Ca(Mg, Fe^{2+})$, consistent with the comparatively high Na_2O, but low CaO contents of the clinopyroxene cores, relative to their mantles and rims. Since the *Mg-numbers* plotted in Fig. 6.4 were calculated assuming all Fe to be in the divalent state, but aegirine contains Fe in the trivalent state, the *Mg-numbers* are likely to be slightly in error, although this does not distract from the fact that the clinopyroxene cores are chemically very different from their mantles and rims. In general, the cores appear to be more evolved compositionally than the mantles and rims. The chemical variations between mantles and rims, on the other hand, are consistent with the expected down-temperature evolution of clinopyroxene in a cooling body of magma (e.g. Ellis, 1976) and are probably the result of quenching at or near the surface: in most phenocrysts analysed, the rims have higher TiO_2 and FeO contents, but lower MgO contents and Mg-numbers than the mantles (Fig. 6.4).

Olivine

Selected analyses of olivines in Mayotte lavas are reported in Table 6.7 and individual analyses are shown in Fig. 6.2. The complete dataset of Mayotte olivine analyses acquired during this study is contained in Table A2.2, Appendix A2. Olivine phenocrysts in the La Grille-type Shield-building lavas tend to have slightly higher Fo-contents (Fo_{82} to Fo_{87}) than olivines in the Karthala-type Shield-building lavas (Fo_{74} to Fo_{86}). Similarly, olivines in the La Grille-type Rejuvenescent Phase lavas are generally more magnesian (Fo_{77} to Fo_{87}) than olivines in the Karthala-type Rejuvenescent Phase lavas (Fo_{73} to Fo_{85}). Most of the olivine phenocrysts analysed from Mayotte lavas appear to be in equilibrium or near-equilibrium with their respective host rocks (Fig. 6.5) and only a relatively small number of the analysed phenocrysts have $K_D^{Fe\text{-}Mg}$ values which are too high or too low for them to be in equilibrium with their host rocks, implying that they might be xenocrysts.

TABLE 6.7
Selected olivine analyses from Mayotte lavas

	KT Shield-building Phase			*LGT Shield-bldg Phase*		*KT Rejuvenescent Phase*	
Sample	*MA-29*	*MA-29*	*MA-30*	*MA-60*	*MA-60*	*MA-1*	*MA-8*
SiO_2	38.15	38.95	39.95	39.59	40.29	37.54	39.00
TiO_2	*n.d.*	*n.d.*	*n.d.*	*n.d.*	*n.d.*	*n.d.*	*n.d.*
Al_2O_3	*n.d.*	*n.d.*	*n.d.*	*n.d.*	*n.d.*	*n.d.*	*n.d.*
Cr_2O_3	*n.d.*	*n.d.*	*n.d.*	*n.d.*	*n.d.*	*n.d.*	*n.d.*
FeO	23.18	19.38	12.67	16.18	12.20	24.33	17.87
MnO	0.31	0.26	0.20	0.20	0.20	0.33	0.22
MgO	37.98	41.16	45.97	42.91	45.85	36.99	42.64
CaO	0.31	0.29	0.28	0.25	0.31	0.20	0.27
NiO	0.21	0.29	0.28	0.27	0.18	0.17	0.27
Total	100.14	100.33	99.35	99.40	99.03	99.55	100.28
Fo	0.74	0.79	0.86	0.82	0.87	0.73	0.81

n.d. = not detected; KT=Karthala-type; LGT=La Grille-type.

TABLE 6.7 ***continued***

	Karthala-type Rejuvenescent Phase			*La Grille-type Rejuvenescent Phase*			
Sample	*MA-11*	*MA-66*	*MA-66*	*MA-7*	*MA-12*	*MA-22*	*MA-33*
SiO_2	38.56	38.96	40.15	38.47	39.01	39.84	40.33
TiO_2	*n.d.*	*n.d.*	*n.d.*	*n.d.*	*n.d.*	*n.d.*	*n.d.*
Al_2O_3	*n.d.*	*n.d.*	*n.d.*	*n.d.*	*n.d.*	*n.d.*	*n.d.*
Cr_2O_3	*n.d.*	*n.d.*	*n.d.*	*n.d.*	*n.d.*	*n.d.*	*n.d.*
FeO	21.60	19.27	13.56	20.41	18.23	14.92	12.51
MnO	0.26	0.27	0.19	0.26	0.22	0.12	*n.d.*
MgO	39.27	41.06	45.06	40.03	42.00	44.49	46.39
CaO	0.22	0.27	0.23	0.16	0.25	0.22	0.20
NiO	0.22	0.19	0.29	0.19	0.24	0.28	0.32
Total	100.12	100.02	99.48	99.51	99.94	99.87	99.75
Fo	0.76	0.79	0.85	0.77	0.80	0.84	0.87

n.d. = not detected.

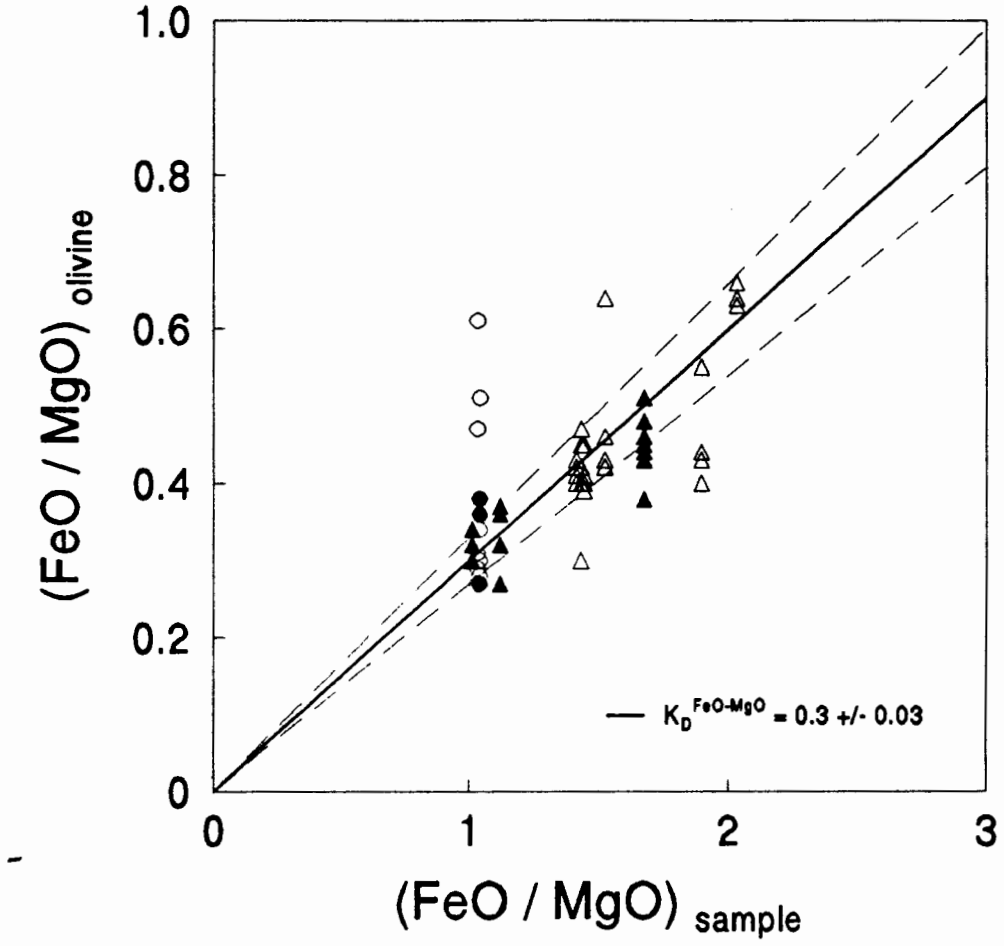

Fig. 6.5. Plot of $(FeO/MgO)_{olivine}$ vs $(FeO/MgO)_{sample}$ for olivine phenocrysts from Mayotte lavas. Symbols as in Fig. 6.1. Solid line: $K_D^{Fe-Mg}=0.3$. Stippled lines: $K_D^{Fe-Mg}=0.33$ and $K_D^{Fe-Mg}=0.27$.

Feldspar

Selected electron microprobe analyses of feldspar phenocrysts from Rejuvenescent Phase Mayotte lavas are presented in Table 6.8 and individual analyses are plotted in Fig. 6.6. The complete set of Mayotte feldspar analyses acquired during this study is contained in Table A2.3, Appendix A2. Feldspar phenocrysts in Karthala-type Rejuvenescent lavas show a considerable range in composition from moderately An-rich plagioclase (labradorite, $An_{64}Ab_{34}Or_2$) through more Ab-rich andesine, oligoclase and anorthoclase to sanidine ($An_1Ab_{50}Or_{49}$). Feldspars in La Grille-type Rejuvenescent Phase lavas overlap in composition with those in the Karthala-type Rejuvenescent Phase lavas, but do not reach the extremes on either end of the compositional trend, although this may reflect

TABLE 6.8
Selected feldspar analyses from Mayotte lavas

	Karthala-type Rejuvenescent Phase						
Sample	*MA-3*	*MA-5*	*MA-6*	*MA-11*	*MA-14*	*MA-18*	*MA-20*
SiO_2	53.77	63.36	59.56	61.54	62.38	60.79	66.81
Al_2O_3	29.47	24.32	25.93	24.77	23.97	25.22	19.87
FeO	0.36	0.24	0.29	0.18	0.26	0.23	0.33
MgO	*n.d.*	*n.d.*	*n.d.*	*n.d.*	*n.d.*	*n.d.*	*n.d.*
CaO	12.75	5.12	7.45	5.83	4.93	6.59	0.23
Na_2O	3.85	5.99	6.37	6.67	7.17	6.43	5.17
K_2O	0.27	1.51	0.73	1.00	1.34	0.82	7.78
Total	100.47	100.54	100.33	99.99	100.05	100.07	100.19
An	0.64	0.29	0.38	0.31	0.25	0.34	0.01
Ab	0.34	0.61	0.58	0.63	0.67	0.61	0.50
Or	0.02	0.10	0.04	0.06	0.08	0.05	0.49

n.d. = not detected.

TABLE 6.8 *continued*

	KT Rejuvenescent Phase			*La Grille-type Rejuvenescent Phase*			
Sample	*MA-59*	*MA-65*	*MA-66*	*MA-17*	*MA-34*	*MA-34*	*MA-34*
SiO_2	63.64	64.00	59.02	58.03	61.51	66.52	63.80
Al_2O_3	23.04	23.14	26.04	26.44	24.10	20.58	21.82
FeO	0.23	0.25	0.33	0.32	0.30	*n.d.*	0.28
MgO	*n.d.*	*n.d.*	*n.d.*	0.06	*n.d.*	*n.d.*	*n.d.*
CaO	4.15	3.62	7.94	8.98	5.89	1.79	3.52
Na_2O	7.52	6.80	5.44	5.89	7.09	7.51	7.75
K_2O	1.83	1.86	0.70	0.49	1.12	4.18	2.44
Total	100.40	99.67	99.47	100.21	100.00	100.57	99.60
An	0.21	0.20	0.43	0.44	0.29	0.09	0.17
Ab	0.68	0.68	0.53	0.53	0.64	0.67	0.69
Or	0.11	0.12	0.04	0.03	0.07	0.24	0.14

n.d. = not detected; KT=Karthala-type.

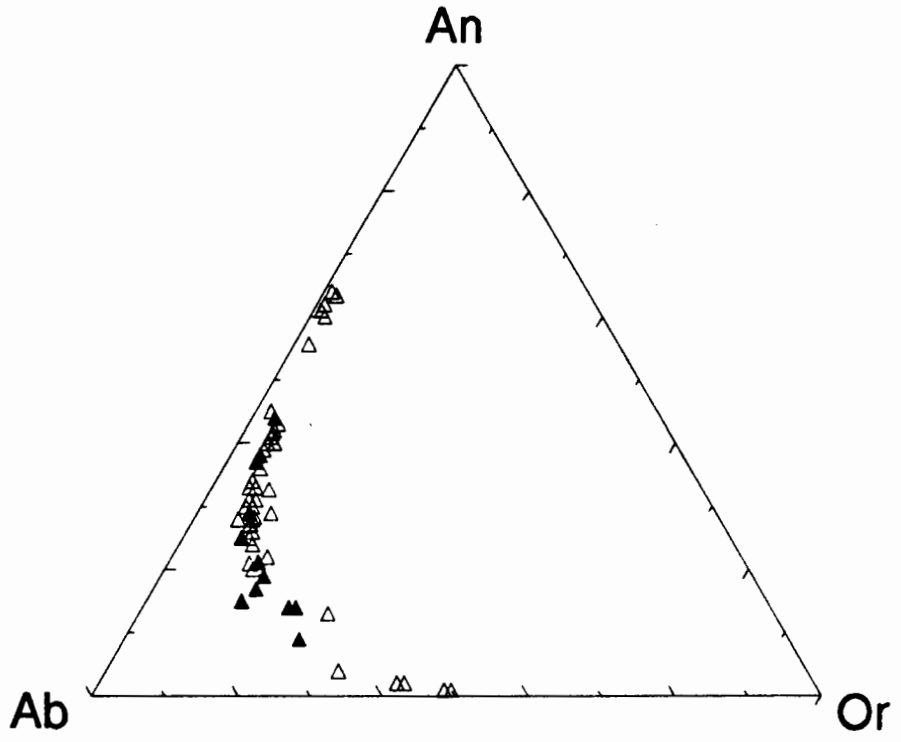

Fig. 6.6. Ab-An-Or triangular diagram showing the composition of feldspar phenocrysts in Rejuvenescent Phase Mayotte lavas. Symbols: open triangles: Karthala-type Rejuvenescent Phase; filled triangles: La Grille-type Rejuvenescent Phase.

the smaller number of analyses from these rocks. CaO contents in Mayotte feldspar phenocrysts range from 0.18 to 12.8 wt.%, whereas Na_2O and K_2O abundances vary from 3.9 to 7.8 wt.% and from 0.23 to 7.9 wt.% respectively.

Fe-Ti oxide

Analyses of Fe-Ti oxide microphenocrysts from Mayotte lavas are reported in Table 6.9 and are presented graphically in Fig. 6.7. All of the Fe-Ti oxides analysed belong to the ulvöspinel-magnetite solid solution series. Fe-Ti oxides from the Post-erosional and Rejuvenescent Phase lavas overlap in composition. The TiO_2 content of Fe-Ti oxides in Mayotte lavas ranges from 15.3 to 25.4 wt.% and tends to be considerably higher in the La Grille-type Rejuvenescent Phase lavas (average = 23.6 wt.%) than in the Post-erosional Phase and Karthala-type Rejuvenescent Phase lavas (average = 17.8 wt.%). Furthermore, Fe-Ti oxides in the La Grille-type Rejuvenescent Phase lavas have significantly greater

TABLE 6.9
Titanomagnetite analyses from Mayotte lavas

	Post-erosional Phase		*Karthala-type Rejuvenescent Phase*								
Sample	*MA-55*	*MA-55*	*MA-3*	*MA-3*	*MA-3*	*MA-6*	*MA-8*	*MA-8*	*MA-11*	*MA-14a*	*MA-35*
SiO_2	*n.d.*	*n.d.*	*n.d.*	0.10	0.10	0.09	*n.d.*	0.14	0.52	0.13	*n.d.*
TiO_2	16.30	16.57	17.71	17.87	16.63	17.51	19.79	19.36	20.46	18.94	15.92
Al_2O_3	5.84	5.40	4.09	3.55	5.86	2.99	6.32	6.73	4.95	1.48	3.67
Cr_2O_3	0.32	0.12	0.14	0.45	*n.d.*	*n.d.*	0.19	1.78	*n.d.*	0.21	*n.d.*
FeO	39.55	40.11	43.33	43.77	41.13	42.26	42.55	43.09	44.74	46.00	40.24
Fe_2O_3	33.02	32.57	31.24	30.86	32.20	33.66	25.70	23.71	24.85	30.26	36.19
MnO	0.92	1.00	0.84	0.92	0.77	0.72	0.38	0.39	0.58	1.13	0.57
MgO	4.20	3.78	2.30	2.27	3.44	3.32	4.53	4.45	3.94	1.13	3.31
CaO	*n.d.*	0.08	*n.d.*	*n.d.*	*n.d.*	*n.d.*	*n.d.*	*n.d.*	0.19	*n.d.*	*n.d.*
Total	100.15	99.63	99.63	99.78	99.94	100.53	99.47	99.65	100.22	99.29	99.91
Us	0.50	0.51	0.53	0.54	0.51	0.51	0.61	0.61	0.62	0.55	0.47
Mt	0.50	0.49	0.47	0.46	0.49	0.49	0.39	0.39	0.38	0.45	0.53

n.d. = *not detected*; Fe_2O_3 calculated according to stoichiometry.

TABLE 6.9 ***continued***

	Karthala-type Rejuvenescent Phase			*La Grille-type Rejuvenescent Phase*						
Sample	*MA-35*	*MA-35*	*MA-59*	*MA-12*	*MA-12*	*MA-12*	*MA-33*	*MA-33*	*MA-33*	*MA-34*
SiO_2	*n.d.*	0.08	0.10	*n.d.*	*n.d.*	*n.d.*	0.10	0.10	0.13	0.08
TiO_2	18.08	17.99	15.34	21.36	24.17	25.38	23.19	25.17	24.47	18.35
Al_2O_3	5.32	5.46	3.60	5.95	4.56	4.54	5.23	3.34	3.85	2.89
Cr_2O_3	*n.d.*	*n.d.*	*n.d.*	0.45	*n.d.*	*n.d.*	1.21	0.23	0.32	*n.d.*
FeO	41.09	41.08	41.47	45.30	47.98	49.22	48.23	50.65	49.67	44.29
Fe_2O_3	31.17	30.78	36.11	22.59	19.43	17.58	18.80	17.35	17.81	30.97
MnO	0.50	0.61	0.95	0.46	0.53	0.67	0.77	0.88	0.70	0.90
MgO	4.26	4.35	2.29	3.80	3.21	3.26	3.12	2.30	2.45	2.16
CaO	*n.d.*	*n.d.*	*n.d.*	*n.d.*	*n.d.*	*n.d.*	*n.d.*	0.11	*n.d.*	*n.d.*
Total	100.41	100.36	99.86	99.92	99.87	100.65	100.65	100.12	99.40	99.64
Us	0.54	0.54	0.46	0.66	0.72	0.75	0.71	0.74	0.74	0.54
Mt	0.46	0.46	0.54	0.33	0.28	0.25	0.29	0.26	0.26	0.46

n.d. = *not detected*; Fe_2O_3 calculated according to stoichiometry.

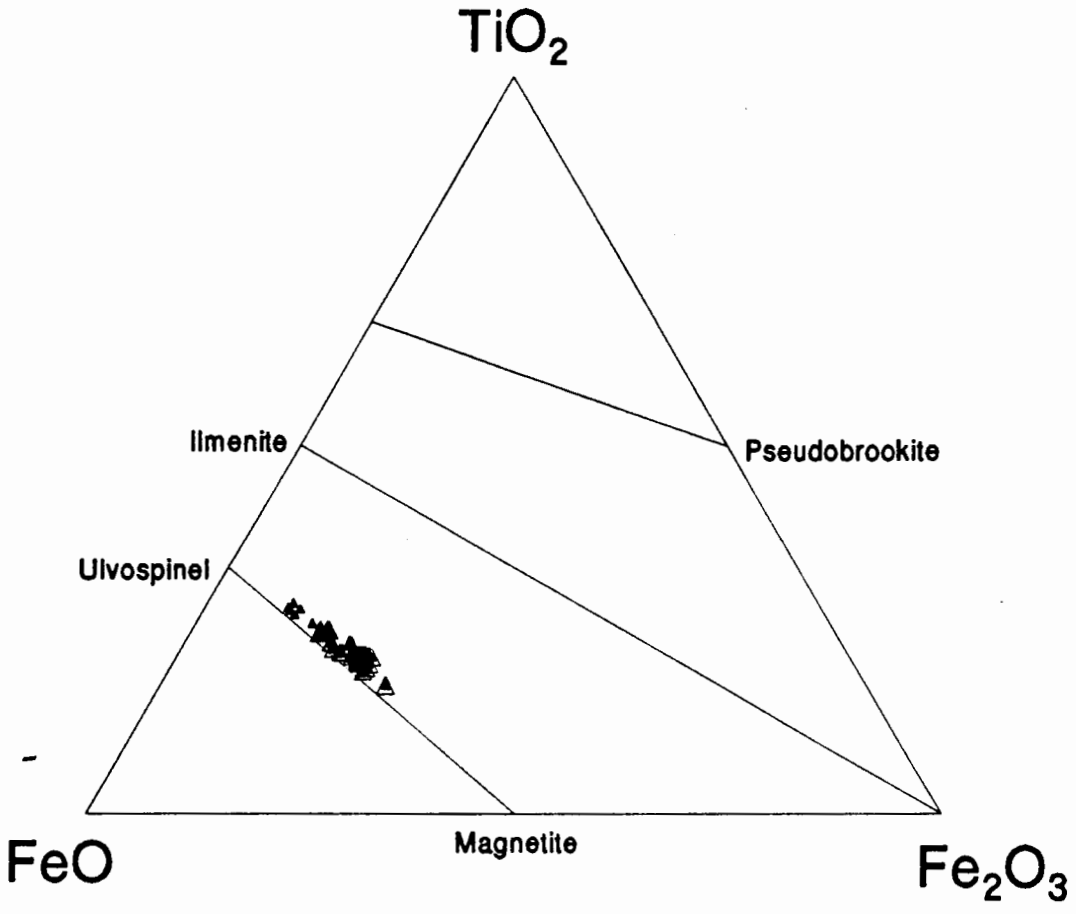

Fig. 6.7. Triangular diagram of FeO, TiO_2 and Fe_2O_3 (molecular proportions) showing the composition of Fe-Ti oxides in Mayotte lavas. Diagonal lines indicate solid-solution series. Symbols: small filled triangles: La Grille-type Rejuvenescent Phase; open triangles: Karthala-type Rejuvenescent Phase; filled squares: Post-erosional Phase.

FeO/Fe_2O_3 ratios[1] (average=2.42) and thus tend to contain comparatively larger proportions of the ulvöspinel molecule (Us_{54}-Us_{75}) than Fe-Ti oxides in the Post-erosional Phase and Karthala-type Rejuvenescent Phase lavas (average FeO/Fe_2O_3=1.39; Us_{46}-Us_{62}), suggesting that the Fe-Ti oxides in the La Grille-type Rejuvenescent Phase lavas crystallised under conditions of appreciably lower oxygen fugacity than those in the Post-erosional Phase and Karthala-type Rejuvenescent Phase lavas.

[1]calculated according to stoichiometry

6.4 Bulk Rock Chemistry

Major and Minor Elements

The major and minor element compositions of Mayotte lavas are presented in Table 6.10 and the compositional range of these lavas is depicted graphically in Figures 6.1, 6.8 and 6.9. Before plotting on diagrams, the major and minor element data were normalised to 100 per cent on a volatile free basis.

The considerable range in compositions and the variety of rock types amongst Mayotte lavas was noted previously (Fig. 6.1). The majority of Mayotte lavas are nepheline-normative, with the exception of several Rejuvenescent Phase lavas, which contain normative hypersthene and rarely quartz (Fig. 6.8).

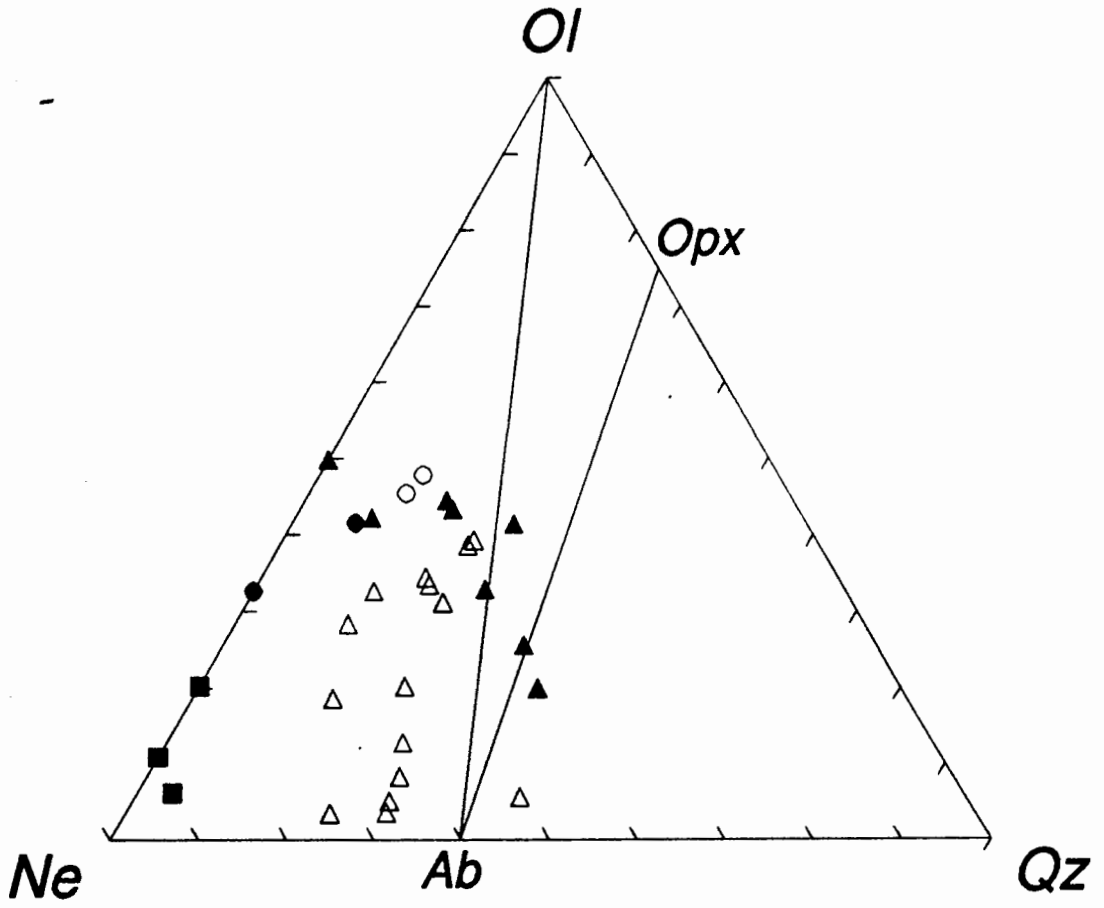

Fig. 6.8. Mayotte lavas plotted on the basal projection of the normative Cpx-Ol-Ne-Qz tetrahedron, projected from Cpx according to Irvine and Baragar (1971). Symbols as in Fig. 6.1.

TABLE 6.10

Bulk-rock analyses and selected trace element ratios of Mayotte lavas

	KT Shield-bldg Phase		*LGT Shield-bldg Phase*		*Post-erosional Phase*			*Karthala-type Rejuvenescent Phase*							
Sample	*MA-29*	*MA-30*	*MA-60*	*MA-61*	*MA-55*	*MA-73*	*MA-81*	*MA-1*	*MA-3*	*MA-5*	*MA-6*	*MA-8*	*MA-9*	*MA-11*	*MA-14a*
	AB	*AB*	*Bas*	*Neph*	*Teph*	*Neph*	*Neph*	*Bas*	*Pt*	*Tr*	*Mu*	*AB*	*Ha*	*PTb*	*Ben*
SiO_2	45.34	45.25	42.56	39.76	40.10	45.49	41.81	44.31	47.39	59.10	50.20	46.73	46.66	46.91	52.80
TiO_2	2.33	2.38	3.43	3.66	3.12	1.19	2.13	3.23	2.01	0.57	2.38	2.90	2.86	3.09	1.57
Al_2O_3	11.82	11.93	11.82	13.83	14.99	18.62	16.48	13.32	17.33	19.58	16.63	14.30	14.12	15.18	17.00
Fe_2O_3	1.61	1.62	1.61	1.65	1.46	0.89	1.26	1.84	1.21	0.49	1.23	1.56	1.55	1.55	0.98
FeO	10.71	10.79	10.76	11.02	9.70	5.94	8.39	12.28	8.09	3.27	8.23	10.39	10.34	10.35	6.52
MnO	0.19	0.19	0.17	0.19	0.23	0.30	0.25	0.19	0.17	0.14	0.18	0.17	0.17	0.18	0.17
MgO	10.42	10.40	10.33	7.38	5.14	2.47	4.70	6.03	4.28	0.44	4.17	7.38	6.81	5.47	2.65
CaO	10.86	11.29	11.08	13.80	11.56	6.46	10.13	8.47	7.78	1.94	7.13	9.45	9.55	8.91	5.38
Na_2O	3.49	3.11	4.08	4.51	5.15	8.11	7.25	4.56	6.23	7.94	5.29	3.13	3.80	3.72	6.02
K_2O	1.11	1.07	0.73	0.84	1.58	3.66	2.49	2.12	2.23	4.83	2.67	1.55	1.61	1.95	3.33
P_2O_5	0.44	0.49	0.58	0.61	1.10	0.45	0.75	1.07	0.83	0.08	0.75	0.66	0.67	0.76	0.49
LOI	1.00	1.25	0.39	3.23	3.87	4.60	1.02	1.85	2.28	0.58	0.23	1.54	1.48	2.24	1.81
H_2O-	0.24	0.27	2.64	0.41	1.31	1.73	3.26	0.82	0.43	1.34	1.32	0.69	0.47	0.67	0.60
Total	99.54	100.03	100.17	100.89	99.32	99.92	99.89	100.08	100.26	100.28	100.41	100.44	100.08	100.97	99.32
Zr	162	166	206	211	289	473	329	390	367	738	470	302	303	296	572
Nb	44	44	62	80	125	199	153	111	130	145	108	71	72	75	116
Y	25	25	24	28	36	46	40	31	32	24	30	28	41	29	25
Rb	24	22	39	35	82	164	116	51	60	154	77	37	38	40	105
Ba	293	300	561	692	848	2623	759	660	946	1333	827	646	660	724	936
Sr	459	484	724	751	1394	1552	1211	1020	1009	514	968	773	767	887	887
Th	3.9	4.7	6.5	8.9	8.3	21	14.4	9.8	19.3	23	12.0	8.0	7.0	6.3	17.6
Co	65	65	66	50	38	14.5	28	56	29	3.5	33	49	55	42	20
Cr	696	661	479	95	26	1.1	66	96	54	6.4	57	188	208	83	38
Ni	254	274	257	63	25	*n.d.*	34	107	39	1.2	53	166	161	82	30
V	232	247	282	358	224	90	182	160	116	3.1	133	193	204	186	75
Zn	122	109	100	77	144	169	127	175	108	95	119	110	115	114	100
Cu	118	103	65	132	91	11.0	41	49	39	4.5	36	51	64	47	21
Sc	29	29	27	26	12.1	2.0	8.5	14.3	9.1	0.6	10.6	15.8	17.1	14.9	6.4
La	-	34	-	-	-	-	99	64	96	80	71	-	67	51	72
Ce	-	69	-	-	-	-	187	131	179	138	136	-	113	109	135
Nd	-	35	-	-	-	-	76	64	68	41	60	-	57	53	51
Zr/Nb	3.7	3.8	3.3	2.6	2.3	2.4	2.2	3.5	2.8	5.1	4.4	4.3	4.2	4.0	4.9
Zr/Y	6.5	6.6	8.6	7.5	8.0	10.3	8.2	12.6	11.5	31	15.7	10.8	7.4	10.2	23
Y/Nb	0.57	0.57	0.39	0.35	0.29	0.23	0.26	0.28	0.25	0.17	0.28	0.39	0.57	0.39	0.22
Ba/Nb	6.7	6.8	9.1	8.7	6.8	13.2	5.0	6.0	7.3	9.2	7.7	9.1	9.2	9.7	8.1
Mg#	0.63	0.63	0.63	0.54	0.49	0.43	0.50	0.47	0.49	0.19	0.47	0.56	0.54	0.49	0.42

Fe_2O_3 calculated assuming Fe_2O_3/FeO = 0.15; La, Ce and Nd determined by XRF; *Mg#* = atomic $Mg/(Mg+Fe^{2+})$ with Fe_2O_3/FeO = 0.15. *KT=Karthala-type; LGT=La Grille-type. AB* = alkali basalt; *Bas* = basanite; *Neph* = nephelinite; *Teph* = tephrite; *Pt* = phonotephrite; *Tr* = trachyte; *Mu* = mugearite; *Ha* = hawaiite; *PTb* = potassic trachybasalt; *Ben* = benmoreite. *n.d.* = *not detected.*

TABLE 6.10 *continued*

	Karthala-type Rejuvenescent Phase							*La Grille-type Rejuvenescent Phase*							
Sample	*MA-18*	*MA-20*	*MA-35*	*MA-59*	*MA-65*	*MA-66*	*MA-67*	*MA-2*	*MA-4*	*MA-7*	*MA-12*	*MA-17*	*MA-22*	*MA-33*	*MA-34*
	Phon	*Tr*	*AB*	*Ben*	*Tr*	*Bas*	*Ha*	*Bas*	*Bas*	*SaB*	*AB*	*Shosh*	*Bas*	*Bas*	*Shosh*
SiO_2	55.97	59.57	44.10	55.59	58.02	46.15	46.99	41.34	42.01	44.75	46.53	49.72	40.74	43.36	49.59
TiO_2	0.90	0.37	3.82	0.96	0.80	2.87	2.65	4.07	3.79	3.04	2.93	2.25	2.95	3.11	2.27
Al_2O_3	19.29	19.83	15.53	20.24	18.93	14.25	13.84	13.70	13.13	14.59	14.54	18.66	10.66	12.34	17.48
Fe_2O_3	0.61	0.40	1.72	0.60	0.67	1.50	1.57	1.76	1.69	1.62	1.52	1.26	1.72	1.66	1.21
FeO	4.09	2.64	11.44	4.0	4.46	9.98	10.44	11.71	11.29	10.82	10.16	8.39	11.46	11.04	8.05
MnO	0.14	0.07	0.20	0.18	0.17	0.18	0.16	0.17	0.16	0.18	0.17	0.15	0.20	0.19	0.16
MgO	1.14	0.26	5.07	1.07	0.78	6.96	7.27	6.84	8.69	6.47	6.07	1.71	11.30	9.86	3.16
CaO	3.41	0.57	9.35	3.63	3.00	8.87	8.32	10.52	10.09	8.86	9.16	3.66	13.02	10.79	6.24
Na_2O	8.20	5.15	2.75	6.63	7.59	5.21	4.26	2.64	3.12	2.63	3.42	4.02	3.52	4.00	3.68
K_2O	4.60	5.59	2.00	4.28	4.35	1.97	1.85	0.99	0.62	1.21	1.08	2.80	0.58	0.95	2.14
P_2O_5	0.27	0.07	0.93	0.28	0.22	0.71	0.79	0.92	0.83	0.68	0.70	0.82	0.92	0.71	0.69
LOI	1.37	2.86	2.93	2.24	1.25	1.27	0.49	4.48	3.33	3.66	2.28	3.59	2.36	2.06	3.39
H_2O-	0.54	1.68	1.01	0.79	0.46	0.32	1.25	1.54	0.95	1.92	0.89	2.40	0.63	0.54	2.20
Total	100.54	99.05	100.84	100.49	100.69	100.24	99.88	100.67	99.69	100.42	99.45	99.43	100.06	100.59	100.24
Zr	689	821	332	566	674	340	327	330	294	307	320	562	254	233	436
Nb	126	132	91	141	136	87	75	88	78	73	77	125	86	77	105
Y	22	62	36	26	46	28	25	30	29	31	31	26	30	30	32
Rb	141	169	43	89	127	76	44	15.4	19.3	11.2	11.4	30	16.1	31	16.9
Ba	822	1903	981	1266	1140	780	608	676	535	779	685	1354	592	836	1474
Sr	753	163	1026	1311	768	898	851	853	807	668	832	944	879	966	1063
Th	23	24	7.2	20	18.7	6.6	6.5	8.2	8.7	7.2	9.1	15.8	9.3	7.4	11.4
Co	8.1	*n.d.*	38	5.6	5.8	49	56	54	59	57	44	23	73	61	23
Cr	7.2	2.3	42	5.1	5.1	194	262	114	171	215	157	59	430	356	42
Ni	2.1	0.4	50	0.1	1.3	144	188	116	167	187	112	44	320	245	33
V	25	*n.d.*	224	27	10	188	164	208	208	211	196	103	246	219	125
Zn	100	158	128	106	95	111	138	114	106	121	113	119	117	102	115
Cu	7.2	2.1	49	5.9	5.2	55	56	72	60	40	46	30	71	43	32
Sc	1.8	0.3	15.3	1.3	1.4	15.3	17.5	17.6	18.8	20	17.1	10.4	27	18.9	9.8
La	73	317	62	86	124	62	49	67	58	58	56	79	-	-	70
Ce	119	66	128	143	158	116	99	140	122	115	114	140	-	-	128
Nd	37	152	63	46	64	53	50	69	59	52	54	57	-	-	57
Zr/Nb	5.5	6.22	3.7	4.0	5.0	3.9	4.4	3.8	3.8	4.2	4.2	4.5	3.0	3.0	4.2
Zr/Y	31	13.2	9.2	22	14.7	12.1	13.1	11.0	10.1	9.9	10.3	22	8.5	7.8	13.6
Y/Nb	0.17	0.47	0.40	0.18	0.34	0.32	0.33	0.34	0.37	0.42	0.40	0.21	0.35	0.39	0.30
Ba/Nb	6.5	14.4	10.8	9.0	8.4	9.0	8.1	7.7	6.9	10.7	8.9	10.8	6.9	10.9	14.0
Mg#	0.33	0.15	0.44	0.32	0.24	0.55	0.55	0.51	0.58	0.52	0.52	0.27	0.64	0.61	0.41

Fe_2O_3 calculated assuming Fe_2O_3/FeO = 0.15; La, Ce and Nd determined by XRF; *Mg#* = atomic $Mg/(Mg+Fe^{2+})$ with Fe_2O_3/FeO = 0.15. *AB* = alkali basalt; *Bas* = basanite; *Tr* = trachyte; *Ha* = hawaiite; *Ben* = benmoreite; *Phon* = phonolite; *SaB* = subalkali basalt; *Shosh* = shoshonite. *n.d.* = *not detected.*

The La Grille-type Shield-building lavas are notably richer in normative nepheline (15.2-21.3 wt.%) than the Karthala-type Shield-building lavas (8.2-10.0 wt.%). The Post-erosional Phase lavas have significantly greater contents of normative nepheline (25.1-37.0 wt.%) than any of the other Mayotte lavas analysed. The normative nepheline content of the Karthala-type Rejuvenescent Phase lavas ranges from 2.3 to 20.0 wt.%, with the only anomalous sample in this group being the highly trachyte MA-20, which contains 5.0 wt.% normative hypersthene and 5.3 wt.% normative quartz. Amongst the La Grille-type Rejuvenescent Phase lavas, the four basanites (MA-2, MA-4, MA-22, MA-33) are moderately to considerably nepheline-normative (4.2-16.6 wt.%). The remaining four La Grille-type Rejuvenescent Phase lavas (MA-7, MA-12, MA-17, MA-34), however, range from the very slightly nepheline-normative (0.55 wt.%) alkali basalt MA-12, through the hypersthene-normative MA-7 and MA-34, to the hypersthene- and quartz-normative MA-17 (Fig. 6.8).

Several major and minor elements are plotted against *Mg-number* in Fig. 6.9. Mayotte lavas display a considerable range in *Mg-numbers* (0.15-0.64) and relatively well-defined linear trends are observed on a number of the variation diagrams. Good negative correlations exist between *Mg-number* and SiO_2, Al_2O_3 and K_2O. Positive correlations exist between CaO and *Mg-number*, FeO and *Mg-number* and, less well-defined, between TiO_2 and *Mg-number*. In lavas with *Mg-numbers* between 0.50-0.64, P_2O_5 appears to be relatively constant in concentration, but from *Mg-number* 0.50, the P_2O_5 content of Mayotte lavas generally decreases with decreasing *Mg-number*, most probably reflecting the effects of apatite fractionation. Samples from the different lava groups identified on Mayotte broadly overlap in their major and minor element compositions. Amongst the Shield-building lavas, which have relatively high *Mg-numbers* (0.54-0.63), the La Grille-type lavas have slightly higher concentrations of TiO_2, Na_2O and CaO than the Karthala-type lavas. The Post-erosional Phase lavas range in *Mg-number* from 0.43-0.50 and tend to be relatively rich in CaO and Na_2O. Of all the groups of lavas identified on Mayotte, the Karthala-type Rejuvenescent Phase lavas show the greatest compositional variability, ranging in *Mg-number* from 0.15 to 0.56. The La Grille-type Rejuvenescent Phase lavas range from *Mg-number* 0.27 to 0.64 and at similar *Mg-numbers* tend to contain less K_2O and Na_2O than the Karthala-type Rejuvenescent Phase lavas. The major and minor

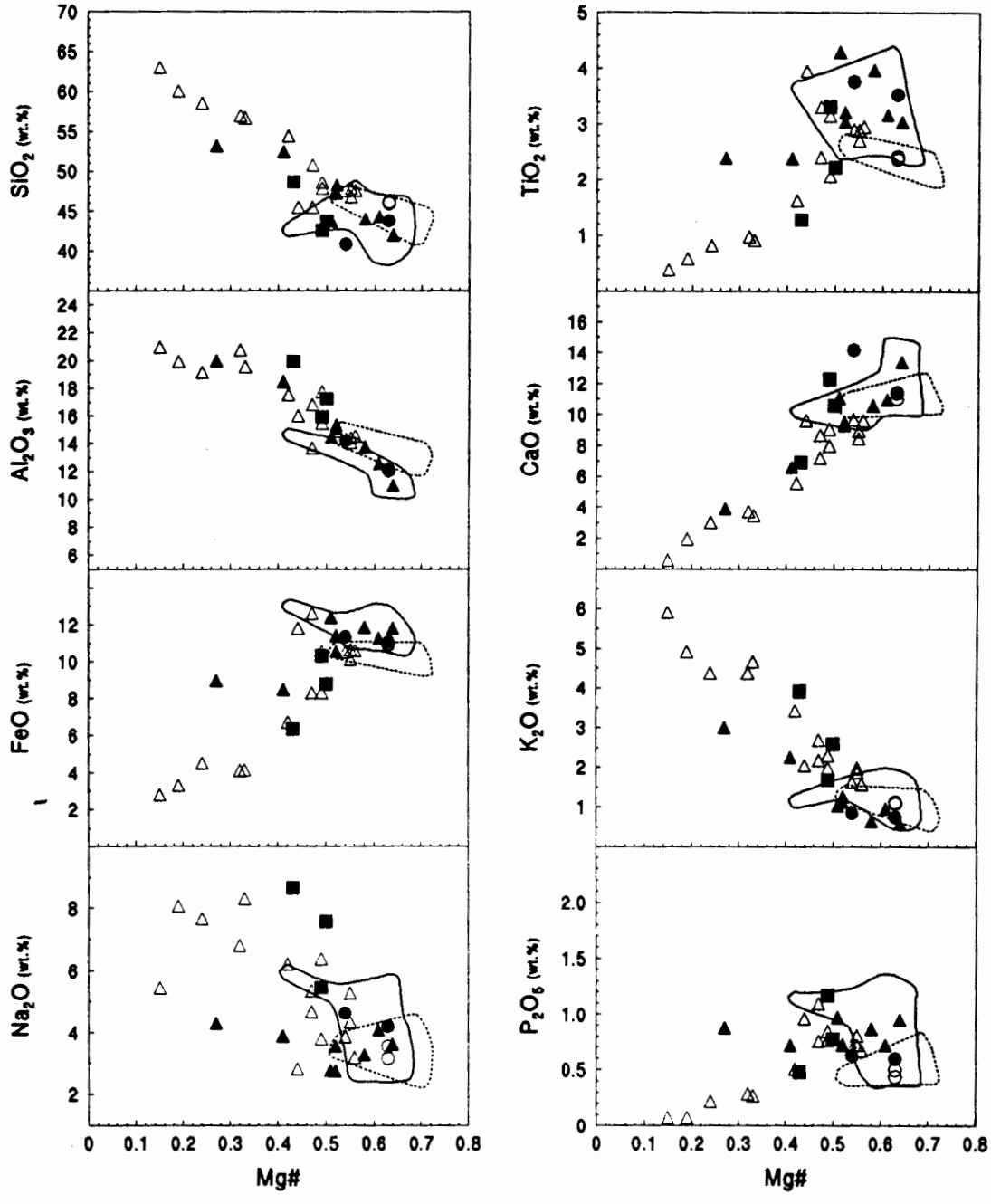

Fig. 6.9. Plots of major and minor elements (wt.%) vs *Mg-number* for Mayotte lavas. Symbols: open circles: Karthala-type Shield-building Phase; filled circles: La Grille-type Shield-building Phase; filled squares: Post-erosional Phase; open triangles: Karthala-type Rejuvenescent Phase; filled triangles: La Grille-type Rejuvenescent Phase. For comparison, the fields for Moheli and Grande Comore data, delineated by solid and stippled lines respectively, are shown.

element compositions of the three Comores islands investigated in this study overlap, although Mayotte lavas range to significantly lower *Mg-numbers*, CaO, TiO_2, FeO and P_2O_5 contents, but significantly higher SiO_2, Al_2O_3, Na_2O and K_2O concentrations than the lavas from Grande Comore and Moheli.

Trace Elements

The trace element contents of Mayotte lavas are presented in Table 6.10. In addition, the REE contents of eight Mayotte lavas were determined by HPIC and are reported in Table 6.11.

TABLE 6.11
REE contents (ppm) of some Mayotte lavas

	Shield-building Phase			*Post-erosional Phase*		*Rejuvenescent Phase*		
Sample	*MA-29*	*MA-60*	*MA-61*	*MA-55*	*MA-73*	*MA-8*	*MA-22*	*MA-33*
La	31.1	44.9	58.6	77.4	101	51.9	76.9	55.1
Ce	59.8	82.7	104	149	166	94.3	140	101
Pr	7.28	9.62	11.8	17.7	17.3	11.0	15.6	12.2
Nd	29.5	39.6	46.1	65.4	63.4	41.9	60.7	46.7
Sm	6.92	8.41	9.23	12.1	10.5	8.46	11.5	9.44
Eu	2.20	2.61	2.53	3.47	3.18	2.70	3.49	2.69
Gd	6.27	7.25	7.40	9.93	8.61	7.14	9.53	7.46
Rb	0.92	1.00	0.98	1.45	1.25	1.03	1.25	1.04
Dy	4.89	4.99	5.28	7.85	7.36	5.27	6.51	5.54
Er	2.52	2.11	2.38	3.54	3.87	2.24	2.60	2.51
Yb	2.22	1.53	2.04	2.96	3.76	1.66	1.99	1.97
$(La/Sm)_n$	2.9	3.4	4.1	4.1	6.2	4.0	4.3	3.8
$(La/Yb)_n$	10.0	21.1	20.6	18.8	19.3	22.4	27.7	20.1
La/Nb	0.71	0.72	0.73	0.62	0.51	0.73	0.89	0.72

$(La/Sm)_n$ and $(La/Yb)_n$ are chondrite-normalised ratios (normalising values from Sun and McDonough, 1989).

Reflecting the effects of olivine and clinopyroxene fractionation, the compatible ferromagnesian trace elements Ni and Cr show well-defined trends in Fig. 6.10, decreasing in concentration with decreasing *Mg-number*, whereas Sc displays a similar, but somewhat more dispersed trend of decreasing concentration with decreasing *Mg-number*

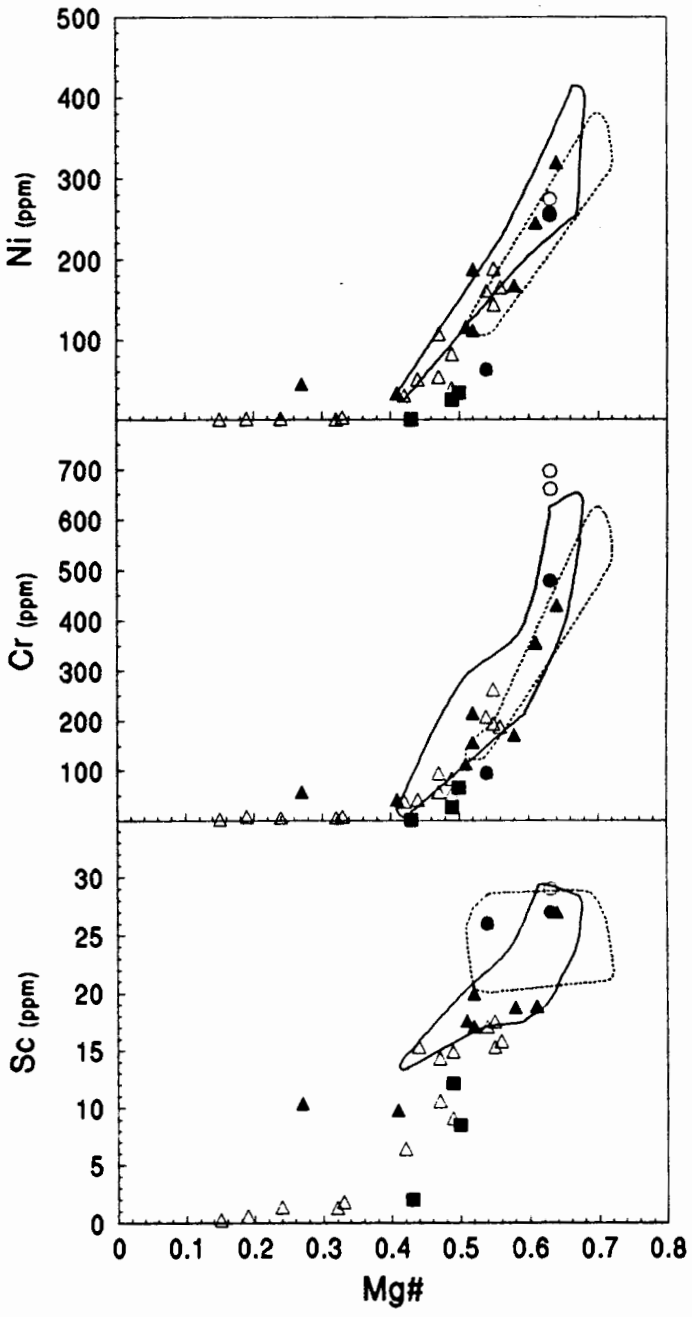

Fig. 6.10. Plots of Ni, Cr and Sc (ppm) vs *Mg-number* for Mayotte lavas. Symbols: open circles: Karthala-type Shield-building Phase; filled circles: La Grille-type Shield-building Phase; filled squares: Post-erosional Phase; open triangles: Karthala-type Rejuvenescent Phase; filled triangles: La Grille-type Rejuvenescent Phase. For comparison, the fields for Moheli and Grande Comore data, delineated by solid and stippled lines respectively, are shown.

Several incompatible trace elements are plotted against Zr in Fig. 6.11. Considered together, Mayotte lavas show considerable variability, with the Zr content ranging from 162 to 821 ppm and a number of relatively well-defined trends are observed on the variation diagrams.

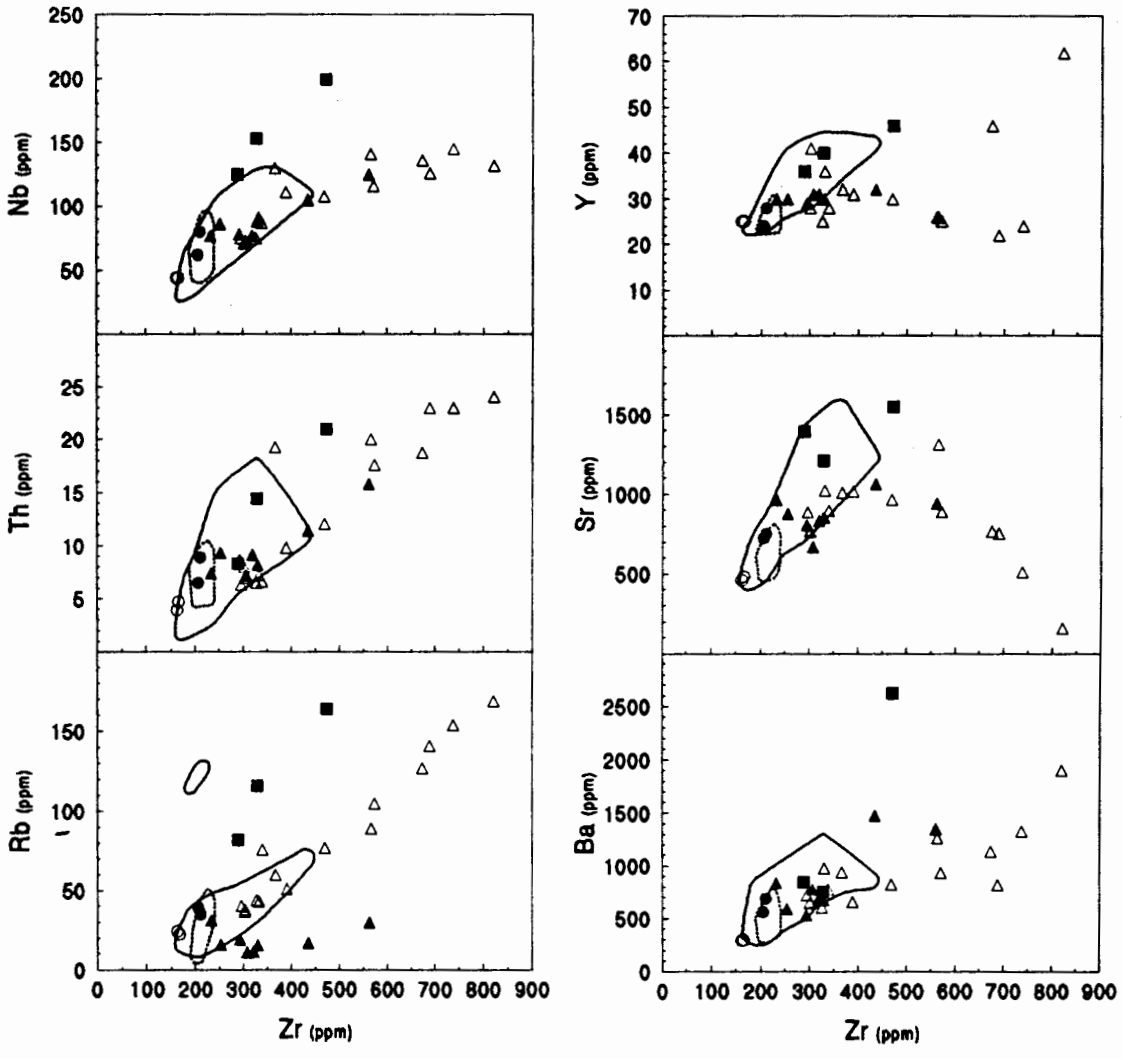

Fig. 6.11. Plots of incompatible trace elements vs Zr (all in ppm) for Mayotte lavas. Symbols: open circles: Karthala-type Shield-building Phase; filled circles: La Grille-type Shield-building Phase; filled squares: Post-erosional Phase; open triangles: Karthala-type Rejuvenescent Phase; filled triangles: La Grille-type Rejuvenescent Phase. For comparison, the fields for Moheli and Grande Comore data, delineated by solid and stippled lines respectively, are shown.

Nb, Th, Rb and Ba all broadly increase with increasing Zr content. The Sr concentration of Mayotte lavas increases, as the Zr concentration increases from 162 to about 450 ppm, but decreases in lavas with higher Zr contents. The La Grille-type Shield-building lavas have somewhat greater concentrations of Zr, Nb, Th, Sr, Rb and Ba than the Karthala-type Shield-building lavas. The Post-erosional Phase lavas display distinct trends on

several of the trace element variation diagrams and at similar Zr contents tend to be enriched in Nb, Y, Sr and Rb relative to the other lava groups. As expected, lavas of the Karthala-type Rejuvenescent Phase display the greatest range in Zr content (296-821 ppm) amongst all Mayotte lavas, following well-defined variation trends on most of the diagrams in Fig. 6.11. The La Grille-type Rejuvenescent Phase lavas range in Zr from 233 to 562 ppm and generally overlap with the Karthala-type Rejuvenescent Phase lavas in terms of incompatible trace element contents. However, they have significantly lower Rb contents than the Karthala-type Rejuvenescent Phase lavas. The incompatible element compositions of Grande Comore and Moheli lavas overlap with those of the lavas from Mayotte, although Mayotte lavas range to higher concentrations of Zr, Nb, Th, Rb, Y and Ba.

Figure 6.12 depicts the variation in several incompatible trace element ratios with respect to Zr.

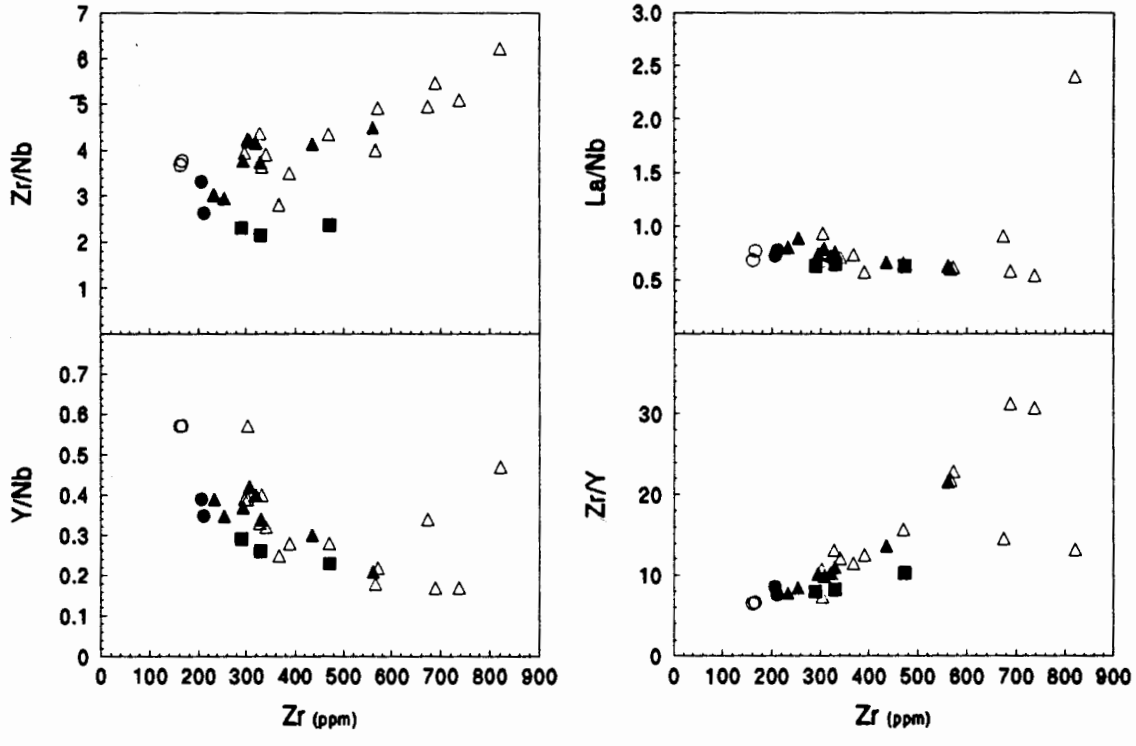

Fig. 6.12. Plots of incompatible trace element ratios vs Zr (ppm) for Mayotte lavas. Symbols: open circles: Karthala-type Shield-building Phase; filled circles: La Grille-type Shield-building Phase; filled squares: Post-erosional Phase; open triangles: Karthala-type Rejuvenescent Phase; filled triangles: La Grille-type Rejuvenescent Phase. (MA-20 is the sample with the highest Zr content).

Notable variations occur in the Zr/Nb (2.2-6.2), Y/Nb (0.17-0.57) and Zr/Y (6.5-31.3) ratios of Mayotte lavas, but very little variation in La/Nb (0.55-0.93; outlier: MA-20: 2.4) is observed. The apparently anomalous behaviour of sample MA-20 on diagrams involving Y or La in the incompatible element ratio (i.e. comparatively high Y/Nb and La/Nb, but low Zr/Y) seems to reflect anomalously high Y and La contents, rather than anomalously low Nb and Zr concentrations (since the Zr/Nb ratio of this sample is consistent with the overall trend of the data) and might suggest that this evolved sample (trachyte) has accumulated appreciable quantities of apatite, a mineral with high distribution coefficients for the REE and Y (see Appendix A3). The Ba/Nb, La/Nb and Y/Nb ratios of all Mayotte lavas tend to overlap, but most of the Karthala-type Shield-building and Karthala-type Rejuvenescent Phase lavas have somewhat greater Zr/Nb ratios (2.8-6.2) than the Post-erosional, La Grille-type Shield-building and La Grille-type Rejuvenescent Phase lavas (2.2-4.5). Fractional crystallisation processes are incapable of causing significant variations in highly incompatible trace element ratios. Partial melting processes, on the other hand, are much more effective in fractionating such ratios, and unless they reflect the involvement of different source materials, the considerable ranges in Zr/Nb, Y/Nb and Zr/Y observed amongst Mayotte lavas point towards the effects of variable degrees of partial melting in the generation of these lavas.

Primitive mantle-normalised incompatible element patterns (spidergrams) of Mayotte lavas are depicted in Fig. 6.13. As in the case of Grande Comore and Moheli, these diagrams clearly show the significant incompatible element enrichment of Mayotte lavas relative to N-type MORB compositions. With reference to the characteristic spidergrams of Karthala and La Grille lavas (Fig. 4.8), these diagrams are the basis for grouping Mayotte samples into Karthala-type and La Grille-type lavas. The incompatible element patterns of the Karthala-type and La Grille-type Shield-building lavas mimic the relationship between Karthala and La Grille lavas to a remarkable degree (compare Figures 6.13a and 6.13b with Figures 4.8a and 4.8b respectively). The lavas of the Post-erosional Phase (Fig. 6.13c) reach greater degrees of overall absolute enrichment than the La Grille-type Shield-building lavas, but also display a relative depletion in K and therefore belong to the La Grille-type lavas. All of the La Grille-type Rejuvenescent Phase lavas (Fig. 6.13d) are depleted in both K and Rb and in several samples, in fact,

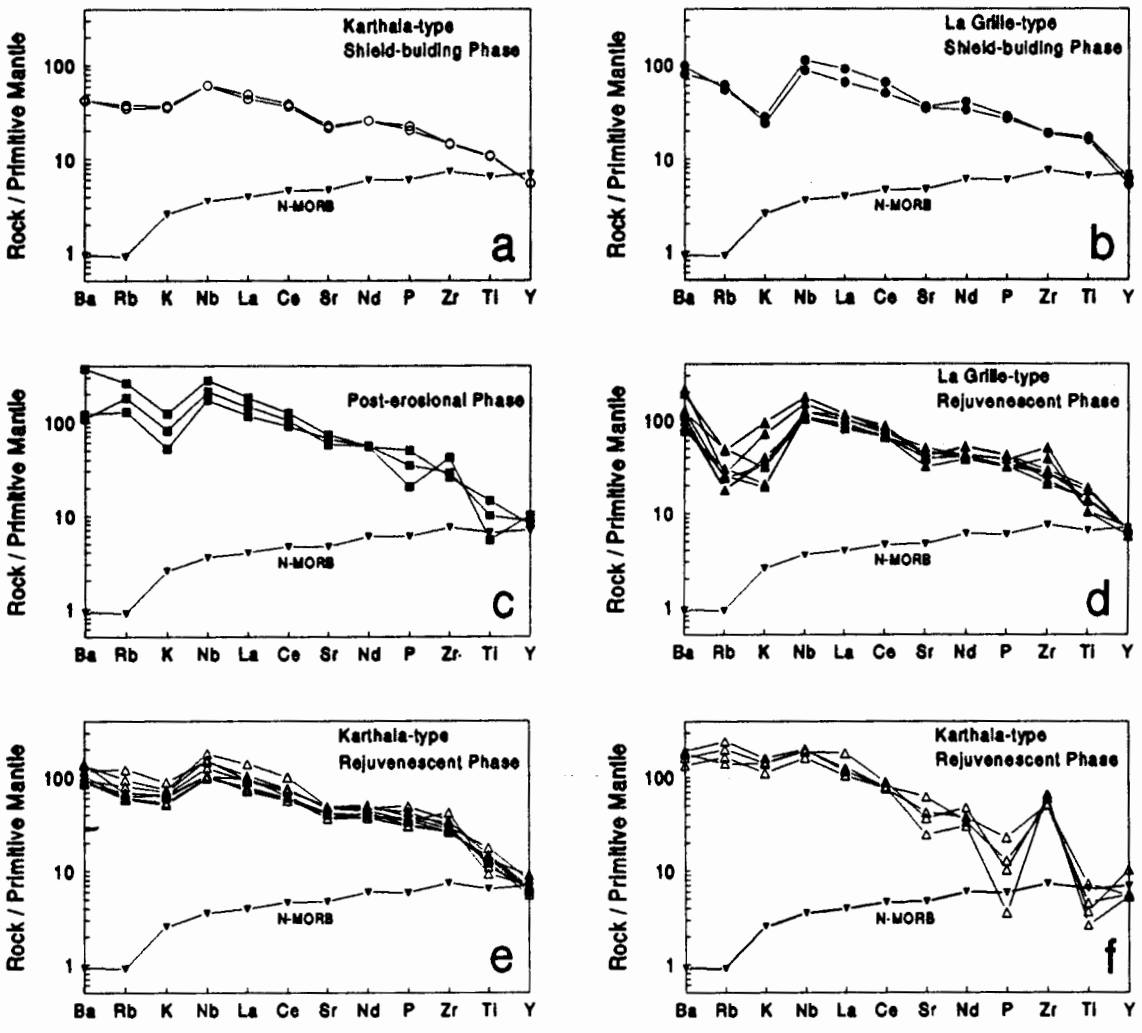

Fig. 6.13. Plots of primitive mantle-normalised incompatible elements for Mayotte lavas, arranged (from left to right) in order of decreasing incompatibility. A pattern of N-type MORB (Sun and McDonough, 1989) is shown for comparison. Normalising values after Sun and McDonough (1989).

Rb is somewhat more depleted than K, possibly implying an enhanced mobility for this element. The evolved members of the Karthala-type Rejuvenescent Phase (benmoreite, trachyte, phonolite) are depicted in Fig. 6.13f. It is important to note that great care must be taken in interpreting a diagram such as Fig. 6.13f, on which spidergrams for considerably evolved lavas are plotted. Strictly speaking, spidergrams should be restricted to primitive lava compositions, since at advanced stages of magmatic differentiation, a number of the elements shown can no longer be considered incompatible. The notably greater variability of elements such as Sr, P, Ti and Y in Fig. 6.13f, compared to the

other diagrams in Fig. 6.13, can thus be ascribed to the effects of significant feldspar (Sr), apatite (P and Y) and titanomagnetite (Ti) fractionation. The greater overall enrichment levels of these lavas, compared to their mafic and intermediate equivalents (Fig. 6.13e), can also be explained as a result of the significant differentiation these lavas have experienced. The reason for including this diagram in Fig. 6.13 is to show that even at such advanced stages of magmatic evolution, these samples show no signs of K or Rb depletion and can clearly be identified as Karthala-type lavas.

The chondrite-normalised REE patterns of eight Mayotte lavas are shown in Fig. 6.14.

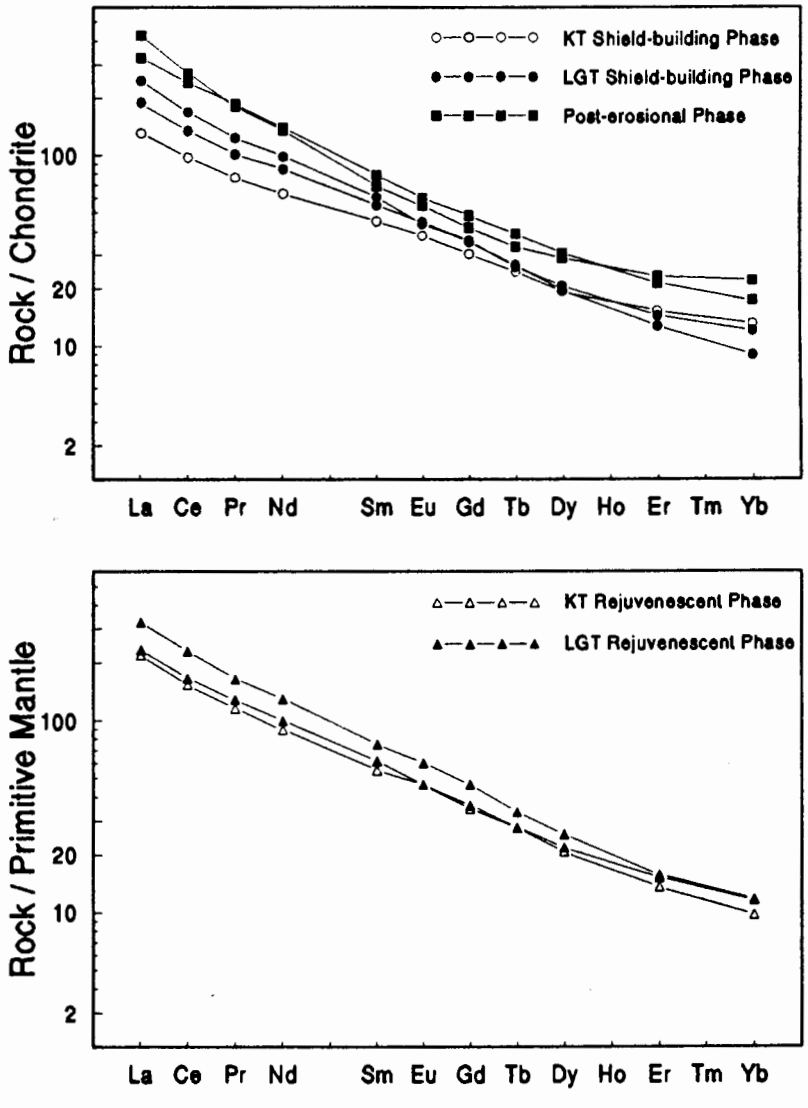

Fig. 6.14. Chondrite-normalised REE patterns of selected Mayotte lavas. Normalising values after Sun and McDonough (1989). KT=Karthala-type; LGT=La Grille-type.

The patterns of the La Grille-type Shield-building lavas, with normalised La/Yb ratios of 20.6 to 21.1 cross-cut the pattern of the single Karthala-type Shield-building lava (normalised La/Yb: 10.1) at Dy. The Post-erosional Phase lavas (normalised La/Yb: 18.8-19.3) are more REE enriched than the Shield-building lavas and have concave-upward REE patterns. The Rejuvenescent Phase lavas analysed for REE have comparatively steep REE patterns and high normalised La/Yb, ratios ranging from 20.1 to 27.7. No distinction can be made between La Grille- and Karthala-type Rejuvenescent Phase lavas in terms of the REE data presented here.

Isotopes

A total of nine samples from Mayotte, including one Karthala-type and one La Grille-type Shield-building lava, one Post-erosional Phase lava, five Karthala-type Rejuvenescent Phase lavas and one La Grille-type Rejuvenescent Phase lava, were analysed for their Sr and Nd isotopic compositions. All isotope data acquired are listed in Table 6.12.

TABLE 6.12
Sr and Nd isotope data for selected Mayotte lavas

	Sample	$^{87}Sr/^{86}Sr$	$^{143}Nd/^{144}Nd$
KT Shield-building Phase	*MA-29*	0.70334±2	0.51279±1
LGT Shield-building Phase	*MA-60*	0.70332±1	0.51283±1
Post-erosional Phase	*MA-55*	0.70328±1	0.51282±4
KT Rejuvenescent Phase	*MA-1*	0.70319±1	0.51288±1
KT Rejuvenescent Phase	*MA-3*	0.70355±1	0.51276±1
KT Rejuvenescent Phase	*MA-8*	0.70338±1	0.51283±1
KT Rejuvenescent Phase	*MA-11*	0.70336±1	0.51284±1
KT Rejuvenescent Phase	*MA-35*	0.70330±1	0.51282±1
LGT Rejuvenescent Phase	*MA-33*	0.70328±1	0.51282±1

KT = Karthala-type; LGT = La Grille-type;
errors are $2\sigma_{mean}$ on in-run statistics and correspond to least significant digits.

The isotopic compositions of all Mayotte lavas analysed overlap, with $^{87}Sr/^{86}Sr$ values ranging from 0.70319±1 to 0.70355±1 and $^{143}Nd/^{144}Nd$ values ranging from 0.51276±1 to 0.51288±1. The $^{87}Sr/^{86}Sr$ values for a number of Mayotte lavas presented by Emerick (1985) lie within the range of the present data (0.703222-0.703401). The isotopic compositions of Mayotte lavas also overlap with those of all Moheli and La Grille lavas analysed (see Chapters 4 and 5). Based only on their Sr and Nd isotopic signatures, no distinction can be made between samples from the different lava suites identified on Mayotte on the basis of age and lava type.

7. PRIMARY MELTS

Before discussing the petrogenesis of Comorean lavas in detail, it is important to ascertain whether any of the present samples have primary magma compositions (i.e compositions that have remained unmodified since segregation from the melting regions). A number of geochemical criteria have been widely used to distinguish possible primary melts from magmas whose compositions have changed since they segregated from their mantle source regions (e.g. Sun and Hanson, 1975; Sato, 1977; Hart and Davis, 1978; Frey *et al.*, 1978; Basaltic Volcanism Study Project [BVSP], 1981; Clague and Frey, 1982). An essential requirement for any primary basalt magma is that its bulk composition be equivalent to that of a liquid (as opposed to, for example, a cumulate) - a requirement which is probably closely met by many aphyric basalts, or basalts containing only minor quantities of phenocrysts and microphenocrysts (BVSP, 1981). The presence of mantle-derived nodules in basaltic lavas has been widely used as a criterion to identify primary or near-primary melts (e.g. BVSP, 1981). The occurrence of such ultramafic nodules is generally accepted as evidence for rapid magma ascent velocities, which are considered to preclude any significant compositional modifications *en route* from the melting regions towards the surface. The *Mg-number* of basaltic lavas is a further criterion which has been frequently employed to distinguish between primary and non-primary magmas. Based on the equilibrium distribution of Fe and Mg between olivine and melt (Roeder and Emslie, 1970) and on assumptions of olivine compositions in the Earth's mantle, the *Mg-number* of primary terrestrial melts has been estimated to range from about 0.68 to 0.75 (e.g. Frey *et al.*, 1978; BVSP, 1981). The ferromagnesian trace element Ni has mineral-melt distribution coefficients exceeding unity for olivine and clinopyroxene, both of which are early crystallising phases in many basaltic magmas and any melt which has experienced fractionation of either or both of these minerals will be significantly depleted in Ni relative to its parental magma. Sun and Hanson (1975) suggested that a primary alkali basalt in equilibrium with typical peridotitic mantle should contain between about 300 and 400 ppm Ni, whereas according to the BVSP (1981), estimates of primary Ni concentrations in terrestrial magmas range from 200-450 ppm (e.g. Sato, 1977; Clague and Frey, 1982). It has furthermore been noted, that unless a magma has a Ni/MgO ratio between about 23 and 39, it is unlikely to be a primary melt complementary to a

residual peridotitic mantle (Hart and Davis, 1978; BVSP, 1981).

Grande Comore

The lavas erupted from *La Grille* volcano are the most likely candidates for primary melts amongst all of the lavas analysed. La Grille lavas tend to contain relatively limited quantities of olivine and clinopyroxene phenocrysts and microphenocrysts. Fig. 4.3 shows that although some of the olivine crystals in some La Grille lavas are too Fe-rich to be in equilibrium with the bulk rock compositions and may be xenocrystic, others fulfil the equilibrium requirements, and overall, La Grille lavas probably represent near-liquid compositions. This conclusion is consistent with Strong's (1972b) suggestion that "that the bulk chemistry of at least some of the porphyritic (La Grille) rocks might represent original liquid compositions". As mentioned in Chapter 3, La Grille lavas are known to commonly contain ultramafic xenoliths (Strong, 1972b; Upton, 1982) and two of the La Grille lavas in the present sample collection (RH-1, RH-2b) have been noted to contain possible peridotite xenoliths (see Chapter 4). The *Mg-numbers* of La Grille lavas range from 0.69 to 0.71, their Ni contents from 327 to 373 ppm and their Ni/MgO ratios from 25.2 to 27.2. Using a $K_D^{Fe\text{-}Mg}$ value of 0.3 (Roeder and Emslie, 1970) and assuming La Grille lavas to represent liquid compositions, the composition of the olivine which would be in equilibrium with these melts is estimated to range from Fo_{88} to Fo_{89}, falling within the presumed range of mantle olivine (Fo_{88}-Fo_{92}; e.g. Hoernle and Schmincke, 1993a). The arguments presented above provide sufficient evidence to suggest that La Grille lavas represent primary or near-primary mantle melt compositions.

In contrast, *Karthala* lavas are clearly non-primary. They only rarely contain ultramafic xenoliths (Strong, 1972b; Upton, 1982), the samples analysed in this study range in *Mg-number* from 0.52 to 0.54, contain 115 to 122 ppm Ni and have Ni/MgO ratios from 16.9 to 18.1.

Moheli

Among the *alkali basalts* of Moheli, three samples are clearly non-primary (RH-16, RH-

28, RH-42), having *Mg-numbers* between 0.56 and 0.59 and Ni contents of 184 to 214 ppm. The remaining two alkali basalts (RH-15, RH-17), however, have *Mg-numbers* (0.66-0.67), Ni concentrations (375-403 ppm) and Ni/MgO ratios (32.0-32.2) consistent with near-primary compositions. The composition of the olivine that would be in equilibrium with these lavas (assuming them to represent liquids) ranges from Fo_{86} to Fo_{87} and is thus very close to mantle olivine compositions. These two lavas are, however, strongly olivine and clinopyroxene phyric, suggesting a cumulate origin, which is further substantiated by Fig. 5.3, which shows the olivine phenocrysts to be out of equilibrium with bulk rock compositions. The fact that a lava is strongly porphyritic does not necessarily preclude it from having a bulk composition which is equivalent to that of a primary melt, if a crystallisation process such as the "compensated crystal settling" model of Cox and Bell (1972) and Cox (1978) is invoked. In this scenario, the amount of crystals lost due to fractional crystallisation is compensated by equal quantities of crystals gained by accumulation. No record exists of ultramafic inclusions in any Moheli lavas, although this may be an artefact of limited sampling. From the present data, it is not possible to conclude whether the two coarsely porphyritic alkali basalts have retained near-primary compositions as a result of compensated crystal settling, or whether they have acquired the geochemical character of such magmas by substantial accumulation of ferromagnesian minerals.

Moheli *basanites* range in *Mg-number* from 0.42 to 0.66 and in Ni content from 34 to 343 ppm and the majority of these lavas are clearly non-primary. This conclusion is further corroborated by the disequilibrium relationship between some olivine phenocrysts in these lavas with respect to bulk rock compositions (Fig. 5.3). Two of the samples may, however, represent exceptions to this: the two basanites with the highest Mg-numbers and Ni concentrations (RH-21, RH-36) also imply relatively magnesian equilibrium olivine compositions of Fo_{86} and Fo_{87} and are closer to near-primary compositions than any of the other Moheli basanites.

The moderately olivine and clinopyroxene phyric Moheli *nephelinites*, which contain olivine phenocrysts in equilibrium with bulk rock compositions (Fig. 5.3), probably represent liquid or near-liquid compositions. The lavas of this group have *Mg-numbers*

between 0.61 an 0.66 and Ni contents ranging from 257 to 318 ppm and, with the exception of one sample (RH-41), which may be relatively close to a near-primary state, are all non-primary lavas.

Mayotte

None of the Mayotte lavas analysed have the characteristics expected of primary mantle magmas. Most of these lavas have *Mg-numbers* below 0.6 and Ni concentrations below 200 ppm. Even the lavas of the Shield-building Phase and two of the primitive La Grille-type Rejuvenescent Phase lavas (MA-22, MA-33), which have higher *Mg-numbers* (0.61-0.64) and Ni contents (245-320 ppm) than the other Mayotte lavas, can not be considered to represent primary magma compositions.

8. FRACTIONAL CRYSTALLISATION

In the previous chapter, it was established that only a small number of the Comorean lavas analysed in this study can be considered to represent potential primary or near-primary melt compositions. The compositions of the majority of the lavas analysed were therefore modified after they segregated from their source regions. Crystal fractionation is one of the processes most frequently invoked to explain the modification and differentiation of terrestrial magmas after they have separated from the residual solids in their melting regions. In this chapter, the bulk rock data of Comorean lavas will be evaluated in order to determine to what extent crystal fractionation may have played a role in their evolution. Although the crystal fractionation processes that are inferred to occur in nature are most probably intermediate between the extreme endmember cases of fractional crystallisation[1] and equilibrium crystallisation[2], the presence of extensively zoned phenocrysts in Comorean lavas (see Chapters 4 to 6 and Appendix A4) suggests that the crystallisation processes involved in the differentiation of these lavas are more closely approximated by fractional rather than equilibrium crystallisation. All of the crystal fractionation models presented in this chapter therefore refer to fractional rather than equilibrium crystallisation.

Grande Comore

The fact that La Grille and Karthala, the two main volcanic centres on Grande Comore, have erupted lavas of distinctly different character has already been noted (Chapter 4). These *intervolcano* geochemical differences are contrasted somewhat by the very limited *intravolcano* variation observed (e.g. Figures 4.5 to 4.8). In the previous chapter, it was shown that La Grille lavas have primary or near-primary compositions, whereas Karthala lavas were modified during ascent towards the surface. The primary to near-primary nature of La Grille lavas is supported by Fig. 8.1, which shows a plot of Ni vs *Mg-*

[1]fractionating solid phases are continuously separated from the residual liquid phase

[2]fractionating phases grow in chemical equilibrium with the liquid phase

number, onto which a partial melting grid for typical mantle melts, generated over a range of temperatures and degrees of melting, has been superimposed (for details on the construction of the melting grid, see caption to Fig. 8.1).

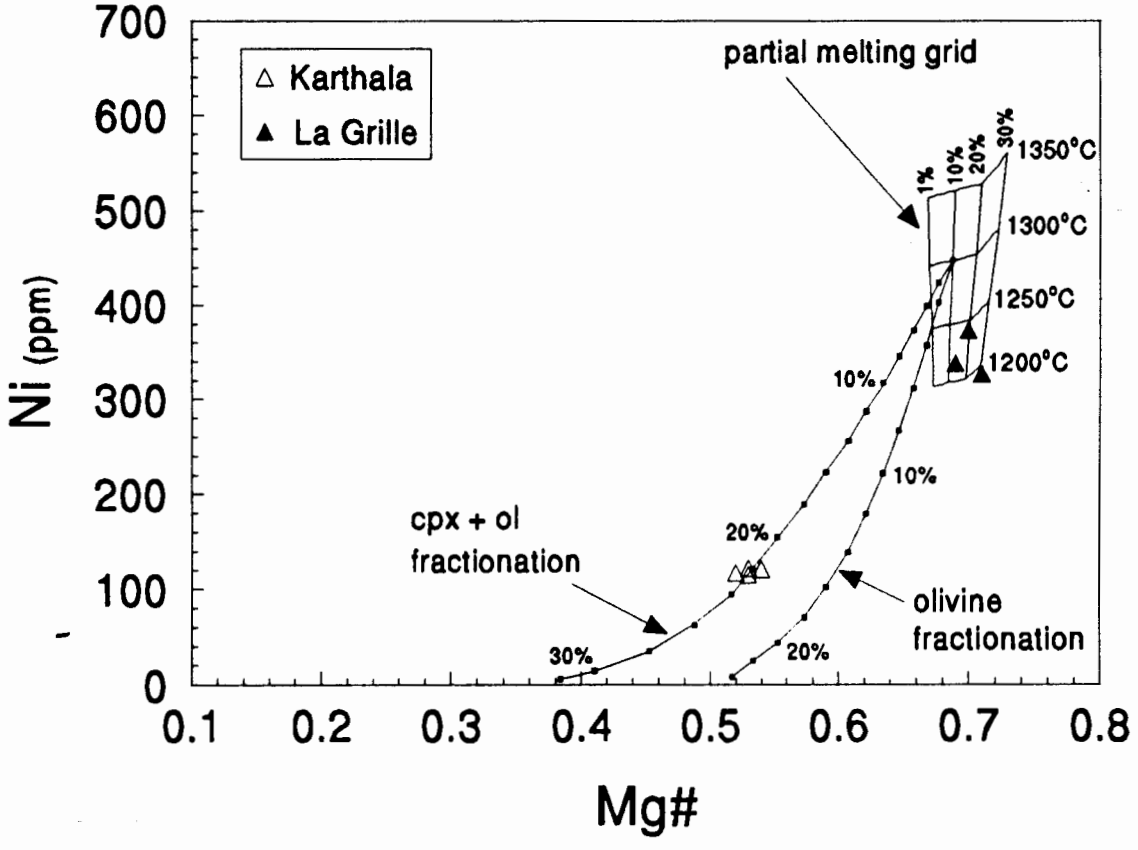

Fig. 8.1. Plot of Ni (ppm) vs *Mg-number* for Grande Comore lavas. Also displayed are: a partial melting grid, showing the variation of Ni and *Mg-number* in liquids produced by variable degrees (1-30%) of non-modal equilibrium partial melting of a mantle source over a temperature range of 1200-1350°C; and trends of olivine and combined olivine plus clinopyroxene (40% ol + 60% cpx) fractional crystallisation (in steps of 2%) of a hypothetical mantle melt, generated by 10% partial melting of the model mantle source at 1300°C. In constructing the melting grid, the approaches of Hanson and Langmuir (1978) and Consolmagno and Drake (1976) were followed for modelling Fe-Mg distributions and Ni abundances respectively. Composition of model mantle source: FeO = 9.13 wt.%, MgO = 34.29 wt.% (Wilkinson, 1991), Ni = 1850 ppm (Sun and Nesbitt, 1977). Source mineralogy: 55% ol, 25% opx, 18% cpx, 2% spinel, entering the melt in proportions of 10:20:68:2 respectively (Johnson *et al.*, 1990). For the fractional crystallisation trends, the variation in *Mg-number* was calculated according to Pearce (1978), assuming $K_D^{Fe-Mg} = 0.3$ for both ol and cpx (Roeder and Emslie, 1970; Kinzler and Grove, 1992a). Ni abundances during fractional crystallisation were calculated, using the mineral-melt distribution coefficients for Ni in ol and cpx listed in Appendix A3 in conjunction with Gast's (1968) fractional crystallisation equation.

La Grille lavas plot within, or very close to, the melting grid and therefore represent possible primary mantle melts generated by partial melting of the hypothetical source composition used.

Also shown in Fig. 8.1 are the compositional trends produced by fractional crystallisation of olivine and olivine plus clinopyroxene (60% clinopyroxene + 40% olivine) from a hypothetical mantle melt generated by 10% melting at 1300°C (for details, see caption to Fig. 8.1). All of the Karthala lavas analysed plot on, or very near to, the olivine plus clinopyroxene fractionation curve, suggesting, that they could have been produced by around 22% of combined olivine and clinopyroxene crystallisation of a parental melt similar to the hypothetical mantle melt considered. This conclusion is consistent with the fact that olivine and clinopyroxene are by far the predominant phenocryst phases in Karthala lavas (Chapter 4). The involvement of clinopyroxene is furthermore supported by the observation that Karthala lavas, relative to La Grille lavas, are significantly depleted in Cr (Fig. 4.6), typical mineral-melt distribution coefficients for Cr in clinopyroxene ranging between approximately 1.5 and 3.8 (e.g. Irving, 1978; Irving and Price, 1981; Hart and Dunn, 1993). Sc, however, is not depleted in Karthala lavas relative to La Grille lavas (Fig. 4.6), necessitating a bulk solid-melt distribution coefficient close to one for Sc during the differentiation of Karthala lavas (literature values for the mineral-melt distribution coefficient of Sc in clinopyroxene range from less than unity to significantly greater than unity; e.g. Irving, 1978; le Roex *et al.*, 1990; Hart and Dunn, 1993).

If the very minor intravolcano geochemical variations observed amongst the lavas of Karthala are the result of fractional crystallisation, only very small degrees of crystallisation would presumably be required to relate different Karthala lavas to one another. This suggestion is confirmed by a major element least-squares calculation using the algorithm of Bryan *et al.* (1969) (Table 8.1), according to which the Karthala lava with the lowest *Mg-number* (GC-1) could have been derived from the Karthala lava with the highest *Mg-number* (RH-1b), by only 1.3% of combined fractional crystallisation of clinopyroxene and olivine (proportions: 78% clinopyroxene, 22% olivine; the clinopyroxene and olivine compositions used for the modelling were taken from Tables

TABLE 8.1

Major element least-squares approximation relating two Karthala lavas

Alkali Basalt → Alkali Basalt

RH-1b = 0.9874 GC-1 + 0.0169 Cpx[a] + 0.0048 Fo_{84}

		SiO_2	TiO_2	Al_2O_3	FeO[t]	MnO	MgO	CaO	Na_2O	K_2O	P_2O_5	
RH-1b	*obs.*	46.91	2.49	14.29	11.98	0.19	6.88	11.09	3.47	1.25	0.42	
	calc.	46.93	2.66	14.26	11.96	0.19	6.87	11.05	3.35	1.32	0.47	
	diff.	0.02	0.17	-0.03	-0.02	0.00	-0.01	-0.04	-0.12	0.07	0.05	$\Sigma R^2 = 0.05$

[a]Cpx = $Wo_{46}En_{44}Fs_{10}$ (TiO_2 = 1.11 wt.%; Al_2O_3 = 3.43 wt.%).

TABLE 8.2

Predicted and observed trace element concentrations (ppm) of GC-1, calculated on the basis of the major element model presented in Table 8.1

	RH-1b parent	*GC-1 differentiate*	
	obs.	*calc.*	*obs.*
Zr	208	210	223
Nb	47	48	52
Y	27	27	29
Rb	29	29	31
Ba	324	328	363
Sr	495	501	542
La	39	40	41
Ce	79	80	81
Nd	39	39	41
Sc	28	27	26
V	248	248	260
Co	53	52	52
Ni	121	119	117
		F=0.9874	

calculated using the fractional crystallisation equation of Gast (1968) and the mineral melt distribution coefficients listed in Appendix A3.

4.1 and 4.2 respectively). The comparatively poor correlation between the calculated and observed TiO_2 concentrations suggests that titanomagnetite may have been an additional fractionating phase. The good agreement between calculated and observed trace element abundances, predicted on the basis of the above major element model using the fractional crystallisation equation of Gast (1968) and the mineral-melt distribution coefficients listed in Appendix A3, supports the proposed model (Table 8.2).

It is important to note at this point that the least-squares models presented in this chapter are not intended to imply that the individual samples considered are necessarily directly related to one another, but rather, these models aim to demonstrate that realistic fractional crystallisation processes are capable of explaining the compositional variations observed amongst Comorean lavas in general.

Moheli

It was noted in Chapter 5, that the major and minor elements of Moheli lavas are only poorly correlated, displaying very few well-defined linear variation trends on Harker diagrams such as the ones shown in Fig. 5.5. Slightly better correlations exist on some of the trace element variation diagrams (Figures 5.6 and 5.7). Olivine and clinopyroxene are the only phenocryst phases observed in the Moheli lavas analysed in this study and it is reasonable to assume that the fractionation of these minerals was involved in the diversification of lavas from this island. The diagram of Ni vs *Mg-number* depicted in Fig. 8.2 is the equivalent of that in Fig. 8.1 for Moheli lavas, showing the same partial melting grid and olivine and olivine plus clinopyroxene fractionation trends. The relatively well-defined variation of Ni with *Mg-number* in Moheli lavas (which is mimicked by the behaviour of Cr and Sc; Fig. 5.6) is approximated reasonably well by the combined olivine plus clinopyroxene fractionation curve shown in Fig. 8.2, implying that the alkali basalts could have resulted from between about 4% and 19% of combined olivine and clinopyroxene fractionation of a primary magma. According to this diagram, the basanites, which show the greatest compositional range of all Moheli lavas, may have experienced between approximately 8% and almost 30% fractional crystallisation of

olivine plus clinopyroxene.

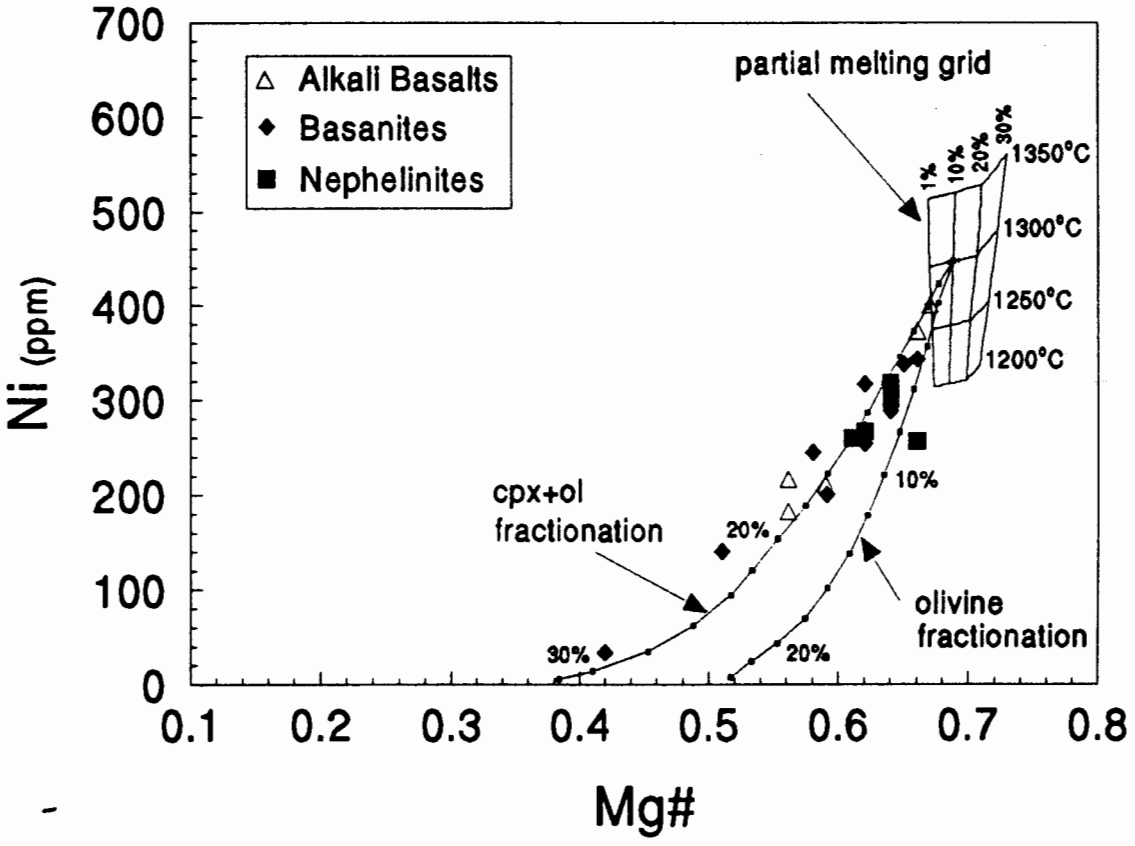

Fig. 8.2. Plot of Ni (ppm) vs *Mg-number* for Moheli lavas. The partial melting grid and the fractional crystallisation trends are the same as in Fig. 8.1.

Although the Ni vs *Mg-number* diagram is effective in evaluating the role of clinopyroxene and olivine during crystallisation, this diagram is not sensitive to the effects of the fractionation of phases in which Ni is incompatible, such as for example feldspar and to a slightly lesser extent amphibole. The fact that olivine and clinopyroxene are the only phenocryst phases present in the rocks considered here, does not necessarily mean that no other phases could have been involved in their crystallisation history. Fractionation of phases other than olivine and clinopyroxene, such as, for example, amphibole and feldspar, as recognised in the more evolved Moheli lavas investigated by Strong (1972a), could have occurred at depth beneath the volcano and may not be apparent from the modal mineralogy of the lavas (amphibole in xenoliths and megacrysts carried by alkaline volcanics is frequently suggested to be the product of crystal fractionation at depth; e.g. le Maitre, 1969; Aoki, 1970; Borley *et al.*, 1971; Kesson and Price, 1972; Ellis, 1976; Wilkinson and Hensel, 1991). In order to evaluate the possible involvement of such alternative (high P ?) fractionating phases, the basanite lavas of Moheli were investigated with the use of Pearce element ratio (PER) diagrams (Figures

8.3 and 8.4).

PER diagrams were introduced by Pearce (1968) as a tool for modelling igneous differentiation processes and as an alternative to using simple Harker diagrams, which tend to be distorted by constant-sum effects. The use of PER diagrams has since been discussed widely (e.g. Pearce, 1987; Nicholls, 1988; Russell and Nicholls, 1988; Ernst *et al.*, 1988; Stanley and Russell, 1989a) and such diagrams have been successfully employed to interpret various petrogenetic problems (e.g. Pearce, 1970; Syme and Forester, 1977; Russell and Nicholls, 1987). PER diagrams involve the plotting of molar ratios with common denominators. Importantly, the common denominator must be a "conserved constituent", i.e. a constituent, the absolute (extensive) quantities of which are not affected by the process under investigation (e.g. fractional crystallisation). Since, for example, elements such as K and P tend to be incompatible with respect to the early crystallising phases of most basaltic magmas, the absolute amounts (i.e. number of moles or grams) of these elements in the liquid phase will remain constant during fractional crystallisation[3] and these elements are therefore commonly used as conserved constituents in Pearce element ratios.

Amongst other things, PER diagrams may be used to distinguish between different potential fractionating assemblages involved in the evolution of a comagmatic suite of rocks. In this type of application, the combination of numerator element coefficients for each axis is chosen to reflect the stoichiometry of specific minerals, resulting in compositional trends that are predictable and different for different fractionating phases or assemblages (e.g. Pearce, 1968, 1970; Russell and Nicholls, 1988; Stanley and Russell, 1989a). On a plot of $0.5(Mg+Fe)/x$ vs Si/x (where x is a conserved element), for instance, geochemical differentiation trends controlled by only olivine, orthopyroxene, clinopyroxene, plagioclase or Fe-Ti oxide would be expected to be straight lines (not passing through the origin) with slopes of 1.0, 0.5, 0.25, 0.00 and ∞ respectively. Fractionation of a combination of these phases would result in a straight line trend of intermediate slope. All Moheli basanites are plotted on such a diagram in Fig. 8.3. The

[3]the *relative* abundances (e.g. in ppm) of these incompatible elements will, of course, increase during fractional crystallisation

data points define a well correlated linear trend approximated by a best-fit linear regression line that intercepts the y-axis at -3.33 and has a slope of 0.39.

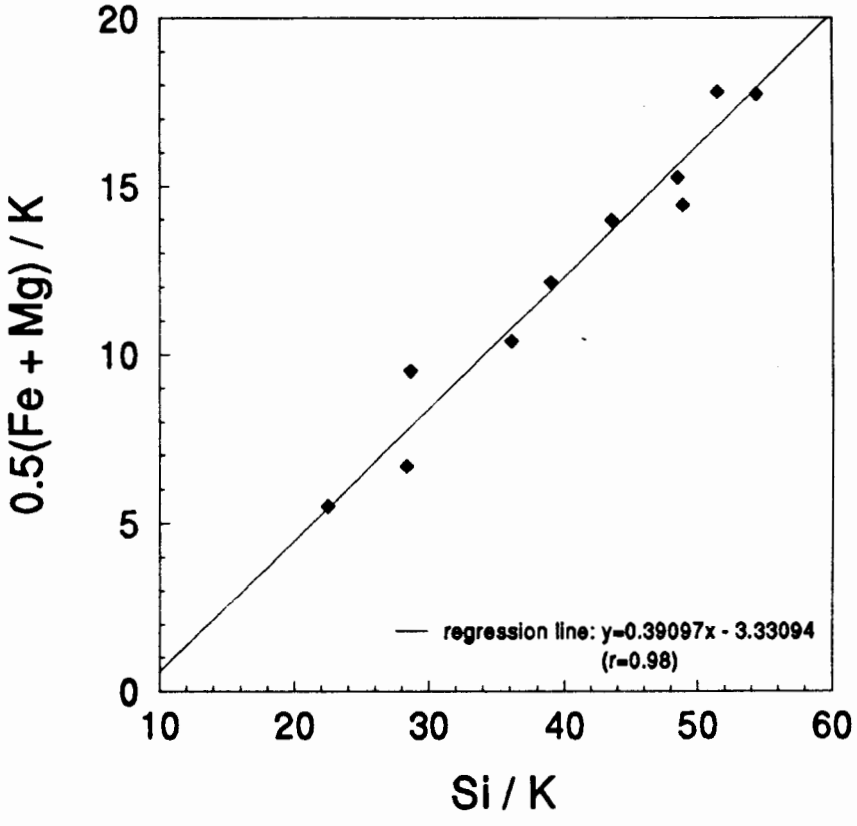

Fig. 8.3. Pearce element ratio diagram for Moheli basanites, plotting 0.5(Fe+Mg)/K vs Si/K. See text for discussion. The Pearce element ratios and the equations of the regression lines on this diagram and in Fig. 8.4 were calculated using the program PEARCE.PLOT (Stanley and Russel, 1989b).

The well-defined linear trend of the data points suggests a systematic petrogenetic relationship between these basanites. The slope of the regression line does, however, not correspond to that predicted for the fractionation of any one single phase, but could be the result of fractionation involving a combination of these minerals.

The Pearce element ratios plotted in Fig. 8.4a and b were chosen so as to distinguish between the effects of olivine, clinopyroxene and plagioclase fractionation. In both Fig. 8.4a and b, the fractional crystallisation of plagioclase only, would result in a straight line trend with a slope of zero. In Fig. 8.4a, pure olivine fractionation would lead to a vertical linear trend (i.e. slope = ∞), whereas clinopyroxene fractionation has no effect on this

diagram at all. In Fig.8.4b, the effects of pure olivine and clinopyroxene fractionation are reversed from those they have in Fig. 8.4a. On both Fig. 8.4a and b, the Moheli basanite data define relatively well-constrained linear trends with slopes intermediate between zero and infinity and with non-zero y-intercepts. From these diagrams, it may be concluded, that besides olivine and clinopyroxene, plagioclase also appears to have been involved in the differentiation of Moheli basanites.

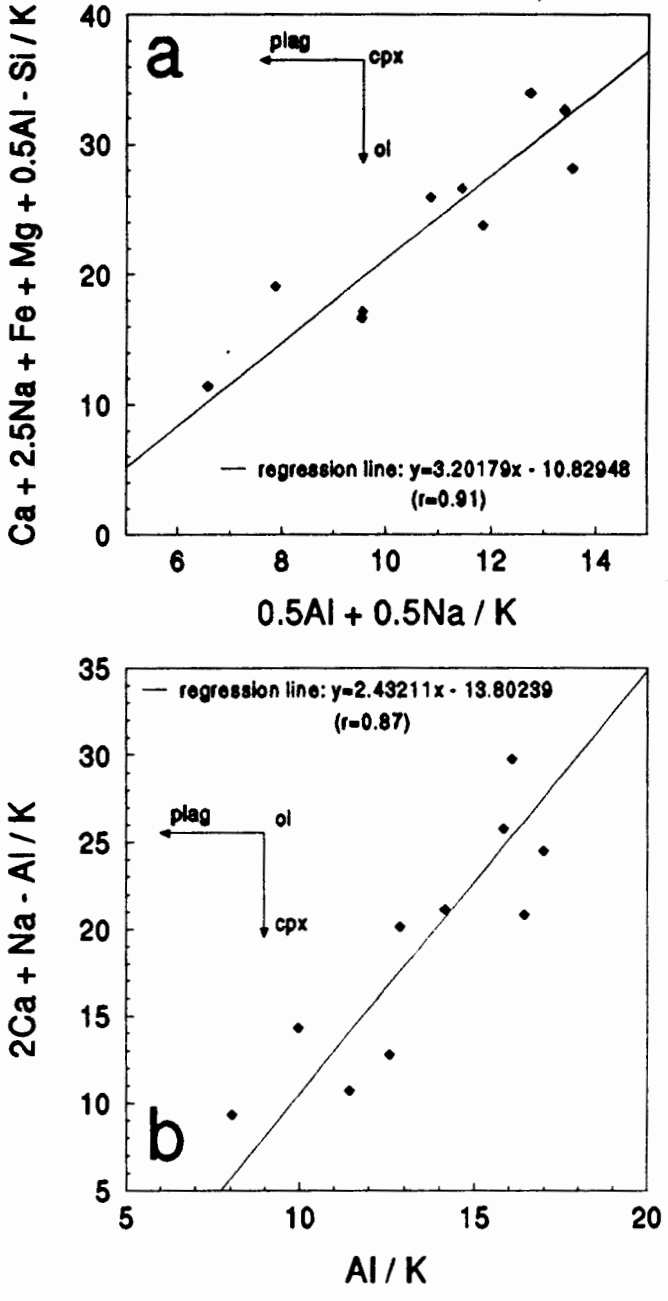

Fig. 8.4. Pearce element diagrams for Moheli basanites, plotting (**a**) (Ca+2.5Na+Fe+Mg+ 0.5Al-Si)/K vs (0.5Al+0.5Na)/K and (**b**) (2Ca+Na-Al)/K vs Al/K. See text for discussion.

In order to further investigate the possible effects of fractional crystallisation on Moheli lavas, attempts were made to relate various promising pairs of basanites and nephelinites by major element least-squares approximations, but only very limited success was achieved. Amongst the basanites, the only mathematically successful combination was one relating RH-12a to RH-13 by approximately 41% crystallisation of predominantly feldspar, clinopyroxene, olivine and titanomagnetite and small amounts of amphibole and apatite (Table 8.3). Amongst the nephelinites, on the other hand, RH-14 can be related to RH-19 by 33% fractionation of mainly amphibole with lesser involvement of clinopyroxene, olivine, titanomagnetite and apatite (Table 8.3). Although amphibole was not recognised as a modal constituent of the Moheli lavas of the present sample collection, Strong (1972a) reported the occurrence of amphibole phenocrysts in some samples from this island and suggested that the observed relative K deficiency in the basanites of this island was probably the result of significant amphibole fractionation. The titanomagnetite and amphibole compositions used for the least-squares approximations were chosen from the analyses of these minerals in Mayotte lavas (Tables 6.8 and 6.9 respectively), whereas the clinopyroxene and olivine compositions were taken from Tables 5.1 and 5.2 respectively. In these and in subsequent models, the proportions of apatite fractionation were estimated from the discrepancy between observed and calculated P_2O_5 concentrations, based on the assumption that P is incompatible in all other phases involved.

Although the two major element models presented in Table 8.3 are mathematically successful (i.e. small differences between observed and calculated oxide abundances), their results appear to be inconsistent with certain earlier observations. The degrees of crystallisation proposed by these models for relating individual samples to one another exceed the estimates for the degrees of fractionation required to generate the entire compositional variation observed amongst the Moheli basanite and nephelinite suites according to Fig. 8.2. Both of the models furthermore involve only very minor quantities of olivine and relatively small amounts of clinopyroxene, the phases previously suggested to have dominated the evolution of Moheli lavas (e.g. Fig. 8.2), but instead require substantial fractionation of amphibole and feldspar, two minerals which are not observed as modal constituents in the present sample collection from Moheli. The validity of the

TABLE 8.3

Major element least-squares approximations for Moheli lavas (according to Bryan *et al.*, 1969)

Basanite → Basanite

RH-13 = 0.587 RH-12a + 0.1058 Cpx[a] + 0.0405 Fo_{87} + 0.2119 Fsp[b] + 0.0012 Amph + 0.0539 TiMgt + 0.0045 Ap

		SiO_2	TiO_2	Al_2O_3	FeO[t]	MnO	MgO	CaO	Na_2O	K_2O	P_2O_5	
RH-13	*obs.*	42.79	2.79	12.68	13.16	0.20	9.16	10.46	3.97	0.93	0.83	
	calc.	42.78	2.75	12.68	13.17	0.21	9.17	10.48	4.04	0.97	0.83	
	diff.	-0.01	-0.04	0.00	0.01	0.01	0.01	0.02	0.07	0.04	0.00	$\Sigma R^2 = 0.01$

Nephelinite → Nephelinite

RH-14 = 0.6681 RH-19 + 0.0358 Cpx[c] + 0.0051 Fo_{83} + 0.2758 Amph + 0.0014 TiMgt + 0.0048 Ap

		SiO_2	TiO_2	Al_2O_3	FeO[t]	MnO	MgO	CaO	Na_2O	K_2O	P_2O_5	
RH-14	*obs.*	39.50	3.25	11.15	12.83	0.22	11.32	12.66	4.41	1.25	0.88	
	calc.	39.56	3.35	11.05	12.81	0.23	11.28	12.59	4.42	1.40	0.88	
	diff.	0.06	0.10	-0.10	-0.02	0.01	-0.04	-0.07	0.01	0.15	0.00	$\Sigma R^2 = 0.05$

[a]Cpx = $Wo_{50}En_{39}Fs_{11}$ (TiO_2 = 2.29 wt.%; Al_2O_3 = 6.23 wt.%); [b]Fsp = $An_{24}Ab_{67}Or_9$; [c]Cpx = $Wo_{50}En_{38}Fs_{12}$ (TiO_2 = 2.70 wt.%; Al_2O_3 = 5.49 wt.%).

TABLE 8.4

Predicted and observed trace element concentrations (ppm) of Moheli lavas, calculated on the basis of the major element model presented in Table 8.3

	RH-13 parent	*RH-12a differentiate*		*RH-14 parent*	*RH-19 differentiate*	
	obs.	*calc.*	*obs.*	*obs.*	*calc.*	*obs.*
Zr	311	508	359	237	268	262
Nb	96	140	124	88	110	105
Y	30	40	42	32	29	39
Rb	31	52	45	20	28	34
Ba	726	994	1003	806	1015	599
Sr	813	629	1404	792	945	1060
La	66	99	111	69	86	98
Ce	131	194	210	135	172	188
Nd	61	79	90	62	73	78
Sc	23	18.3	17.9	23	18.1	22
V	242	176	208	257	237	235
Zn	159	178	158	109	123	125
Ni	245	146	201	301	331	318
Co	63	48	59	71	68	67
		F=0.587			F=0.6681	

calculated using the fractional crystallisation equation of Gast (1968) and the mineral melt distribution coefficients listed in Appendix A3.

major element models described above is furthermore brought into question by the relatively poor correspondence between the predicted and observed abundances of certain trace elements (Table 8.4; e.g. Zr and Sr in the basanite model and Ba in the nephelinite model). The models presented in Table 8.3 thus represent a good illustration of the dangers of basing fractionation models on major element least-squares approximations only, without validation by corresponding trace element calculations or taking into account the modal mineralogy.

In general then, the semi-quantitative observations made in this section suggest that the differentiation of the alkali basalts, basanites and nephelinites of Moheli was dominated by fractional crystallisation of clinopyroxene and olivine. PER diagrams are furthermore consistent with the involvement of plagioclase as an additional fractionating phase, at least during the evolution of Moheli basanites. Although the possible fractionation of amphibole, as proposed by Strong (1972a), cannot be entirely disregarded, the failure to produce any satisfactory quantitative models for both major and trace elements which involve amphibole places the validity of this proposal into question.

Mayotte

The relatively well-correlated major, minor and trace element variations of Mayotte lavas, extending over a significant compositional range, have been described in Chapter 6 and are apparent in Figures 6.9 to 6.11 as reasonably well-defined linear trends. The samples from the different lava suites defined in Chapter 6 behave coherently in most of these variation diagrams and it will be argued below, that the *within-suite* geochemical variations observed, are consistent with being the results of fractional crystallisation processes. Different parental magmas (e.g. produced by different degrees of partial melting at different mantle depths; see Chapter 9), different physico-chemical conditions (e.g. pressure, temperature, presence of volatiles) and different fractionating mineral assemblages are regarded as having caused the geochemical differences *between* the lava suites.

As in the case of Grande Comore and Moheli, Mayotte lavas are plotted on a diagram of Ni vs *Mg-number* with superimposed melting grid and fractionation trends (Fig. 8.5).

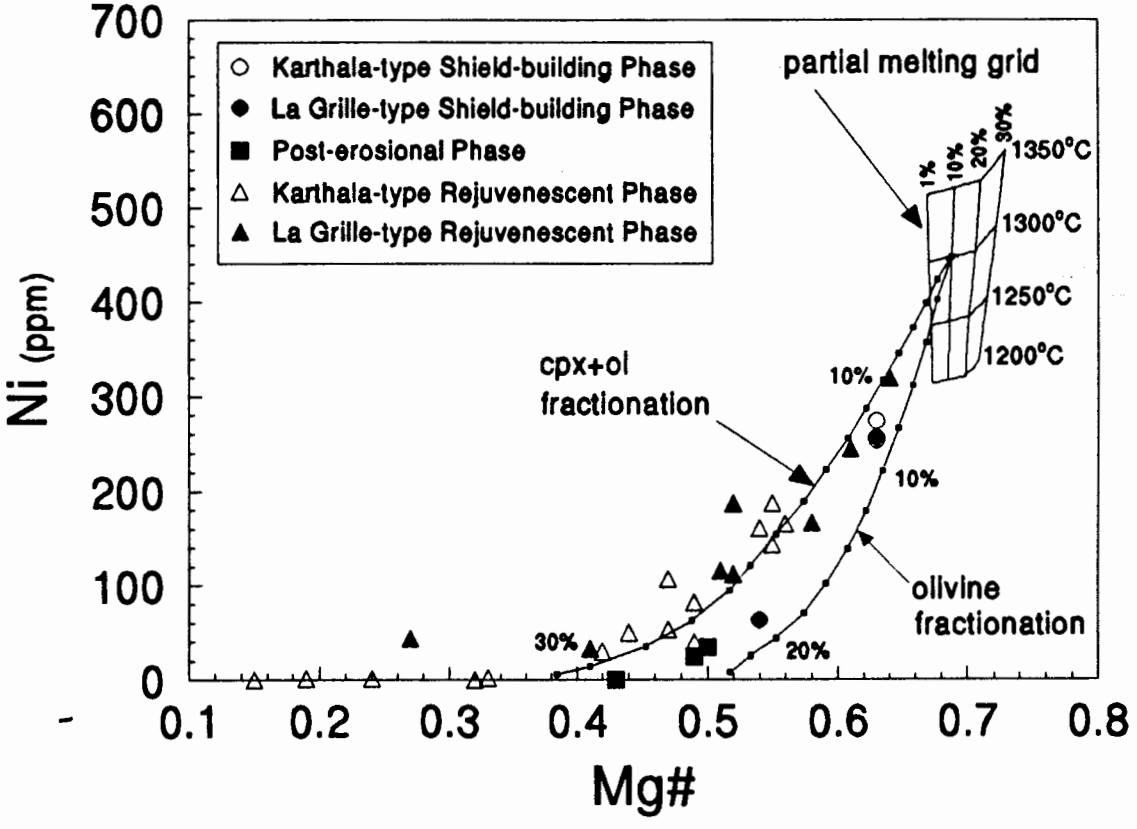

Fig. 8.5. Plot of Ni (ppm) vs *Mg-number* for Mayotte lavas. The partial melting grid and the fractional crystallisation trends are the same as in Fig. 8.1.

The concave upward trend defined by the Mayotte data (mimicked by Cr and Sc; Fig. 6.10) corresponds closely to the combined olivine and clinopyroxene fractional crystallisation trend. If, for simplicity's sake (and ignoring differences in age and lava type), we consider all Mayotte lavas to have been derived from a common hypothetical mantle melt (generated by 10% partial melting at 1300°C), then Fig. 8.5 suggests that somewhere between about 10% and 20% of combined olivine and clinopyroxene fractionation would have been required to produce the lavas of the Shield-building Phase and about 26% to almost 30% fractionation of the same minerals could have generated the Post-erosional lavas. The lavas of the Rejuvenescent Phase are shown to span a compositional range that appears to require degrees of fractionation which lie beyond the sensitivity of the Ni vs *Mg-number* diagram.

Although Fig. 8.5 illustrates the importance of olivine and clinopyroxene fractionation in the petrogenesis of Mayotte lavas, this diagram is insensitive to the possible involvement of other fractionating phases, such as feldspar and to a lesser extent amphibole and Fe-Ti oxide, and the highly simplified model discussed in the previous paragraph is in no way intended to suggest that the complex and extensive geochemical differentiation history of Mayotte lavas involved only two fractionating minerals. In an attempt to establish a more realistic fractionation model for Mayotte lavas, least-squares major element calculations were carried out for all potentially related samples from this island. Only models which yielded internally consistent results (sum of squares of differences between predicted and observed concentrations < 0.1) and which were consistent with observed trace element abundances are presented here. Mineral compositions used for modelling were chosen from the analyses listed in Tables 6.1, 6.3, 6.5 and 6.6. Feldspar compositions used fall into the compositional range of Mayotte feldspars listed in Table 6.4.

Amongst the Karthala-type Rejuvenescent Phase lavas, three excellent least-squares major element approximations, substantiated by good agreement between observed and calculated trace element abundances, were achieved (Tables 8.5 and 8.6), relating a potassic trachybasalt (MA-11) to a mugearite (MA-6), the same mugearite to a benmoreite (MA-14a) and one trachyte (MA-65) to another trachyte (MA-5). In combination, these models can account for a significant portion of the geochemical differentiation observed amongst this group of lavas. The models involve the fractionation of variable amounts of clinopyroxene, feldspar and titanomagnetite and very small quantities of apatite. The involvement of feldspar and apatite in the evolution of these lavas is consistent with the observed decrease in Sr and P_2O_5 concentrations with increasing differentiation respectively (see Figures 6.9 and 6.11). The anomalously high calculated Y and La abundances (compared to the observed values) in the trachyte model suggest a somewhat greater involvement of apatite than estimated for this model (typical mineral-melt distribution coefficients for Y and La in apatite range to extremely high values; see Appendix A3). Olivine fractionation is only required in one of the models, while amphibole is suggested to be the predominant fractionating phase in the transition from the mugearite to the benmoreite. A very small amount of titanite

TABLE 8.5

Major element least-squares approximations for Karthala-type Rejuvenescent Phase Mayotte lavas

Potassic Trachybasalt ⇒ Mugearite

MA-11 = 0.5782 MA-6 + 0.1559 Cpx[a] + 0.0671 TiMgt + 0.0198 Fo80 + 0.1671 Fsp[b] + 0.0079 Ap

		SiO_2	TiO_2	Al_2O_3	FeO[t]	MnO	MgO	CaO	Na_2O	K_2O	P_2O_5	
MA-11	obs.	46.91	3.09	15.18	11.74	0.18	5.47	8.91	3.72	1.95	0.76	
	calc.	46.90	3.05	15.17	11.75	0.18	5.47	8.92	3.80	2.05	0.76	
	diff.	-0.01	-0.04	-0.01	0.01	0.00	0.00	0.01	0.08	0.10	0.00	$\Sigma R^2 = 0.02$

Mugearite ⇒ Benmoreite

MA-6 = 0.7258 MA-14a + 0.0352 Cpx[c] + 0.0248 TiMgt + 0.1436 Amph + 0.0763 Fsp[d] + 0.0093 Ap

		SiO_2	TiO_2	Al_2O_3	FeO[t]	MnO	MgO	CaO	Na_2O	K_2O	P_2O_5	
MA-6	obs.	50.20	2.38	16.63	9.34	0.18	4.17	7.13	5.29	2.67	0.75	
	calc.	50.22	2.38	16.61	9.34	0.16	4.19	7.08	5.16	2.79	0.75	
	diff.	0.02	0.00	-0.02	0.00	-0.02	0.02	-0.05	-0.13	0.12	0.00	$\Sigma R^2 = 0.04$

Trachyte ⇒ Trachyte

MA-65 = 0.8962 MA-5 + 0.0445 Cpx[e] + 0.017 TiMgt + 0.0465 Fsp[f] + 0.0036 Ap + 0.004 Titanite

		SiO_2	TiO_2	Al_2O_3	FeO[t]	MnO	MgO	CaO	Na_2O	K_2O	P_2O_5	
MA-65	obs.	58.02	0.80	18.93	5.06	0.17	0.78	3.00	7.59	4.35	0.22	
	calc.	58.01	0.86	18.97	5.04	0.16	0.91	2.95	7.57	4.34	0.22	
	diff.	-0.01	0.06	0.04	-0.02	-0.01	0.13	-0.05	-0.02	-0.01	0.00	$\Sigma R^2 = 0.03$

[a]Cpx = $Wo_{46}En_{38}Fs_{16}$ (TiO_2 = 1.63 wt.%; Al_2O_3 = 5.42 wt.%); [b]Fsp = $An_{45}Ab_{37}Or_{18}$; [c]Cpx = $Wo_{47}En_{40}Fs_{13}$ (TiO_2 = 2.01 wt.%; Al_2O_3 = 5.67 wt.%); [d]Fsp = $An_{41}Ab_{42}Or_{17}$; [e]Cpx = $Wo_{50}En_{32}Fs_{18}$ (TiO_2 = 1.89 wt.%; Al_2O_3 = 6.14 wt.%); [f]Fsp = $An_{22}Ab_{77}Or_1$.

TABLE 8.6

Predicted and observed trace element concentrations (ppm) of Karthala-type Rejuvenescent Phase Mayotte lavas, calculated on the basis of the major element models presented in Table 8.5

	Potassic Trachybasalt ⇒ Mugearite			*Mugearite ⇒ Benmoreite*			*Trachyte ⇒ Trachyte*		
	MA-11	MA-6		MA-6	MA-14a		MA-65	MA-5	
	parent	differentiate		parent	differentiate		parent	differentiate	
	obs.	calc.	obs.	obs.	calc.	obs.	obs.	calc.	obs.
Zr	296	487	470	470	561	572	674	744	738
Nb	75	107	108	108	120	116	136	146	145
Y	29	30	30	30	25	25	46	43	24
Rb	40	69	77	77	103	105	127	142	154
Ba	724	871	827	827	908	736	1140	1239	1333
Sr	887	962	968	968	883	887	768	593	514
La	51	71	71	71	73	72	124	108	80
Ce	109	137	136	136	135	135	158	139	138
Nd	53	59	60	60	52	51	64	49	41
Sc	14.9	10.5	10.6	10.6	7.1	6.4	1.4	1.3	0.6
V	186	104	133	133	75	75	10	7.7	3.1
Co	42	31	33	33	24	20	5.8	5.6	3.5
Zn	114	120	119	119	123	100	95	97	95
Ni	82	57	53	53	36	30	1.3	1.1	1.2
		F = 0.5782			F = 0.7258			F = 0.8962	

Calculated using the fractional crystallisation equation of Gast (1968) and the mineral-melt distribution coefficients listed in Appendix A3.

(sphene), a phase which is present in many evolved Mayotte lavas in minor quantities, was included in the model relating the two trachytes.

Two successful major and trace element models relating La Grille-type Rejuvenescent Phase lavas to one another are presented in Tables 8.7 and 8.8. Fractional crystallisation of clinopyroxene, feldspar, amphibole, titanomagnetite, apatite and in one of the models olivine is suggested to have been involved in producing sample MA-34 (shoshonite) from MA-7 (sub-alkali basalt) and sample Ma-17 (shoshonite) from MA-34. The only unsatisfactory result in these models is the discrepancy between the observed and calculated Ba abundances in the model relating the two shoshonites to one another (Table 8.8). In Fig. 6.8, the La Grille-type Rejuvenescent Phase lavas have been shown to define a trend of increasing silica-saturation from the nepheline-normative basanites to the hypersthene- and in one case quartz-normative shoshonites, cutting across both the critical plane of silica-undersaturation (Ab-Ol-Cpx) and the plane of silica saturation (Ab-Opx-Cpx). Since, at low pressures (1 atm), the critical plane of silica-undersaturation is regarded to be a thermal divide that cannot be breached during fractional crystallisation (e.g. Yoder and Tilley, 1962), the trend followed by this suite of lavas suggests fractionation at elevated pressures.

No successful least-squares approximations relating any of the highly undersaturated Post-erosional Phase lavas to one another were achieved. Nevertheless, the geochemical similarity of these samples and their close association in space and time support the contention that they form part of the same, comagmatic suite of lavas. The significantly different mineralogy of these rocks, particularly that of MA-73 (i.e. aegirine-augite, nepheline and schorlomite phenocrysts), when compared to that of other Mayotte lavas, suggests that they evolved under markedly different physico-chemical conditions. Although schorlomite is not a typical mantle garnet and its stability limits are not known, the presence of garnet phenocrysts in Ma-73, apparently in textural equilibrium with their host lava, may point to fractionation a relatively high pressures.

TABLE 8.7

Major element least-squares approximations for La Grille-type Rejuvenescent Phase Mayotte lavas

Sub-alkali Basalt → Shoshonite

MA-7 = 0.6078 MA-34 + 0.1678 Cpx[a] + 0.0563 TiMgt + 0.0461 Fo_{77} + 0.0328 Amph + 0.0702 Fsp[b] + 0.0062 Ap

		SiO_2	TiO_2	Al_2O_3	FeO[t]	MnO	MgO	CaO	Na_2O	K_2O	P_2O_5	
MA-7	*obs.*	44.75	3.04	14.59	12.28	0.18	6.47	8.86	2.63	1.20	0.68	
	calc.	44.74	2.97	12.59	12.30	0.16	6.47	8.88	2.68	1.35	0.68	
	diff.	-0.01	-0.07	0.00	0.02	-0.02	0.00	0.02	0.05	0.15	0.00	$\Sigma R^2 = 0.03$

Shoshonite → Shoshonite

MA-34 = 0.7739 MA-17 + 0.1111 Cpx[c] + 0.0102 TiMgt + 0.0179 Amph + 0.0852 Fsp[d] + 0.0014 Ap

		SiO_2	TiO_2	Al_2O_3	FeO[t]	MnO	MgO	CaO	Na_2O	K_2O	P_2O_5	
RH-34	*obs.*	49.59	2.26	17.48	9.13	0.16	3.16	6.24	3.68	2.14	0.69	
	calc.	49.58	2.17	17.49	9.15	0.14	3.18	6.25	3.73	2.20	0.69	
	diff.	-0.01	-0.09	0.01	0.02	-0.02	0.02	0.01	0.05	0.06	0.00	$\Sigma R^2 = 0.02$

[a]Cpx = $Wo_{48}En_{38}Fs_{14}$ (TiO_2 = 2.66 wt.%; Al_2O_3 = 6.93 wt.%); [b]Fsp = $An_{64}Ab_{35}Or_1$; [c]Cpx = $Wo_{45}En_{42}Fs_{13}$ (TiO_2 = 1.42 wt.%; Al_2O_3 = 3.95 wt.%); [d]Fsp = $An_{45}Ab_{54}Or_1$.

TABLE 8.8

Predicted and observed trace element concentrations (ppm) of La Grille-type Rejuvenescent Phase Mayotte lavas, calculated on the basis of the major element model presented in Table 8.9

	MA-7 parent	*MA-34 differentiate*		*MA-34 parent*	*MA-17 differentiate*	
	obs.	*calc.*	*obs.*	*obs.*	*calc.*	*obs.*
Zr	307	466	436	436	544	562
Nb	73	100	105	105	130	125
Y	31	32	32	32	35	26
Rb	11.2	17.9	16.9	16.9	22	30
Ba	779	1246	1474	1474	1609	1354
Sr	668	921	1063	1063	982	944
La	58	71	70	70	83	79
Ce	115	131	128	128	151	140
Nd	52	57	57	57	63	57
Sc	20	9.6	9.8	9.8	11.1	10.4
V	211	122	125	125	106	103
Zn	121	117	115	115	131	119
Ni	187	39	33	39	37	44
Co	57	22	23	23	23	23
		F=0.6078			F=0.7739	

calculated using the fractional crystallisation equation of Gast (1968) and the mineral melt distribution coefficients listed in Appendix A3.

Green-core Clinopyroxenes

The occurrence in Comorean lavas, of complex clinopyroxene phenocrysts with green cores, pale grey to pale tan mantles and darker tan rims, was noted in Chapters 5 and 6 and the chemical characteristics of such clinopyroxenes from Mayotte were described in Chapter 6 (Figures 6.3 and 6.4). Clinopyroxenes fitting this description are quite frequently reported from alkaline basaltic lavas and they clearly document significant variations in the physico-chemical conditions under which they crystallised. The continuous chemical transition from the mantles to the rims observed in the green-core clinopyroxenes of Mayotte (e.g. Fig. 6.4) reflect the effects of normal clinopyroxene evolution with decreasing temperature at constant pressure, such as increasing Fe, Al and Ti, but decreasing Si and Mg (e.g Thompson, 1974; Duda and Schmincke, 1985;). Barton *et al.* (1982) suggested that the mantles, together with the bulk of the "normal" phenocrysts and microphenocrysts, represent the equilibrium, pre-eruption clinopyroxene composition, whereas the rims correspond chemically to groundmass clinopyroxene and grew during eruption and quenching. The chemically distinct green clinopyroxene cores in Comorean lavas were clearly not in equilibrium with their host lavas under the same conditions at which the titaniferous clinopyroxenes (i.e. clinopyroxene mantles and rims, "normal" clinopyroxene phenocrysts, groundmass clinopyroxene) were crystallising prior to, and during, eruption at near-atmospheric pressures. Disequilibrium conditions are also suggested by the rounded appearance of many of the green cores and the frequent occurrence of sieve-textured clinopyroxene cores.

Several possible modes of origin have been proposed for green clinopyroxene cores in alkaline basaltic lavas. It has been suggested, that these clinopyroxene cores could be cognate with respect to their host lavas, having been formed under pressure, temperature and fO_2 regimes significantly different from those under which the mantles and rims were precipitated (Scott, 1976; Brooks and Printzlau, 1978; Duda and Schmincke, 1985). Barton and van Bergen (1981), on the other hand, concluded that green clinopyroxenes in a potassic alkaline lava from Leucite Hills, Wyoming, originated by disagregation of mantle xenoliths which were accidentally sampled by the host lava during ascent. Several workers have proposed that the green cores represent xenocrysts which were

incorporated into their present host lavas as a result of magma mixing (Brooks and Printzlau, 1978; Barton *et al.*, 1982; Duda and Schmincke, 1985; Haase and Devey, 1994). In this scenario, the green clinopyroxenes are believed to have crystallised at depth from relatively evolved liquids produced by the differentiation of alkali basaltic magmas which were subsequently mixed with more voluminous, more primitive, Mg-rich magmas, resulting in the partial resorption of the green clinopyroxenes and their eventual overgrowth by more magnesian titanaugite at shallow depths.

Aoki and Kushiro (1968) proposed that the relative proportions of Al in the tetrahedral and octahedral sites of clinopyroxene crystals may be related to the physico-chemical conditions under which they crystallised. These authors suggested, that at high temperatures, Al prefers the tetrahedral sites to the octahedral ones, but that at high pressures, the converse is true. Based on this relationship, a diagram of Al^{VI} vs Al^{IV} may thus be used to evaluate the pressure and temperature conditions under which a particular clinopyroxene crystal equilibrated (Aoki and Kushiro, 1968; Aoki and Shiba, 1973; Wass, 1979; Haase and Devey, 1994). Fig. 8.6 shows such a diagram for the green-core clinopyroxenes from Mayotte lavas.

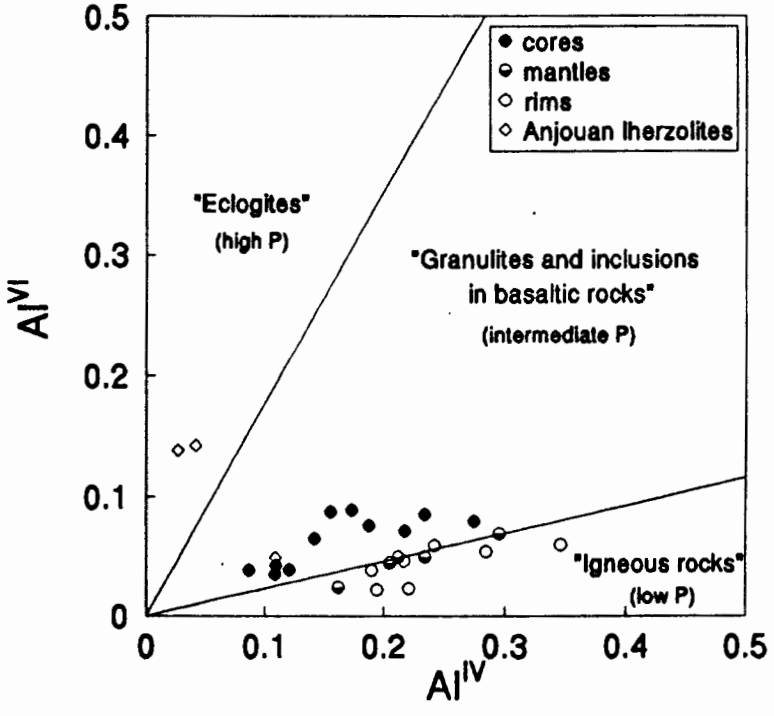

Fig. 8.6. Plot of Al^{VI} vs Al^{IV} for cores, mantles and rims of green-core clinopyroxenes from Mayotte lavas and three clinopyroxenes from spinel-lherzolite xenoliths found in Anjouan lavas (Ludden, 1977). The diagram has been divided into fields occupied by clinopyroxenes in "igneous rocks", "granulites + inclusions in basaltic rocks" and "eclogites" according to Aoki and Kushiro (1968). These fields are considered to correspond broadly to low, intermediate and high pressure conditions respectively.

Also shown in Fig. 8.6, are the fields representative of the pressure and temperature conditions appropriate for clinopyroxenes in "igneous rocks", "granulites and inclusions in basaltic rocks" and "eclogites" as delineated empirically by Aoki and Kushiro (1968).

All of the green cores analysed in this study fall into the field of "granulites and inclusions in basaltic rocks", whereas with very few exceptions, the mantles and rims of these clinopyroxenes have lower Al^{VI}/Al^{IV} ratios and plot in the field of "igneous rocks". This relationship suggests that the green cores crystallised at greater pressures than their mantles and rims. Based on the Al^{VI} vs Al^{IV} diagram, Aoki and Kushiro (1968) suggested that clinopyroxenes from Dreiser Weiher, Eifel (which plot in the "granulites and inclusions in basaltic rocks" field) possibly crystallised at relatively deep levels (20-30 km) in the continental crust and Haase and Devey (1994) argued that the green cores of clinopyroxenes in the alkaline lavas of Vesteris Seamount, Greenland Basin (which plot in the same field) were generated at depths corresponding to pressures of 5-15 kb in the upper oceanic mantle.

Also plotted on Fig. 8.6, are three clinopyroxene analyses from spinel lherzolite xenoliths found in Anjouan lavas (Ludden, 1977). Ludden (1977) proposed that these lherzolite xenoliths are residual after basalt extraction and originate from mantle depths corresponding to pressures of < 20-25 kb. Two of these analyses plot in the high-pressure "eclogite" field and the green cores of Mayotte clinopyroxenes could clearly not have been generated by the disagregation of such xenoliths. The third clinopyroxene, however, has an Al^{VI}/Al^{IV} ratio identical to that of the green cores of Mayotte clinopyroxenes and based only on Fig. 8.6, the disintegration of xenoliths bearing similar clinopyroxenes could therefore represent a potential source of green core clinopyroxenes in Mayotte lavas. Importantly, however, all three of the xenolith clinopyroxenes from Anjouan are Cr-diopsides which are chemically very different from the green clinopyroxene cores, containing much less FeO^t (2.3-2.8 wt.%), but significantly more MgO (16.4-16.7 wt.%) than the green clinopyroxene cores (FeO^t: 10.5-15.4 wt.%; MgO: 7.6-10.6 wt.%), making any genetic relationship between mantle-derived lherzolite xenoliths and the green-core clinopyroxenes observed in Comorean lavas very unlikely.

The present data thus support a magma mixing model similar to that outlined above for the formation of green-core clinopyroxenes in Comorean lavas. The chemically evolved green cores are suggested to have crystallised from differentiated alkaline magmas at depth. These magmas subsequently mixed with more voluminous, more primitive magmas that carried the green clinopyroxenes towards the surface as xenocrysts. Being in chemical disequilibrium with their new host magmas the green clinopyroxenes were partially corroded, resulting in their rounded and often sieve-textured appearance. Finally, the green clinopyroxene xenocrysts were overgrown by equilibrium titaniferous clinopyroxene mantles and rims as the magma cooled under low-pressure, near-surface conditions.

Amphibole Fractionation

The phenocrysts of kaersutitic amphibole in Mayotte lavas are generally surrounded by thick rims of Fe-Ti oxides - a feature commonly observed amongst phenocrysts of this phase and which clearly indicates the unstable nature of this mineral in the eruption environment (e.g. Baxter, 1975b; le Roex *et al.*, 1990). Amphibole is a relatively common phenocryst phase in lavas erupted on oceanic islands (e.g. Upton and Wadsworth, 1972a; Flower, 1973a; Baxter, 1975b; le Roex *et al.*, 1990; Weaver, 1990) and its presence is generally regarded to indicate elevated water pressures at some time during the evolution of a magma, typically towards the more evolved stages of a differentiation sequence (e.g. Flower, 1973a; Baxter, 1975b). In some instances, low and fractionated K/Rb ratios of ocean island lavas have been attributed to the removal of amphibole (e.g. Strong, 1972a, Flower, 1973b; Baxter, 1975a). Besides its occurrence as a phenocryst phase, kaersutite is frequently found as megacrysts and in ultramafic and mafic xenoliths included in alkaline basaltic lavas worldwide (e.g. le Maitre, 1969; Aoki, 1970; Borley *et al.*, 1971; Kesson and Price, 1972; Green *et al.*, 1974; Ellis, 1976; Reid and le Roex, 1988; Wilkinson and Hensel, 1991). These amphiboles are widely regarded to have formed as cognate, near-liquidus phases at relatively high pressures under hydrous conditions. The depth of formation of such megacrysts and xenocrysts has generally been estimated at somewhere between 5 and 30 km (le Maitre, 1969; Aoki, 1970; Borley *et al.*, 1971; Green

et al., 1974). Since kaersutite is therefore a potential fractionating phase in alkaline basaltic liquids over a wide range of pressures under hydrous conditions, it is worthwhile to consider whether there exists any evidence that the amphiboles in Mayotte lavas may have crystallised at depths greater than expected for "normal" near-surface conditions.

It appears that mantle-derived kaersutites are generally somewhat poorer in Ti, but richer in Al than kaersutites which crystallised at shallow crustal levels (Best, 1974; Vinx and Jung, 1977). Fig. 8.8 shows a diagram of Ti vs Al for amphiboles from Mayotte lavas. Rather than plotting in the field defined by amphiboles of shallow intrusive origin, with very few exceptions, Mayotte amphiboles fall into the field occupied by mantle-derived kaersutites. Although the Ti and Al contents of Mayotte amphiboles on their own represent insufficient evidence to prove that they originated at mantle depths, they make derivation from regions of relatively elevated pressure a distinct possibility.

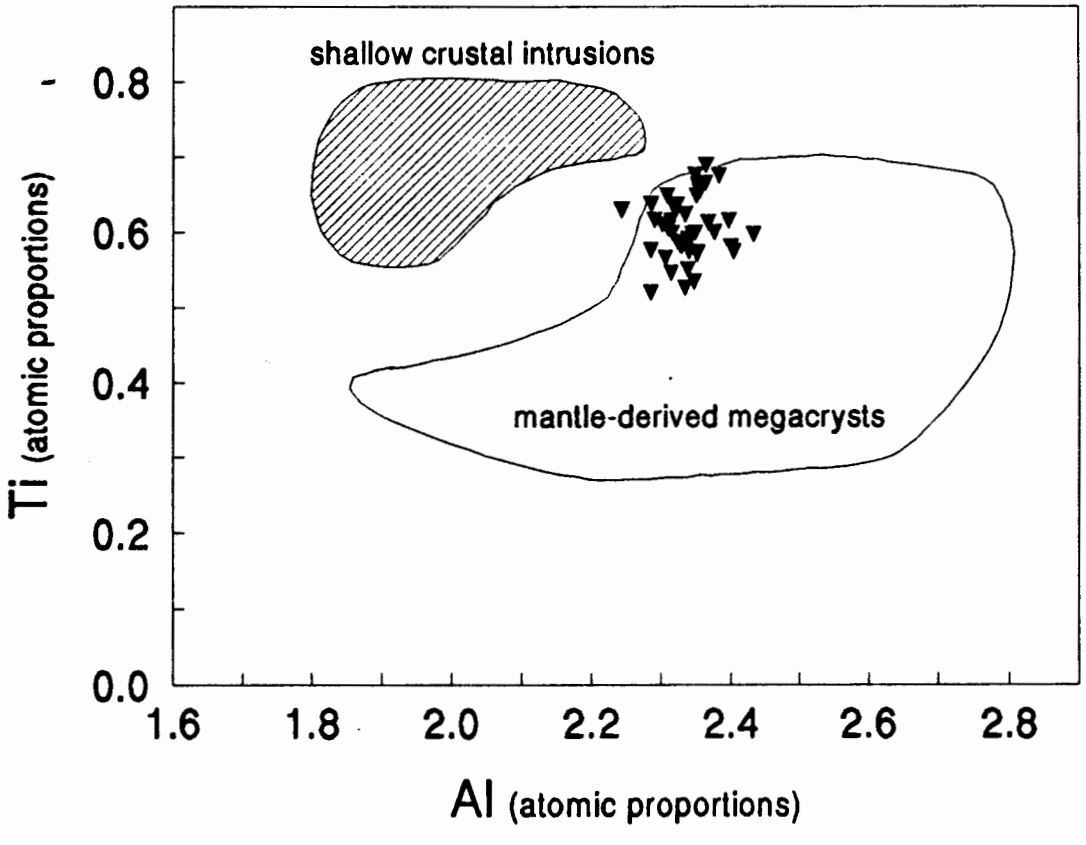

Fig. 8.7. Plot of Ti vs Al (atomic proportions) for Mayotte amphiboles. Also shown are fields representative of amphiboles from shallow crustal intrusions and of mantle-derived amphibole megacrysts (Best, 1974; Vinx and Jung, 1977).

Depth of Crystallisation

Although much of the differentiation of Comorean magmas by processes of fractional crystallisation may have occurred at relatively shallow levels, close to the Earth's surface, several pieces of evidence presented in this chapter suggest that this differentiation may in fact have started at greater depths and may have continued over a significant pressure range. Such evidence for polybaric fractionation in Comores lavas includes the presence of potentially high-pressure garnet phenocrysts in the Mayotte Post-erosional Phase nephelinite MA-73, the trend of increasing silica-saturation amongst the La Grille-type Rejuvenescent lavas of Mayotte, the occurrence of green-core clinopyroxenes and the presence of amphibole phenocrysts potentially crystallised at elevated pressures.

The results of melting and crystallisation experiments conducted on alkalic basalts at different pressures may shed more light on the possible polybaric origin of Comores lavas. Such experiments have shown that at pressures between 0 and 5 kb the order of crystallisation for lavas similar in composition to those of the Comores is olivine, followed by plagioclase, followed by clinopyroxene (ol→plag→cpx; Tilley *et al.*, 1971; Thompson, 1972; Mahood and Baker, 1986; Fisk *et al.*, 1988). The order of crystallisation changes to ol→cpx→plag between 5 and 8 kb (Fisk *et al.*, 1988) and to cpx→ol→plag at pressures above 8 kb (Mahood and Baker, 1986; Fisk *et al.*, 1988). Based on these experimental constraints, Albarede and Tamagnan (1988) concluded that lavas from Piton de la Fournaise on Réunion, for which they established a crystallisation order of ol→cpx→plag, started to differentiate by fractional crystallisation at depths greater than 15 km. Similar conclusions were drawn by Hoernle and Schmincke (1993a) for lavas from Gran Canaria.

The petrography of the mafic lavas from all three Comores islands investigated is dominated by olivine and clinopyroxene (see Chapters 4, 5 and 6), plagioclase only becoming important as a phenocryst phase in the more evolved rocks of Mayotte. The crystallisation sequence thus appears to have been ol→cpx→plag (or even cpx→ol→plag), rather than ol→plag→cpx, and based on the experimental results described above, would suggest that fractional crystallisation started at depths equivalent to pressures of more

than 5 kb.

One-atmosphere melting experiments conducted on Anjouan lavas have, however, shown that in at least some Comorean lavas, clinopyroxene is a low-pressure liquidus or near-liquidus phase together with olivine, followed at much lower temperatures by the crystallisation of plagioclase (Thompson and Flower, 1971; Thompson, 1972). The early olivine- and clinopyroxene-dominated differentiation of lavas from the other Comores islands does therefore not necessarily imply fractionation at depth, although this possibility can not be entirely disregarded either.

In closing this chapter, two of the main conclusions regarding the petrogenesis of Comorean lavas may be summarised as follows: firstly, the differentiation of Comorean lavas was largely the result of early fractionation of olivine and clinopyroxene, followed at more evolved stages by Fe-Ti oxide, feldspar, amphibole, as well as small amounts of apatite and in some cases titanite; secondly, the fractional crystallisation processes involved in the differentiation of Comorean lavas were not confined to shallow, sub-volcanic levels, but rather, several lines of evidence suggest that these processes were more complex and may have started at mantle depths corresponding to pressures as high as 15 kb.

9. PARTIAL MELTING

The formation of mafic, silica-undersaturated, alkaline magmas, such as the alkali basalts, basanites and nephelinites erupted on the Comores, has been the subject of intense study and debate in the Earth science community for several decades, resulting in a wealth of experimental data and theoretical conclusions on the issue. Although the fractional crystallisation of orthopyroxene, clinopyroxene, olivine and garnet at high pressures has previously been put forward as a possible model for the formation of silica-undersaturated alkali basalts, basanites and nephelinites from more silica-rich primary mantle melts (Green and Ringwood, 1964; O'Hara and Yoder, 1967; Bultitude and Green, 1967; Green, 1969, 1970), such fractional crystallisation schemes, which would lead to significant iron-enrichment and anomalously low *Mg-numbers*, have generally been abandoned more recently in favour of an origin of such magmas by partial melting processes (e.g. Bultitude and Green, 1971; Edgar, 1987).

The most important factors determining the composition of magmas produced by partial melting in the Earth's mantle are the mineralogy and chemistry of the parental material, the depth of melt generation and segregation, the volatile content (H_2O, CO_2) of the source material and the degree of partial melting. Several workers have proposed that the genesis of basic, silica-undersaturated, alkaline magmas by realistic degrees of partial melting requires mantle source regions which are significantly enriched in incompatible elements relative to the estimated compositions of primitive mantle and the source of N-type MORB (e.g. Sun and Hanson, 1975; Frey *et al.*, 1978; Clague and Frey, 1982). The results of numerous melting experiments conducted on a variety of natural and synthetic mantle compositions have been published and the most important of these experimental studies pertinent to the generation of alkaline magmas were reviewed by Edgar (1987). Kushiro and Kuno (1963) pointed out the dependence of magma compositions on the depth of partial melt generation, suggesting that with increasing depth, partial melting of mantle peridotite produces increasingly silica-undersaturated liquids. In contradiction to this, Chen and Frey (1983) proposed a model for Hawaiian volcanism according to which Hawaiian tholeiites segregated from their source at greater depth than Hawaiian alkalic magmas. More recently, however, Clague (1987) has

suggested that there exists a general consensus that all of the alkalic Hawaiian lavas did, in fact, originate from greater mantle depths than the Hawaiian tholeiites. According to Green (1970, 1971), progressively more silica-undersaturated, alkali-rich magmas may be produced at progressively greater depth by decreasing degrees of partial melting of a hydrous peridotite (pyrolite) mantle. The hypothesis that the extent of partial melting increases in the sequence nephelinite to basanite to alkali basalt has furthermore been widely confirmed by trace element studies (e.g. Kay and Gast, 1973; Sun and Hanson, 1975; Frey *et al.*, 1978). Significant advances have recently been made in quantifying the behaviour of major and minor elements during partial melting in the upper oceanic mantle (e.g. Niu and Batiza, 1991; Kinzler and Grove, 1992a,b), but these models are only applicable to the relatively shallow melting processes in operation beneath mid-oceanic ridges and are probably not strictly appropriate to the more deep-seated melting events that generate silica-undersaturated alkaline magmas. The important role of the H_2O and CO_2 contents of the source in the formation of silica-undersaturated magmas was emphasised by Eggler (1978) and Wyllie (1979), who argued that an increasing CO_2/H_2O source ratio leads to increasingly silica-undersaturated melts. Trends of increasing silica-undersaturation among primary mantle melts have been ascribed to an expansion of the primary-phase field of orthopyroxene as a result of increasing pressure with increasing mantle depth (Green and Ringwood, 1964), the presence of H_2O (Green, 1969, 1970) and the presence of CO_2 (Eggler, 1978). Green (1970, 1971) published a schematic petrogenetic grid for mantle-derived basaltic magmas, according to which magmas with the compositions of alkali basalts, basanites and nephelinites could be generated by respectively 15-20%, 5-15% and 5% partial melting of a hydrous pyrolite source at pressures of about 13-20 kb. Based on the results of partial melting experiments, Green (1973a) concluded that olivine-rich basanite could be produced by 6% partial melting of a hydrous pyrolite (0.2-0.4% H_2O) at pressures of 25-30 kb. More recently, Foley (1988) outlined the possible generation of alkaline basaltic magmas by "redox melting" (Taylor and Green, 1989) in the upper mantle. Redox melting involves the interaction of CH_4-rich fluids rising from reduced, deep asthenospheric levels, with relatively oxidised overlying material, during which the oxidation of CH_4 results in the precipitation of solid carbon and in the formation of H_2O, which in turn leads to increased αH_2O, a subsequent depression of mantle solidus temperatures and eventually

to the initiation of melting.

Although it is thus difficult to constrain the exact conditions of partial melting for a primary magma of a particular composition, the general trend is apparent and based on the above discussion, it is suggested that the chemical differences between the alkali basalts, basanites and nephelinites erupted on the Comores Archipelago are primarily the result of decreasing degrees of partial melting at increasing mantle depths. On *Grande Comore*, it is therefore proposed, that the basanitic La Grille lavas were generated by smaller degrees of partial melting at greater depths than the primary precursors of the alkali basaltic Karthala lavas. This proposal is consistent with Strong's (1972b) suggestion that La Grille and Karthala lavas were produced by less than 10% and more than 10% partial melting of a garnet-lherzolite source respectively, although he proposed pressures of around 25 to 30 kb for both cases (see Chapter 3). The geochemical differences between the alkali basalts, basanites and nephelinites of *Moheli* are suggested to be the results of progressively smaller degrees of partial melting at progressively greater mantle depths (Strong's (1972a) "high-pressure trend"; see Chapter 3), whereas on *Mayotte*, the primary magmas from which the La Grille-type lavas (including the Post-erosional Phase lavas) were derived, are proposed to have been produced by smaller degrees of partial melting at greater depths than the primary magmas that gave rise to the typically somewhat less silica-undersaturated Karthala-type magmas. The suggestion that the compositional variations observed amongst basic Comorean lavas reflect predominantly the effects of variable degrees of partial melting, rather than the effects of source region heterogeneities, is supported by the fact that all Comorean lavas analysed have overlapping ranges of incompatible element ratios and, with the exception of Karthala lavas, also have nearly identical Sr and Nd isotopic compositions, suggesting a broadly homogeneous mantle source for all Comorean lavas (see Chapter 11).

A question of considerable interest in basalt petrogenesis, which is directly related to the depth of melting, is whether or not the mantle source which melted to produce the magma contained residual garnet. At depths corresponding to pressures of between about 10 and 25 kb (~33-80 km), spinel-lherzolite represents the stable mineralogy in the

Earth's mantle (e.g. BVSP, 1981). At pressures above 25 kb, however, spinel is unstable and spinel-lherzolite gives way to garnet-lherzolite as the equilibrium mineral assemblage. Since garnet strongly prefers the heavy REE (HREE) over the light REE (LREE) during magmatic processes, chondrite-normalised REE plots may be useful in evaluating the role of garnet during partial melting. If garnet is a residual phase during melting, it will strongly retain the HREE relative to the LREE and the REE pattern of a melt produced in equilibrium with residual garnet would be expected to be steeper and possibly cutting across the REE pattern of a comparable melt generated from a garnet-free source. Residual garnet in a mantle melting region should therefore lead to melts with relatively high chondrite-normalised ratios of La/Yb and La/Y (in which case Y is assumed to mimic the geochemical behaviour of the HREE Ho), compared to melts produced from sources without residual garnet. The REE patterns of Comorean lavas are, of course, not only dependant on the degree of partial melting and the presence or absence of residual garnet in their source regions, but they are also a function of the REE pattern of their source materials. Although it is difficult to ascertain the shape of the chondrite-normalised REE pattern of the Comorean mantle source (e.g. flat or LREE enriched), it should be noted here that the mantle source of Comorean lavas is probably relatively enriched in incompatible elements compared to primitive mantle (as described in more detail in Chapter 11) and it is therefore a reasonable assumption that this source is, in fact, also enriched in the LREE relative to the less incompatible HREE. Small degrees of partial melting of such a LREE-enriched source could generate the high LREE concentrations of Comorean lavas in general, but the presence of residual garnet in the source would be expected to result in particularly low HREE abundances and chondrite-normalised REE patterns which cut across those of lavas produced by partial melting of a similar source in the absence of residual garnet.

In the case of *Grande Comore*, it was shown in Chapter 4 that La Grille lavas have significantly steeper REE patterns and greater $(La/Yb)_n$ ratios than Karthala lavas, all of the La Grille REE patterns cutting across one of the Karthala patterns (Fig. 4.9). La Grille lavas also have significantly greater $(La/Y)_n$ ratios (13.8-17.8) than Karthala lavas (9.4-10.2) and it is therefore suggested that La Grille lavas were derived from a garnet-bearing mantle source, whereas garnet was not a residual phase during melting of the

source of Karthala lavas. Small degrees of partial melting of a LREE-enriched Comorean mantle source could easily account for the high LREE concentrations observed amongst Grande Comore lavas in general and La Grille lavas in particular. The comparatively low chondrite-normalised HREE abundances of La Grille lavas (in relation to Karthala lavas), however, point towards the effects of residual garnet in the La Grille source which preferentially retains the HREE relative to the LREE, resulting in high $(La/Yb)_n$ and $(La/Y)_n$ ratios and steep chondrite-normalised REE patterns which cut across those of the Karthala lavas.

It was noted in Chapter 5, that of the *Moheli* lavas analysed for the REE, all of the nephelinites have steeper REE patterns and greater $(La/Yb)_n$ ratios than the basanites and alkali basalts and cross-cut the REE patterns of these lavas in the middle to heavy REE range (Fig. 5.10). The nephelinites also tend to have greater $(La/Y)_n$ ratios (14.3-21.2) than the basanites (12.7-17.5) and the samples from both of these lava suites have greater $(La/Y)_n$ ratios than the alkali basalts (8.6-11.6). It is proposed that the nephelinites and probably the basanites of Moheli were formed as the result of partial melting of a garnet-bearing mantle source, whereas the source of the Moheli alkali basalts was probably shallower and free of garnet.

The role of garnet in the source regions of Moheli basanites and nephelinites is substantiated by the behaviour of certain incompatible trace element ratios in these lavas. The incompatible trace element ratios Zr/Nb and Y/Nb show a considerable range amongst Moheli lavas and when plotted against Zr, the majority of the alkali basalts in particular, define a linear trend over a relatively large range of Zr/Nb and Y/Nb ratios (Fig. 5.8). Although magmatic processes such as partial melting and fractional crystallisation can cause only limited variation in such incompatible trace element ratios (e.g. Erlank and Kable, 1976; Weaver *et al.*, 1987), partial melting is appreciably more effective in changing such ratios than is fractional crystallisation. It is proposed here, that the observed variations are the result mainly of partial melting processes. This suggestion is supported by Fig. 9.1, which shows the variation in Zr/Nb ratio with respect to Zr abundance in Moheli lavas, onto which model trends for partial melting and fractional crystallisation have been superimposed. While the partial melting

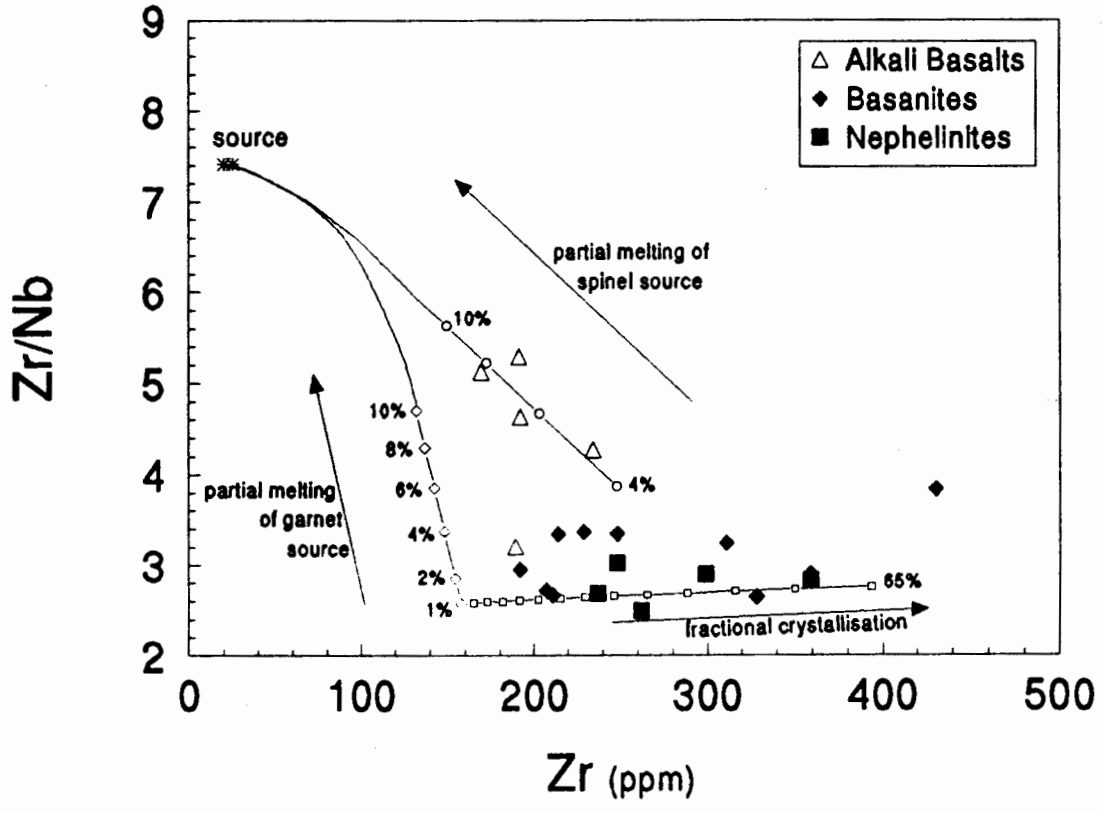

Fig. 9.1. Plot of Zr/Nb vs Zr (ppm) for Moheli lavas. The lines joining the open diamonds and circles represent trends of non-modal equilibrium partial melting of a garnet-lherzolite source and a spinel-lherzolite source respectively (calculated according to Hertogen and Gijbels, 1976 and Consolmagno and Drake, 1976). The line joining the open squares represents the trend of combined fractional crystallisation of cpx, ol, Fe-Ti oxide, feldspar and amphibole (in proportions of 35:15:7:35:8 respectively) in steps of 5%, calculated using the fractional crystallisation equation of Gast (1968). Mineral-melt distribution coefficients used in all models are listed in Appendix A3. Parameters used for partial melting models: spinel-lherzolite source mineralogy: 55%ol+25%opx+18%cpx+2%spinel, melting in proportions of 10:20:68:2 respectively (Johnson *et al.*, 1990); garnet-lherzolite source mineralogy: 55%ol+20%opx+11%cpx+7%gt+7%amph, melting in proportions of 3:3:21:23:50 respectively (*cf.* Johnson *et al.*, 1990). Reasons for including amphibole in the garnet-bearing source will become apparent in Chapter 10. Before plotting, the alkali basalt compositions, which do not represent primary melts, were recalculated to approximately primary melt compositions by adding olivine and clinopyroxene in amounts estimated from Fig. 8.2. Amounts of ol and cpx (in proportions of 40:60) added: RH-15: 3%, RH-17: 5%, RH-28: 17%, RH-16: 17%.

trends are quite steep, indicating relatively large changes in Zr/Nb ratio, the fractional crystallisation trend is almost horizontal and is clearly incapable of generating significant variations in this ratio (for details on the crystallisation and partial melting models, see caption to Fig. 9.1). According to the partial melting models shown in Fig. 9.1, the data from Moheli alkali basalts (with the exception of RH-42) are consistent with a derivation

by about 4 to 8% partial melting of a spinel-lherzolite source. The basanites and nephelinites, on the other hand, are consistent with having been derived by fractional crystallisation following comparatively smaller degrees (~1-4%) of partial melting of a garnet-lherzolite source. In more detail, Fig. 9.1 suggests that the nephelinites resulted from relatively smaller degrees of partial melting than most of the basanites.

The La Grille-type Shield-building lavas of *Mayotte* were shown to have greater $(La/Yb)_n$ ratios and steeper REE patterns than the Karthala-type Shield-building lavas (Fig. 6.14). The former also have greater $(La/Y)_n$ ratios (12.4-14.7) than the latter (7.9-9.0) and probably resulted from partial melting of a garnet-bearing mantle source. The La Grille-type and Karthala-type Rejuvenescent Phase lavas of Mayotte have steep, overlapping REE patterns (Fig. 6.14) as well as overlapping $(La/Yb)_n$ and $(La/Y)_n$ ratios and based purely on their REE data, no conclusion can be drawn about the possible role of garnet in their source regions.

Hoernle and Schmincke (1993a) used a plot of mole% MgO vs mole% FeO^t to estimate the depths of melting for the mafic volcanics of Gran Canaria. On such a diagram, lines of olivine fractionation or accumulation are nearly perpendicular to the FeO^t axis (Hanson and Langmuir, 1978) and the FeO content of mafic melts may be regarded as a petrogenetic indicator which should reflect the FeO content of their parental primary mantle melts relatively closely, even if the melts have experienced considerable olivine fractionation or accumulation (Langmuir and Hanson, 1980). The FeO (and MgO) content of melts is, however, affected by the pressure at which melting begins, the extent of melting and the FeO/MgO ratio of the source material (Langmuir and Hanson, 1980). Based on a comparison between data from Gran Canaria and the results of high-pressure melting experiments conducted on mantle compositions, Hoernle and Schmincke (1993a) concluded that mafic Gran Canaria volcanics were produced by partial melting at pressures greater than 30 kb. Fig. 9.2 shows a diagram of mole% MgO vs mole% FeO^t for all Comores lavas analysed in this study. Also shown are the field defined by the mafic volcanics from Gran Canaria investigated by Hoernle and Schmincke (1993a), the fields occupied by experimental mantle melts produced at pressures of 20, 30 and 35 kb and the field of melting for Hawaiian pyrolite.

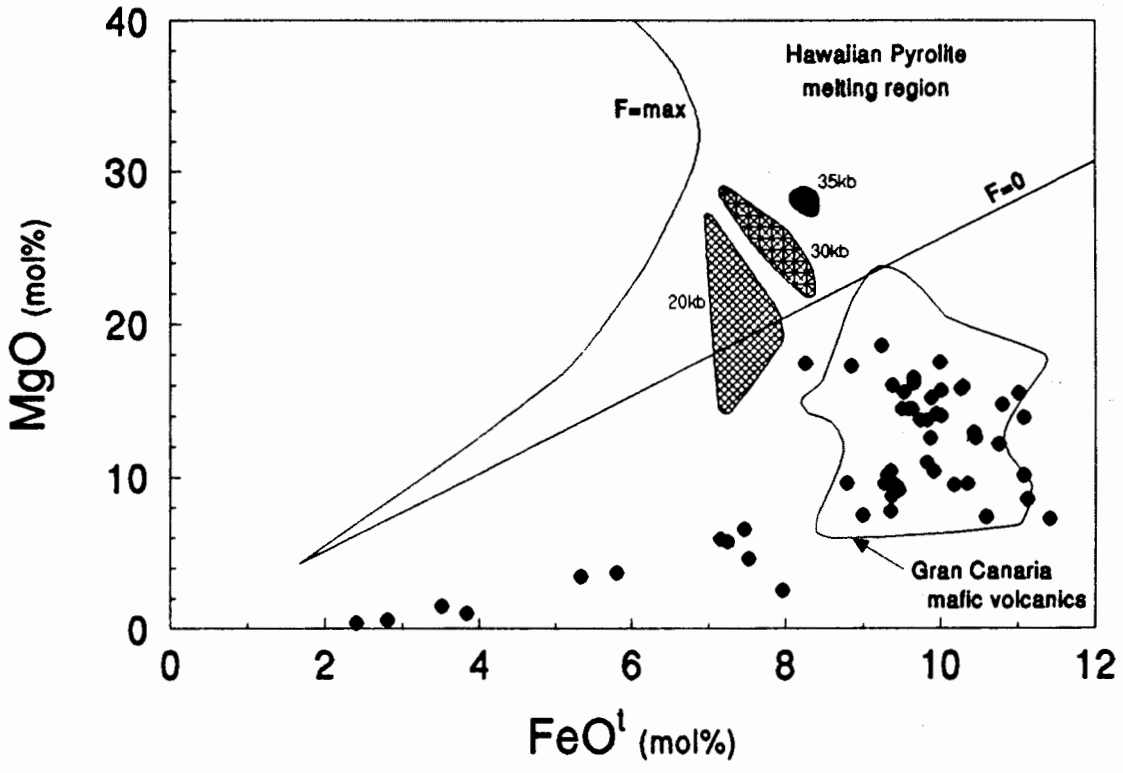

Fig. 9.2. Plot of MgO vs FeO^t (both in mole%) for all Comorean lavas analysed in this study. Also shown: field of melting for Hawaiian pyrolite at 1 atm (Hanson and Langmuir, 1978), field occupied by mafic volcanics from Gran Canaria (Hoernle and Schmincke, 1993a) and fields for experimental mantle melts generated at pressures of 20, 30 and 35 kb (Hoernle and Schmincke, 1993a and references therein).

Although the more evolved Comores lavas reach very low FeO^t values, indicative of significant fractionation involving minerals other than olivine, the majority of the more primitive lavas plot within the field defined by the mafic volcanic of Gran Canaria. The high FeO content of mafic Comorean lavas illustrated by Fig. 9.2 is consistent with the derivation of these lavas by comparatively deep-seated mantle melting. To attach any rigid, quantitative estimate of depth of melting to this conclusion is, however, unwarranted. Langmuir and Hanson (1980) noted the importance of the FeO/MgO ratio of source materials on the FeO content of resulting melts and estimated that a variation of one mole% FeO in the source may be equivalent to a difference of about 7 kb in the pressure at which melting begins, thus making accurate determinations of melting depths impossible.

In summary, the evidence and arguments presented in this chapter point towards the derivation of primary Comorean magmas by partial melting at considerable mantle depths, spanning the transition from spinel-lherzolite to garnet-lherzolite. It appears that, in general, Karthala and Karthala-type lavas owe their origin to comparatively larger (compared to La Grille and La Grille-type lavas) degrees of partial melting of spinel-lherzolite at mantle depths corresponding to pressures of less than about 25 kb (~80 km). La Grille lavas and the primary melts giving rise to La Grille-type lavas, on the other hand, are consistent with having been produced by somewhat smaller degrees of melting of garnet-lherzolite at mantle pressures above 25 kb. This model for the generation of Comorean magmas is broadly consistent with Wyllie's (1989) proposal that a variety of alkalic melts (including nephelinitic ones) may be produced at a mantle depth of approximately 70 to 90 km (the location of a solidus ledge in the system peridotite-CO_2-H_2O).

10. THE ORIGIN OF LA GRILLE-TYPE INCOMPATIBLE ELEMENT PATTERNS

It was shown in Chapters 4 (Fig. 4.8), 5 (Fig. 5.9) and 6 (Fig. 6.13) that all samples analysed in this study may be assigned to one of two distinct lava types: all lavas erupted by La Grille volcano on Grande Comore, all basanites and nephelinites from Moheli and more than half of the lavas from Mayotte are La Grille-type lavas, whereas all lavas erupted by Karthala volcano, as well as all alkali basalts from Moheli and all remaining samples from Mayotte are Karthala-type lavas. This classification is based solely on the primitive mantle-normalised incompatible element patterns of Comorean volcanics: the La Grille-type lavas displaying a significant relative depletion in K (and in many cases Rb) which is not observed in the Karthala-type lavas. The aim of this chapter is to establish the most likely mode of origin for these two Comorean lava types.

Derivation of the two lava types by partial melting of geochemically different mantle sources appears to be an obvious possibility for their origin and the fact that the Nd and Sr isotopic signatures of lavas from the La Grille and Karthala volcanoes are notably different (Chapter 4) seems to be in accordance with this hypothesis. The isotopic signature of Karthala lavas is, however, not only different to that of La Grille lavas, but also to that of all other Comorean lavas. No distinction can be made between the $^{87}Sr/^{86}Sr$ and $^{143}Nd/^{144}Nd$ values of the lavas from Moheli, Mayotte and La Grille, but all of these lavas have Sr and Nd isotopic compositions which are significantly different to those of Karthala lavas (Chapter 11). In addition, it will be shown in Chapter 11 that all of the Comores lavas analysed have overlapping highly incompatible element ratios, making it impossible to distinguish between the two lava types. It is therefore concluded, that the difference between La Grille- and Karthala-type Comorean lavas is not the result of derivation from geochemically different mantle source materials.

It should be noted at this point that of the two lava types, the La Grille-type is really the anomalous one, since the undepleted (with respect to K and Rb) Karthala-type pattern approximates the pattern which would be expected to result from partial melting of a "normal", incompatible element enriched lherzolitic mantle. During small degrees of partial melting of a mantle source consisting of olivine, orthopyroxene, clinopyroxene and

spinel or garnet, the relative incompatibilities of the elements plotted on the spidergrams are expected to increase fairly consistently from right to left and therefore, the mantle-normalised abundances of these elements in the resulting partial melts are expected to increase reasonably consistently in the same direction. The very highly incompatible elements plotted on the left side of the spidergrams (Nb, K, Rb, Ba) all have very similar incompatibilities (e.g. Sun and McDonough, 1989) and small degree partial melts produced from a lherzolite source may thus show relatively flat patterns in this part of the spidergrams, similar to those of the Karthala-type lavas, but they are certainly not expected to display the very distinct K-depletions typical of the La Grille-type lavas. The important issue at hand is thus to evaluate possible modes of origin for the La Grille-type incompatible element patterns.

It is also worth noting that K-depleted incompatible element patterns very similar to those of La Grille-type Comorean lavas may be found amongst the volcanics erupted on a number of ocean islands worldwide (Fig. 10.1) and the conclusions drawn from the present discussion may have some relevance to the petrogenesis of these lavas.

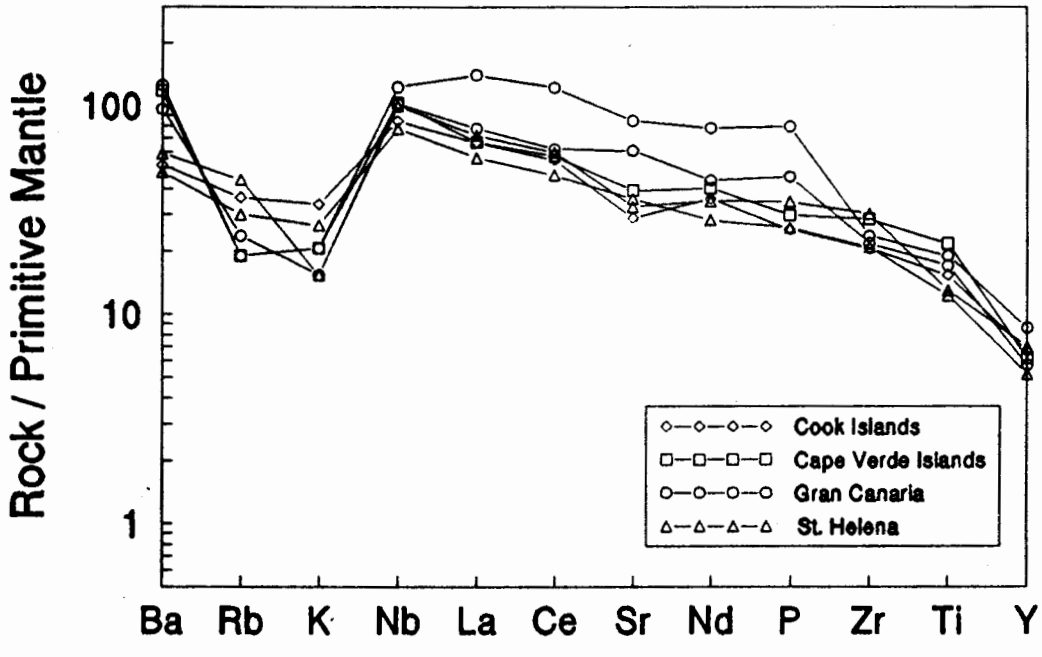

Fig. 10.1. Primitive mantle-normalised incompatible element patterns of selected alkaline basaltic lavas from Gran Canaria (Hoernle and Schmincke, 1993a), St. Helena (Weaver *et al.*, 1987), the Cape Verde Islands (Gerlach *et al.*, 1988) and the Cook Islands (Palacz and Saunders, 1986), showing relative depletions in K (and Rb). Normalising values from Sun and McDonough (1989).

Assuming derivation from a broadly homogeneous source, the relative K-depletion of La Grille-type lavas may be the result of one of the following magmatic processes:

- fractional crystallisation of amphibole,
- fractional crystallisation of phlogopite,
- partial melting of a phlogopite-bearing source,
- partial melting of an amphibole-bearing source.

To what extent each of these possibilities are consistent with the present data will be discussed in a semi-quantitative manner below.

Fractional Crystallisation of Amphibole

Strong (1972a) suggested that, what he termed a "potassium deficiency" in Moheli basanites may have resulted from about 20% fractional crystallisation of amphibole. Without doubt, kaersutitic amphibole was in equilibrium with lavas from Moheli (Strong, 1972a) and Mayotte (Chapters 6 and 8) at some stage during their evolution, but whether fractionation of this mineral lead to the significant relative K-depletions observed in La Grille-type lavas is questionable. Well-constrained major element least-squares approximations and corresponding trace element models have confirmed the importance of amphibole fractionation during the later stages of the differentiation history of Comorean lavas, particularly the Rejuvenescent Phase lavas of Mayotte (Chapter 8). The evolution of both the La Grille- and Karthala-types of Rejuvenescent Mayotte lavas appears to have involved significant amphibole fractionation, but no signs of progressive K-depletion or compositional trends from Karthala-type lavas towards La Grille-type lavas are discernable. Although, in the case of lavas erupted from La Grille volcano, the absence of amphibole crystals does not necessarily invalidate the possibility of extensive amphibole fractionation (all petrographic evidence of which could have been eliminated by crystal settling at depth), the removal of significant quantities of this phase would inevitably have led to a decrease in the *Mg-number* of residual liquids. This observation is, however, in total contradiction to the fact that La Grille lavas have primary or near-primary *Mg-numbers* and that Karthala lavas, which do not show the K-depletion have evolved *Mg-numbers*.

Simple calculations were carried out to evaluate the effect of amphibole fractionation on an undepleted (with respect to K) model primary melt produced from a hypothetical lherzolitic mantle source. A 6% partial melt with overall incompatible element abundances approximating those of Comorean lavas has a higher concentration of K than Mayotte kaersutites[1] and fractionation of such amphiboles would lead to a relative enrichment in K, rather than a depletion. Even if anomalously high K-contents are assumed for the fractionating amphibole, unrealistically large amounts (> >50%) of pure amphibole removal would be required to generate relative K-depletions comparable to those observed in La Grille-type lavas.

Fractional crystallisation of amphibole is therefore not considered to be a viable mechanism for the origin of La Grille-type Comorean lavas.

Fractional Crystallisation of Phlogopite

Phlogopite is significantly more K-rich than amphibole and the fractional crystallisation of this mineral could conceivably have generated the K-depletion typical of La Grille-type incompatible element patterns.

Although the occurrence of modal phlogopite in Comores lavas would have strengthened the case for its fractionation, the absence of this phase in the rocks investigated does not eliminate the possibility of phlogopite crystallisation and removal by gravitational settling at depth (an origin by crystal fractionation at depth has been suggested for mica megacrysts in several alkaline volcanics; e.g. Ellis, 1976; Wilkinson and Hensel, 1991) .

Fig. 10.2 shows model incompatible element patterns which illustrate the effect of phlogopite fractionation on a liquid generated by 6% partial melting of a hypothetical garnet-lherzolite mantle. Shown for comparison are the patterns of a La Grille-type lava (RH-7) and a Karthala-type lava (GC-3). For clarity, the model patterns were calculated

[1]in fact, most real Comorean lavas in general and the majority of Karthala-type Comorean lavas in particular contain more K than Mayotte kaersutites

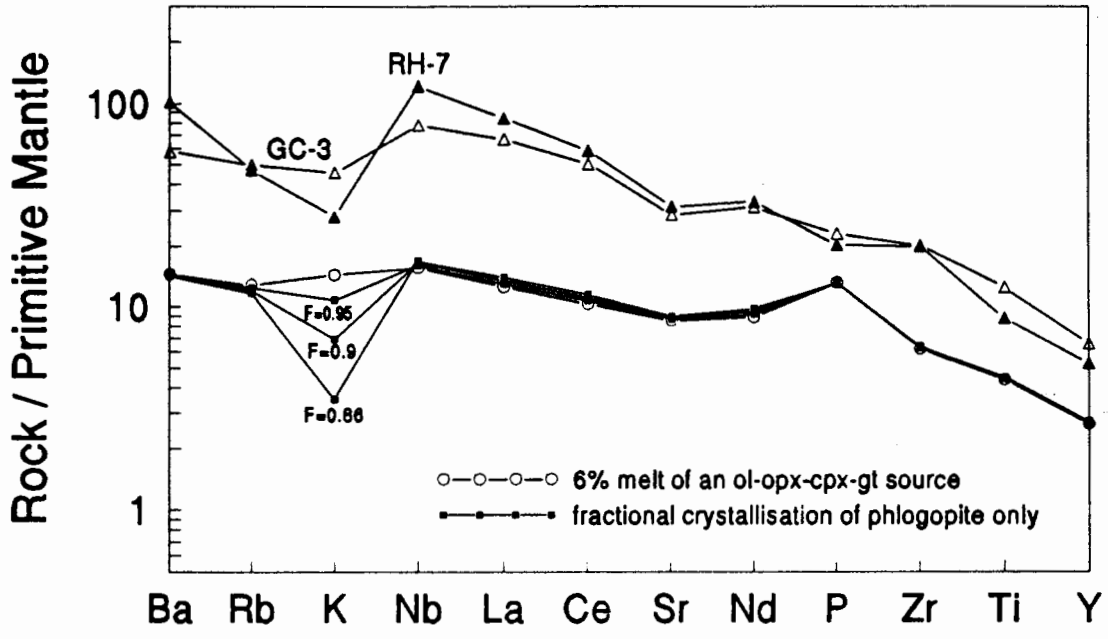

Fig. 10.2. Primitive mantle-normalised incompatible element patterns illustrating the effect of pure phlogopite fractionation on a liquid produced by 6% non-modal equilibrium melting of a hypothetical garnet-lherzolite mantle source. The patterns for a La Grille lava (RH-7) and a Karthala lava (GC-3) are shown for comparison. Normalising values from Sun and McDonough (1989). For the partial melting model, calculated according to Hertogen and Gijbels (1976) and Consolmagno and Drake (1976): source mineralogy: 55%ol+20%opx+15%cpx+10%gt, melting in proportions of 3:3:44:50 respectively (Johnson *et al.*, 1990); source element abundances: primitive mantle composition of Sun and McDonough (1989). For the phlogopite fractionation models, the fractional crystallisation equation of Gast (1968) was used to calculate the abundances of all elements, except K. Because K is a stoichiometric component of phlogopite, K abundances for the crystallisation models were calculated by mass balance, using a phlogopite with 9.8 wt.% K_2O (Deer *et al.*, 1962b). Since the incompatible element abundances of real Comorean lavas are enriched by a factor of about four, relative to small degree melts of Sun and McDonough's (1989) primitive mantle, the K content of the fractionating phlogopite was scaled down by the same factor in order to produce realistic model patterns. The scaling avoids overlapping of the model patterns with the patterns of RH-7 and GC-3 and thus makes comparison easier. Using a model mantle source enriched four times relative to primitive mantle (i.e. a source approaching the composition of the real Comorean mantle source) and using an unscaled K content in the crystallising phlogopite would result in model element abundances approximating those of real Comorean lavas. The mineral-melt distribution coefficients (for all elements except K) used in melting and crystallisation models are listed in Appendix A3.

at abundance levels below those of real Comorean lavas by scaling the parameters involved in the calculations (for details of the models, see caption of Fig. 10.2), but all discussions and conclusions are directly applicable to abundance levels of real Comorean samples. The model patterns displayed in Fig. 10.2 imply that on the order of 14% of pure phlogopite fractionation is required to generate a relative K-depletion comparable

to that observed in the La Grille lava RH-7. It is also clear from this diagram, however, that phlogopite removal is incapable of producing any significant degree of Rb-depletion (which would be required in the case of at least some La Grille-type lavas). Furthermore, as in the case of amphibole fractionation, phlogopite fractionation, presumably in combination with other phases such as olivine and clinopyroxene, would be expected to result in a decrease in the *Mg-number* of the derivative magmas, which is inconsistent with the primary to near-primary *Mg-numbers* of La Grille lavas.

Partial Melting of a Phlogopite-bearing Source

Phlogopite has been widely suggested to be an important hydrous, K-bearing phase in the Earth's mantle, which may play a significant role in the genesis of alkaline basaltic magmas and in the distribution of elements such as K and Rb in such melts (e.g. Flower, 1971b; Forbes and Flower, 1974; Beswick, 1976; Greenough, 1988). High pressure experiments have shown that, depending on parameters such as phlogopite composition, ambient water pressure and the nature of the local geotherm, phlogopite may have an upper stability limit ranging from at least 32 kb to more than 40 kb, suggesting that this mineral may be a stable mantle phase at depths of well over 100 km (Kushiro *et al.*, 1967; Kushiro, 1970). The occurrence of phlogopite in the Earth's mantle is supported by reports of what appears to be primary, mantle-derived mica in peridotite xenoliths from Lashaine volcano, northern Tanzania (Dawson and Powell, 1969) and as xenocrysts from Jan Mayen Island (Flower, 1971b). Primary phlogopite has also been recognised in mantle-derived xenoliths found in kimberlites (e.g. Erlank *et al.*, 1987; Harte *et al.*, 1987).

Curiously, partial melting of phlogopite-bearing mantle source material has been postulated to generate both magmas with relative K-depletions (e.g. Mertes and Schmincke, 1985; Hoernle and Schmincke, 1993a,b), as well as magmas strongly enriched in K (e.g. Sheraton and Cundari, 1980; Cullers *et al.*, 1985). Flower (1971b) suggested that during partial melting at low pressures, Ti-rich phlogopite behaves as a supra-liquidus phase which withholds elements such as K from the liquid phase, whereas "at higher pressures, small degrees of partial melting, involving mainly phlogopite, would be

expected to produce liquids enriched in these elements".

Späth and le Roex (1994) proposed that the K-depletion observed in La Grille-type Comorean lavas is the result of very small degree (~1%) partial melting of a residual phlogopite-bearing mantle source. The melting models on which this suggestion was based, were calculated using published mineral-melt distribution coefficients in conjunction with "normal" trace element melting equations (Hertogen and Gijbels, 1976; Consolmagno and Drake, 1976) for all elements, including K. The fact that K is a stoichiometric constituent of phlogopite means, however, that it can not be reliably treated as a trace element in this mineral and the applicability of mineral-melt distribution coefficients and trace element melting equations therefore becomes suspect (Hanson and Langmuir, 1978; Greenough, 1988).

In the present study, the behaviour of K during partial melting of a phlogopite-bearing source is modelled following the method outlined by Greenough (1988). Assuming that all K in the source is contained in phlogopite (contributions by all other mantle phases are considered to be trivial), the concentration of K in the melt is dependent only on the proportion in which phlogopite enters the melt and will remain constant as long as any residual phlogopite remains. All phlogopite will be consumed at relatively small degrees of melting (e.g. Forbes and Flower, 1974; Greenough, 1988) and this mineral is therefore assumed to enter the melt in a fixed proportion of 0.5 relative to other minerals in the source (*cf.* Greenough, 1988). Using a K_2O content of 9.8% for phlogopite (Deer et al., 1962b), the concentration of K in the model melt generated will remain constant at just over 40 000 ppm (~163 times primitive mantle) as long as phlogopite remains a residual solid. The K content of most La Grille-type Comorean lavas is, however, only on the order of about 20 to 50 times primitive mantle, making an origin by small degree partial melting of a phlogopite-bearing source highly unlikely. Even if phlogopite with an anomalously low K content is considered, the low K abundances of La Grille-type lavas can not be achieved by melting in the presence of residual phlogopite. Only if melting continues beyond the stage when all phlogopite and therefore all K has entered the melt, will the K abundance of the magma start to decrease as a result of dilution. Incompatible element abundances (with the exception of K) of Comorean lavas are enriched by a

factor of about four, relative to small degree (~1-6%) partial melts produced from a source with the composition of Sun and McDonough's (1989) primitive mantle, suggesting that the source of Comorean lavas is enriched by approximately the same factor, relative to this primitive mantle. Following this argument and keeping in mind previous assumptions, the source of Comores lavas would be expected to contain on the order of 1000 ppm K and approximately 1.2% phlogopite. In order to dilute the K content of a partial melt derived from such a source to levels of abundance comparable to those observed in La Grille-type lavas would require degrees of melting of around 15% - a suggestion which is inconsistent with the low degree of partial melting generally considered to give rise to such alkaline, silica-undersaturated magmas.

It is thus concluded from the discussion above, that partial melting of a phlogopite-bearing mantle source is not capable of generating the La Grille-type lavas erupted on the islands of the Comores Archipelago.

Partial Melting of an Amphibole-bearing Source

Amphibole is another hydrous, K-bearing mineral which could potentially play an important role in the distribution of K during partial melting in the mantle. Experimental estimates of the upper stability limit of this mineral, which has been suggested by several workers to be present as an accessory phase in the Earth's mantle (Oxburgh, 1964; Kesson and Price, 1972; Wyllie, 1978; Wilkinson and le Maitre, 1987), range from as little as 22 kb to as much as 35 kb (Green, 1973b; Allen and Boettcher, 1973; Holloway and Ford, 1973; Allen *et al.*, 1975; Olafsson and Eggler, 1983) and Varne (1970) reported supposedly primary, mantle-derived amphibole in lherzolite nodules from Kirsh volcano, Arabia. Mertes and Schmincke (1985) proposed that amphibole was an accessory phase in the source region of an olivine nephelinite and basanite suite from the Quaternary West Eifel, Germany, and Haase and Devey (1994) suggested that relative depletions of K and Rb in lavas from Vesteris Seamount, Greenland Basin, could be explained as a result of residual amphibole (or phlogopite) in their source.

As is the case for phlogopite, most appeals for the presence of residual amphibole in the source regions of alkaline basaltic magmas appear to be intuitive and qualitative, rather than quantitative. In an attempt to evaluate the possible role of residual amphibole in the mantle source of Comorean lavas, a semi-quantitative approach analogous to that employed in the previous section of this chapter is adopted here. Since K is a major constituent of amphibole, "normal" trace element melting equations can not be reliably employed to model the behaviour of K during partial melting of an amphibole-bearing source. In analogy to the treatment of partial melting of a phlogopite-bearing source in the previous section, a mass-balance approach following Greenough (1988) is taken to determine the abundance of K in partial melts of a model amphibole-bearing source.

Fig. 10.3 shows the primitive mantle-normalised incompatible element pattern of a 1% non-modal equilibrium melt generated from a hypothetical amphibole-bearing garnet-lherzolite source. The patterns of a La Grille lava (RH-7) and a Karthala lava (GC-3) are shown for comparison. For the sake of clarity, the melting model was scaled to plot at abundance levels below those of real Comorean lavas, analogous to the model patterns in Fig. 10.2. The details of the melting model are outlined in the caption to Fig. 10.3 and only the most important aspects need to be mentioned here. All K in the source is assumed to reside in the amphibole (contributions from all other phases are considered irrelevant) and, being an early melting phase, this mineral is considered to dominate the composition of all small degree melts which it enters in a proportion of 0.5 relative to the other phases comprising the source. As argued previously, the source region of Comorean lavas appears to be enriched by a factor of about four, relative to Sun and McDonough's (1989) primitive mantle composition, suggesting a K content of 1000 ppm, corresponding to an estimated 7% amphibole. The melting model shown in Fig. 10.3 mimics the shape of the La Grille lava RH-7 very closely. In addition to being able to account for the significant K-depletion, the presence of residual amphibole during melting also results in a notable relative Rb-depletion. This partial melting model is preferred to all other models discussed here as the most likely mode of origin for La Grille-type lavas.

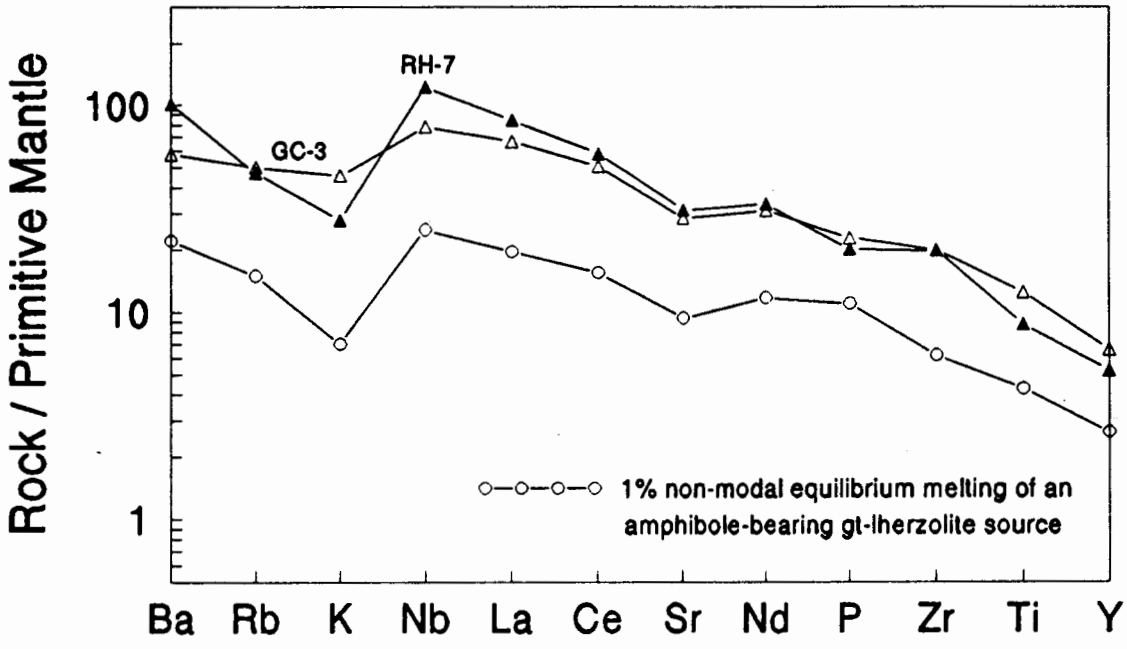

Fig. 10.3. Primitive mantle-normalised incompatible element pattern of a 1% non-modal equilibrium melt of a hypothetical, amphibole-bearing model mantle source. The patterns for a La Grille lava (RH-7) and a Karthala lava (GC-3) are shown for comparison. Normalising values from Sun and McDonough (1989). With the exception of K, all element abundances for the partial melting model were calculated according to Hertogen and Gijbels (1976) and Consolmagno and Drake (1976), using the mineral-melt distribution coefficients listed in Appendix A3. Source mineralogy: 55%ol+20%opx+11%cpx+7%gt+7%amph, melting in proportions of 3:3:21:23:50 respectively (*cf.* Johnson *et al.*, 1990). Source element abundances: primitive mantle composition of Sun and McDonough (1989). The abundance of K, being a major constituent of amphibole, was calculated by mass balance, using an amphibole containing 1.7 wt.% K_2O (Deer *et al.*, 1962c). To facilitate easy comparison with the patterns of real Comorean lavas, the model pattern was calculated at abundances lower than those of real Comorean samples by using Sun and McDonough's (1989) primitive mantle composition and scaling down the abundance of K in the amphibole by a factor of four (since Comorean source regions appear to be enriched by this factor relative to primitive mantle). The Comorean mantle source is suggested to contain approximately 1000 ppm K, contained in 7% amphibole which is completely consumed after 14% of partial melting.

The most important conclusion drawn from the discussion presented in this chapter is therefore that the distinct differences between La Grille- and Karthala-type Comorean lavas are best explained as a result, not of differences in source geochemistry, but rather of differences in residual source mineralogy. Small degree partial melting of an amphibole-bearing garnet-lherzolite source is considered to be the most likely mode of origin of the K-depleted La Grille-type lavas erupted on the Comores. The Karthala-type lavas, which do not display any relative depletion in K, are consistent with having been produced by partial melting of a "normal", amphibole-free mantle source.

11. SOURCE REGION CHARACTERISTICS

Volcanic rocks erupted on ocean islands such as the Comores may yield invaluable information about the geochemical characteristics and evolution of their mantle source regions, particularly since their extrusion through relatively thin, basaltic, oceanic crust minimizes the potential for crustal contamination. The radiogenic isotopes of Sr, Nd, Pb and He have proved to be of great value in investigating the evolution of mantle source regions of ocean island lavas, and it is now widely believed that the range of isotopic signatures from different ocean islands may be explained as being the result of mixing relationships between several distinct mantle source components (e.g. Kurz *et al.*, 1982, 1983; McKenzie and O'Nions, 1983; Hart, 1984; Allègre and Turcotte, 1985; White, 1985; Zindler and Hart, 1986). In addition to the radiogenic isotopes, incompatible trace element concentrations and highly incompatible element ratios, have come to play an important role in evaluating the nature of suboceanic magma source regions (e.g. le Roex, 1985; Weaver *et al.*, 1986, 1987).

Incompatible Elements

All of the Comorean lavas analysed in this study have been shown to be strongly enriched in incompatible elements when compared to N-type MORB and primitive mantle compositions (Figures 4.8, 5.9 and 6.13) and in Chapter 10 it was suggested that a source, enriched in incompatible elements by a factor of about four relative to primitive mantle, was required to generate Comorean lavas at reasonable degrees of partial melting. Relatively incompatible element enriched mantle sources are frequently proposed for alkaline basaltic lava suites and are commonly regarded to be the result of mantle enrichment events involving the migration of incompatible- and volatile-rich melts or fluids (e.g. Sun and Hanson, 1975; Frey et al., 1978; Clague and Frey, 1982).

Highly incompatible element ratios such as Ba/Nb, Zr/Nb, K/Ba and K/Rb can not be fractionated significantly by magmatic processes like partial melting and fractional crystallisation, and such ratios should therefore reflect the geochemical characteristic of

the mantle source regions of lavas quite reliably. Diagrams on which highly incompatible element ratios are plotted against one another thus allow comparisons between the source regions of different mantle-derived lava suites. Fig. 11.1 shows the covariation between selected incompatible element ratios for lavas from the Comores and other Indian Ocean islands.

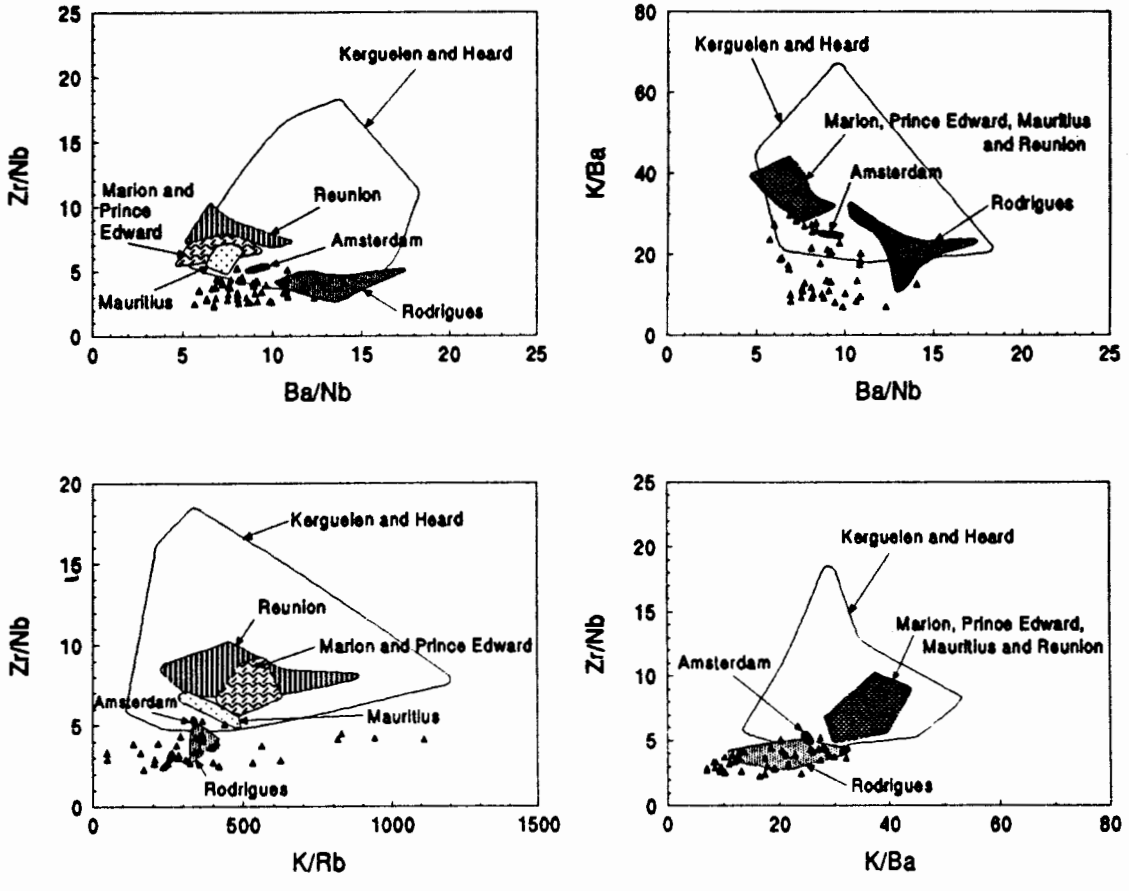

Fig. 11.1. Diagrams of incompatible element ratios, comparing Comorean lavas analysed in this study with lavas from other Indian Ocean islands. Sources: Kerguelen and Heard: Kable (1972), Storey *et al.* (1988), Davies *et al.* (1989), Gautier *et al.* (1990), Weis *et al.* (1993); Amsterdam: Kable (1972); Rodrigues: Baxter *et al.* (1985); Marion and Prince Edward: Kable *et al.* (1971), Kable (1972); Mauritius: Baxter (1975b, 1976); Réunion: Upton and Wadsworth (1972).

Comorean lavas tend to be quite distinct in these diagrams, although on some they show similarities with Amsterdam and Rodrigues. Comorean lavas display relatively large ranges in the Ba/Nb and K/Nb ratios and are characterised by comparatively low Zr/Nb and K/Ba ratios, significantly lower than those of most Marion, Prince Edward, Réunion, Mauritius, Kerguelen and Heard lavas.

The incompatible element abundances and ratios of Comorean lavas thus appear to suggest a relatively enriched mantle source which is distinctly different from that of other ocean islands in the Indian Ocean.

Radiogenic Isotopes

The Nd and Sr isotopic ratios of selected Comores lavas are shown in Fig. 11.2 and these isotopic compositions are compared to those of other ocean islands in Fig. 11.3.

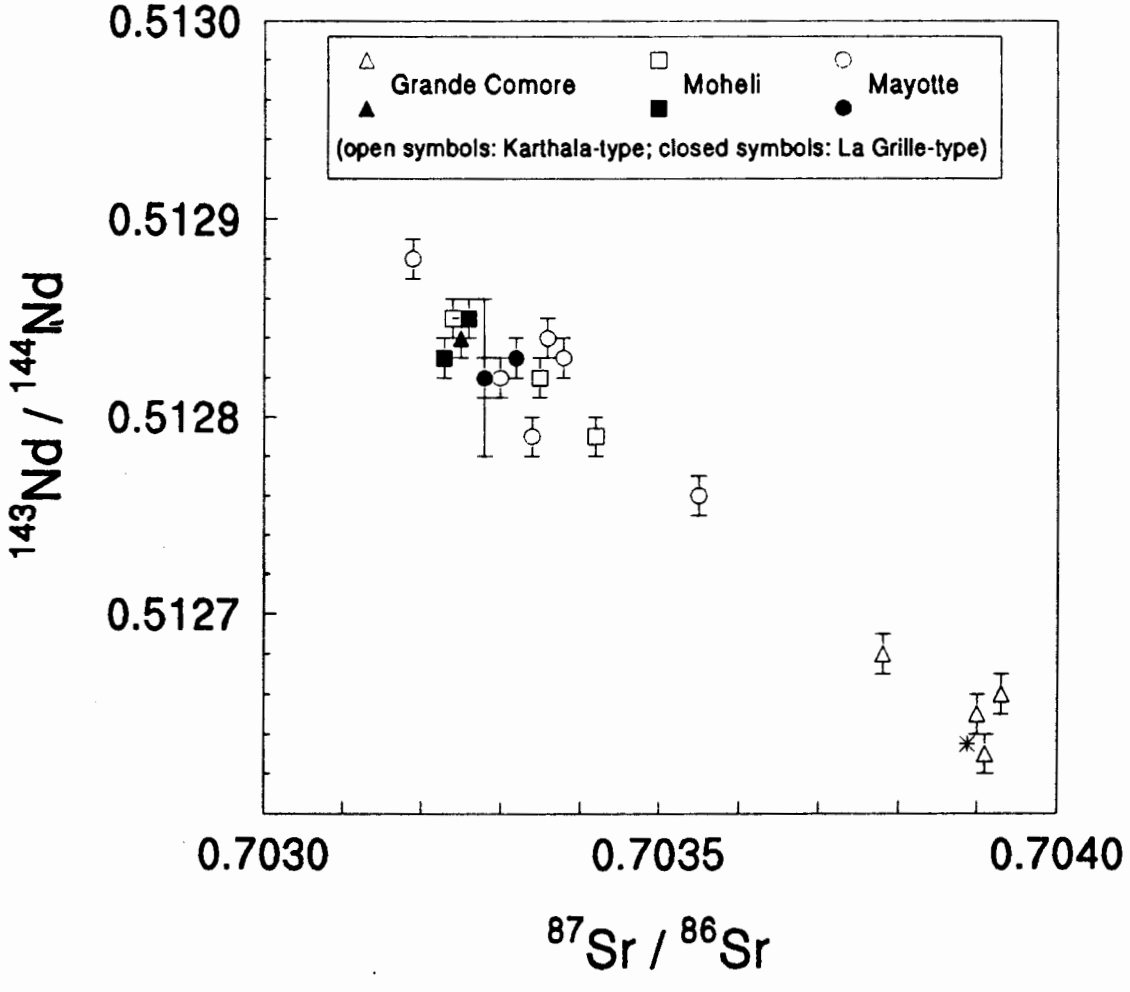

Fig. 11.2. Nd-Sr isotope correlation diagram for selected lavas from Grande Comore, Moheli and Mayotte. $2\sigma_{mean}$ error bars are shown for individual samples. The isotopic composition of one Comorean sample published by Hart *et al.* (1986) is also shown (asterisk).

Like the majority of ocean island and mid-ocean ridge lavas erupted worldwide, most Comores lavas analysed have higher $^{143}Nd/^{144}Nd$ and lower $^{87}Sr/^{86}Sr$ ratios than bulk Earth estimates, indicative of a time-averaged incompatible element depletion.

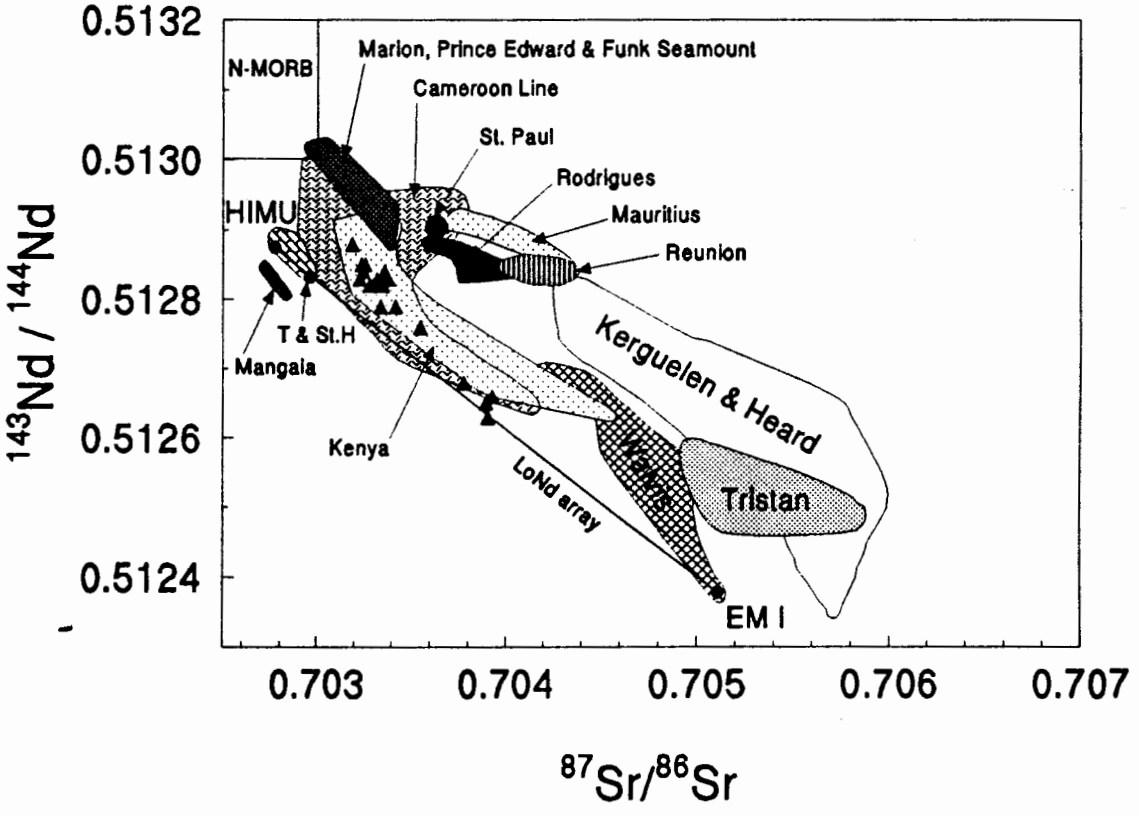

Fig. 11.3. Nd-Sr isotope correlation diagram, comparing selected Comorean lavas analysed in the present study with basaltic lavas from other oceanic and continental localities. T & St.H = Tubuaii and St. Helena. Also shown is the LoNd array of Hart *et al.* (1986). Sources of data: Kerguelen & Heard: Dosso and Murthy (1980), White and Hofmann (1982), Barling and Goldstein (1990), Gautier *et al.* (1990), Weis *et al.* (1993); Rodrigues: Baxter *et al.* (1985); Marion, Prince Edward & Funk Seamount: Hart (1988), Mahoney *et al.* (1992); Mauritius: Hamelin *et al.* (1985/86), Mahoney *et al.* (1989); St. Paul: Dupré and Allègre (1983), Michard *et al.* (1986); Réunion: Dupré and Allègre (1983), Fisk *et al.* (1988); Kenya: Norry *et al.* (1980); Walvis Ridge: Richardson *et al.* (1982); Tristan da Cunha: le Roex *et al.* (1990); Cameroon Line: Halliday *et al.* (1988, 1990); St. Helena: White and Hofmann (1982), Hart *et al.* (1986); Tubuaii: Hart *et al.* (1986); Mangaia: Palacz and Saunders (1986).

The Nd and Sr isotopic signature of Comorean lavas is unlike that of any other Indian Ocean island and in fact unlike that of most volcanic rocks from around the world, falling between the "mantle array" (defined by the majority of ocean islands) and the "LoNd array" of Hart *et al.* (1986). Lavas from Kenya and the Cameroon Line, which

overlap the field defined by Comorean lavas, appear to be two exceptions in this regard. Based on their Nd, Sr and Pb isotopic compositions, White (1985) suggested that the Comores may be assigned to the "St. Helena group" of oceanic basalts.

All of the lavas from Mayotte, Moheli and La Grille volcano analysed for their isotopic composition define a relatively small cluster of data points with restricted ranges in $^{87}Sr/^{86}Sr$ (0.70319±1 - 0.70355±1) and $^{143}Nd/^{144}Nd$ (0.51276±1 - 0.51288±1) (Fig. 11.2). These lavas appear to define a short, broad trend towards the EM I mantle component of Zindler and Hart (1986) (Fig. 11.3). Based only on their isotopic signatures, no distinction can be made between these lavas, which include representatives of both the La Grille- and Karthala-types, suggesting that they were derived from isotopically indistinguishable source regions. Lavas from Karthala volcano, the youngest lavas analysed, on the other hand, have significantly greater $^{87}Sr/^{86}Sr$ (0.70378±1 - 0.70393±1) and smaller $^{143}Nd/^{144}Nd$ (0.51263±1 - 0.51268±1) ratios, implying a different, less incompatible element depleted source.

The Sr and Nd isotopic data for Comorean lavas thus appear to suggest a change from an isotopically more or less homogeneous, depleted mantle source, which gave rise to most lavas erupted on the archipelago (La Grille, Moheli and Mayotte lavas), to a less depleted source during the formation of the youngest Comores lavas (Karthala lavas). More isotopic measurements and coupled age determinations are required to determine whether this change was gradual or abrupt.

Hart *et al.* (1986) suggested that the isotopic variations observed in the lavas of a number of ocean islands, including the Comores, which fall below the mantle array on the Nd-Sr correlation diagram, define linear trends extending from points on the LoNd array towards the mantle array, rather than forming trends collinear with the mantle array. Such isotopic trends were proposed to result from mixing between the two endmember components of the LoNd array (Tubuaii/HIMU and Walvis Ridge/EM I), followed by mixing with sources on the mantle array. With respect to the Comores, this model was based on a very limited dataset and the isotopic variations amongst the Comorean lavas analysed in the present study, which do in fact define a trend more or less parallel to

both the mantle and LoNd arrays, are entirely inconsistent with the conclusions drawn by Hart *et al.* (1986).

If the isotopic compositions of Comorean lavas are to be defined in terms of mixing relationships between distinct mantle components (e.g. those of Zindler and Hart, 1986), it is suggested here, that the source of all Comores lavas other than those erupted by Karthala represents a mixture of at least three components, namely HIMU, plus one of the depleted components (DMM or PREMA), plus either primitive mantle (BSE/PUM) or one of the enriched components (EM I or EM II). The following model is preferred for the present data: the prevailing upper mantle beneath the Comores Archipelago contains at least two mantle components, namely HIMU plus one of the depleted components (DMM or PREMA) or, as an alternative to the latter, a component on the mantle array. These components are reasonably well-mixed over a horizontal distance spanning at least the length of the archipelago. The thermal anomaly associated with the rising Comores mantle plume, an EM I plume, resulted in partial melting of this ambient sub-Comorean mantle. The isotopic signatures of the lavas produced are dominated by the components comprising the sub-Comorean upper mantle, but limited and variable contributions of material from the plume itself resulted in the short trend towards the EM I component observed amongst these lavas on the Nd-Sr correlation diagram.

The isotopic composition of the mantle source region of Karthala lavas, on the other hand, is explicable as a mixture of the same endmember components, but the substantial increase in $^{87}Sr/^{86}Sr$ and decrease in $^{143}Nd/^{144}Nd$ compared to Mayotte, Moheli and La Grille lavas suggests more substantial contributions by one of the enriched mantle components. In particular, the isotopic variation from Mayotte, Moheli and La Grille lavas to Karthala lavas defines a trend towards the EM I component. It is proposed that this trend is the result of significantly increased involvement of the EM I-type Comores mantle plume, upwelling from greater mantle depths (e.g. from the upper mantle-lower mantle boundary or the core-mantle boundary), in the genesis of the youngest Comorean lavas.

The model for the origin of the isotopic compositions of Comorean lavas presented here

appears to be broadly consistent with Class and Goldstein's (1994) proposal that the isotopic variation observed in Grande Comore lavas are the result of mixing between three components: components "G" and "X", located in the lithosphere and component "K", representing the Comores mantle plume component.

An alternative model to the one presented above involves a sub-Comorean mantle comprised of a depleted component (DMM, PREMA or a component on the mantle array) which is mixed with a Comores mantle plume that contains both HIMU and EM I components. In this scenario, the character of the plume would have to change from one dominated by the HIMU component during most of the volcanic history of the Comores, to one dominated by the EM I component during the generation of Karthala lavas. Both models (i.e. depleted component + HIMU mixing with EM I plume, and depleted component mixing with combined HIMU-EM I plume) are consistent with the present data.

Whether or not the mantle source regions of Kenyan and Cameroon Line volcanics have had similar histories as those of the lavas from the Comores must remain a matter of speculation for the time being. It is interesting to note, however, that Halliday et al. (1988, 1990) proposed that the Sr, Nd and Pb isotopic characteristics of Cameroon Line volcanics are the result of partial melting of an upper mantle source that was impregnated by the St. Helena mantle plume during the opening of the Atlantic Ocean. Lee *et al.* (1994) argued that the Sr, Nd and Pb isotopic compositions of the islands of Pagalu, São Tomé and Principe, representing the oceanic sector of the Cameroon Line, may be explained in terms of mixing of the three mantle components HIMU, EM I and DMM. According to these authors, the volcanics of the Cameroon Line originate from a sublithospheric enriched "hot zone" that is periodically fed and melted by HIMU mantle plumes which rise from greater mantle depths and entrain ambient mantle material (a mixture of EM I and DMM) during their ascent. These models thus suggest that, although the same mantle components may have been involved in producing the volcanics of the Cameroon Line and the lavas of the Comores, the relative spatial disposition of these components was different (Cameroon Line: HIMU plume mixing with ambient upper mantle comprising EM I + DMM; Comores: EM I plume mixing

with ambient upper mantle comprising HIMU + depleted component, or alternatively HIMU-EM I plume mixing with depleted component).

Mantle Depletion and Enrichment Events

The isotopic data summarised above clearly requires a mantle source for the majority of Comorean lavas which experienced an event of incompatible element depletion at some stage in its history. It was, however, also noted, that the incompatible element abundances of the same Comores lavas imply derivation from a relatively incompatible element enriched source. Examples of such an apparently paradoxical decoupling between the behaviour of incompatible element concentrations and isotopic ratios are reported quite frequently for ocean island basalts (e.g. Clague and Frey, 1982; Norry and Fitton, 1983) and such lavas are generally regarded to have been generated by partial melting of sources which suffered time-integrated incompatible element depletion, but were subsequently enriched in incompatible elements at a time sufficiently close to magma genesis to not have resulted in noticeable variations of the isotopic signature.

It is suggested that (with the exception of the material contributed by the Comores plume itself) the mantle source regions of Comorean lavas were previously depleted in incompatible elements, resulting in the low $^{87}Sr/^{86}Sr$ and high $^{143}Nd/^{144}Nd$ ratios observed, but were subsequently significantly enriched in incompatible elements relatively shortly before magma generation and segregation. Although it is conceivable that this recent enrichment event was directly or indirectly linked to the uprising Comorean mantle plume, the present data do not allow any conclusive answers in this regard.

Evidence for enrichment processes such as the one envisaged for Comorean mantle sources, commonly referred to as "mantle metasomatism", has been reported widely (e.g. Best, 1974; Boettcher and O'Neil, 1980; Menzies and Murthy, 1980a,b; Menzies *et al.*, 1987; Schiano and Clocchiatti, 1994) and metasomatising, incompatible element- and volatile-rich melts and/or fluids are thought to be ubiquitous throughout large parts of the upper reaches of the Earth's mantle. During mantle metasomatism, such melts or

fluids are considered to rise from deeper mantle levels, scavenging incompatible elements *en route* to eventually infiltrate and modify the peridotites of the upper mantle. A distinction is made between two basic types of mantle metasomatism (Dawson, 1984): *patent* or *modal metasomatism* involves the development of new, incompatible element-rich, hydrous phases, such as amphibole and mica, along grain boundaries or in metasomatic veins, whereas *cryptic metasomatism* results in incompatible element enrichment of existing minerals in the absence of newly precipitated phases. Foley (1988) suggested that in mantle regions where the ambient heat flow is too low for redox melting[1] to occur, the interaction between CH_4-rich fluids, rising from deep, reduced levels of the asthenosphere, and relatively oxidizing overlying material, may result in extensive amphibole and/or mica crystallisation. Evidence for the derivation of La Grille-type Comores lavas from an amphibole-bearing source was put forward in the previous chapter and in cognisance of the arguments presented in the present chapter, it is proposed that the amphibole in La Grille-type source regions was produced by recent modal mantle metasomatism. The mantle source of Karthala-type Comorean lavas, on the other hand, is considered to have experienced only cryptic metasomatism shortly prior to magma generation.

Schiano and Clocchiatti (1994) and Schiano *et al.* (1994) have recently reported the presence of apparently cogenetic, volatile-rich fluid and melt inclusions in the olivine, orthopyroxene and clinopyroxene crystals of ultramafic xenoliths from La Grille and other oceanic and continental localities. These authors considered the inclusions to represent trapped metasomatic melts, unrelated to their host minerals or the basaltic host magmas which transported the xenoliths to the surface. Micrometer-sized crystals of K-rich amphibole (kaersutite) and other phases, crystallised from the trapped melt droplets, were observed in some of the inclusions and Schiano *et al.* (1994) furthermore suggested that the emplacement of such melt inclusions in anhydrous peridotite xenoliths from Kerguelen was contemporaneous with the crystallisation of metasomatic amphibole in hydrous peridotites (biotitite, hornblendite) from this island. These observations provide support for the widespread existence of small amounts of migrating metasomatic

[1]for a very brief outline of the processes involved in redox melting, see Chapter 9

melts in the Earth's mantle in general and for the suggestion of a metasomatised mantle beneath the Comores in particular.

12. THE EVOLUTION OF COMOREAN VOLCANISM IN SPACE AND TIME - A SYNTHESIS

Numerous conclusions concerning various aspects of the petrogenesis and mantle source region characteristic of Comorean magmas have been drawn throughout this study and it is the aim of the present chapter to combine these independent pieces of evidence into an internally-consistent model of the nature and history of volcanic activity on the Comores Archipelago. The model proposed here will be presented with the help of a series of "cartoon" diagrams (Figures 12.1 to 12.3) which, it must be emphasised, represent highly schematic and simplistic pictures of very complex natural processes, but nevertheless serve as useful aids in depicting the envisaged scenarios. Although the model will present the evolution of Comorean volcanism in a broadly chronological order, it should be noted, that some of the events described as strictly sequential, undoubtably overlapped in time (e.g. some of the volcanic activity on the islands was most certainly synchronous).

The model described here is based on the premise that the volcanism of the Comores Archipelago represents the manifestation of an upwelling plume of mantle material - the Comores mantle plume.

The source region of all Comorean lavas experienced incompatible element depletion at some time in the relatively distant past, leading to lower $^{87}Sr/^{86}Sr$, but higher $^{143}Nd/^{144}Nd$ values than those observed for "bulk Earth". This depleted source was subsequently subjected to a mantle enrichment process, at a time close enough to the generation of the first Comorean magma so as not to affect the isotopic signature to any significant extent. It is proposed that incompatible element- and volatile-rich metasomatic melts or fluids, possibly related to the rising Comores mantle plume itself and originating from greater depth, infiltrated and pervasively modified the upper mantle underlying the Comores Archipelago (Fig. 12.1). It is furthermore suggested that the sub-Comorean mantle at depths below approximately the level of the transition from spinel-lherzolite to garnet-lherzolite (~80 km) experienced extensive modal metasomatism resulting in the precipitation of several vol.% of amphibole, whereas the spinel-lherzolite mantle

above this transition underwent cryptic metasomatism only, without the introduction of new phases.

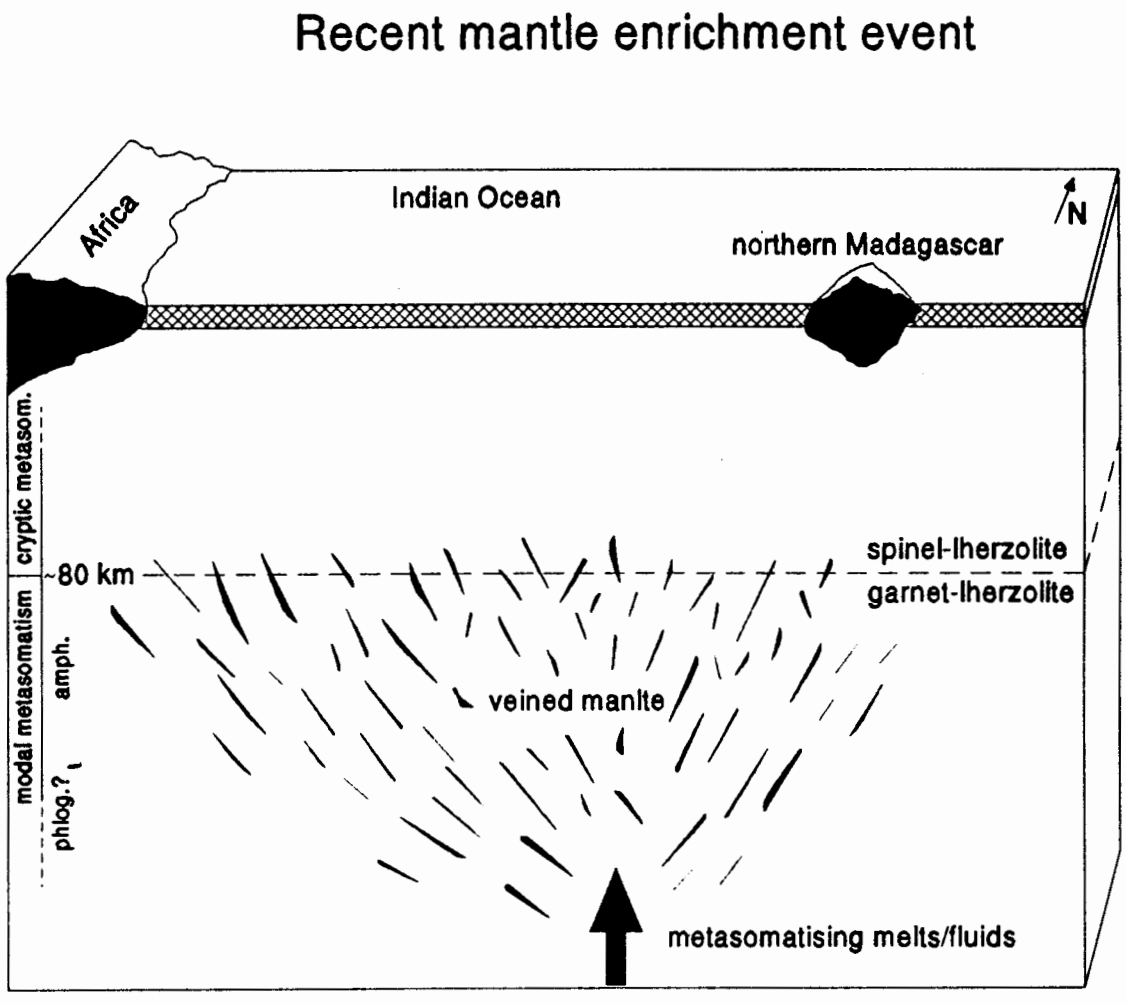

Fig. 12.1. Schematic "cartoon" cross-section through the crust and upper mantle beneath the Mozambique Channel in the vicinity of the present location of the Comores Archipelago, showing the effects of a recent mantle enrichment event. The garnet- lherzolite mantle below about 80 km depth experienced modal metasomatism resulting in the introduction of amphibole (and possibly phlogopite at greater depth). This modally metasomatised mantle is shown schematically as "veined mantle". The spinel-lherzolite above 80 km experienced cryptic metasomatism only, without the precipitation of any new minerals. See text for more detail. Not to scale.

Relatively shortly after this mantle enrichment event, the progressive increase in ambient mantle temperature as a result of the thermal anomaly associated with the rising Comores mantle plume, aided by a lowering of the mantle solidus as a result of the episode of hydrous metasomatism, led to the initiation of partial melting in the ambient

sub-Comorean mantle, generating the magmas of the Shield-building Phase of Mayotte (Fig. 12.2a).

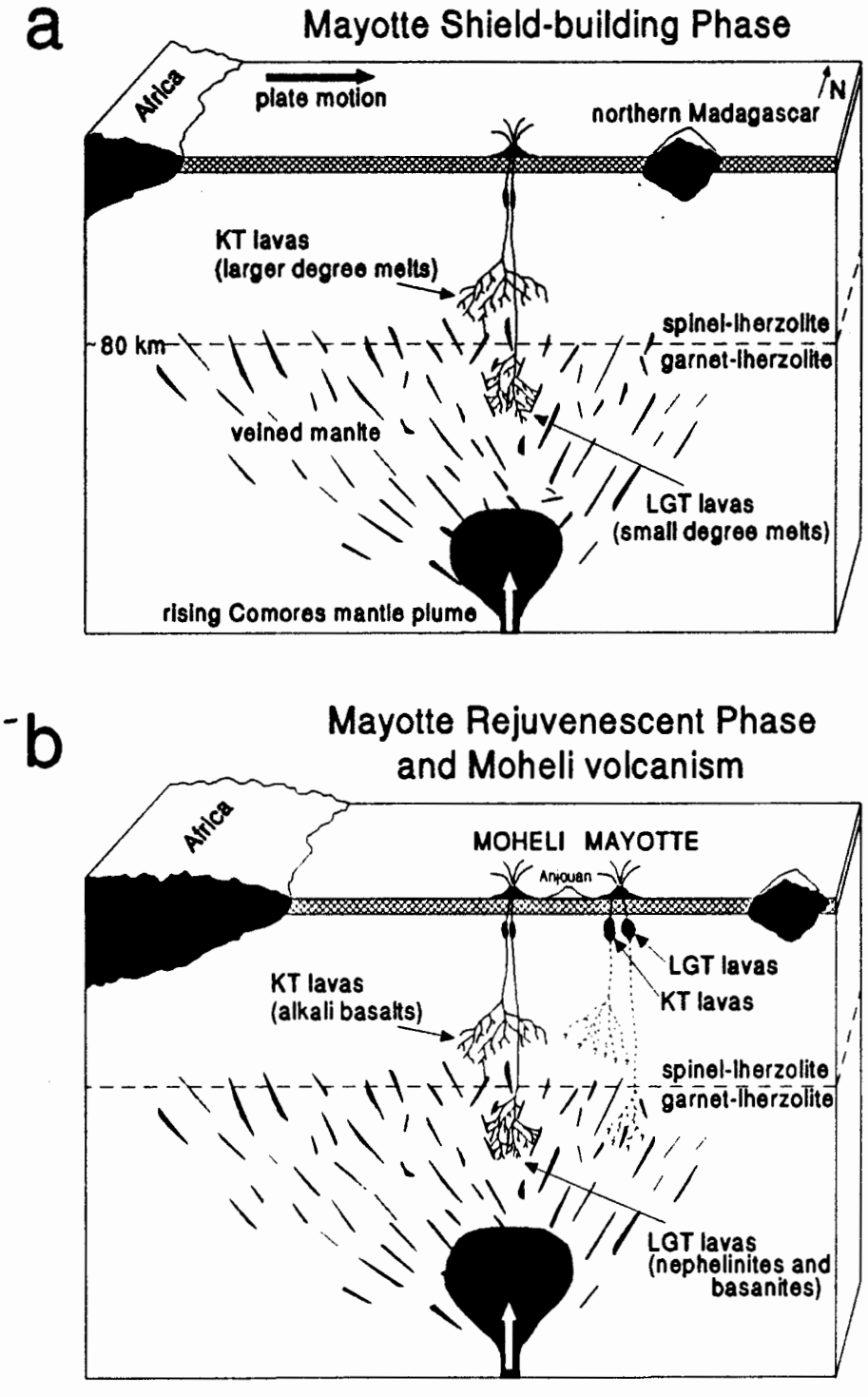

Fig. 12.2. Chronological series of schematic "cartoon" cross-sections through the crust and upper mantle beneath the Comores Archipelago, illustrating the evolution of Comorean volcanism. See text for more detail. KT = Karthala-type, LGT = La Grille-type. Sub-crustal "magma chambers" signify polybaric crystallisation. Not to scale. **(a)** Genesis of the Shield-building Phase lavas of Mayotte; **(b)** Genesis of the Rejuvenescent Phase lavas of Mayotte and the lavas of Moheli.

Only limited quantities of magma produced by decompression melting of the rising plume material itself were contributed to the formation of these lavas. Typical of the majority of Comorean lavas, the melts produced were relatively incompatible element enriched, but carried low $^{87}Sr/^{86}Sr$ and high $^{143}Nd/^{144}Nd$ isotopic signatures, being the consequences of the recent mantle metasomatism and the more ancient, time-integrated depletion respectively. The La Grille-type Shield-building lavas were the result of small degree partial melting of an amphibole-bearing garnet-lherzolite source (ol-opx-cpx-gt-amph) at depths corresponding to mantle pressures greater than about 25 kb (>80 km). The Karthala-type Shield-building lavas, on the other hand, originated from slightly larger degrees of partial melting of amphibole-free spinel-lherzolite (ol-opx-cpx-sp) at somewhat shallower depths (<80 km). None of the Shield-building lavas of Mayotte represent truly primary melts and at some stage before eruption, they experienced relatively small amounts of predominantly olivine and clinopyroxene fractionation.

The actual melting and melt migration processes involved in the generation of both La Grille- and Karthala-type lavas may possibly best be visualised in terms of an inverted "fractal tree" of melt-filled channels (Fig. 12.3, at the end of this chapter). Melting is initiated at polymineralic grain intersections in the lherzolitic mantle. In analogy to the twigs, larger branches and the trunk of a tree, microscopic, intergranular conduits, filled with buoyantly rising melt, are envisaged to coalesce into a complex network of fewer and fewer, ever-widening channelways and eventually into a single vent, transporting magma from the mantle melting region towards the surface. The analogy to a tree, as opposed to for example the drainage system of a river, accounts for the three-dimensionality of mantle melting. The possibly synchronous eruption of two quite distinct lava types on the Comores Islands implies the existence of separate and independent mantle plumbing systems for the La Grille- and Karthala-type lavas throughout the volcanic history of the Archipelago.

The generation of the Post-erosional Phase lavas of Mayotte (not shown in Fig. 12.2), following the Shield-building Phase of activity, remains somewhat enigmatic, although the highly undersaturated nature and the La Grille-type incompatible element patterns of these lavas imply very small degree melting of an amphibole-bearing source. Furthermore, the presence of garnet phenocrysts in these lavas may imply fractionation

at elevated pressures, although it must be emphasised that schorlomite is not a typical mantle garnet and that its stability limits are not known. More samples from this phase of Mayotte volcanism are required to draw more definitive conclusions concerning the origin of these lavas.

Whether the La Grille- and Karthala-type Rejuvenescent Phase lavas of Mayotte, which bear evidence for extensive polybaric fractional crystallisation of olivine, clinopyroxene, amphibole, feldspar and minor amounts of apatite and possibly titanite (sphene), were derived directly from La Grille- and Karthala-type Shield-building Phase precursors respectively or whether their genesis involved a separate episode of partial melting, is not clear (Fig. 12.2b), but considering the time interval between the Shield-building and Rejuvenescent Phases, the latter apears more likely.

The volcanic activity on Anjouan, which probably started relatively soon after the initiation of Mayotte volcanism, will not be dealt with here.

As on Mayotte, the La Grille-type lavas (nephelinites and basanites) and Karthala-type lavas (alkali basalts) of Moheli are suggested to be the result of partial melting of amphibole-bearing garnet-lherzolite and amphibole-free spinel-lherzolite sources respectively (Fig. 12.2b). After melt generation, these magmas experienced variable degrees of probably polybaric fractional crystallisation, dominated by olivine and clinopyroxene, but possibly also involving amphibole and feldspar.

The lavas erupted by La Grille volcano on Grande Comore are the products of relatively small degree partial melting of an amphibole-bearing garnet-lherzolite mantle source (Fig. 12.2c) which were rapidly transported through the mantle and crust to reach the Earth's surface in a primary or near-primary state. Typical of all Comorean lavas erupted up to this time, La Grille lavas carry relatively depleted Sr and Nd isotopic signatures (relatively high $^{143}Nd/^{144}Nd$, but low $^{87}Sr/^{86}Sr$), which are interpreted to be the result of predominant contributions by the mantle components comprising the ambient sub-Comorean lithosphere (HIMU plus DMM, PREMA or a component on the mantle array) and variable but limited contributions by the Comores mantle plume itself (alternatively, they may be the result of mixing between sub-Comorean mantle consisting

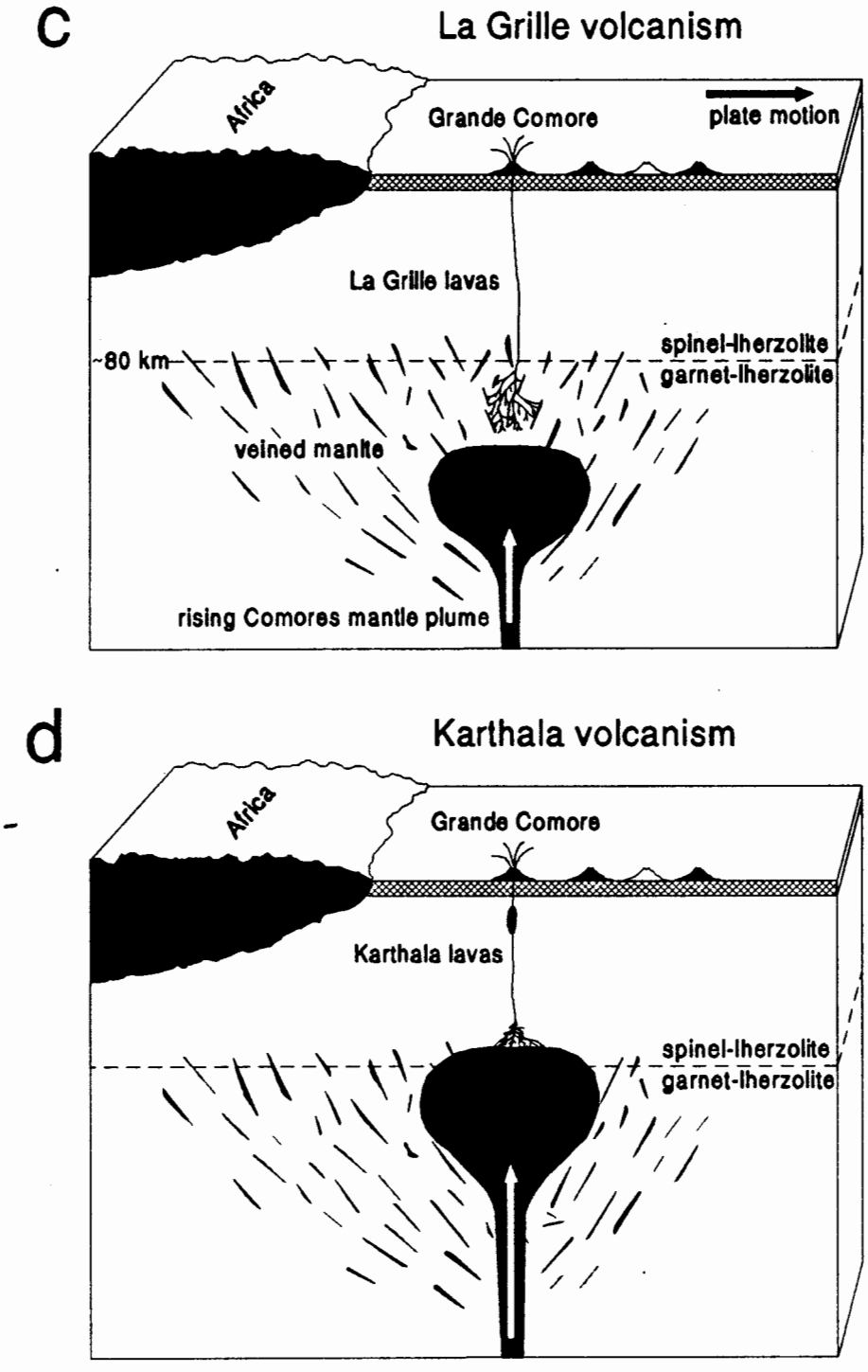

Fig. 12.2 ***continued.*** **(c)** Genesis of La Grille lavas; **(d)** Genesis of Karthala lavas.

of a depleted component and a HIMU-dominated HIMU-EM I Comores mantle plume). The lavas erupted by Karthala volcano are the result of larger degree partial melting of an amphibole-free spinel-lherzolite mantle at shallower levels, followed by olivine and

clinopyroxene dominated fractional crystallisation (Fig. 12.2d). Importantly, however, since the time of the formation of Karthala lavas , the Comores mantle plume has finally risen to a level where it contributes appreciably more material to the generation of partial mantle melts (Fig. 12.2d). The significantly enriched Nd and Sr isotopic signature of Karthala lavas compared to all other Comorean lavas is therefore considered to be the direct result of increased contributions from the enriched, EM I-type Comores mantle plume (or alternatively, an EM I-dominated HIMU-EM I Comores mantle plume).

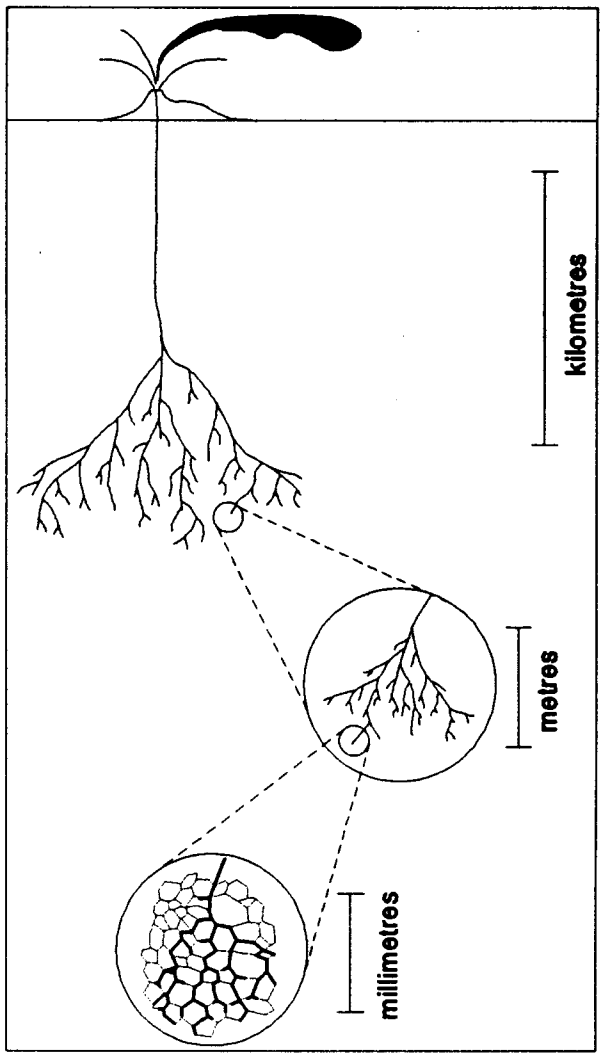

Fig. 12.3. Highly schematic depiction of the partial melting and melt propagation processes envisaged for the generation of Comorean lavas. The magma drainage system is considered to have a three-dimensional geometry analogous to that of an upside-down "fractal tree" (a fractal being a self-same geometric object, i.e. it "looks the same" at any magnification). An increase in the ambient mantle temperature as a result of the upwelling Comores mantle plume, aided by a lowering of the solidus due to hydrous metasomatism, initiates partial melting at polymineralic grain intersections ("millimetre" scale). The buoyant partial melts rise along grain edge intersections and coalesce into progressively fewer, but progressively wider, melt-filled channels ("millimetre"→"metre"→"kilometre" scales), forming the "twigs" and "branches" of the "tree" and finally collect in a single vent- the "trunk"- leading towards the surface. The efficiency at which the melt is extracted from the source region and migrates through the mantle is controlled by factors such as the dihedral angles (i.e. angle extended by the liquid between two adjacent grains) in the source material, the density contrast between melt and residual solid, the melt viscosity and the porosity of the mantle (e.g. Turcotte and Ahern, 1978; Bulau *et al.*, 1979; Stolper *et al.*, 1981; Richter and McKenzie, 1984; McKenzie, 1985; Nicolas, 1986).

13. CONCLUSIONS

The most important conclusions drawn in this study, concerning the petrology, petrogenesis and source region characteristics of lavas from the Comores Archipelago are listed below.

- The Comorean rocks investigated in this study are generally slightly vesicular, sparsely to moderately and on occasion strongly porphyritic lavas. They contain phenocrysts and microphenocrysts of olivine, clinopyroxene, amphibole, feldspar, Fe-Ti oxide and in one case nepheline and garnet. These phenocrysts are typically set in a fine- to very fine-grained or cryptocrystalline and sometimes partly glassy groundmass of clinopyroxene, Fe-Ti oxide, feldspar or nepheline, lesser olivine and accessory amounts of apatite and occasionally titanite (sphene).

- With the exception of some Rejuvenescent Phase Mayotte lavas, which are hypersthene- and even quartz-normative, all Comores lavas analysed are moderately to strongly silica-undersaturated, nepheline-normative, alkaline rocks.

- Basic alkaline lavas (alkali basalts, basanites and nephelinites) were analysed from all three islands investigated. On Mayotte, however, more compositional variation, ranging from alkali basalt through trachybasalt, basaltic trachyandesite and trachyandesite to trachyte and from basanite and nephelinite through phonotephrite to phonolite, was encountered.

- All samples analysed are significantly enriched in incompatible elements relative to N-type MORB, primitive mantle or melts produced from such primitive mantle and display strong LREE enrichment relative to the HREE.

- All lavas analysed may be assigned to one of two very distinct Comorean lava types on the basis of their primitive mantle-normalised incompatible element patterns: La Grille-type lavas display a strong relative depletion in K (and sometimes Rb), which is not observed amongst Karthala-type lavas.

- Although many of the lavas analysed are relatively primitive and some have near-primary compositions, only those erupted by La Grille volcano on Grande Comore have the petrographic and geochemical characteristics expected of truly primary melts.

- Much of the compositional variation amongst Comorean lavas is explicable in terms of fractional crystallisation, initially dominated by olivine and clinopyroxene, but joined at more evolved stages by Fe-Ti oxide, feldspar, amphibole and small amounts of apatite and titanite. The presence of amphibole phenocrysts implies reasonably hydrous conditions at some stage during the evolution of Comorean lavas.

- Although much of the differentiation of Comorean lavas may have taken place at shallow, near-surface levels, several lines of mainly petrographic and mineralogical evidence are consistent with the initiation of fractional crystallisation at relatively elevated pressures within the upper mantle, suggesting an evolution by polybaric fractionation.

- The data presented in this study are consistent with the derivation of primary La Grille-type lavas by relatively small degree partial melting of an amphibole-bearing garnet-lherzolite mantle source at depths greater than about 80 km, whereas Karthala-type lavas are probably the products of somewhat larger degrees of melting of an amphibole-free spinel-lherzolite source at shallower depths.

- The Nd and Sr isotopic compositions of Comores lavas bear evidence for a time-averaged depletion in incompatible elements, whereas the highly enriched incompatible element abundances of these lavas relative to N-type MORB are proposed to be the result of a recent mantle enrichment event. It is suggested that the garnet-lherzolite mantle source of La Grille-type Comorean lavas experienced modal metasomatism, resulting in the precipitation of amphibole, whilst the shallower spinel-lherzolite source of Karthala-type lavas underwent cryptic metasomatism only, without the introduction of any new phases.

- It is proposed that the Nd and Sr isotopic signature carried by the majority of Comorean lavas, which is similar to that of Cameroon Line and Kenyan lavas (i.e. located between the mantle and LoNd arrays on the Nd-Sr isotope correlation diagram) and not unlike that of St. Helena (HIMU), is largely representative of the ambient sub-Comorean upper mantle. This isotopic signature may be explained in terms of mixing between several mantle components, namely HIMU plus a depleted component (DMM, PREMA or a component on the mantle array), with variable and limited contributions from the Comores mantle plume (EM I) itself. The low $^{143}Nd/^{144}Nd$ and high $^{87}Sr/^{86}Sr$ isotopic composition of Karthala lavas, however, is distinctly different and is suggested to indicate a significantly increased contribution from the EM I-type Comores mantle plume, rising from greater mantle depths. Alternatively, the ambient sub-Comorean mantle could consist of a depleted component which is mixed with a HIMU-EM I Comores mantle plume that is dominated by the HIMU component during most of the volcanic history of the Comores, but becomes dominated by the EM I component during the generation of Karthala lavas.

- An internally consistent, broadly chronological, petrogenetic model for the evolution of Comorean volcanism in space and time can be constructed on the basis of the conclusions drawn in this study.

ACKNOWLEDGEMENTS

I am deeply indebted to a host of people without whose committed support and encouragement I would not have been able to complete this dissertation - thank you very much to all of them.

My supervisor, Prof. Anton le Roex, has been an invaluable source of inspiration, scientific insight and expert guidance during the last two years.

Prof. R. A. Duncan of Oregon State University, USA, is thanked for supplying the sample collection on which this study is based. Leon Myburg's expert assistance in preparing and running many of the XRF samples is greatly appreciated and he is furthermore thanked for showing me the ropes in the REE chemistry and HPIC labs. A special thanks must go to Dr. Rich Armstrong for introducing me to the ins and outs of radiogenic isotope chemistry and mass-spectrometry during a somewhat turbulent and busy period in his own life. Dr. Stephen Richardson is thanked for helping to prepare the last batch of Nd samples and analysing them on the mass-spectrometer. David Wilson once again provided expertly prepared petrographic thin-sections. The tireless efforts of Dick Rickard in keeping the ageing UCT probe in excellent working order year after year are greatly appreciated. Many thanks also to "magic" Ted Mills for making computer troubles and viruses disappear at the push of a button or two. Charlie Basson provided quality photographic services. Many thanks to Neville Buchanan for helping to print this dissertation and for letting me stay on in "sy tannie se ou huis" despite repeated threats of eviction. Had it not been for the friendship and support of my fellow post-graduates in the Department, the last few years would not have been as enjoyable as they have been. A special note of thanks to my office-mates Steve, Ingrid, Gail, Karen, Esmé and Roxy.

I am very grateful to my parents, whose continuing hard work, support (both financially and emotionally), love and encouragement have played an unfathomable role in getting me to where I am today. Thanks for never asking: "and when are you going to get a real job ?".

This dissertation is dedicated to Sam - above all it was her love, understanding and support throughout the last three years that have allowed me to complete this dissertation.

Much needed financial support for this work came from the Foundation of Research and Development and a UCT Research Associateship.

REFERENCES

Albarede, F. and Tamagnan, V. (1988). Modelling the recent geochemical evolution of the Piton de la Fournaise volcano, Réunion Island. *J. Petrol.*, **29**, 997-1030.

Albee, A. L. and Ray, L. (1970). Correction factors for electron probe microanalysis of silicates, oxides, carbonates, phosphates, and sulfates. *Anal. Chem.*, **42**, 1408-1414.

Allègre, C. J. and Turcotte, D. L. (1985). Geodynamic mixing in the mesosphere boundary layer and the origin of oceanic islands. *Geophys. Res. Lett.*, **12**, 207-210.

Allen, J. C. and Boettcher, A. L. (1973). Phase relations and the stability of amphiboles in an olivine nephelinite at high pressures. *EOS*, **54**, 481.

Allen, J. C., Boettcher, A. L. and Marland, G. (1975). Amphiboles in andesite and basalt: I. Stability as a function of P-T-f_{O2}. *Am. Mineral.*, **60**, 1069-1085.

Aoki, K.-I. (1970). Petrology of kaersutite-bearing ultramafic and mafic inclusions in Iki Island, Japan. *Contrib. Mineral. Petrol.*, **25**, 270-283.

Aoki, K.-I. and Kushiro, I. (1968). Some clinopyroxenes from ultramafic inclusions in Dreiser Weiher, Eifel. *Contrib. Mineral. Petrol.*, **18**, 326-337.

Aoki, K.-I. and Shiba, I. (1973). Pyroxenes from lherzolite inclusions of Itinome-gata, Japan. *Lithos*, **6**, 41-51.

Baker, B. H. and Miller, J. A. (1963). Geology and geochronology of the Seychelles Islands and structure of the floor of the Arabian Sea. *Nature*, **199**, 346-348.

Barling, J. and Goldstein, S. L. (1990). Extreme isotopic variations in Heard Island lavas and the nature of mantle reservoirs. *Nature*, **348**, 59-62.

Barton, M. and van Bergen, M. J. (1981). Green clinopyroxenes and associated phases in a potassium-rich lava from the Leucite Hills, Wyoming. *Contrib. Mineral. Petrol.*, **77**, 101-114.

Barton, M., Varekamp, J. C. and van Bergen, M. J. (1982). Complex zoning of clinopyroxenes in the lavas of Vulsini, Latium, Italy: evidence for magma mixing. *J. Volcanol. Geotherm. Res.*, **14**, 361-388.

Basaltic Volcanism Study Project (1981). *Basaltic volcanism on the terrestrial planets*. Pergamon Press, New York, 409-432.

Bassias, Y. (1992). Petrological and geochemical investigation of rocks from the Davie Fracture Zone (Mozambique Channel) and some tectonic implications. *J. Afr. Earth Sci.*, **15**, 321-339.

Baxter, A. N. (1975a). K/Rb ratios in some volcanic rocks from Mauritius, Indian Ocean. *Geochim. Cosmochim. Acta*, **39**, 1573-1576.

Baxter, A. N. (1975b). Petrology of the Older Series lavas from Mauritius, Indian Ocean. *Geol. Soc. Am. Bull.*, **86**, 1449-1458.

Baxter, A. N. (1976). Geochemistry and petrogenesis of primitive alkali basalt from Mauritius, Indian Ocean. *Geol. Soc. Am. Bull.*, **87**, 1028-1034.

Baxter, A. N. (1990). Major and trace element variations in basalts from leg 115. *Proc. ODP, Sci. Results*, **115**, 11-21.

Baxter, A. N., Upton, B. G. J. and White, W. M. (1985). Petrology and geochemistry of Rodrigues Island, Indian Ocean. *Contrib. Mineral. Petrol.*, **89**, 90-101.

Bence, A. B. and Albee, A. L. (1967). Empirical correction factors for the electron microanalysis of silicates and oxides. *J. Geol.*, **76**, 382-403.

Best, M. G. (1974). Mantle-derived amphibole within inclusions in alkalic-basaltic lavas. *J. Geophys. Res.*, **79**, 2107-2113.

Beswick, A. E. (1976). K and Rb relations in basalts and other mantle derived materials. Is phlogopite the key ? *Geochim. Cosmochim. Acta*, **40**, 1167-1183.

Boettcher, A. L. and O'Neil, J. R. (1980). Stable isotope, chemical, and petrographic studies of high-pressure amphiboles and micas: evidence for metasomatism in the mantle source regions of alkali basalts and kimberlites. *Am. J. Sci.*, **280**, 594-621.

Borley, G. D., Suddaby, P. and Scott, P. (1971). Some xenoliths from the alkalic rocks of Teneriffe, Canary Islands. *Contrib. Mineral. Petrol.*, **31**, 102-114.

Brooks, C. K. and Printzlau, I. (1978). Magma mixing in mafic alkaline volcanic rocks: the evidence from relict phenocryst phases and other inclusions. *J. Volcanol. Geotherm. Res.*, **4**, 315-331.

Bryan, W. B., Finger, L. W. and Chayes, F. (1969). Estimating proportions in petrographic mixing equations by least-squares approximation. *Science*, **163**, 926-927.

Bulau, J. R. and Waff, H. S. (1979). Mechanical and thermodynamic constraints on fluid distribution in partial melts. *J. Geophys. Res.*, **84**, 6102-6108.

Bultitude, R. J. and Green, D. H. (1967). Experimental study at high pressures on the origin of olivine nephelinite and olivine melilite nephelinite magmas. *Earth Planet. Sci Lett.*, **3**, 325-337.

Bultitude, R. J. and Green, D. H. (1971). Experimental study of crystal-liquid relationships at high pressures in olivine nephelinite and basanite compositions. *J. Petrol.*, **12**, 121-147.

Bunce, E. T. and Molnar, P. (1977). Seismic reflection profiling and basement topography in the Somali Basin: possible fracture zones between Madagascar and Africa. *J. Geophys. Res.*, **82**, 5305-5311.

Burke, K. C. and Wilson, J. T. (1976). Hot spots on the Earth's surface. *Sci. Am.*, **235**, 46-57.

Chen, C.-Y. and Frey, F. A. (1983). Origin of Hawaiian tholeiite and alkalic basalt. *Nature*, **302**, 785-789.

Clague, D. A. (1987). Hawaiian alkaline volcanism. In: Fitton, J. G. and Upton, B. G. J. (eds.), Alkaline Igneous Rocks. *Geol. Soc. Spec. Publ.*, **30**, 227-252.

Clague, D. A. and Frey, F. A. (1982). Petrology and trace element geochemistry of the Honolulu Volcanics, Oahu: implications for the oceanic mantle below Hawaii. *J. Petrol.*, **23**, 447-504.

Class, C. and Goldstein, S. L. (1994). Isotope arrays and plume sources: the Ninetyeast Ridge & Comoro plumes. ICOG 8 Abstract Volume, *U.S. Geol. Survey Circular*, **1107**, 60.

Consolmagno, G. J. and Drake, M. J. (1976). Equivalence of equations describing trace element distribution during equilibrium partial melting. *Geochim. Cosmochim. Acta*, **40**, 1421-1422.

Cox, K. G. (1978). Komatiites and other high-magnesia lavas: some problems. *Phil. Trans. R. Soc. Lond. A.*, **288**, 599-609.

Cox, K. G. and Bell, J. D. (1972). A crystal fractionation model for the basaltic rocks of the New Georgia Group, British Solomon Islands. *Contrib. Mineral. Petrol.*, **37**, 1-13.

Crough, S. T. (1983). Hotspot swells. *Ann. Rev. Earth Planet. Sci.*, **11**, 165-193.

Cullers, R. L., Ramakrishnan, S., Berendsen, P. and Griffin, T. (1985). Geochemistry and petrogenesis of lamproites, Late Cretaceous age, Woodson County, Kansas, U.S.A. *Geochim. Cosmochim. Acta*, **49**, 1383-1402.

Davies, H. L., Sun, S-s., Frey, F. A., Gautier, I., McCulloch, M. T., Price, R. C., Bassias, Y. Klootwijk, C. T. and Leclaire, L. (1989). Basalt basement from the Kerguelen Plateau and the trail of a Dupal plume. *Contrib. Mineral. Petrol.*, **103**, 457-469.

Dawson, J. B. (1984). Contrasting types of upper-mantle metasomatism? In: Kornprobst, J. (ed.), *Kimberlites II: The mantle and crust-mantle relationships*. Elsevier, Amsterdam, 289-294.

Dawson, J. B. and Powell, D. G. (1969). Mica in the upper mantle. *Contrib. Mineral. Petrol.*, **22**, 233-237.

Deer, W. A., Howie, R. A. and Zussman, J. (1962a). *Rock-forming minerals*, Vol.1, Ortho- and ring silicates. Longmans, London, 89-93.

Deer, W. A., Howie, R. A. and Zussman, J., (1962b). *Rock-forming minerals*, Vol.3, Sheet silicates. Longmans, London, 46-47.

Deer, W. A., Howie, R. A. and Zussman, J., (1962c). *Rock-forming minerals*, Vol.2, Chain silicates. Longmans, London, 322-323.

Dickin, A. P., Fallick, A. E., Halliday, A. N., Macintyre, R. M. and Stephens, W. E. (1986/1987). An isotopic and geochronological investigation of the younger igneous rocks of the Seychelles microcontinent. *Earth Planet. Sci. Lett.*, **81**, 46-56.

Dionex® (1987). Determination of lanthanide metals. Dionex Corp., Sunnyvale, Calif., *Tech. Note* No.**23**, 4 pp.

Dosso, L. and Murthy, V. R. (1980). A Nd isotopic study of the Kerguelen Islands: inferences on enriched oceanic mantle sources. *Earth Planet. Sci. Lett.*, **48**, 268-276.

Dostal, J., Dupuy, C., Nicollet, C. and Cantagrel, J. M. (1992). Geochemistry and petrogenesis of Upper Cretaceous basaltic rocks from southern Malagasy. *Chem. Geol.*, **97**, 199-218.

Duda, A. and Schmincke, H.-U. (1985). Polybaric differentiation of alkali basaltic magmas: evidence from green-core clinopyroxenes (Eifel, FRG). *Contrib. Mineral. Petrol.*, **91**, 340-353.

Duncan, A. R., Erlank, A. J. and Betton, P. J. (1984). Appendix 1. Analytical techniques and database descriptions. *Spec. Publ. Geol. Soc. S. Afr.*, **13**, 389-395.

Duncan, R. A. (1981). Hotspots in the southern oceans - an absolute frame of reference for motion of the Gondwana continents. *Tectonophysics*, **74**, 29-42.

Duncan, R. A. (1990). The volcanic record of the Réunion hotspot. *Proc. ODP, Sci. Results*, **115**, 3-10.

Duncan, R. A., Backman, J. and Peterson, L. (1989). Reunion hotspot activity through Tertiary time: initial results from the Ocean Drilling Program, leg 115. *J. Volcanol. Geotherm. Res.*, **36**, 193-198.

Duncan, R. A. and Hargraves, R. B. (1990). $^{40}Ar/^{39}Ar$ geochronology of basement rocks from the Mascarene Plateau, the Chagos Bank, and the Maldives Ridge. *Proc. ODP, Sci. Results*, **115**, 43-51.

Dupré, B. and Allègre, C. J. (1983). Pb-Sr isotope variation in Indian Ocean basalts and mixing phenomena. *Nature*, **303**, 142-146.

Du Toit, A. L. (1937). *Our wandering continents*. Oliver and Boyd, London, 120-125.

Edgar, A. D. (1987). The genesis of alkaline magmas with emphasis on their source regions: inferences from experimental studies. In: Fitton, J. G. and Upton, B. G. J. (eds.), Alkaline Igneous Rocks, *Geol. Soc. Spec. Publ.*, **30**, 29-52.

Eggler, D. H. (1978). The effect of CO_2 upon partial melting of peridotite in the system Na_2O-CaO-Al_2O_3-MgO-SiO_2-CO_2 to 35 kb, with an analysis of melting in a peridotite-H_2O-CO_2 system. *Am. J. Sci.*, **278**, 305-343.

Ellis, D. J. (1976). High pressure cognate inclusions in the Newer Volcanics of Victoria. *Contrib. Mineral. Petrol.*, **58**, 149-180.

Emerick, C. (1980). A new chronology for the Comoro Islands, western Indian Ocean, and implications for Somali plate tectonics. *EOS*, **61**, 1106.

Emerick, C. M. (1985). Age progressive volcanism in the Comores Archipelago and northern Madagascar. *Unpubl. Ph.D. thesis*, Oregon State University.

Emerick, C. M. and Duncan, R. A. (1982). Age progressive volcanism in the Comores Archipelago, western Indian Ocean and implications for Somali plate tectonics. *Earth Planet. Sci. Lett.*, **60**, 415-428.

Emerick, C. M. and Duncan, R. A. (1983). Age progressive volcanism in the Comores Archipelago, western Indian Ocean and implications for Somali plate tectonics. Errata. *Earth Planet. Sci. Lett.*, **62**, 439.

Erlank, A. J. and Kable, E. J. D. (1976). The significance of incompatible elements in Mid-Atlantic Ridge basalts from 45°N with particular reference to Zr/Nb. *Contrib. Mineral. Petrol.*, **54**, 281-291.

Erlank, A. J., Waters, F. G., Hawkesworth, C. J., Haggerty, S. E., Allsopp, H. L., Rickard, R. S. and Menzies, M. (1987). In: Menzies, M. A. and Hawkesworth, C. J. (eds.), *Mantle metasomatism*. Academic Press, London, 221-311.

Ernst, R. E., Fowler, A. D. and Pearce, T. H. (1988). Modelling of igneous fractionation and other processes using Pearce diagrams. *Contrib. Mineral. Petrol.*, **100**, 12-18.

Esson, J., Flower, M. F. J., Strong, D. F., Upton, B. G. J. and Wadsworth, W. J. (1970). Geology of the Comores Archipelago, western Indian Ocean. *Geol. Mag.*, **107**, 549-557.

Fisher, R. L., Johnson, G. L. and Heezen, B. C. (1967). Mascarene Plateau, western Indian Ocean. *Geol. Soc. Am. Bull.*, **78**, 1247-1266.

Fisk, M. R., Upton, B. G. J., Ford, C. E. and White, W. M. (1988). Geochemical and experimental study of the genesis of magmas of Reunion Island, Indian Ocean. *J. Geophys. Res.*, **93**, 4933-4950.

Fisk, M. R., Duncan, R. A., Baxter, A. N., Greenough, J. D., Hargraves, R. B. and Tatsumi, Y. (1989). Reunion hotspot magma chemistry over the past 65 m.y.: results from leg 115 of the Ocean Drilling Program. *Geology*, **17**, 934-937.

Flores, G. (1970). Suggested origin of the Mozambique Channel. *Trans. Geol. Soc. S. Afr.*, **73**, 1-16.

Flower, M. F. J. (1971a). Rare earth element distribution in lavas and ultramafic xenoliths from the Comores Archipelago, western Indian Ocean. *Contrib. Mineral. Petrol.*, **31**, 335-346.

Flower, M. F. J. (1971b). Evidence for the role of phlogopite in the genesis of alkali basalts. *Contrib. Mineral. Petrol.*, **32**, 126-137.

Flower, M. F. J. (1972). Petrology of volcanic rocks from Anjouan, Comores Archipelago. *Bull. Volcanol.*, **36**, 238-250.

Flower, M. F. J. (1973a). Evolution of basaltic and differentiated lavas from Anjouan, Comores Archipelago. *Contrib. Mineral. Petrol.*, **38**, 237-260.

Flower, M. F. J. (1973b). Trace-element distribution in lavas from Anjouan and Grande Comore, western Indian Ocean. *Chem. Geol.*, **12**, 81-98.

Flower, M. F. J. and Strong, D. F. (1969). The significance of sandstone inclusions in lavas of the Comores Archipelago. *Earth Planet. Sci. Lett.*, **7**, 47-50.

Foley, S. F. (1988). The genesis of continental basic alkaline magmas - an interpretation in terms of redox melting. *J. Petrol.*, Special Lithosphere Issue, 139-161.

Forbes, W. C. and Flower, M. F. J. (1974). Phase relations of titan-phlogopite, $K_2Mg_4TiAl_2Si_6O_{20}(OH)_4$: a refractory phase in the upper mantle ? *Earth Planet. Sci. Lett.*, **22**, 60-66.

Frey, F. A., Bryan, W. B. and Thompson, G. (1974). Atlantic ocean floor: geochemistry and petrology of basalts from legs 2 and 3 of the Deep-Sea Drilling Project. *J. Geophys. Res.*, **79**, 5507-5527.

Frey, F. A., Green, D. H. and Roy, S. D. (1978). Integrated models of basalt petrogenesis: a study of quartz tholeiites to olivine melilitites from south eastern Australia utilizing geochemical and experimental petrological data. *J. Petrol.*, **19**, 463-513.

Gast, P. W. (1968). Trace element fractionation and the origin of tholeiitic and alkaline magma types. *Geochim. Cosmochim. Acta*, **32**, 1057-1086.

Gautier, I., Weis, D., Mennessier, J.-P., Vidal, P., Giret, A. and Loubet, M. (1990). Petrology and geochemistry of the Kerguelen Archipelago basalts (South Indian Ocean): evolution of the mantle sources from ridge to intraplate position. *Earth Planet. Sci. Lett.*, **100**, 59-76.

Gerlach, D. C., Cliff, R. A., Davies, G. R., Norry, M. and Hodgson, N. (1988). Magma sources of the Cape Verdes archipelago: Isotopic and trace element constraints. *Geochim. Cosmochim. Acta*, **52**, 2979-2992.

Green, A. G. (1972). Seafloor spreading in the Mozambique Channel. *Nature*, **236**, 19-21.

Green, D. H. (1969). The origin of basaltic and nephelinitic magmas in the Earth's mantle. *Tectonophysics*, **7**, 409-422.

Green, D. H. (1970). A review of experimental evidence on the origin of basaltic and nephelinitic magmas. *Phys. Earth Planet. Interiors*, **3**, 221-235.

Green, D. H. (1971). Composition of basaltic magmas as indicators of conditions of origin: application to oceanic volcanism. *Phil. Trans. Roy. Soc. Lond. A*, **268**, 707-725.

Green, D. H. (1973a). Conditions of melting of basanite magma from garnet peridotite. *Earth Planet. Sci. Lett.*, **17**, 456-465.

Green, D. H. (1973b). Experimental melting studies on a model upper mantle composition at high pressure under water-saturated and water-undersaturated conditions. *Earth Planet. Sci. Lett.*, **19**, 37-53.

Green, D. H. and Ringwood, A. E. (1964). Fractionation of basalt magmas at high pressures. *Nature*, **201**, 1276-1279.

Green, D. H., Edgar, A. D., Beasley, P., Kiss, E. and Ware, N. G. (1974). Upper mantle source for some hawaiites, mugearites and benmoreites. *Contrib. Mineral. Petrol.*, **48**, 33-43.

Greenough, J. D. (1988). Minor phases in the Earth's mantle: evidence from trace- and minor-element patterns in primitive alkaline magmas. *Chem. Geol.*, **69**, 177-192.

Guilcher, A. (1965). Coral reefs and lagoons of Mayotte Island, Comoro Archipelago, Indian Ocean, and of New Caledonia, Pacific Ocean. In: Whittard, W. F. and Bradshaw, R. (eds.), *Submarine geology and geophysics*. Butterworths, London, 21-32.

Haase, K. M. and Devey, C. W. (1994). The petrology and geochemistry of Vesteris Seamount, Greenland Basin-an intraplate alkaline volcano of non-plume origin. *J. Petrol.*, **35**, 295-328.

Hajash, A. and Armstrong, R. L. (1972). Paleomagnetic and radiometric evidence for the age of the Comores Islands, west central Indian Ocean. *Earth Planet. Sci. Lett.*, **16**, 231-236.

Halliday, A. N., Dickin, A. P., Fallick, A. E. and Fitton, J. G. (1988). Mantle dynamics: a Nd, Sr, Pb and O isotopic study of the Cameroon Line volcanic chain. *J. Petrol.*, **29**, 181-211.

Halliday, A. N., Davidson, J. P., Holden, P., DeWolf, C., Lee, D.-C. and Fitton, J. G. (1990). Trace-element fractionation in plumes and the origin of HIMU mantle beneath the Cameroon line. *Nature*, **347**, 523-528.

Hamelin, B., Dupré, B. and Allègre, C. J. (1985/86). Pb-Sr-Nd isotopic data of Indian Ocean ridges: new evidence of large-scale mapping of mantle heterogeneities. *Earth Planet. Sci. Lett.*, **76**, 288-298.

Hanson, G. N. and Langmuir, C. H. (1978). Modelling of major elements in mantle-melt systems using trace element approaches. *Geochim. Cosmochim. Acta*, **42**, 725-741.

Hart, S. R. (1984). A large-scale isotope anomaly in the southern hemisphere mantle. *Nature*, **309**, 753-757.

Hart, S. R. (1988). Heterogeneous mantle domains: signatures, genesis and mixing chronologies. *Earth Planet. Sci. Lett.*, **90**, 273-296.

Hart, S. R. and Brooks, C. (1977). The geochemistry and evolution of early Precambrian mantle. *Contrib. Mineral. Petrol.*, **61**, 109-128.

Hart, S. R. and Davis, K. E. (1978). Nickel partitioning between olivine and silicate melt. *Earth Planet. Sci. Lett.*, **40**, 203-219.

Hart, S. R., Gerlach, D. C. and White, W. M. (1986). A possible new Sr-Nd-Pb mantle array and consequences for mantle mixing. *Geochim. Cosmochim. Acta*, **50**, 1551-1557.

Hart, S. R. and Dunn, T. (1993). Experimental cpx/melt partitioning of 24 trace elements. *Contrib. Mineral. Petrol.*, **113**, 1-8.

Harte, B., Winterburn, P. A. and Gurney, J. J., M. (1987). In: Menzies, M. A. and Hawkesworth, C. J. (eds.), *Mantle metasomatism*. Academic Press, London, 145-220.

Hartnady, C. J. H. (1986). Amirante Basin, western Indian Ocean: possible impact site of the Cretaceous/Tertiary extinction bolide ? *Geology*, **14**, 423-426.

Heirtzler, J. R. and Burroughs, R. H. (1971). Madagascar's paleoposition: new data from the Mozambique Channel. *Science*, **174**, 488-490.

Hertogen, J. and Gijbels, R. (1976). Calculation of trace element fractionation during partial melting. *Geochim. Cosmochim. Acta*, **40**, 313-322.

Hoernle, K. and Schmincke, H.-U. (1993a). The petrology of the tholeiites through melilite nephelinites on Gran Canaria, Canary Islands: crystal fractionation, accumulation, and depths of melting. *J. Petrol.*, **34**, 573-597.

Hoernle, K. and Schmincke, H.-U. (1993b). The role of partial melting in the 15-Ma geochemical evolution of Gran Canaria: A blob model for the Canary hotspot. *J. Petrol.*, **34**, 599-626.

Holloway, J. R. and Ford, C. E. (1973). The effect of fluorine on hornblende: Fluid-absent melting of F-OH pargasite to 35 kb. *EOS*, **54**, 478.

Irvine, T. N. and Baragar, W. R. A. (1971). A guide to the chemical classification of the common volcanic rocks. *Can. J. Earth Sci.*, **8**, 523-548.

Irving, A. J. (1978). A review of experimental studies of crystal/liquid trace element partitioning. *Geochim. Cosmochim. Acta*, **42**, 743-770.

Irving, A. J. and Price, R. C. (1981). Geochemistry and evolution of lherzolite-bearing phonolitic lavas from Nigeria, Australia, East Germany and New Zealand. *Geochim. Cosmochim. Acta*, **45**, 1309-1320.

Johnson, K. T. M., Dick, H. J. B. and Shimizu, N. (1990). Melting in the oceanic upper mantle: an ion microprobe study of diopsides in abyssal peridotites. *J. Geophys. Res.*, **95**, 2661-2678.

Kable, E. J. D. (1972). Some aspects of the geochemistry of selected elements in basalts and associated lavas. *Unpubl. Ph.D thesis*, University of Cape Town.

Kable, E. J. D., Erlank, A. J. and Cherry, R. D. (1971). Geochemical features of lavas. In: van Zinderen Bakker, E. M., Winterbottom, J. M. and Dyer, R. A. (eds.), *Marion and Prince Edward islands. Report on the South African biological and geological expedition / 1965-1966*. Balkema, Cape Town, 78-88.

Kay, R. W. and Gast, P. W. (1973). The rare earth content and origin of alkali-rich basalts. *J. Geol.*, **81**, 653-682.

Kent, P. E. (1972). Mesozoic history of the east coast of Africa. *Nature*, **238**, 147-148.

Kesson, S. and Price, R. C. (1972). The major and trace element chemistry of kaersutite and its bearing on the petrogenesis of alkaline rocks. *Contrib. Mineral. Petrol.*, **36**, 119-124.

Kinzler, R. J. and Grove, T. L. (1992a). Primary magmas of mid-ocean ridge basalts 1. Experiments and methods. *J. Geophys. Res.*, **97**, 6885-6906.

Kinzler, R. J. and Grove, T. L. (1992b). Primary magmas of mid-ocean ridge basalts 2. Applications. *J. Geophys. Res.*, **97**, 6907-6926.

Krenkel, E. (1925). *Geologie Afrikas*. Erster Teil, 377-379. Borntraeger, Berlin.

Kurz, M. D., Jenkins, W. J. and Hart, S. R. (1982). Helium isotopic systematics of oceanic islands: implications for mantle heterogeneity. *Nature*, **297**, 43-47.

Kurz, M. D., Jenkins, W. J., Hart, S. R. and Clague, D. (1983). Helium isotopic variations in volcanic rocks from Loihi Seamount and the island of Hawaii. *Earth Planet. Sci. Lett.*, **66**, 388-406.

Kushiro, I. (1970). Stability of amphibole and phlogopite in the upper mantle. *Carnegie Inst. Year Book*, **68**, 245-247.

Kushiro, I. and Kuno, H. (1963). Origin of primary basalt magmas and classification of basaltic rocks. *J. Petrol.*, **4**, 75-89.

Kushiro, I., Syono, Y and Akimoto, S. (1967). Stability of phlogopite at high pressures and possible presence of phlogopite in the Earth's upper mantle. *Earth Planet. Sci. Lett.*, **3**, 197-203.

Lacroix, A. (1922). *Minéraolie de Madagascar*. Tome 1, 141-148. Paris.

Langmuir, C. H. and Hanson, G. N. (1980). An evaluation of major element heterogeneity in the mantle sources of basalts. *Phil. Trans. Roy. Soc. Lond. A*, **297**, 383-407.

Leake, B. E. (1978). Nomenclature of amphiboles. *Am. Mineral.*, **63**, 1023-1052.

le Bas, M. J., le Maitre, R. W., Streckeisen, A. and Zanettin, B. (1986). A chemical classification of volcanic rocks based on the total alkali-silica diagram. *J. Petrol.*, **27**, 745-750.

Lee, D.-C., Halliday, A. N., Fitton, J. G. and Poli, G. (1994). Isotopic variations with distance and time in the volcanic islands of the Cameroon line: evidence for a mantle plume origin. *Earth Planet. Sci. Lett.*, **123**, 119-138.

Lemarchand, F., Villemant, B. and Calas, G. (1987). Trace element distribution coefficients in alkaline series. *Geochim. Cosmochim. Acta.*, **51**, 1071-1081.

le Maitre, R. W. (1969). Kaersutite-bearing plutonic xenoliths from Tristan da Cunha, South Atlantic. *Mineral. Mag.*, **37**, 185-197.

le Roex, A. P. (1980). Geochemistry and mineralogy of selected Atlantic Ocean basalts. Unpublished Ph.D. thesis, University of Cape Town.

le Roex, A. P. (1985). Geochemistry, mineralogy and magmatic evolution of the basaltic and trachytic lavas from Gough Island, South Atlantic. *J. Petrol.*, **26**, 149-186.

le Roex, A. P. and Dick, H. J. B. (1981). Petrography and geochemistry of basaltic rocks from the Conrad fracture zone on the America-Antarctica Ridge. *Earth Planet. Sci. Lett.*, **54**, 117-138.

le Roex, A. P., Erlank, A. J. and Needham, H. D. (1981). Geochemical and mineralogical evidence for the occurrence of at least three distinct magma types in the 'Famous' region. *Contrib. Mineral. Petrol.*, **77**, 24-37.

le Rσex, A. P., Cliff, R. A. and Adair, B. J. I. (1990). Tristan da Cunha, South Atlantic: geochemistry and petrogenesis of a basanite-phonolite lava series. *J. Petrol.*, **31**, 779-812.

le Roex, A. P. and Watkins, R. T. (1990). Analysis of rare-earth elements in geological samples by gradient ion chromatography: an alternative to ICP and INAA. *Chem. Geol.*, **88**, 151-162.

Ludden, J. N. (1977). The mineral chemistry and origin of xenoliths from the lavas of Anjouan, Comores Archipelago, western Indian Ocean. *Contrib. Mineral. Petrol.*, **64**, 91-107.

Mahoney, J. J., Natland, J. H., White, W. M., Poreda, R., Bloomer, S. H., Fisher, R. L. and Baxter, A. N. (1989). Isotopic and geochemical provinces of the western Indian Ocean spreading centres. *J. Geophys. Res.*, **94**, 4033-4052.

Mahoney, J., le Roex, A. P., Peng, Z., Fisher, R. L. and Natland, J. H. (1992). Southwestern limits of Indian Ocean Ridge mantle and the origin of low $^{206}Pb/^{204}Pb$ mid-ocean ridge basalt: isotope systematics of the central Southwest Indian Ridge (17°-50°E). *J. Geophys. Res.*, **97**, 19771-19790.

Mahood, G. A. and Baker, D. R. (1986). Experimental constraints on depth of fractionation of mildly alkalic basalts and associated felsic rocks: Pantelleria, Strait of Sicily. *Contrib. Mineral. Petrol.*, **93**, 251-264.

Matthews, D. H. and Davies, D. (1966). Geophysical studies of the Seychelles Bank. *Phil. Trans. Roy. Soc. Lond. A*, **259**, 227-239.

McCallum, I. S. and Charette, M. P. (1978). Zr and Nb partition coefficients: implications for the genesis of mare basalts, KREEP, and sea floor basalts. *Geochim. Cosmochim. Acta*, **42**, 859-869.

McKenzie, D. (1985). The extraction of magma from the crust and mantle. *Earth Planet. Sci. Lett.*, **74**, 81-91.

McKenzie, D. and O'Nions, R. K. (1983). Mantle reservoirs and ocean island basalts. *Nature*, **301**, 229-231.

Menzies, M. and Murthy, V. R. (1980a). Mantle metasomatism as a precursor to the genesis of alkaline magmas - isotopic evidence. *Am. J. Sci.*, **280**, 622-638.

Menzies, M. and Murthy, V. R. (1980b). Nd and Sr isotope geochemistry of hydrous mantle nodules and their host alkali basalts: implications for local heterogeneities in metasomatically veined mantle. *Earth Planet. Sci. Lett.*, **46**, 323-334.

Menzies, M., Rogers, N., Tindle, A. and Hawkesworth, C. (1987). Metasomatic and enrichment processes in lithospheric peridotites, an effect of asthenosphere-lithosphere interaction. In: Menzies, M. A. and Hawkesworth, C. J. (eds.), *Mantle metasomatism*. Academic Press, London, 313-361.

Mertes, H. and Schmincke, H.-U. (1985). Mafic potassic lavas of the Quaternary West Eifel volcanic field. I. Major and trace elements. *Contrib. Mineral. Petrol.*, **89**, 330-345.

Meyerhoff, A. A. and Kamen-Kaye, M. (1981). Petroleum prospects of Saya de Malha and Nazareth Banks, Indian Ocean. *Am. Assoc. Petrol. Geol. Bull.*, **65**, 1344-1347.

Michard, A., Montigny, R. and Schlich, R. (1986). Geochemistry of the mantle beneath the Rodriguez Triple Junction and the South-east Indian Ridge. *Earth Planet. Sci. Lett.*, **78**, 104-114.

Miller, J. A. and Mudie, J. D. (1961). Potassium-Argon age determinations on granite from the island of Mahé in the Seychelles Archipelago. *Nature*, **192**, 1174-1175.

Morgan, W. J. (1971). Convection plumes in the lower mantle. *Nature*, **230**, 42-43.

Morgan, W. J. (1972). Deep mantle convection plumes and plate motions. *Am. Assoc. Petrol. Geol. Bull.*, **56**, 203-213.

Morgan, W. J. (1978). Rodriguez, Darwin, Amsterdam,.., a second type of hotspot island. *J. Geophys. Res.*, **83**, 5355-5360.

Nicholls, J. (1988). The statistics of Pearce element diagrams and the Chayes closure problem. *Contrib. Mineral. Petrol.*, **99**, 11-24.

Nicolas, A. (1986). A melt extraction model based on structural studies in mantle peridotites. *J. Petrol.*, **27**, 999-1022.

Niu, Y. and Batiza, R. (1991). An empirical method for calculating melt compositions produced beneath mid-ocean ridges: application for axis and off-axis (Seamounts) melting. *J. Geophys. Res.*, **96**, 21753-21777.

Norrish, K. and Hutton, J. T. (1969). An accurate X-ray spectrographic method for the analysis of a wide range of geological samples. *Geochim. Cosmochim. Acta*, **33**, 431-453.

Norry, M. J., Truckle, P. H., Lippard, S. J., Hawkesworth, C. J., Weaver, S. D. and Marriner, G. F. (1980). Isotopic and trace element evidence from lavas, bearing on mantle heterogeneity beneath Kenya. *Phil. Trans. R. Soc. Lond. A*, **297**, 259-271.

Norry, M. J. and Fitton, J. G. (1983). Compositional differences between oceanic and continental basic lavas and their significance. In: Hawkesworth, C. J. and Norry, M. J. (eds.), *Continental basalts and mantle xenoliths*. Shiva, London, 5-19.

Norton, I. O. and Sclater, J. G. (1979). A model for the evolution of the Indian Ocean and the breakup of Gondwanaland. *J. Geophys. Res.*, **84**, 6803-6830.

Nougier, J., Cantagrel, J.M. and Karche, J. P. (1986). The Comores archipelago in the western Indian Ocean: volcanology, geochronology and geodynamic setting. *J. Afr. Earth Sci.*, **5**, 135-145.

O'Hara, M. J. and Yoder, H. S. (1967). Formation and fractionation of basic magmas at high pressures. *Scott. J. Geol.*, **3**, 67-117.

Olafsson, M. and Eggler, D. H. (1983). Phase relations of amphibole, amphibole-carbonate, and phlogopite-carbonate peridotite: petrologic constraints on the asthenosphere. *Earth Planet. Sci. Lett.*, **64**, 305-315.

Oxburgh, E. R. (1964). Petrological evidence for the presence of amphibole in the upper mantle and its petrogenetic and geophysical implications. *Geol. Mag.*, **101**, 1-19.

Palacz, Z. A. and Saunders, A. D. (1986). Coupled trace element and isotope enrichment in the Cook-Austral-Samoan islands, southwest Pacific. *Earth Planet. Sci. Lett.*, **79**, 270-280.

Pearce, J. A. and Norry, M. J. (1979). Petrogenic implications of Ti, Zr, Y and Nb variations in volcanic rocks. *Contrib. Mineral. Petrol.*, **69**, 33-47.

Pearce, T. H. (1968). A contribution to the theory of variation diagrams. *Contrib. Mineral. Petrol.*, **19**, 142-157.

Pearce, T. H. (1970). Chemical variations in the Palisade Sill. *J. Petrol.*, **11**, 15-32.

Pearce, T. H. (1978). Olivine fractionation equations for basaltic and ultrabasaltic liquids. *Nature*, **276**, 771-774.

Pearce, T. H. (1987). The identification and assessment of spurious trends in Pearce-type ratio variation diagrams: a discussion of some statistical arguments. *Contrib. Mineral. Petrol.*, **97**, 529-534.

Philpotts, J. A. and Schnetzler, C. C. (1970). Phenocryst-matrix partition coefficients for K, Rb, Sr and Ba, with applications to anorthosite and basalt genesis. *Geochim. Cosmochim. Acta*, **34**, 307-322.

Rabinowitz, P. D., Coffin, M. F. and Falvey, D. (1983). The separation of Madagascar and Africa. *Science*, **220**, 67-69.

Reid, A. M. and le Roex, A. P. (1988). Kaersutite-bearing xenoliths and megacrysts in volcanic rocks from the Funk Seamount in the southwest Indian Ocean. *Mineral. Mag.*, **52**, 359-370.

Richardson, S. H., Erlank, A. J., Duncan, A. R. and Reid, D. L. (1982). Correlated Nd, Sr and Pb isotope variation in Walvis Ridge basalts and implications for the evolution of their mantle source. *Earth Planet. Sci. Lett.*, **59**, 327-342.

Richter, F. M. and McKenzie, D. (1984). Dynamical models for melt segregation from a deformable matrix. *J. Geol.*, **92**, 729-740.

Roeder, P. L. and Emslie, R. F. (1970). Olivine-liquid equilibrium. *Contrib. Mineral. Petrol.*, **29**, 275-289.

Russell, J. K. and Nicholls, J. (1987). Early crystallisation history of alkali olivine basalts, Diamond Craters, Oregon. *Geochim. Cosmochim. Acta*, **51**, 143-154.

Russell, J. K. and Nicholls, J. (1988). Analysis of petrologic hypotheses with Pearce element ratios. *Contrib. Mineral. Petrol.*, **99**, 25-35.

Sato, H. (1977). Nickel content of basaltic magmas: identification of primary magmas and a measure of the degree of olivine fractionation. *Lithos*, **10**, 113-120.

Schiano, P. and Clocchiatti, R. (1994). Worldwide occurrence of silica-rich melts in sub-continental and sub-oceanic mantle minerals. *Nature*, **368**, 621-624.

Schiano, P., Clocchiatti, R., Shimizu, N., Weis, D. and Mattielli, N. (1994). Cogenetic silica-rich and carbonate-rich melts trapped in mantle minerals in Kerguelen ultramafic xenoliths: implications for metasomatism in the oceanic upper mantle. *Earth Planet. Sci. Lett.*, **123**, 167-178.

Schnetzler, C. C. and Philpotts, J. A. (1968). Partition coefficients of rare-earth elements and barium between igneous matrix material and rock-forming-mineral phenocrysts-I. In: Ahrens, L. H. (ed.), *Origin and distribution of the elements*. Pergamon, London, 929-938.

Schnetzler, C. C. and Philpotts, J. A. (1970). Partition coefficients of rare-earth elements between igneous matrix material and rock-forming mineral phenocrysts-II. *Geochim. Cosmochim. Acta*, **34**, 331-340.

Scott, P. W. (1976). Crystallization trends of pyroxenes from the alkaline volcanic rocks of Tenerife, Canary Islands. *Mineral. Mag.*, **40**, 805-816.

Scrutton, R. A. (1978). Davie Fracture Zone and the movement of Madagascar. *Earth Planet. Sci. Lett.*, **39**, 84-88.

Sheraton, J. W. and Cundari, A. (1980). Leucitites from Gaussberg, Antarctica. *Contrib. Mineral. Petrol.*, **71**, 417-427.

Shimizu, N. (1974). An experimental study of the partitioning of K, Rb, Cs, Sr and Ba between clinopyroxene and liquid at high pressures. *Geochim. Cosmochim. Acta*, **38**, 1789-1798.

Shor, G. G. and Pollard, D. D. (1963). Seismic investigations of Seychelles and Saya de Malha Banks, Northwest Indian Ocean. *Science*, **142**, 48-49.

Späth, A. and le Roex, A. P. (1994). The geochemistry of the Comores Archipelago, western Indian Ocean. *Supplement to EOS*, **75**, 368.

Stanley, C. R. and Russell, J. K. (1989a). Petrologic hypothesis testing with Pearce element ratio diagrams: derivation of diagram axes. *Contrib. Mineral. Petrol.*, **103**, 78-89.

Stanley, C. R. and Russel, J. K. (1989b). PEARCE.PLOT: Interactive graphics-supported software for testing petrologic hypotheses with Pearce element-ratio diagrams. *Am. Mineral.*, **74**, 273-276.

Stoddart, D. R., Taylor, J. D., Fosberg, F. R. and Farrow, G. E. (1971). Geomorphology of Aldabra Atoll. *Phil. Trans. Roy. Soc. Lond. B*, **260**, 31-65.

Stolper, E., Walker, D., Hager, B. H. and Hays, J. F. (1981). Melt segregation from partially molten source regions: the importance of melt density and source region size. *J. Geophys. Res.*, **86**, 6261-6271.

Storey, M., Saunders, A. D., Tarney, J., Leat, P., Thirlwall, M. F., Thompson, R. N., Menzies, M. A. and Marriner, G. F. (1988). Geochemical evidence for plume-mantle interactions beneath Kerguelen and Heard Islands, Indian Ocean. *Nature*, **336**, 371-374.

Strong, D. F. (1972a). Petrology of the island of Moheli, western Indian Ocean. *Geol. Soc. Am. Bull.*, **83**, 389-406.

Strong, D. F. (1972b). The petrology of the lavas of Grande Comore. *J. Petrol.*, **13**, 181-217.

Strong, D. F. and Jacquot, C. (1970). The Karthala caldera, Grande Comore. *Bull. Volcanol.*, **34**, 663-680.

Sun, S. S. and Hanson, G. N. (1975). Origin of Ross Island basanitoids and limitations upon the heterogeneity of mantle sources for alkali basalts and nephelinites. *Contrib. Mineral. Petrol.*, **52**, 77-106.

Sun, S.-S. and Nesbitt, R. W. (1977). Chemical heterogeneity of the Archean mantle, composition of the Earth and mantle evolution. *Earth Planet. Sci. Lett.*, **35**, 429-448.

Sun, S.-s. and McDonough, W. F. (1989). Chemical and isotopic systematics of oceanic basalts: implications for mantle composition and processes. In: Saunders, A. D. and Norry, M. J. (eds.), Magmatism in the ocean basins, *Geol. Soc. Spec. Publ.*, **42**, 313-345.

Syme, E. C. and Forester, R. W. (1977). Petrogenesis of the Boundary intrusion in the Flin Flon area of Saskatchewan and Manitoba. *Can. J. Earth Sci.*, **14**, 444-455

Taylor, W. R. and Green, D. H. (1989). The role of reduced C-O-H fluids in mantle partial melting. *Geol. Soc. Australia Spec. Publ.*, **14**, 592-602.

Thompson, R. N. (1972). The 1-atmosphere melting patterns of some basaltic volcanic series. *Am. J. Sci.*, **272**, 901-932.

Thompson, R. N. (1974). Some high-pressure pyroxenes. *Mineral. Mag.*, **39**, 768-787.

Thompson, R. N. and Flower, M. F. J. (1971). One-atmosphere melting and crystallisation relations of lavas from Anjouan, Comores Archipelago, western Indian Ocean. *Earth Planet. Sci. Lett.*, **12**, 97-107.

Tilley, C. E., Thompson, R. N., Wadsworth, W. J. and Upton, B. G. J. (1971). Melting relations of some lavas of Réunion Island, Indian Ocean. *Mineral. Mag.*, **38**, 344-352.

Turcotte, D. L. and Ahern, J. L. (1978). A porous flow model for magma migration in the asthenosphere. *J. Geophys. Res.*, **83**, 767-772.

Upton, B. G. J. (1982). Oceanic islands. In: Nairn, E. M. and Stehli, F. G. (eds.), *The ocean basins and margins*, **6**, 585-647. Plenum.

Upton, B. G. J. and Wadsworth, W. J. (1972). Aspects of magmatic evolution on Réunion Island. *Phil. Trans. R. Soc. Lond. A*, **271**, 105-130.

Upton, B. G. J., Wadsworth, W. J. and Latrille, E. (1974). The 1972 eruption of Karthala volcano, Grande Comore. *Bull. Volcanol.*, **38**, 136-148.

Varne, R. (1970). Hornblende lherzolite and the upper mantle. *Contrib. Mineral. Petrol.*, **27**, 45-51.

Vink, G. E., Morgan, W. J. and Vogt, P. R. (1985). The Earth's hot spots. *Sci. Am.*, **252**, 32-39.

Vinx, R. and Jung, D. (1977). Pargasitic-kaersutitic amphibole from a basanitic diatreme at the Rosenberg, north of Kassel (North Germany). *Contrib. Mineral. Petrol.*, **65**, 135-142.

Wass, S. Y. (1979). Multiple origins of clinopyroxenes in alkali basaltic rocks. *Lithos*, **12**, 115-132.

Wasserburg, G. J., Craig, H., Menard, H. W., Engel, A. E. J. and Engel, C. G. (1963). Age and composition of a Bounty Islands granite and age of a Seychelles Islands granite. *J. Geol.*, **71**, 785-789.

Watkins, R. T. and le Roex, A. P. (1992). The rare-earth element content of GSJ rock reference samples determined by gradient ion chromatography. *Geochem. J.*, **26**, 241-249.

Watkins, R. T. and le Roex, A. P. (1993). Rare earth element concentrations in USGS and CCRMP igneous rock standards determined by high performance ion chromatography. *Geostandards Newsletter*, **17**, 105-111.

Weaver, B. L. (1990). Geochemistry of highly-undersaturated ocean island basalt suites from the South Atlantic Ocean: Fernando de Noronha and Trinidade islands. *Contrib. Mineral. Petrol.*, **105**, 502-515.

Weaver, B. L., Wood, D. A., Tarney, J. and Joron, J. L. (1986). Role of subducted sediment in the genesis of ocean-island basalts: geochemical evidence from South Atlantic Ocean islands. *Geology*, **14**, 275-278.

Weaver, B. L., Wood, D. A., Tarney, J. and Joron, J. L. (1987). Geochemistry of ocean island basalts from the South Atlantic: Ascension, Bouvet, St. Helena, Gough and Tristan da Cunha. In: Fitton, J. G. and Upton, B. G. J. (eds.), Alkaline Igneous Rocks, *Geol. Soc. Spec. Publ.*, **30**, 253-267.

Wegener, A. (1924). *The origin of continents and oceans.* Methuen & Co., London.

Weis, D., Frey, F. A., Leyrit, H. and Gautier, I. (1993). Kerguelen Archipelago revisited: geochemical and isotopic study of the Southeast Province lavas. *Earth Planet. Sci. Lett.*, **118**, 101-119.

White, W. M. (1985). Sources of oceanic basalts: radiogenic isotopic evidence. *Geology*, **13**, 115-118.

White, W. M. and Hofmann, A. W. (1982). Sr and Nd isotope geochemistry of oceanic basalts and mantle evolution. *Nature*, **296**, 821-825.

White, W. M., Cheatham, M. M. and Duncan, R. A. (1990). Isotope geochemistry of leg 115 basalts and inferences of the history of the Réunion mantle plume. *Proc. ODP, Sci. Results*, **115**, 53-61.

Wilkinson, J. F. G. (1991). Mauna Loan and Kilauean tholeiites with low 'ferromagnesian-fractionated' 100 $Mg/(Mg+Fe^{2+})$ ratios: primary liquids from the upper mantle ? *J. Petrol.*,**32**, 863-907.

Wilkinson, J. F. G. and le Maitre, R. W. (1987). Upper mantle amphiboles and micas and TiO_2, K_2O and P_2O_5 abundances and 100 $Mg/(Mg+Fe^{2+})$ ratios of common basalts and andesites: Implications for modal mantle metasomatism and undepleted mantle compositions. *J. Petrol.*, **28**, 37-73.

Wilkinson, J. F. G. and Hensel, H. D. (1991). An analcime mugearite-megacryst association from north-eastern New South Wales: implications for high-pressure amphibole-dominated fractionation of alkaline magmas. *Contrib. Mineral. Petrol.*, **109**, 240-251.

Wright, J. B. and McCurry, P. (1970). Letter to the editor. The significance of sandstone inclusions in lavas of the Comores Archipelago, M.F.J. Flower and D.F. Strong. *Earth Planet. Sci. Lett.*, **8**, 267-268.

Wyllie, P. J. (1978). Mantle fluid compositions buffered in peridotite-CO_2-H_2O by carbonates, amphibole and phlogopite. *J. Geol.*, **86**, 687-713.

Wyllie, P. J. (1979). Magmas and volatile components. *Am. Mineral.*, **64**, 469-500.

Wyllie, P. J. (1989). The genesis of kimberlites and some low-SiO_2, high-alkali magmas. *Geol. Soc. Australia Spec. Publ.*, **14**, 603-615.